Doctoral thesis 2013

GEOLOGY AND METALLOGENY OF THE CERRO QUEMA AU-CU DEPOSIT (AZUERO PENINSULA, PANAMA)

Isaac Corral Calleja

Universitat Autònoma de Barcelona
Departament de Geologia

Universitat Autònoma de Barcelona

Geology and Metallogeny of the Cerro Quema Au-Cu deposit

(Azuero Peninsula, Panama)

Isaac CORRAL CALLEJA

Geology and Metallogeny of the Cerro Quema Au-Cu deposit

(Azuero Peninsula, Panama)

PhD Dissertation presented by

Isaac CORRAL CALLEJA

In candidacy for the degree of Doctor in Geology at the Universitat Autònoma de Barcelona.

PhD thesis supervised by

Dr. Esteve Cardellach López

Unitat de Cristal·lografia I Mineralogia
Departament de Geologia
Universitat Autònoma de Barcelona

Cerdanyola del Vallès, March 2013

Esteve Cardellach López, Catedràtic de Cristal·lografia i Mineralogia del Departament de Geologia de la Universitat Autònoma de Barcelona (UAB).

CERTIFICO:

Que els estudis recollits en la present memòria sota el títol "**Geology and Metallogeny of the Cerro Quema Au-Cu deposit (Azuero Peninsula, Panama)**" han estat realitzats sota la meva direcció per Isaac Corral Calleja, llicenciat en Geologia, per optar al grau de Doctor en Geologia.

I perquè així consti, signo la present certificació.

Cerdanyola del Vallès, Març de 2013

Dr. Esteve Cardellach López

The development of this thesis has been done within the framework of the PhD program in Geology of the Universitat Autònoma de Barcelona (RD 778/1998), and supported by the Spanish Ministry of Science and Education (MEC), project CGL2007-62690/BTE.

Isaac Corral acknowledges a PhD research grant (FI 2008) from the "Departament d'Universitats, Recerca i Societat de la Informació (Generalitat de Catalunya)" as well as the research mobility grant within the framework of the "Beques per a estades de recerca a l'estranger (BE 2009)" of the "Agència de Gestió d'Ajuts Universitaris i de Recerca (Generalitat de Catalunya). Moreover, the corresponding author would like to express his gratitude to the Society of Economic Geology Foundation and the Society of Economic Geology Canada Foundation for the 2009, 2010 and 2011 Hugh E. McKinstry student research grants. Part of the experimental work of this thesis was performed in collaboration with:

- Central Mineral and Environmental Resources Science Center. United States Geological Survey, Denver, CO (USA).
- Departamento de Geología, Universidad Complutense de Madrid (UCM), Madrid (Spain).

Con todo mi cariño y agradecimiento,

a mi Yayo Emilio y a mis Padres.

« The best geologist is the one who has seen the most rocks »

H. H. Read (1889-1970)

TABLE OF CONTENTS

SUMMARY

Cerro Quema, located in the Azuero Peninsula (SW Panama) is a structurally and lithologically controlled Au-Cu deposit. It is hosted by a dacite dome complex intruded within the Río Quema Formation, a volcanosedimentary sequence of Late Campanian to Maastrichtian age deposited in a fore-arc basin. Mineralization and hydrothermal alteration is controlled by E-W trending regional faults. Cerro Quema is a controversial deposit because it has been interpreted as a high sulfidation epithermal deposit, but also as a hybrid epithermal-volcanogenic massive sulfide deposit. Despite previous geologic and metallogenetic studies, the geodynamic framework of the area and the relationship with mineral deposits is not understood. The aim of this thesis is to unravel the relationship between the geological evolution of the area and the origin and evolution of the mineralizing fluids.

In Chapter 1, the main characteristics of high sulfidation epithermal deposits and their link with other economically important deposits (e.g., porphyry copper and VMS) are revised. Chapters 2 and 3 comprise the tectonostratigraphy, geochemistry and biostratigraphy of the Azuero Peninsula. A new geologic map of the area, complemented with geochemical data and a biostratigraphical study of radiolarian and planctonic foraminifera, is presented. Finally, a paleogeographic reconstruction of the Cretaceous volcanic arc is proposed.

Chapters 4 and 5 deal with the geology, mineralogy, geochemistry and age of the deposit. Ore and alteration (hydrothermal and supergene) mineral parageneses are described. The origin and evolution of mineralizing fluids is discussed from fluid inclusion (homogenization temperature and salinity) and stable isotopes (S, O and H) data. The chemical characterization of the hydrothermal fluids is strengthened from trace metal content of hydrothermally altered host rocks, and EMPA analyses on pyrite, alunite and aluminum phosphate-sulfate (APS) minerals. In order to constrain the age of the mineralization, Ar/Ar dating (hornblende) have been performed on Cerro Quema host rocks (67.9 ±1.3 to 65.6 ±1.3 Ma) and on plutonic rocks of the area (El Montuoso batholith: 65.7 ±1.4 Ma; Valle Rico batholith: 54.8 ±1.2 Ma; Parita batholith: 40.8 ±1.4 Ma). $\delta^{34}S$ values have been measured on pyrite, chalcopyrite, enargite, barite and aluntie. $\delta^{18}O$ was analyzed on barite, aluntie, quartz, kaolinite and dickite, and δD on kaolinite and dickite. Microthermometircal measurements were performed on secondary fluid inclusions from hydrothermally altered igneous quartz. A conceptual model integrating the genesis of the deposit within the geodynamic framework of the Azuero Peninsula is presented.

Chapter 6 includes the conclusions of the thesis. According to field observations coupled with geochronological and biostratigraphical data, Cerro Quema is a high sulfidation epithermal deposit emplaced during Lower Eocene (~55-49 Ma) times, and is probably related to an underlying porphyry copper system. Mineralizing fluids were of variable temperature (140 - 240ºC) and low salinity (< 5 wt% NaCl eq.). Hydrothermal fluids were sulfide dominant with sulfur of magmatic origin ($\delta^{34}S_{\Sigma S}$= -0.5‰). $\delta^{18}O$ of fluids in equilibrium with vuggy silica (-2.6 to +3.0‰), and $\delta^{18}O/\delta D$ values of fluids in equilibrium with kaolinite/dickite ($\delta^{18}O$= -10.0 to +13.3‰; δD= -72 to -13‰, respectively), indicate that mineralization was produced by the mixing of hydrothermal fluids with meteoric waters. Cerro Quema is only a part of an extensive hydrothermal system that produced similar deposits in the southern portion of the Azuero Peninsula. The present study has revealed the relationship of Au-Cu deposits with E-W trending regional faults, an important feature that might be used as exploration tool.

RESUM

Cerro Quema és un dipòsit d'or-coure situat a la Península d'Azuero (SO Panamà). Està encaixat dins d'un complex de doms dacítics que intrueixen la Formació Río Quema, seqüència vulcanosedimentària d'edat Campanià superior - Maastrichtià dipositada en una conca d'avantarc. La mineralització i l'alteració hidrotermal estan controlades per falles regionals d'orientació E-O i litològicaments per la presència de doms dacítics. Es tracta d'un dipòsit d'origen controvertit, ja que ha estat interpretat com a epitermal d'alta sulfuració, i també com a un híbrid epitermal - sulfurs massius. Malgrat els estudis geològics i metal·logenètics previs, la geodinàmica de la zona i la seva relació amb el dipòsits minerals, no es coneixia en detall. En conseqüència, l'objectiu d'aquesta Tesi és el esbrinar la relació entre l'evolució geològica de la zona i l'origen i evolució dels fluids mineralitzants.

Al Capítol 1, es revisen les característiques principals dels dipòsits epitermals d'alta sulfuració i la seva possible relació amb d'altres dipòsits d'interès econòmic (p.e. pòrfirs cuprífers i sulfurs massius). Els Capítols 2 i 3 comprenen l'estudi tectonoestratigràfic, geoquímic i bioestratigràfic de la part sud de la Península d'Azuero. És presentat també un nou mapa geològic de la zona d'estudi, completat amb dades geoquímiques i bioestratigràfiques de radiolaris i foraminífers planctònics. Finalment, es proposa un model de reconstrucció de l'arc volcànic durant el Cretaci.

Els Capítols 4 i 5 tracten la geologia, mineralogia, geoquímica i l'edat del dipòsit. Es descriuen les paragènesis minerals de la mineralització i de les alteracions (hidrotermal i supergènica). A partir de dades d'incllusions fluides (temperatura d'homogenització i salinitat), i d'isòtops estables (S, O i H), es discuteix l'origen i evolució dels fluids mineralitzants. La caracterització geoquímica dels fluids hidrotermals és completada dades de contingut en metalls de les roques de caixa alterades hidrotermalment i per anàlisis amb microsonda electrònica (EMPA) de pirites, alunites i minerals alumino-fosfats-sulfats (APS). Per tal de concretar l'edat de la mineralització, s'han realitzat datacions radiomètriques Ar/Ar (hornblendes), en les roques caixa (67.9 ±1.3 - 65.6 ±1.3 Ma) i en les roques plutòniques de la zona (batòlit de El Montuoso: 65.7 ±1.4 Ma; batòlit de Valle Rico: 54.8 ±1.2 Ma; batòlit de Parita: 40.8 ±1.4 Ma). Per tal de conèixer l'origen dels fluids, s'ha analitzat la $\delta^{34}S$ en pirita, calcopirita, enargita, barita i alunita, la $\delta^{18}O$ en barita, alunita, quars, caolinita i dickita, i la δD en caolinita i dickita. Les mesures microtermomètriques s'han realitzat en inclusions fluides secundàries contingudes en quarsos ignis alterats hidrotermalment. El conjunt d'aquestes dades ha permès desenvolupar un model genètic conceptual on s'integra la gènesi del dipòsit en el marc geodinàmic de la Península d'Azuero.

El Capítol 6 inclou les conclusions de la tesi. D'acord amb les observacions de camp, juntament amb les dades geocronològiques i bioestratigràfiques, podem afirmar que Cerro Quema és un dipòsit epitermal d'alta sulfuració emplaçat durant l'Eocè inferior (~55-49 Ma), i que probablement està relacionat amb un sistema de pòrfir cuprífer subjacent. Els fluids mineralitzants van ser de temperatura variable (140 – 240ºC) i de baixa salinitat (< 5% en pes eq. de NaCl). L'espècie de sofre dominant en els fluids hidrotermals era el H_2S, d'origen magmàtic ($\delta^{34}S_{\Sigma S}$= -0.5‰). Els valors de $\delta^{18}O$ dels fluids en equilibri amb el vuggy silica (-2.6 - +3.0‰) i els valors de $\delta^{18}O/\delta D$ dels fluids en equilibri amb caolinites/dickites ($\delta^{18}O$= -10.0 - +13.3‰; δD= -72 - -13‰, respectivament) indiquen que la mineralització es va produir per la barreja de fluids hidrotermals amb aigües meteòriques. Cerro Quema és només una part d'un extens sistema hidrotermal que va donar lloc a dipòsits similars a la regió sud de la Península d'Azuero. Aquest estudi ha posat de manifest la interrelació entre els dipòsits d'or-coure de la Península d'Azuero amb falles regionals d'orientació E-O, una característica important que pot ser utilitzada com a eina d'exploració.

RESUMEN

Cerro Quema es un depósito de oro-cobre situado en la Península de Azuero (SO Panamá). Está encajado dentro de un complejo de domos dacíticos que intruyen la Formación Río Quema, secuencia volcanosedimentaria de edad Campaniense superior – Maastrichtiense depositada en una cuenca de antearco. La mineralización y la alteración hidrotermal están controladas por fallas regionales de orientación E-O y litológicamente por la presencia de domos dacíticos. Se trata de un depósito de origen conrovertido, pues ha sido considerado como un depósito epitermal de alta sulfuración, pero también como un deposito híbrido epitermal - sulfuros masivos. A pesar de los estudios geológicos y metalogenéticos previos, la geodinámica de la zona y su relación con los yacimientos minerales, no se conocía en detalle. En consecuencia, el objetivo de esta Tesis es averiguar la relación entre la evolución geológica de la zona y el origen y evolución de los fluidos mineralizantes.

En el Capítulo 1 se describen las características principales de los depósitos epitermales de alta sulfuración y su posible relación con otros yacimientos de interés económico (p.e. pórfidos cupríferos y sulfuros masivos). Los Capítulos 2 y 3 comprenden el estudio tectonoestratigráfico y geoquímico de la parte sur de la Península de Azuero. Se presenta también un nuevo mapa geológico de la zona de estudio, complementado con datos geoquímicos y bioestratigráficos de radiolarios y foraminíferos planctónicos. Finalmente se propone un modelo de reconstrucción paleogeográfica del arco volcánico durante el Cretácico.

Los Capítulos 4 y 5 tratan sobre la geología, mineralogía, geoquímica y la edad del yacimiento. Se describen las paragénesis minerales de la mineralización y de las alteraciones (hidrotermal y supergénica). A partir de los datos de inclusiones fluidas (temperatura de homogenización y salinidad) y de isotopos estables (S, O y H), se discute el origen y evolución de los fluidos mineralizantes. La caracterización geoquímica de los fluidos hidrotermales es complementada con los datos de contenido de metales de las rocas caja alteradas hidrotermalmente y con los análisis con microsonda electrónica (EMPA), de piritas, alunitas y minerales alumino-fosfato-sulfatos (APS). Para concretar la edad de la mineralización, se han realizado dataciones radiométricas Ar/Ar (en hornblenda), en las rocas caja (67.9 ±1.3 - 65.6 ±1.3 Ma) y en las rocas plutónicas de la zona (batolito de El Montuoso: 65.7 ±1.4 Ma; batolito de Valle Rico: 54.8 ±1.2 Ma; batolito de Parita: 40.8 ±1.4 Ma). Para conocer el origen de los fluidos, se ha analizado la $\delta^{34}S$ en pirita, calcopirita, enargita, barita y alunita, la δ^{18} en barita, alunita, cuarzo, caolinita y dickita, y la δD en caolinita y dickita. Las mediciones microtermométricas se han realizado en inclusiones fluidas secundarias contenidas en cuarzos ígneos alterados hidrotermalmente. El conjunto de estos datos ha permitido desarrollar un modelo genético conceptual donde se integra la génesis del yacimiento en el marco geodinámico de la Península de Azuero.

El Capítulo 6 incluye las conclusiones de la tesis. De acuerdo con las observaciones de campo, junto con los datos geocronológicos y bioestratigráficos, podemos afirmar que Cerro Quema es un depósito epitermal de alta sulfuración emplazado durante el Eoceno inferior (~55-49 Ma), y que probablemente está relacionado con un sistema de pórfido cuprífero subyacente. Los fluidos mineralizantes fueron de temperatura variable (140 – 240ºC), y de baja salinidad (< 5% en peso eq. de NaCl). La espécie de azufre dominante en el fluido hidrotermal era el H_2S, de origen magmático ($\delta^{34}S_{\Sigma S}$= -0.5‰). Los valores de $\delta^{18}O$ de los fluidos en equilibrio con vuggy silica (-2.6 - +3.0‰) y los valores de $\delta^{18}O/\delta D$ de los fluidos en equilibrio con caolinitas/dickitas ($\delta^{18}O$= -10.0 - +13.3‰; δD= -72 - -13‰, respectivamente) indican que la mineralización se produjo por la mezcla de fluidos hidrotermales con aguas meteóricas. Cerro Quema es solo una parte de un extenso sistema hidrotermal que dio lugar a depósitos similares en la región sur de la Península de Azuero. Este estudio ha puesto de manifiesto la interrelación entre los depósitos de oro-cobre con las fallas regionales de orientación E-O, una característica importante que puede ser utilizada como herramienta de exploración.

Chapter 1

Introduction

1.1. Motivations

1.2. Objectives

1.2.1. General objectives

1.2.2. Specific objectives

1.3. Structure of the thesis

1.4. References

1.1. Motivations

High sulfidation epithermal deposits are one of the most economically important sources of gold. They are usually found within volcanic fields and are thought to have formed from hydrothermal fluids of igneous origin (e.g., Sillitoe and Bonham, 1984; White, 1991; Hedenquist and Lowenstern, 1994; Arribas, 1995). As shown in Figure 1.1, high sulfidation epithermal deposits may be related to deeper porphyry-copper systems (e.g., Sillitoe, 1973; Arribas *et al*., 1995; Hannington, 1997; Muntean and Einaudi, 2001; Kouzmanov *et al*., 2009), to volcanic massive sulfide type (VMS), particularly when they form in submarine environments (e.g., Sillitoe *et al*., 1996; Poulsen and Hannington, 1996; Hannington, 1997; Huston, 2000; Robert *et al*., 2007), and also to low sulfidation epithermal systems (Hedenquist and Lowenstern, 1994; Sillitoe, 1995; Corbett and Leach, 1998).

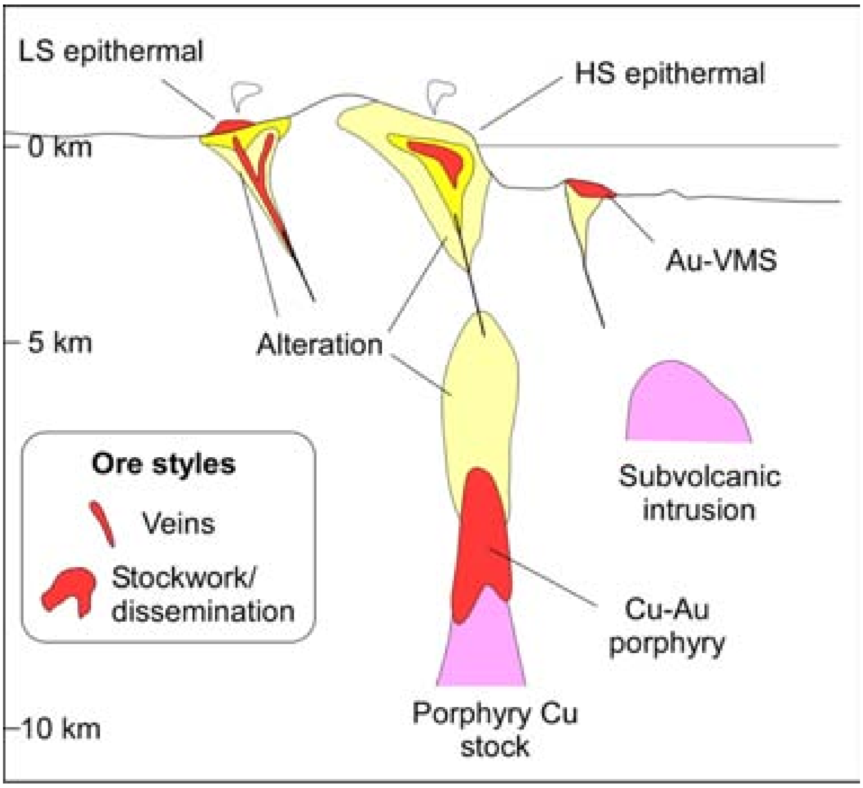

Figure 1.1: Schematic cross section showing the relationship between the main ore deposit types discussed in the text, and their crustal depth of emplacement. Modified from Poulsen *et al*., (2000) and Robert *et al*., (2004, 2007). HS: High Sulfidation, LS: Low Sulfidation.

Research in magmatic-hydrothermal systems in volcano-plutonic arcs has focused on active geothermal systems as analogs for ore-forming systems, and on the potentially genetic links between relatively deep-seated porphyry Cu-(Au) deposits and volcanic-hosted epithermal precious metal deposits (Hedenquist and Lowenstern, 1994). Spatial and temporal links between epithermal and porphyry copper deposits, including overlapping alteration, have been documented in many areas (e.g., Lepanto, Philippines, Arribas *et al*., 1995; Hedenquist et. al., 1998; Maricunga Belt, Chile, Muntean and Eunaudi, 2001; Colquijirca, Perú, Bendezú and Fontboté, 2002). Although the contemporaneity between both styles of mineralization is not clear, they seem to be typically associated with the same magmatic event (Hannington, 1997).

Central America is host to a variety of metallic mineral resources including gold, silver, lead, zinc, nickel, cobalt, antimony, tungsten, aluminum and copper, spanning a broad range of deposit types. In the near past, and due to political and economical reasons, Central America has not been very attractive to mining companies and investments on metal exploration and research have been low, especially when compared to North and South America. In some countries, recent changes led to an increase in the exploration, with discoveries and new mines coming into production. Panama is one of these examples, where Au and Cu mining projects are currently under development. Cerro Quema, the objective of the present study, recently announced reserves of 7.23 Mt with an average gold grade of 1.10 g/T (Valiant *et al*., 2011; Puritch, *et al*., 2012). Viability studies are currently conducted on Cerro Colorado and Petaquilla porphyry copper deposits.

The purpose of this work is to contribute to the knowledge of epithermal deposits and their possible link with porphyry copper and/or VMS deposits. The study is centered in the Cerro Quema deposit, located in the Azuero Peninsula, SW Panama (Fig. 1.2). It is considered one of the most promising Au-Cu prospects of Panama. Cerro Quema is constituted by three mineralized bodies, named from West to East: La Pava, Cerro Quemita and Cerro Quema. From the geological and mineralogical characteristics, Cerro Quema has been considered as a high sulfidation epithermal system related to a underlying porphyry copper intrusion (Leach, 1992; Nelson, 1995), and as an oxidized Au-

Cu deposit that shares characteristics of epithermal and VMS deposits (Nelson and Nietzen, 2000; Nelson, 2007). Thus, the definition of the deposit type for Cerro Quema is still a matter of debate.

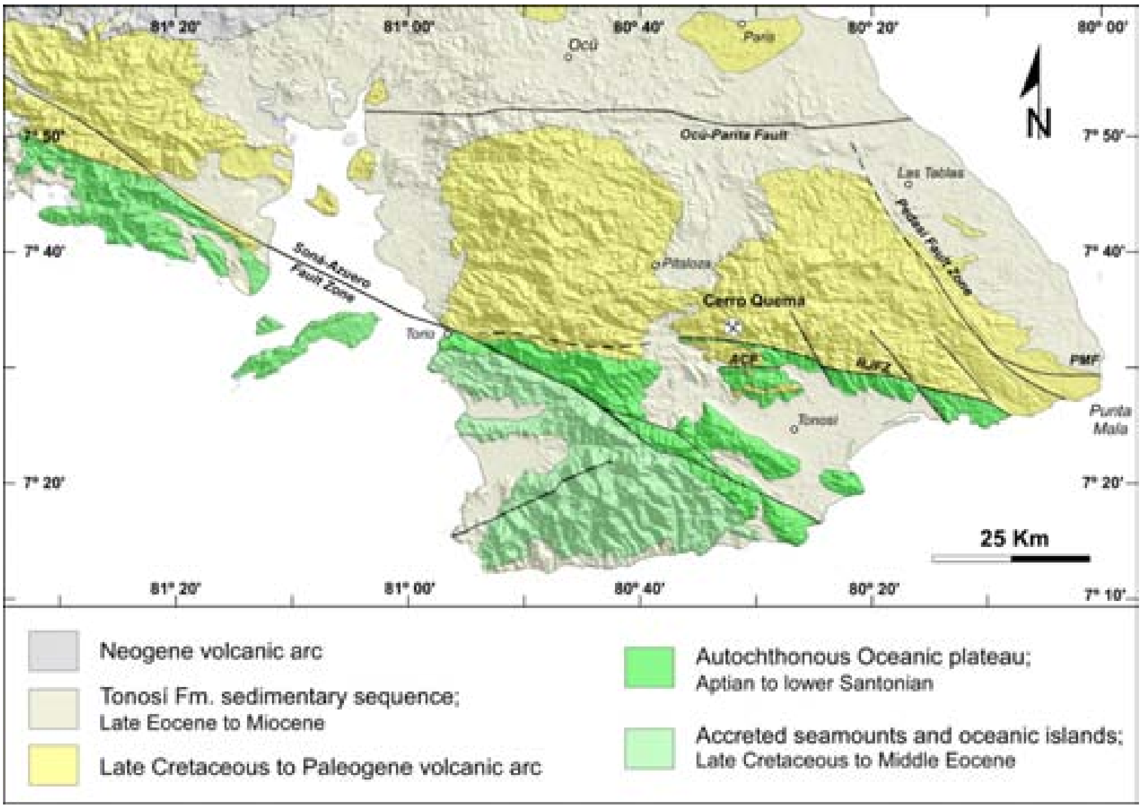

Figure 1.2: Simplified geological map of the volcanic arcs cropping out in the Azuero Peninsula. RJFZ: Río Joaquín Fault Zone, ACF: Agua Clara Fault, PMF: Punta Mala Fault (After Dirección General de Recursos Minerales, 1976; Buchs *et al*., 2010; Corral *et al*., 2011).

The Azuero Peninsula is characterized by a long-lived intra-oceanic subduction zone formed in the Late Cretaceous (Wörner *et al*., 2009; Buchs *et al*., 2010; Wegner *et al*., 2011), produced by the subduction of the ancient Farallon Plate beneath the Caribbean Plate. The volcanic arc of calc-alkaline affinity developed on the western edge of the Caribbean Plate, displays all the necessary characteristics for the development of epithermal, porphyry copper and VMS deposits.

Despite the number of geological studies on the Azuero Peninsula (Del Giudice and Recchi, 1969; Ferencic, 1970; Kesler *et al*., 1977; Buchs *et al*., 2010, 2011) and on Cerro Quema (Leach, 1992; Horlacher and Lehmann, 1993; Torrey and Keenan, 1994), the geology, the age of the deposit and the host rock, the hydrothermal alteration and the mineralization stages, are poorly known. As a consequence, the relationship between magmatism, volcanism and Au-Cu epithermal mineralization, the composition, origin and evolution of the mineralizing fluid, and the possible link of the Cerro Quema deposit with other deposit types (e.g., porphyry copper, VMS) are not well understood.

1.2. Objectives

1.2.1. General objectives

The aim of the present thesis is the study the Cerro Quema Au-Cu deposit, integrating geological, structural, petrological, biostratigraphical, geochronological and geochemical data in order to understand the role of volcanic domes and associated volcanoclastic rocks in the formation of high sulfidation systems in vulcano-plutonic arcs. Additionally, the possible link between this deposit and porphyry Cu systems and/or volcanogenic massive sulfide deposits is also evaluated.

1.2.2. Specific objectives

- Identification of the geological environment of the Cerro Quema deposit, the possible connection with the volcanism and the regional tectonic framework of the Azuero Peninsula.
- Dating the sedimentary, volcanic and plutonic rocks of the Azuero Peninsula related with the Cerro Quema Au-Cu deposit.
- Recognition of the hydrothermal alteration zones and identification of their mineralogical composition.
- Determining the ore paragenetic stages and their respective composition, defining and describing the ore mineral textures.
- Constraining the age of the hydrothermal alteration and/or mineralization.

- Microthermometrical and isotopic characterization of mineralizing fluid in order to infer its origin and evolution.
- Development of a conceptual model for the Cerro Quema deposit within the geological framework of the Azuero Peninsula.
- Defining prospecting criteria for this type of Au-Cu deposit in geologically similar terrains.

1.3. Structure of the thesis

This PhD thesis contains six chapters presented in article-like format, except Chapter 1 (Introduction) and Chpater 6 (Conclusions). Chapters 2 and 3 have already been published in indexed journals (ISI):

Corral, I. Griera, A., Gómez-Gras, d., Corbella, M., Canals, À., Pineda-Falconett, M., Cardellach, E., 2011. Geology of the Cerro Quema Au-Cu deposit (Azuero Peninsula, Panama). Geologica Acta, 9 (3-4), 481-498.

Corral, I., Gómez-Gras, D., Griera, A., Corbella, M. and Cardellach, E., 2013. Sedimentation and volcanism in the Panamanian Cretaceous intra-oceanic arc and fore-arc: New insights from the Azuero Peninsula, (SW Panama). Bulletin de la Société Géologique de France 184 (1), 35-45.

In Chapter 1 (Introduction), the interest of the present study and the main objectives are exposed. Chapter 2 is focused on the geology of the Azuero Peninsula and the Río Quema Formation, the host-rock of the Cerro Quema Au-Cu deposit. Here, an overview of the tectonostratigraphy and geochemistry of the main litostratigraphic units of the Azuero Peninsula is presented. A detailed study of the stratigraphy, biostratigraphy and the facies distribution of the Río Quema Formation throughout the Azuero Peninsula is exposed in Chapter 3. A paleogeographical reconstruction of the Cretaceous volcanic arc is also proposed. Chapter 4 is devoted to the mineralogical and geochemical study of ore and gangue minerals and of the hydrothermal alteration zones. Chemical analyses of hydrothermally altered rocks, sulfides and sulfates are presented. In order to constrain the age of the deposit, this chapter also includes geochronological dating (Ar/Ar) of the Cerro Quema host rock and of the igneous rocks of the Azuero Peninsula related with the mineralization. Finally, a geologic model for the Cerro Quema mineralization within the tectonic framework of the Azuero Peninsula is proposed. In oreder to unravel the origin and evolution of the mineralizing fluids, Chapter 5 includes fluid inclusion data obtained on quartz and stable isotope analyses (S, O and H) of sulfates, silicates and sulfides from hydrothermally altered zones of the Cerro Quema deposit. Finally, a genetic model for the emplacement of the Cerro Quema deposit integrating the geological and geochemical data is proposed. The final conclusions drawn from the data obtained in the present study are presented in Chapter 6. The chapter also includes guidelines for exploration of high sulfidation epithermal deposits in the Azuero Peninsula, and proposals for future work.

1.4. References

Arribas, A., 1995, Characteristics of high-sulfidation epithermal deposits, and their relation to magmatic fluid: In: Thompson, J. F. H. (Ed.), Magmas, Fluids, and Ore Deposits, Mineralogical Association of Canada Short Course, v. 23, p. 419-454.

Arribas, A., Jr., Hedenquist, J. W., Itaya, T., Okada, T., Concepcion, R. A., and Garcia, J. S., Jr., 1995, Contemporaneous formation of adjacent porphyry and epithermal Cu-Au deposits over 300 ka in northern Luzon, Philippines: Geology, v. 23, p. 337-340.

Bendezú, R., and L., F., 2002, Late timing for high sulfidation cordilleran base metal lode and replacement deposits in porphyry-related districts: The case of Colquijirca, central Peru: SGA News, v. 13, p. 1 and 9-13.

Buchs, D. M., Arculus, R. J., Baumgartner, P. O., Baumgartner-Mora, C., and Ulianov, A., 2010, Late Cretaceous arc development on the SW margin of the Caribbean Plate: Insights from the Golfito, Costa Rica, and Azuero, Panama, complexes: Geochemistry, Geophysics, Geosystems, v. 11, p. Q07S24.

Buchs, D. M., Baumgartner, P. O., Baumgartner-Mora, C., Flores, K., and Bandini, A. N., 2011, Upper Cretaceous to Miocene tectonostratigraphy of the Azuero area (Panama) and the discontinuous accretion and subduction erosion along the Middle American margin: Tectonophysics, v. 512, p. 31-46.

Corbett, G. J., and Leach, T. M., 1998, Southwest Pacific Rim gold-copper systems; structure, alteration, and mineralization: Special Publication (Society of Economic Geologists (U. S.)), v. 6, 237 pp.

Corral, I., Griera, A., Gómez-Gras, D., Corbella, M., Canals, À., PIneda-Falconett, M., and Cardellach, E., 2011, Geology of the Cerro Quema Au-Cu deposit (Azuero Peninsula, Panama): Geologica Acta, v. 9, p. 481-498.

Del Giudice, D., and Recchi, G., 1969, Geologia del area del Proyecto Minero de Azuero., Informe técnico preparado para el gobierno de la Republica de Panama por las Naciones Unidas. Gobierno de la República de Panamá, Panama City, Panama, 48 pp.

Dirección General de Recursos Minerales, 1976, Mapa Geológico de Panamá. Escala 1:500,000. Panamá.

Ferencic, A., 1970, Porphyry copper mineralization in Panama: Mineralium Deposita, v. 5, p. 383-389.

Hannington, M. D., 1997, The Porphyry-Epithermal-VMS Transition: Lessons from the Iskut River Area, British Columbia, and Modern Island Arcs: SEG Newsletter, v. 29, p. 12-13.

Hedenquist, J. W., Arribas, A., and Reynolds, T. J., 1998, Evolution of an intrusion-centered hydrothermal system; Far Southeast-Lepanto porphyry and epithermal Cu-Au deposits, Philippines: Economic Geology, v. 93, p. 373-404.

Hedenquist, J. W., and Lowenstern, J. B., 1994, The role of magmas in the formation of hydrothermal ore deposits: Nature, v. 370, p. 519-527.

Horlacher, C. F., and Lehmann, J. H., 1993, Regional Geology, Geochemistry and Exploration potential of the central Cerro Quema concession, Panamà. Unpublished report, 36 pp.

Huston, L. D., 2000, Gold in volcanic-hosted massive sulfide deposits; distribution, genesis and exploration: Reviews in Economic Geology, v. 13, p. 401-426.

Kesler, S. E., Sutter, J. F., Issigonis, M. J., Jones, L. M., and Walker, R. L., 1977, Evolution of porphyry copper mineralization in an oceanic island arc; Panama: Economic Geology, v. 72, p. 1142-1153.

Kouzmanov, K., Moritz, R., von Quadt, A., Chiaradia, M., Peytcheva, I., Fontignie, D., Ramboz, C., and Bogdanov, K., 2009, Late Cretaceous porphyry Cu and epithermal Cu-Au association in the Southern Panagyurishte District, Bulgaria: the paired Vlaykov Vruh and Elshitsa deposits: Mineralium Deposita, v. 44, p. 611-646.

Leach, T. M., 1992, Petrological Evaluation of the High Sulphidation Systems in the La Pava and Cerro Quema Prospect Areas, Panama, for Cyprus Gold Company. Unpublished report, 55 pp.

Muntean, J. L., and Einaudi, M. T., 2001, Porphyry-Epithermal Transition: Maricunga Belt, Northern Chile: Economic Geology, v. 96, p. 743-772.

Nelson, C. E., 1995, Porphyry copper deposits of southern Central America: Arizona Geological Society Digest, v. 20, p. 553-565.

Nelson, C. E., 2007, Metallic mineral resources, *in* Bundschuh., J and Alvarado., G., Eds., Central America, Geology, Resources and Hazards. V. 1, p. 885-915.

Nelson, C. E., and Nietzen, F., 2000, Metalogenia del oro y cobre en américa central: Revista Geológica de América Central., v. 23, p. 25-41.

Poulsen, K. H., and Hannington, M. D., 1996, Volcanic-associated massive sulphide gold: In: Eckstrand R. O., Sinclair, W. D., Thorpe, R. I., (Eds.). Geology of Canadian Mineral Deposit Types: Gological Society of America. Geology of Canada, v. 8, p. 183-196.

Poulsen, K. H., Robert, F., and Dubé, B., 2000, Geological classification of Canadian gold deposits: Geological Surveo of Canada Bulletin p. 106.

Puritch, E. J., Sutcliffe, R. H., Wu, Y., Armstrong, T., and Yassa, A., 2012, Technical report and mineral resource estimate on the Cerro Quema Project, Los Santos province, Panama, Prepared for Preshimco Resources Inc., by P&E Mining Consultants Inc., 123 pp.

Robert, F., 2004, Geologic footprints of gold systems: In: Muhling, J., Goldfarb, R., Vielreicher, N., Bierlein, F., Stumpfl, E., groves, D. I., Kenworthy, S. (Eds.). SEG 2004 - Predictive Mineral Discovery Under cover: Extended Abstracts Volume. Centre for global metallogeny, The University of Western Australia., v. 33, p. 97-101.

Robert, F., Brommecker, R., Bourne, B. T., Dobak, P. J., McEwan, C., Rowe, R. R., and Zhou, X., 2007, Models and exploration methods for major gold deposit types: In: Milkereit, B. (Ed.), Proceedings of Exploration 07: Fifth Decennial International Conference on Mineral Exploration, v. 5. p. 691-711.

Sillitoe, R. H., 1973, The tops and bottoms of porphyry copper deposits: Economic Geology, v. 68, p. 799-815.

Sillitoe, R. H., 1995, The influence of magmatic-hydrothermal models on exploration strategies for volcano-plutonic arcs: In: Thompson, J. F. H. (Ed.), Magmas, fluids and ore deposits, Mineralogical Association of Canada Short Courses, v. 23, p. 511-525.

Sillitoe, R. H., and Bonham, H. F., 1984, Volcanic landforms and ore deposits: Economic Geology, v. 79, p. 1286-1298.

Sillitoe, R. H., Hannington, M. D., and Thompson, J. F. H., 1996, High sulfidation deposits in the volcanogenic massive sulfide environment: Economic Geology, v. 91, p. 204-212.

Torrey, C., and Keenan, J., 1994, Cerro Quema Project, Panama, Prospecting in tropical and arid terrains: Toronto, Ontario, Canada. Unpublished report, 23 pp.

Valiant, W. W., Collins, S. E., and Krutzelmann, H., 2011, Technical report on the Cerro Quema Project, Panama., Prepared for Preshimco Resources Inc., by Scott Wilson Roscoe Postle Associates Inc., 109 pp.

Wegner, W., Worner, G., Harmon, R. S., and Jicha, B. R., 2011, Magmatic history and evolution of the Central American Land Bridge in Panama since Cretaceous times: Geological Society of America Bulletin, v. 123, p. 703-724.

White, N. C., 1991, High sulfidation epithermal gold deposits; characteristics and a model for their origin: Chishitsu Chosajo Hokoku = Report - Geological Survey of Japan, p. 9-20.

Wörner, G., Harmon, R. S., and Wegner, W., 2009, Geochemical evolution of igneous rocks and changing magma sources during the formation and closure of the Central American land bridge of Panama: Backbone of the Americas: Shallow Subduction, Plateau Uplift, and Ridge Terrane Collision, Geological Society of America Memoir 204, p. 183-196.

CHAPTER

2

Tectonostratigraphy and Geochemistry of the Azuero Peninsula and the Río Quema Formation

2.1. Introduction

Central America is a region with important mineral resources where precious metals such as Au and Ag, and Cu are currently attracting the interest of mining companies. A significant portion of their investment is focused on gold-bearing epithermal vein deposits (e.g. alavera, Bonanza and La Libertad, Nicaragua; Marlín, Guatemala), on porphyry copper deposits (e.g. Petaquilla and Cerro Colorado, Panama) and on base metal skarn and replacement deposits (e.g. Mochito, Honduras) (Nelson, 2007). Compared to other Central America countries such as Honduras, Guatemala, Belize, Costa Rica and Nicaragua, our knowledge of the geology and metallogeny of Panama is still limited.

In Panama first geological studies were carried out in 1965 by the United Nations Development Program (UNDP), with the main objective of evaluating Panama's mineral resource potential. Areas with important copper and gold anomalies were found, especially in the Azuero Peninsula (Fig. 2.1). Later studies of Del Giudice and Recchi (1969), Frencic (1970, 1971) and Kesler *et al*. (1977), related the copper and gold anomalies to porphyry copper and epithermal deposits, respectively. In 1988, the Cerro Quema deposit, a potentially mineable Au-Cu target, was discovered in the Azuero Peninsula. In the same region several little epithermal deposits were found (e.g., Juan Diaz, Pitaloza, Las Minas, Cerro Viejo, see Fig. 2.2), becoming the Azuero Peninsula in a high gold potential region. After those discoveries, some geologic studies were centered in the Cerro Quema deposit, the most promising gold project of the region (e.g., Leach, 1992; Horlacher and Lehmann, 1993; Torrey and Keenan, 1994). Nowadays estimated gold resources are 7.23 Mt with an average gold grade of 1.10 g/T (Valiant *et al*., 2011; Puritch, *et al*., 2012).

Unraveling the geologic evolution of the mining area is the first step towards understanding the processes responsible for mineralization and associated hydrothermal alteration. The Azuero Peninsula provides a unique opportunity to study an intra-oceanic arc evolution. Exposures of arc basement rocks and arc related volcanic, intrusives and sediments, provides an exceptional setting to unraveling the geochemical and geodynamic evolution of this type of volcanic arc. In order to achieve this objective, a regional study in the Azuero Peninsula with special emphasis in the Cerro Quema area was carried out. Moreover, fieldwork was complemented with geochemical analyses (major, trace element and REE) of local and regional rocks.

In this study we present an overview of the main tectonostratigraphic units of the Azuero Peninsula, which is supported by our field-based evidences and geochemical data. Moreover, we define a new lithostratigraphic unit, the Río Quema Formation, which hosts the Cerro Quema deposit. The characterization of this unit allows us to constrain the geodynamic and geochemical evolution of the Azuero Peninsula and its relationship with the Cerro Quema deposit.

2.2. Geologic setting

The Azuero Peninsula consists of volcanic, plutonic, sedimentary and volcano-sedimentary rocks ranging in age from ~71Ma to ~40Ma (Del Giudice and Recchi, 1969; Bourgois *et al*., 1982; Kolarsky *et al*., 1995; Lissinna *et al.,* 2002, 2006; Wörner *et al.,* 2005, 2006, 2009; Buchs *et al*., 2009, 2010; Wegner *et al.,* 2011). The main tectonic structures in the Azureo Peninsula are several regional subvertical faults delimiting variously uplifted blocks (Fig. 2.1B), such as the Soná-Azuero fault zone which strikes NW-SE or the Ocú-Parita (Kolarsky *et al*., 1995) and the Río Joaquín fault zones (Buchs, 2008) with broad E-W orientation.

Panama is situated in the southern part of Central America and represents the youngest segment of the land bridge between the North and South American plates. It is considered to be a tectonic block that lies at the junction of four tectonic plates, namely the Caribbean, South American, Cocos, and Nazca plates (Fig. 2.1). The Panama microplate is considered to be part of the Caribbean plate but new GPS data indicates a decoupling motion and relative convergence between Panama and the Caribbean plate (Trenkamp *et al*., 2002). The northern boundary of the Panama microplate is defined by a system of thrust and transform faults known as the North Panama Deformed Belt (Adamek *et al*., 1988; Silver *et al*., 1990). Towards the West, these faults shift to the diffuse thrust belt of the Cordillera Central of Costa Rica (Marshall *et al*., 2003; Denyer and Alvarado, 2007).

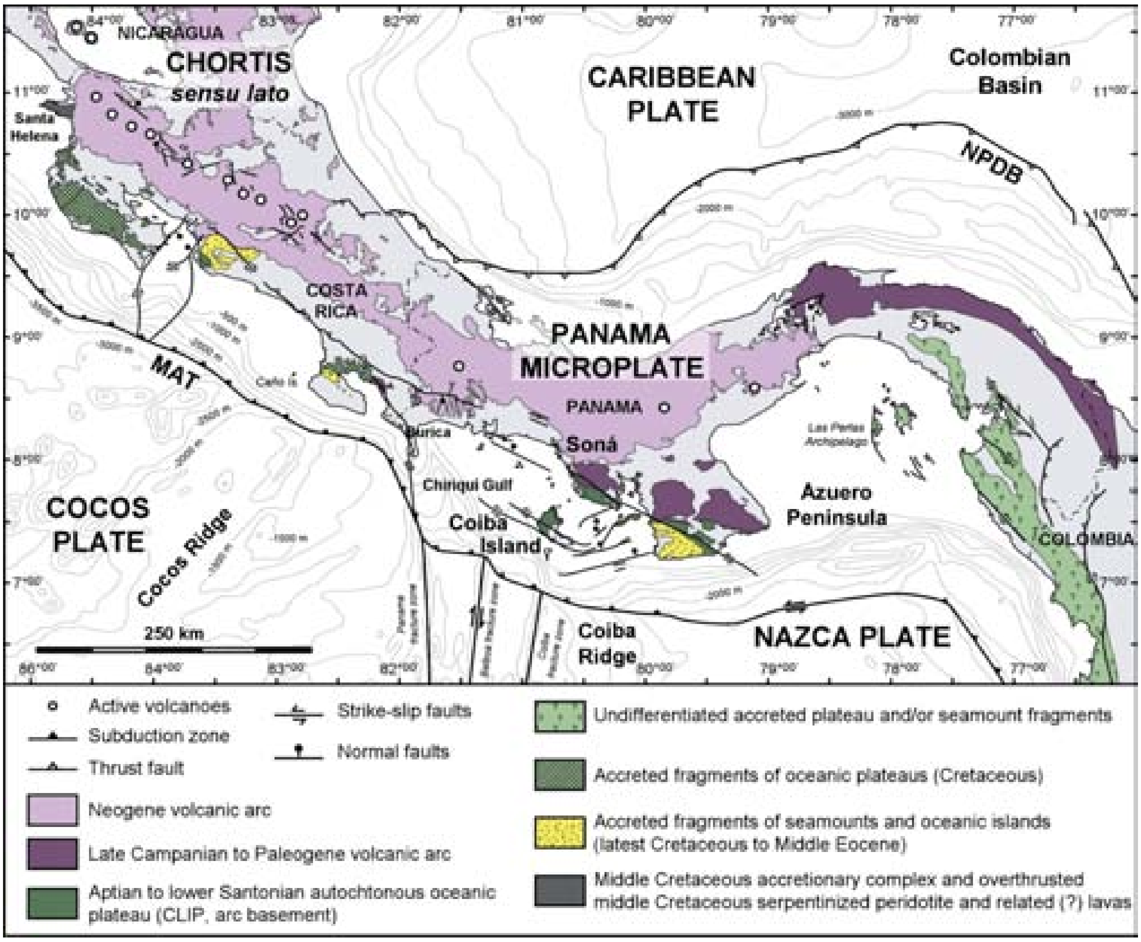

Figure 2.1: A) Present-day tectonic setting of South Central America (after Buchs *et al*., 2010; Duque-Caro, 1990; de Boer *et al*., 1995; Kellogg *et al*., 1995; Mann and Kolarsky, 1995; Harmon, 2005). Bathimetry based on Smith and Sandwell (1997). Quaternary faults from Cowan *et al*. (1998), Montero *et al*. (1998) and Paris *et al*., (2000). NPDB: North Panama Deformed Belt, MAT: Mid American Trench.

The eastern boundary with the South American continental plate is located along the dextral shear zone of the Atrato Valley (Taboada *et al*., 2000; Trenkamp *et al*., 2002). The southern edge is characterized by the subduction of the Nazca and Cocos oceanic plates beneath the Panama microplate. The initiation of the intra-oceanic subduction and the evolution of the magmatic island arc on the Azuero Peninsula is dated as Late Cretaceous and continued until Middle Miocene time (Buchs *et al*., 2009, 2010; Wörner *et al*., 2009).

Compression along the southern border of the Panama microplate controlled the formation of the South Panama Deformed Belt. Deformation is mainly accommodated by bending of the arc and sinistral NW-SE strike-slip faults (Mann and Corrigan, 1990; Coates *et al*., 2004).

The morphology of the subducting oceanic plates along the Central American Isthmus has a strong influence on the tectonics of the overriding plate and the suprasubduction magmatic processes. Subduction of relatively buoyant plates with irregular topographic highs (e.g. aseismic ridges and/or oceanic islands) causes the uplift and exposure of the fore-arc area along its margin (Fisher *et al*., 1998; Gardner *et al*., 2001; Sak *et al*., 2004). Such exposures provide the opportunity to study deep sections of the inner and outer fore-arc margin, which is composed of a complicated arrangement of arc-related volcanic rocks, accreted material and overlapped sequences (Buchs, 2008).

The Azuero Peninsula forms a pronounced prominence in the western Pacific coastline of Panama (Fig. 2.2). Its present configuration results from crustal mobility driven by escape tectonics and coastwise transport of fore-arc units (Krawinkel and Seyfried, 1994). The first regional mapping and stratigraphy definition was made through a joint program of the United Nations Development Program and the Dirección General de Recursos Minerales, 1976 (Del Giudice and Recchi, 1969; Metti *et al*., 1972; Metti and Recchi, 1976; Recchi and Miranda, 1977). The results of this work have been expanded upon in more recent contributions (Escalante, 1990; Krawinkel and Seyfried, 1994; Kolarsky and Mann, 1995; Kolarsky *et al*., 1995; Di Marco *et al*., 1995; Buchs, 2008; Buchs *et al*., 2009, 2010; Corral, 2008).

The basement of the Azuero Peninsula mainly consists of massive and pillowed basalt rocks with characteristic flat chondritic REE patterns which have been interpreted as tholeiitic basalts with plateau affinity (Hoernle *et al*., 2002, 2004; Hoernle and Hauff, 2007). Similar rocks have been identified in central and eastern Panama (i.e. Chagres and Darien regions) and along the Pacific onshore of Costa Rica (i.e Nicoya, Burrica and Osa Peninsula) and are interpreted as the western margin of the Caribbean large igneous province (Di

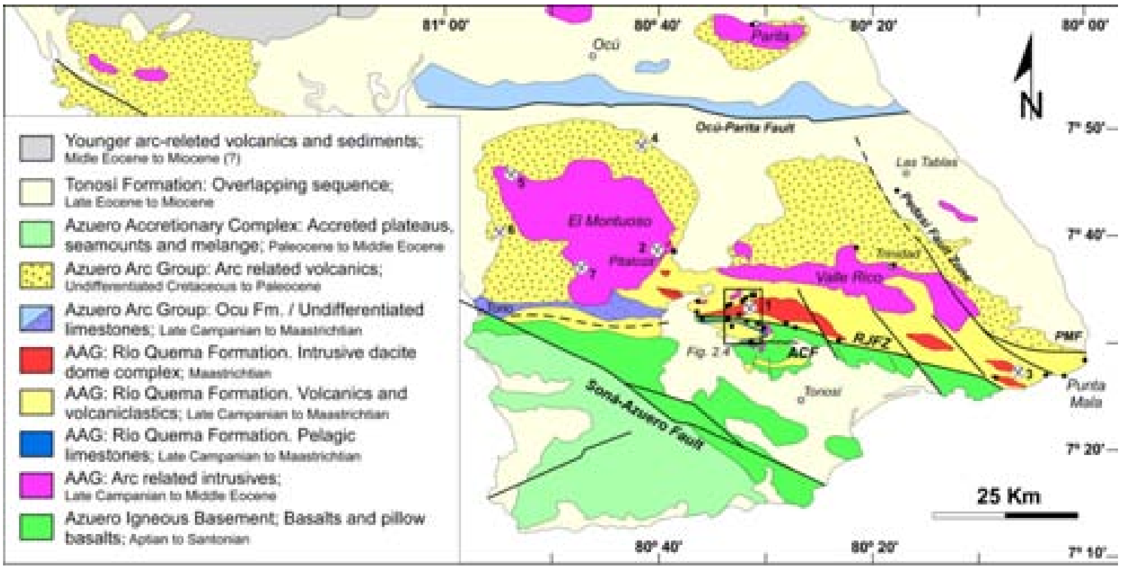

Figure 2.2: Simplified geological map of the Azuero Peninsula. AAG: Azuero Arc Group, RJFZ: Río Joaquín Fault Zone, ACF: Agua Clara Fault, PMF: Punta Mala Fault (After Dirección General de Recursos Minerales, 1976; Buchs *et al.*, 2010). Black dots correspond to analyzed samples in this study. Mineral deposits: 1) Cerro Quema, 2) Pitaloza, 3) Juan Díaz, 4) Las Minas, 5) Quebrada Barro, 6) Quebrada Iguana, 7) Cerro Viejo.

Marco *et al.*, 1995; Sinton *et al.*, 1997; Hauff *et al.*, 2000; Hoernle *et al.*, 2002, 2004). Radiometric and paleontological ages range from 139 to 69 Ma (Bourgois *et al.*, 1982; Kolarsky *et al.*, 1995; Kerr *et al.*, 1997; Sinton *et al.*, 1997, 1998; Revillon *et al.*, 2000; Hauff *et al.*, 2000; Hoernle *et al.*, 2002, 2004; Lissinna, 2005; Buchs *et al.*, 2009, 2010). Although these rocks were interpreted initially as accreted oceanic terranes by Goossens *et al.* (1977), the current accepted interpretation is that they represent uplifted portions of the western margin of the Caribbean plate (Hauff *et al.*, 2000; Hoernle *et al.*, 2002, 2004).

In spite of the abundance of radiometric studies of the igneous rocks of the area (e.g. Del Giudice and Recchi, 1969; Lissinna, 2005), the age of the onset of subduction and the development of the volcanic arc remains a matter of debate. Proposed ages of arc initiation range between 88Ma (Lissinna *et al.*, 2006) to 66Ma (Hoernle *et al.*, 2002; Wörner *et al.*, 2006). Recently, intermediate ages between both extremes have been proposed, (69-71Ma by Wenger *et al.*, 2011; 84-71Ma by Pindell and Kenan, 2009). Buchs *et al.* (2010) reported unusual geochemical compositions for basaltic lava flows and dikes emplaced in the Azuero basement with intermediate signatures, ranging from typical oceanic plateau to intraoceanic island arc. These authors defined these rocks as the Azuero Proto-arc Group (APAG) and interpreted them to have developed from early magmatism produced during the onset of subduction at 73-75 Ma. These rocks are equivalent to some of those described by Wörner *et al*. (2009) and Wenger *et al*. (2011) as Caribbean Large Igneous Province (CLIP oceanic basement) of the Sona-Azuero Arc. These observations suggest a possible overlap in ages between plateau and arc magmatism during early stages of subduction. Here we group all this rocks in the tectonostratigraphic unit of the Azuero Primitive Volcanic Arc (APVA).

After de initiation of subduction, an arc-magmatism was developed on top of the Azuero Igneous Basement and the Azuero Primitive Volcanic Arc rocks, corresponding to The Azuero Arc Group (Buchs *et al*., 2010). This group is composed of an arc-related sequence of volcanic rocks and associated tuffites and volcaniclastic rocks. The Azuero Arc Group crops out mainly in the Azuero Peninsula, however to the West, in the Soná Peninsula is found the lateral continuation of this volcanic arc (see Fig. 2.1 for location). Existing ages indicate that the arc is at least Maastrichtian (~71 Ma), and expands up to ~40 Ma (Del Giudice and Recchi, 1969; Maury *et al*., 1995; Lissinna, 2005; Lissinna *et al*., 2002, 2006; Wörner *et al*., 2005, 2006, 2009; Wegner *et al*., 2011). Maturation of magma sources during growth of the volcanic arc is not well understood, although radiometric ages suggest an overlap of basic and acid igneous rocks (Wörner *et al*., 2009; Buchs *et al*., 2010).

Cerro Quema is a high sulfidation epithermal Au-Cu deposit situated in the central part of the Azuero Peninsula (Fig. 2.2). It is composed by several mineralized ore bodies, named from West to East, La Pava, Cerro Quemita and Cerro Quema. The mining area is constituted by andesites, dacites, limestones, basalts and turbidites, developed in a fore-arc basin environment. These rocks expand from the West to the East of the Azuero peninsula (Fig. 2.2). First geological studies in the Azuero peninsula (Del Giudice and Recchi, 1969; Weyl, 1980) did not distinguish between the different stratigraphic units of this area, and named all these rocks Ocú Formation. They made this assignment because of the similarities between the limestones that occur in the Cerro

Quema area and the grayish-white micritic limestones that crop out in the northern part of the Azuero Peninsula (Ocú locality, Fig. 2.2). Based on microfossil biostratigraphy and field observations, Weyl (1980) proposed a Campanian-Maastrichtian age for these rocks. Later, Horlacher and Lehmann (1993), after field mapping of the area, distinguished two units: 1) the Ocú Formation that included all limestones and volcanosedimentary rocks, and 2) the Quema Formation, that was restricted to dacites and massive andesites.

2.3. Stratigraphy

The Ocú Formation was initially described as well bedded fine-grained limestones with locally nterbedded siltstones, tuffs and intermediate lava flows, deposited on top of basaltic basement rocks (Del Giudice and Recchi, 1969). The assumed age for the Ocú Formation is late Campanian-Maastrichtian on the basis of the association of planktonic foraminifera (*Globotruncana Lapparenti, Globotruncana ventricosa* and *Globotruncana contusa*) as first noted by Del Giudice and Recchi (1969), Weyl (1980) and Bourgois *et al*. (1982). Later, Kolarsky *et al*. (1995) defined the Ocú Formation as thin to medium-bedded grayish-white limestone and calcareous siltstone, and light brown, fine grained calcareous siltstone and sandstone, mainly interbedded with basaltic rocks with 1,500m of apparent thickness. Del Giudice and Recchi (1969) and Weyl (1980) and other recent studies (Buchs, 2008; Buchs *et al*., 2010) describe interbedded basaltic lava flows within the Ocú Formation (e.g. Coiba Island) locally crosscut by basaltic dikes of the Azuero Primitive Volcanic Arc. The limestones of the Ocú Formation which show syn-volcanic soft deformation were dated by Buchs *et al*. (2010) as Late Campanian (~75-73 Ma) in agreement with two limestone samples from the Ocú type locality which gave a Campanian age.

The rocks in the Cerro Quema area neither correspond with the classical definition of the Ocú Formation nor have the same genetic implications. Therefore, the rocks cropping out in the study area need to be defined and reinterpreted as a new lithostratigraphic unit. Our data, together with the work of previous authors, allow us to propose a new formation, named hereafter the Río Quema Formation, consisting of volcanic and volcaniclastic sediments interbedded with hemipelagic limestones, submarine dacite lava domes and crosscut by basaltic to andesitic dikes. The Río Quema Formation belongs to the Azuero Arc Group and is interpreted as the infill sequence of the fore-arc basin of the Cretaceous–Paleogene volcanic arc and is integrated within the five major units of the Azuero Peninsula as follows: 1) Azuero Igneous Basement, 2) Azuero Primitive Volcanic Arc, 3) Río Quema Formation, 4) arc-related intrusive rocks, and 5) Tonosí Formation. The main characteristics of these units are described below and shown in Figure 2.3.

1) The Azuero Igneous Basement (Fig. 2.3A) is composed of massive, agglomerate and pillowed basaltic lavas, diabases, gabbros, minor occurrences of hemipelagic sediments and radiolarites interlayered with lavas, and basaltic dikes crosscutting all materials. Geochronological dating of the basalts indicates ages ranging from Turonian to Santonian (Lissinna, 2005) and is consistent with a Coniacian age obtained from interlayered radiolarian sediments (Kolarsky *et al*, 1995), recently revised by Buchs *et al*. (2009) who reported a Coniacian-Early Santonian age. Dikes of the Azuero Primitive Volcanic Arc crosscut the AIB at several sites of the Azuero Peninsula (e.g., Río Joaquín, Río Torio and in the Tonosí-Las Tablas Road; Buchs *et al*., 2010).

2) The Azuero Primitive Volcanic Arc locally overlies the Azuero Igneous Basement. In the Río Quema stratigraphical section it is composed of massive and pillowed basaltic lavas of irregular thickness (0-40m?) overlain by well bedded greenish shales, cherts and thin basaltic lava flows, and crosscut by basaltic dikes. These volcanic rocks were described in the Torio river by Buchs (2008) and Buchs *et al*. (2010) as basaltic trachyandesitic lava flows and dikes, locally interbedded with hemipelagic limestones of the Ocú Formation.

3) The Río Quema Formation includes all sedimentary, volcaniclastic and extrusive volcanic units deposited in a fore-arc basin, overlying both the Azuero Igneous Basement and locally the Azuero Primitive Volcanic Arc. The total thickness of the Río Quema Formation is approximately 1,700m. In the Quema river, some dikes of the APVA have been observed crosscutting the

volacanosedimentary sequence. The following units have been distinguished in the Cerro Quema district:

- A Lower Unit, made up of andesitic lava flows (0.20-2m thick) and well bedded crystal-rich sandstone to siltstone turbidites interbedded with hemipelagic thin limestone beds (Fig. 2.3B). W-SW paleocurrents were deduced from cross bedding, ripples and tool marks.

- A Limestone Unit, corresponding to a 100-150m thick light grey biomicritic hemipelagic limestone which is interlayered with well bedded cherts, thinly bedded turbidites and ash layers (Fig. 2.3C). The presence of planktonic foraminifera (*Globotruncana sp., Globotruncanita sp.,* and *Globotruncanella sp.*) indicates a Late Cretaceous age. The similarities with the foraminifera found in the limestones described by Del Giudice and Recchi (1969), Tournon *et al*. (1989), Di Marco *et al*. (1995) and Buchs *et al*. (2010) allow us to infer a late Campanian–early Maastrichtian age. Similar limestone beds have also been found in the Torio and Güera rivers, following the southernmost E-W trend fault zone of the Azuero Peninsula.

- An Upper Unit, which crops out both in the northern and southern part of the Río Quema section. The northern part is composed of volcaniclastic sediments interlayered with massive to laminar andesitic lava flows (1 to 3m thick), andesitic hyaloclastites (0.1 to 0.5m thick), and massive dacites overlain by dacite lava flows and dacitic and resedimented hyaloclastites (the latter up to 3m thick). However, in the southern part, this unit is characterized by volcaniclastic turbidites, crystal rich sandstones (up to 1m thick), siltstones and thin pelagic limestone beds (up to 0.2m). Whereas massive lava flows and extrusive rocks prevail in the northern part of the section, volcaniclastic turbidites are dominant in the southern region. W-SW paleocurrents are deduced from cross bedding. Basaltic-andesitic dikes intrude part of the series (Fig. 2.3D), but are more common in the northern part of the study area.

4) The arc-related intrusive unit is composed of diorites, quartz-diorites and granodiorites. They are exposed as large batholiths in the central and northern part of the Azuero Peninsula, although small quartz-diorite stocks and/or dikes

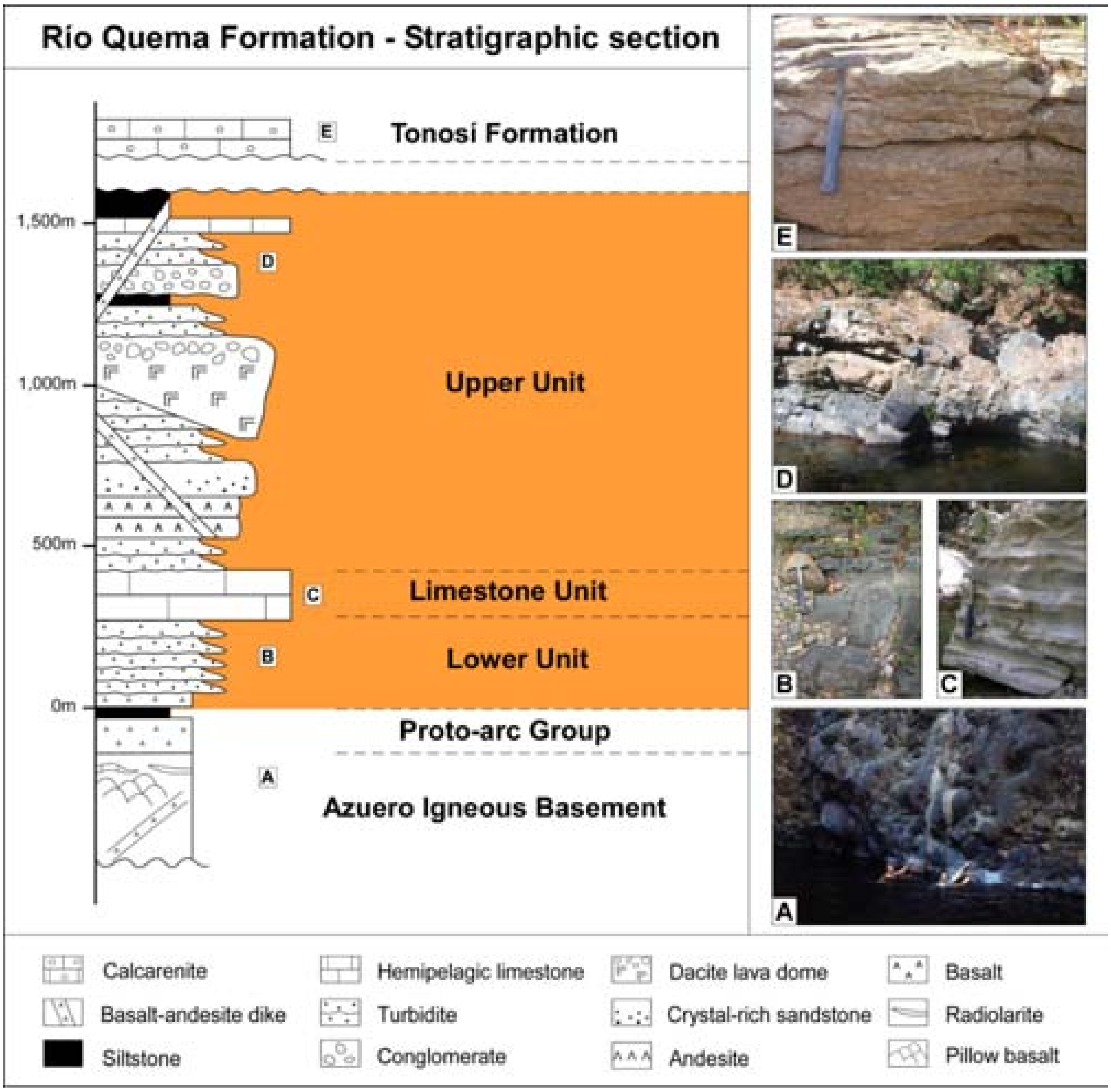

Figure 2.3: Idealized stratigraphic section of the Río Quema Formation. A) Pillow basalts of the Azuero Igneous Basement at Río Joaquín. B) volcaniclastic sediments of the Río Quema Formation lower unit at Río Quema. C) Hemipelagic limestones from the Río Quema Formation limestone unit, south of Río Quema. D) Volcaniclastic and hemipelagic sediments crosscut by a basaltic-andesitic dike of the Río Quema Formation upper unit, north of the Río Quema. E) Fossiliferous calcarenite of the Tonosí Formation at Río Güerita.

occur South of Cerro Quema. Ages of these igneous rocks range from 66 to 42 Ma (Maury *et al*., 1995; Lissinna, 2005; Wörner *et al*., 2009; Wenger *et al*., 2011).

5) The Tonosí Formation consists of a sedimentary sequence unconformably overlapping all of the previous units. Recchi and Miranda (1977) defined the Tonosí Fm. as conglomerates, reefal limestones and associated calcarenites of

Middle Eocene to Early Oligocene age, overlying the basaltic basement northeast of the Azuero-Soná fault zone. More recent studies (Kolarsky *et al*., 1995; Krawinkel and Seyfried, 1994) divided the formation into two major lithological units: 1) A lower unit composed of minor coal seams, conglomerate, coarse sandstone and reefal limestone, and 2) an upper unit composed of deeper marine interbedded sandstone, siltstone and calcarenite. The age of the Lower unit range from Middle Eocene to Early Oligocene (~40 to 30 Ma) whereas the age of the Upper unit range from Late Oligocene to Early Miocene (~30 to 15 Ma) (Kolarsky *et al*., 1995; Krawinkel and Seyfried, 1994; Krawinkel *et al*., 1999).

Our interpretation assumes that the Azuero Igneous Basement is equivalent to the Caribbean large igneous province described by Hauff *et al*. (2000), Hoernle *et al*. (2002, 2004), and represents the autochthonous basement of the Azuero Peninsula at the onset of subduction. At the initial stages of magmatism, a Primitive volcanic arc was developed locally on top of the Azuero Igneous Basement (Buchs *et al*., 2009, 2010). Simultaneously, the deposition of the Ocú Formation took place (this formation does not crop out in the study area). The Río Quema Formation is the expression of a fore-arc basin infill submarine sequence of a more mature volcanic arc. The Lower Unit, formed by andesitic lava flows, crystal-rich sandstones and turbidites interbedded with hemipelagic limestone beds, represents a proximal depositional environment with respect to the volcanic front. The Limestone Unit records a period of time with minor volcanic activity in which autochthonous sedimentation was dominant over volcanic sedimentation. The Upper Unit records both distal and proximal depositional environments due to the presence of submarine dacite lava domes which played a paleo-barrier role in terms of sedimentation. These dacite lava domes compartmentalized the fore-arc basin, producing changes in the sedimentation. The northern slope of the dacitic domes is mainly composed of massive volcanic rocks, minor turbidites, limestone layers and abundant basalticandesitic dikes, suggesting a proximal depositional environment with respect to the volcanic front. In contrast, the southern slope is characterized by a large fraction of volcaniclastic sediments, turbidites, shales and siltstones and by a minor presence of andesitic lava flows, suggesting a distal depositional environment whith respect to the volcanic front. The arc-related intrusive unit represents a period of time characterized by quartz-diorite and granodiorite intrusions. These intrusions are abundant to the North of the study area, but minor quartz-diorite batholiths are also present in the southern part. The intrusions produced contact metamorphism on the Río Quema Formation close to the batholiths (Tonosí – Las Tablas road). Finally, the sedimentary sequence of the Tonosí Formation represents a regional transgressive event that affected the Azuero Peninsula (Kolarsky *et al*., 1995; Krawinkel *et al*., 1999).

2.4. Structure

A large network of faults can be recognized in the area. Predominant faults trend NW-SE and NE-SW, show subvertical dip and normal sense of offset. A left-lateral strikeslip component has been observed along faults which trend NW-SE trend. Another main tectonic structure of the area is the Río Joaquín fault zone, a 30km regional scale fault zone with a broad E-W orientation (Fig. 2.4). It was originally identified by Buchs (2008) combining fieldwork and interpretation of satellite images. In the Cerro Quema area, our observations indicate that the Río Joaquín fault zone maintains the general E-W orientation and does not change to a NE-SW trend as proposed by Buchs (2008). A secondary fault, the Agua Clara Fault with a E-W orientation, parallel to the RJFZ is also observed near the mining area. Along the Río Joaquín fault, the Azuero igneous basement is directly in contact with the upper series of the Río Quema Formation (Fig. 2.4). A reverse dip-slip motion is observed at the Río Joaquín fault with the southern block uplifted with respect to the northern block. The inferred minimum vertical offset is 300-400m. Faulting caused a strong deformation, forming cataclasites and a network of tension gashes oblique to the fault.

In addition, ENE-WSW trending folds and minor faults parallel to E-W trending lithological boundaries have also been identified in the area. All these structures are slightly oblique to the Río Joaquín fault zone and are partly cut by it. The northern part of the area is characterized by abundant decametric open

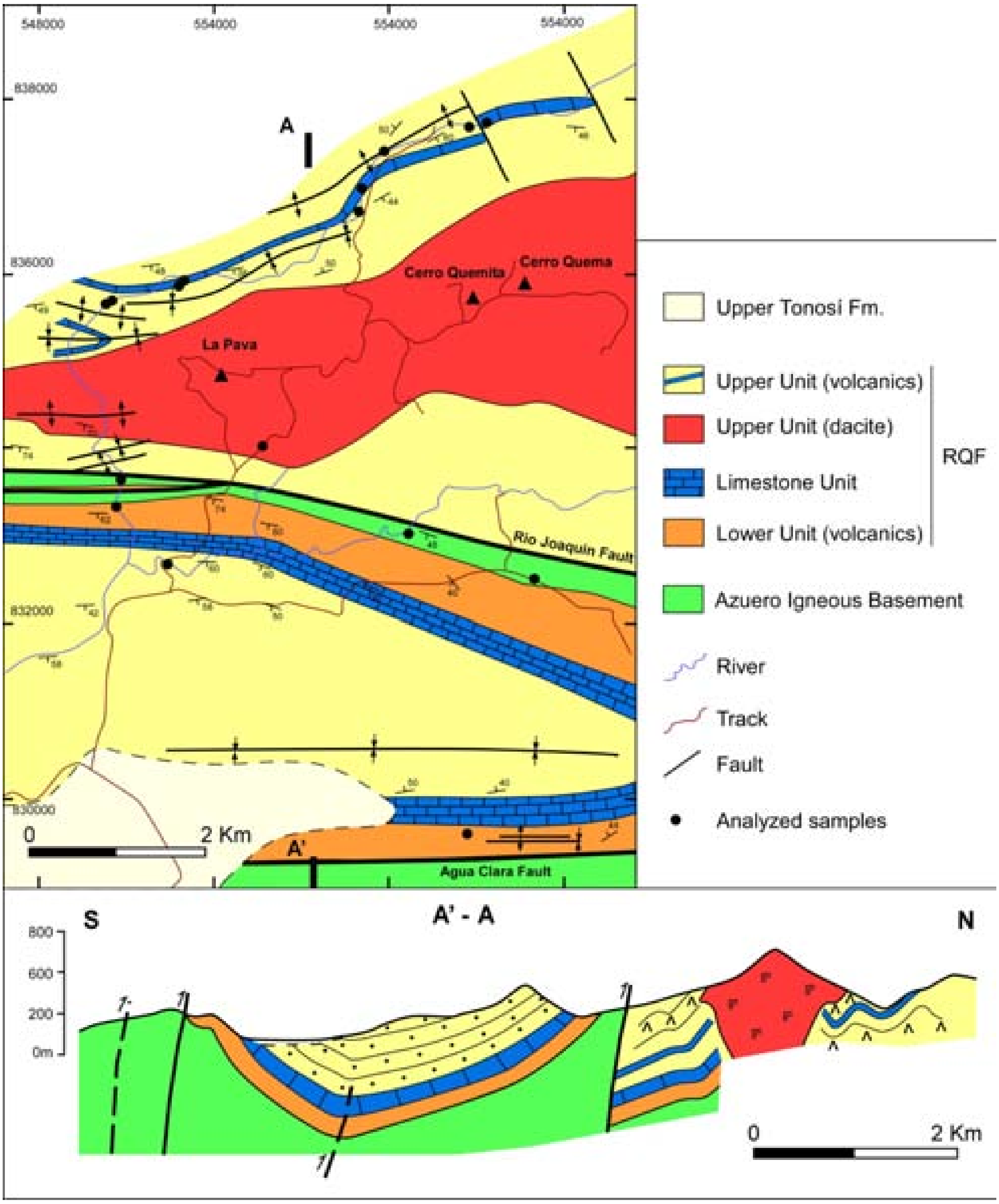

Figure 2.4: Geologic map and cross section of the Cerro Quema deposit and the structure and distribution of the Río Quema Formation and the Azuero igneous Basement.

folds with moderate limb dips and fold axes gently plunging to the SW. The southern area is characterized by a kilometerscale E-W trending syncline that affects the entire forearc basin (Fig. 2.4). All these structures are covered by the Tonosí Fm., which overlaps the Azuero Igneous Basement, the Río Quema Fm. and the arc-related intrusives.

2.5. Geochemistry

Whole rock analysis (major, trace and REE elements) was performed on 34 representative samples of unaltered igneous and rocks of the Central and SE Azuero Peninsula (Table 2.1), with special emphasis in the mining area. Samples were mainly collected in rivers and in tracks, however, some samples have been collected in the slope of the main roads. Sampling includes five samples from the Azuero Igneous Basement, six samples from the Azuero Primitive Volcanic Arc, and twenty three samples from the Azuero Arc Group (Río Quema Formation, Arc-related intrusives and Arc-related volcanic rocks), representing the entire arc sequence. Samples were cut, crushed and reduced to powder using a tungsten carbide mill. Analyses were carried out by Actlabs (Canada) using X-ray fluorescence (XRF) and inductively coupled plasma-mass spectrometry (ICP-MS). Results are presented in Table 2.2.

2.5.1. Chemistry of the Azuero Igneous Basement (AIB)

Analyzed volcanic rocks of the Azuero Igneous Basement are basaltic flows and pillow basalts which are found in the mining area and in the Macaracas-Tonosí Road. As shown in the Total Alkali-Silica (TAS; Fig. 2.5A) diagram, the rocks belong to the sub-alcaline series, and plot in the basalt field. This grup is also characterized by a high-Fe and low-K (tholeiitic) differentiation trend (Fig. 2.5B, 2.5C). In terms of incompatible elements, (Fig. 2.5D), AIB rocks display relatively high values of (Nb/La) and generally low values of (La/Sm). Trace element content (Fig. 2.6A and 2.6D) has a flat or slightly enriched pattern, typical of plateau-like affinities.

The Azuero Igneous Basemet rocks are in agreement, in terms of composition and chemical affinities, with those described by Buchs *et al* (2010) as Azuero Plateau Group I. However, two samples (LS-12 and RQ-102I), corresponding to basalt flows found in the Río Quema, present a more enriched trace element pattern (Fig. 2.6A and 2.6D). This samples correspond to the rocks of the Azuero Plateau Group II defined by Buchs *et al*., (2010), interpreted to reflect melting of an enriched source component.

Sample	Rock Type	Locallity	Coordinates (°WGS84) Latitude	Longitude	Unit
			Azuero Igneous Basement		
AN-02	Basalt	Finca AN	7.52955	-80.51127	Azuero Igneous Basement
CW-04	Basalt	Macaracas-Tonosi Road	7.55086	-80.60711	Azuero Igneous Basement
GUE-5Bis	Basalt	Macaracas-Tonosi Road	7.54121	-80.59680	Azuero Igneous Basement
LS-12	Basalt	Quebrada Quema	7.53530	-80.52937	Azuero Igneous Basement
RQ-102I	Basalt	Rio Quema	7.54167	-80.55694	Azuero Igneous Basement
			Azuero Primitive Volcanic Arc		
CE-1	Basalt	Las Tablas-Tonosi Road	7.73563	-80.29159	Azuero Primitive Volcanic Arc
DES-112	Basalt	Destiladeros Beach	7.45013	-80.03409	Azuero Primitive Volcanic Arc
RJ-11	Basaltic dike	Rio Joaquin	7.52555	-80.45427	Azuero Primitive Volcanic Arc
RJ-13B	Basalt	Rio Joaquin	7.53212	-80.46867	Azuero Primitive Volcanic Arc
RQ-09A	Basaltic dike	Rio Quema	7.56787	-80.53265	Azuero Primitive Volcanic Arc
RQ-26	Basaltic dike	Rio Quema	7.57840	-80.51868	Azuero Primitive Volcanic Arc
			Azuero Arc		
AC-04	Diorite	Agua Clara	7.50593	-80.52091	Azuero arc-related intrusives
AC-11	Diorite	Agua Clara	7.50593	-80.52091	Azuero arc-related intrusives
AN-04	Trachyandesite	Finca AN	7.52417	-80.50457	Azuero arc-related intrusives
CE-3B	Andesite	Las Tablas-Tonosi Road	7.64964	-80.35556	Azuero Arc
CE-11	Basalt	Las Tablas-Tonosi Road	7.50663	-80.38614	Rio Quema Formation
CW-02	Qz-diorite	Macaracas-Tonosi Road	7.56901	-80.60845	Azuero arc-related intrusives
DES-03	Andesite	Destiladeros Beach	7.45147	-80.05903	Rio Quema Formation
LI-01	Andesite	Limón	8.05753	-80.77187	Azuero Arc
LP-111	Andesite	Rio Quema	7.53256	-80.55244	Rio Quema Formation
LP-204	Dacite	La Pava ore body	7.54497	-80.54238	Rio Quema Formation
PA-01	Diorite	Parita	7.99420	-80.52715	Azuero arc-related intrusives
PIT-02	Qz-diorite	Pitaloza	7.64392	-80.64646	Azuero arc-related intrusives
PLA-06	Dacite	Tonosi-Pedasi Road	7.44627	-80.14053	Rio Quema Formation
PM-01	Qz-diorite dike	Punta Mala	7.47301	-80.00174	Azuero arc-related intrusives
RQ-03	Basalt-andesite dike	Rio Quema	7.57547	-80.52980	Rio Quema Formation
RQ-07	Andesite	Rio Quema	7.57075	-80.53175	Rio Quema Formation
RQ-11	Basaltic dike	Rio Quema	7.56283	-80.54958	Rio Quema Formation
RQ-12	Andesite dike	Rio Quema	7.56195	-80.55050	Rio Quema Formation
RQ-13	Basaltic dike	Rio Quema	7.56063	-80.55647	Rio Quema Formation
RQ-15 And	Andesite	Rio Quema	7.56003	-80.55763	Rio Quema Formation
RQ-24	Andesite dike	Rio Quema	7.57837	-80.52027	Rio Quema Formation
RQ-M	Andesite	Rio Quema	7.53847	-80.55772	Rio Quema Formation
TRI-01	Qz-diorite	Trinidad	7.62080	-80.30061	Azuero arc-related intrusives

Table 2.1: Localization of analyzed igneous samples of the Azuero Peninsula

2.5.2. Chemistry of the Azuero Primitive Volcanic Arc (APVA)

Igneous rocks of the Azuero Primitive Volcanic Arc consist of basalt to basaltic andesitic lava flows, pillows and dikes. In the TAS diagram (Fig. 2.5A) these rocks plot in the field of basalts and basaltic andesites of the sub-alkaline series. The APVA defines a hig-Fe and low-K differentiation trend which indicates a tholeiitic character (Fig. 2.5B, 2.5C). This trend is quite similar to the previously described AIB. As shown in Figure 2.5D, in terms of incompatible elements, the APVA is slightly dissimilar to the AIB, having lower values of (Nb/La) for approximately the same values of (La/Sm). Trace elements patterns (Fig. 2.6B and 2.6E) are slightly different in comparison with the AIB rocks.

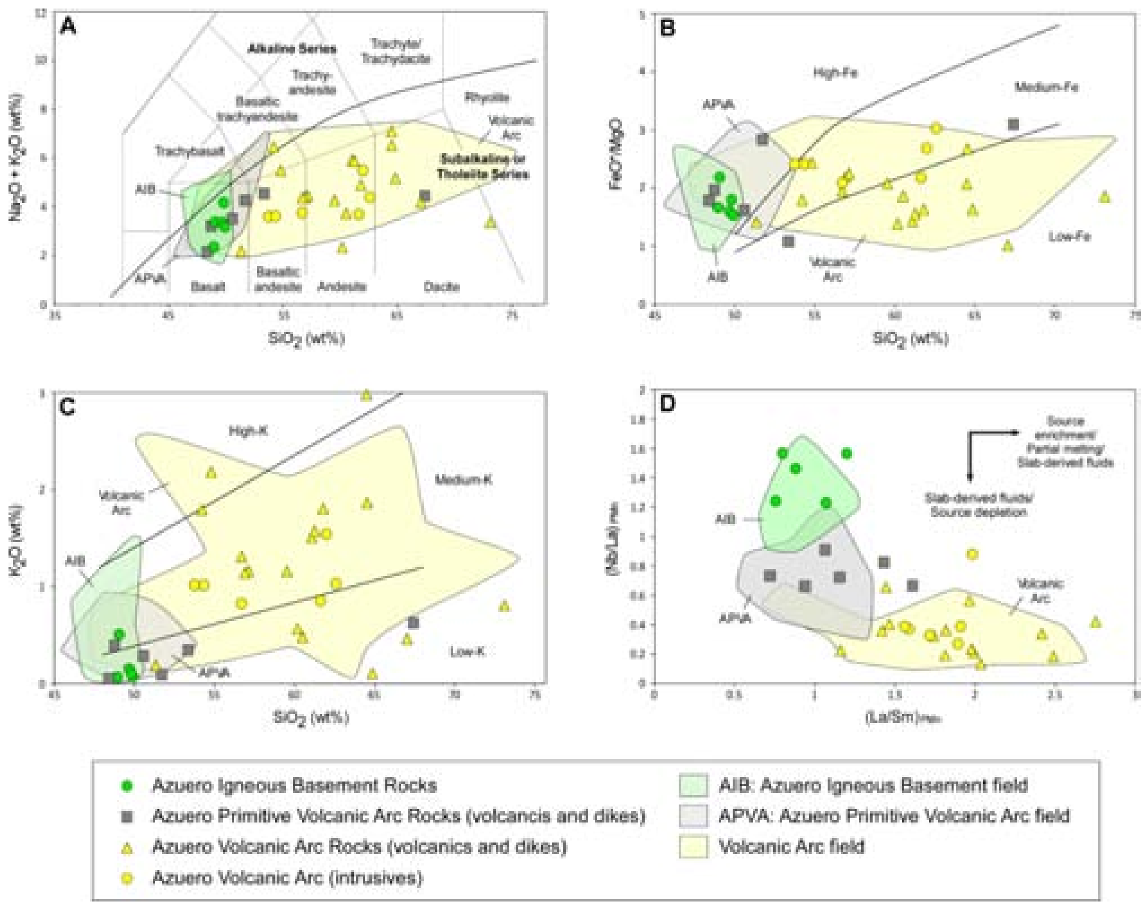

Figure 2.5: Geochemical characteristics of the igneous rocks of the Azuero Peninsula and the Río Quema Formation in comparison with rocks of Lissinna (2005), Wörner *et al*, (2009), Wenger *et al*, (2011) and Buchs *et al*, (2010) with AIB affinity, APVA affinity and Volcanic Arc affinity. A) Chemical composition of igneous rocks in the Total Alkali-Silica (TAS) diagram (Le Maitre *et al*., 1989). B) FeO*-SiO_2 diagram (Arculus, 2003). C) K_2O-SiO_2 diagram (Le Maitre *et al*., 1989). D) Plot of (La/Sm) PMn vs (Nb/La) PMn. Primitive mantle after McDonough and Sun (1995).

In the Primitive Mantle normalized diagrams the APVA rocks display a flat pattern with enrichment in Ba, and contrary to the AIB, depletion in Nb and Ti, whereas in the Chondrite normalized diagrams, APVA rocks display a flat pattern, sometimes difficult to distinguish from the AIB.

Samples of our APVA are similar to the rocks defined by Buchs *et al*, (2010) as Protoarc group and some of the samples defined by Wörner *et al*, (2009) and Wenger *et al*, (2011) as CLIP oceanic basement (Fig. 2.6B and 2.6E). Three of the APVA rocks correspond to basaltic flows and pillow basalts (DES-112, CE-1 and RJ-13B) whereas the rest, correspond to basaltic dikes. Those dikes are found crosscutting AIB rocks (RJ-11), as noted by Buchs *et al*, (2010). However

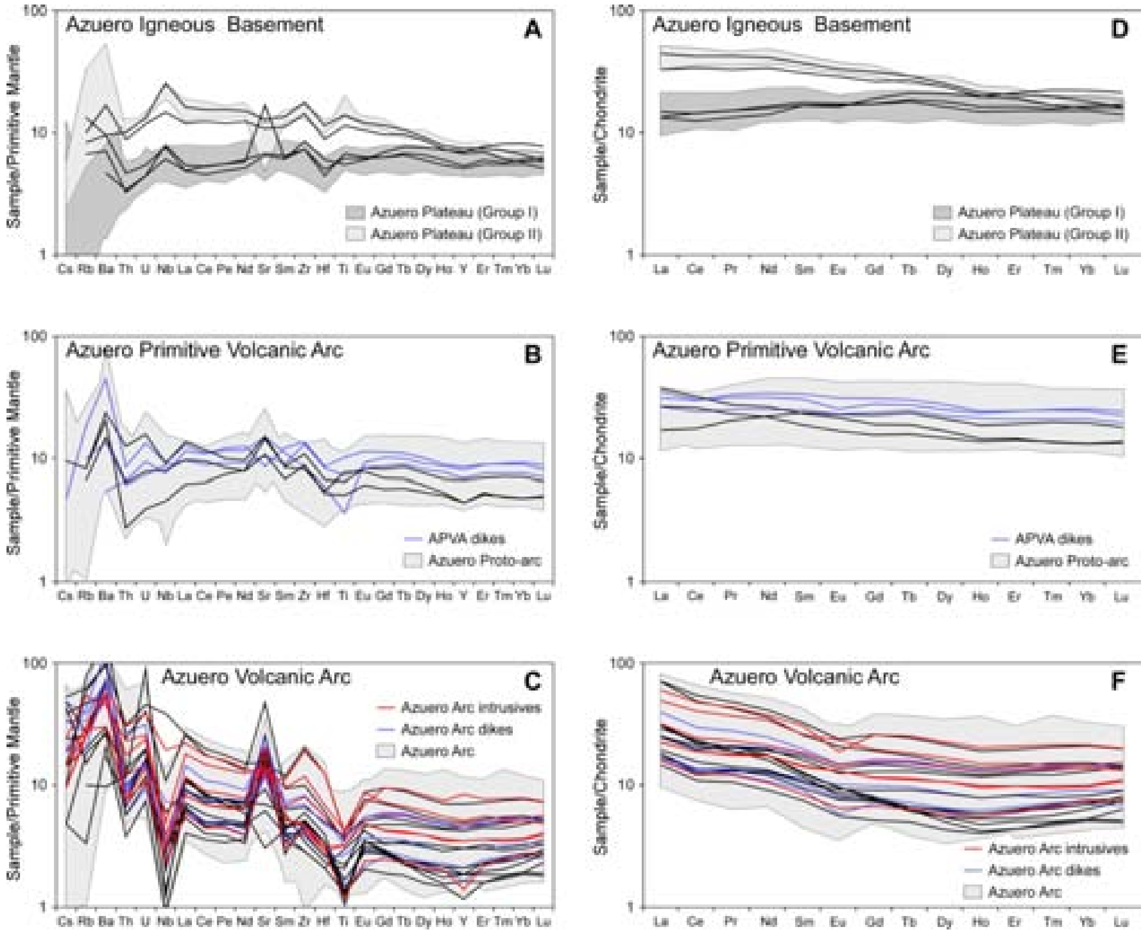

Figure 2.6: Primitive mantle-normalized multielement diagrams (A, B, C) and Chondrite-normalized REE diagrams (D, E, F). Primitive mantle and Chondrite abundances from McDonough and Sun (1995). Azuero Plateau (Group I and Group II) after Buchs *et al*, (2010). Azuero Proto-arc after Buchs *et al*, (2010) and some of the CLIP Oceanic Basement of Wörner *et al*., (2009) and Wenger *et al*., (2011). Azuero Arc after Buchs *et al*., (2010), Paleocene-Early Eocene Arc rocks from Lissinna (2005), Early Arc rocks from Wörner *et al*., (2009) and Sona-Azuero Arc rocks from Wenger *et al*., (2011).

the new contribution is the discovery of some APVA dikes (RQ-9A and RQ-26) crosscutting the Río Quema Formation, a calc-alkaline volcanic arc sequence.

2.5.3. Chemistry of the Azuero Arc Group and the Río Quema Formation

The Azuero Arc Group includes a series of volcanic, volcanosedimentary, sedimentary and plutonic rocks corresponding to the Río Quema Formation, arc-related intrusives and undifferentiated arc rocks. Those rocks belong to the sub-alkaline series, spanning all the compositional range from basalt to dacite

		Major Elements (wt%)												Trace Elements (ppm)							
Sample	Rock Type	SiO_2	TiO_2	Al_2O_3	Fe_2O_3	MnO	MgO	CaO	Na_2O	K_2O	P_2O_5	LOI	Total	Sc	V	Co	Cr	Ni	Zn	Rb	Sr
Azuero Igneous Basement																					
AN-02	Basalt	47.87	1.09	13.34	13.50	0.17	7.51	7.07	3.91	0.10	0.09	3.82	98.49	44.4	378	47.5	96.8	56	53	5	130
CW-04	Basalt	48.58	1.35	14.05	12.27	0.19	7.38	12.32	2.25	0.07	0.11	0.74	99.31	50.2	366	64.1	205	95	72		135
GUE-5Bis	Basalt	48.70	1.25	13.81	12.02	0.19	7.84	10.89	3.03	0.07	0.08	2.43	100.30	47.9	343	58.2	241	111	71	4	334
LS-12	Basalt	48.33	2.81	14.06	11.54	0.18	7.21	10.23	3.12	0.15	0.23	2.70	100.50	41.6	448	42.2	173	76	80	8	257
RQ-102I	Basalt	48.17	2.32	14.30	14.07	0.23	6.43	10.10	2.83	0.50	0.19	1.79	101.00	40.0	389	55.9	159	77	84	6	216
Azuero Primitive Volcanic Arc																					
CE-1	Basalt	47.90	1.57	16.88	12.18	0.19	6.19	10.43	2.78	0.39	0.18	1.75	100.50	41.0	440	54.2	47.2	38	74	5	301
DES-112	Basalt	49.09	1.03	14.71	8.88	0.15	8.27	6.11	3.86	0.32	0.16	8.03	100.60	33.8	249	36.6	274	130	53	4	214
RJ-11	Basaltic dike	50.33	2.05	14.18	12.82	0.19	4.53	8.74	4.06	0.09	0.29	2.66	99.95	40.1	390	39.5	32.1	17	84		172
RJ-13B	Basalt	49.09	1.32	16.53	9.63	0.16	5.96	11.59	3.11	0.28	0.14	2.93	100.70	38.3	252	46.2	107	42	62	5	287
RQ-09A	Basaltic dike	64.56	0.74	14.37	5.79	0.15	1.87	4.31	3.65	0.60	0.32	4.24	100.60	23.5	56	16.2			79	11	298
RQ-26	Basaltic dike	45.86	1.48	14.82	11.46	0.16	6.42	12.66	1.99	0.05	0.16	5.24	100.30	48.3	325	49.9	186	57	71	6	207
Azuero Arc																					
AC-04	Diorite	52.88	0.65	16.63	11.27	0.20	4.68	8.01	2.54	0.99	0.25	2.70	100.80	36.9	313	49.8	26.2	23	89	15	404
AC-11	Diorite	52.24	0.64	16.04	10.97	0.19	4.55	7.89	2.52	0.99	0.25	2.76	99.03	37.2	309	50.1	27.1	23	86	16	387
AN-04	Trachyandesite	53.48	0.69	16.76	8.24	0.17	3.40	7.87	3.20	2.13	0.32	2.36	98.61	24.0	207	18.3	34.2	16	117	47	938
CE-3B	Andesite	50.43	0.61	18.67	9.00	0.16	6.39	11.42	1.94	0.19	0.07	1.77	100.60	41.2	280	44.8	67.5	33	53	2	283
CE-11	Basalt	60.66	0.45	12.80	5.13	0.10	3.16	6.79	4.70	0.10	0.09	6.50	100.50	20.1	134	19.0	27	14	56		122
CW-02	Qz-diorite	58.07	0.26	15.37	8.74	0.15	4.22	6.56	3.00	1.13	0.09	2.44	100.00	38.7	281	36.8	26.1	10	56	16	502
DES-03	Andesite	63.41	0.27	12.89	5.45	0.16	5.41	3.56	3.47	0.44	0.07	5.43	100.60	24.9	149	37.8	91	21	82	6	61
LI-01	Andesite	62.92	0.79	15.74	5.41	0.13	2.03	3.52	4.49	1.82	0.24	2.47	99.56	18.0	96		12.3	5	68	37	304
LP-111	Andesite	56.15	0.26	12.57	7.85	0.15	5.71	7.11	1.62	0.53	0.06	6.59	98.59	35.3	267	27.1	208	24	61	11	370
LP-204	Dacite	62.90	0.22	13.61	7.33	0.13	3.55	3.56	3.99	2.91	0.07	2.47	100.70	30.8	210	19.9	113	18	58	35	506
PA-01	Diorite	61.23	0.81	15.32	6.33	0.11	2.09	6.00	3.29	1.01	0.13	2.12	98.43	18.6	133	48.6	10.9	9	60	18	231
PIT-02	Qz-diorite	60.36	0.24	15.31	7.24	0.08	3.32	6.49	2.78	0.84	0.07	2.01	98.75	29.2	216	68.6	20.3	13	46	17	296
PLA-06	Dacite	57.45	0.25	12.70	6.93	0.09	4.27	6.39	2.86	1.68	0.09	7.00	99.71	30.0	177	27.5	150	33	47	28	184
PM-01	Qz-diorite dike	61.48	0.85	15.24	8.21	0.13	3.06	5.23	3.93	1.53	0.20	0.81	100.70	24.4	185	39.4	51.3	19	73	32	283
RQ-03	Basalt-andesite dike	51.67	0.54	18.34	8.80	0.17	4.93	4.65	4.43	1.71	0.07	4.68	99.98	33.1	323	37.2	27.1	19	72	20	369
RQ-07	Andesite	55.32	0.77	15.08	10.05	0.14	4.60	7.02	3.12	1.11	0.13	2.78	100.10	34.6	385	27.5	23.6	24	71	15	501
RQ-11	Basaltic dike	55.55	0.76	15.13	10.21	0.14	4.54	7.09	3.16	1.13	0.13	2.78	100.60	34.7	382	27.6	22.3	25	71	12	477
RQ-12	Andesite dike	58.27	0.30	13.69	8.50	0.08	5.48	1.87	4.04	1.50	0.06	4.81	98.60	36.9	246	23.8	53.5	15	61	26	257
RQ-13	Basaltic dike	57.86	0.34	14.44	7.85	0.15	5.47	2.93	4.12	1.43	0.08	5.27	99.93	33.5	256	30.1	45.3	17	59	16	236
RQ-15 And	Andesite	57.94	0.33	14.61	7.84	0.11	4.23	6.77	3.10	0.46	0.10	4.23	99.72	36.3	255	23.5	49.9	16	50	9	315
RQ-24	Andesite dike	54.01	0.64	16.01	8.45	0.16	4.36	7.29	2.89	1.25	0.11	4.73	99.92	30.8	272	22.7	64	26	61	23	410
RQ-M	Andesite	70.32	0.41	10.91	5.76	0.11	3.11	1.55	2.45	0.78	0.18	3.77	99.35	21.3	138	15.2	8.9	7	77	12	138
TRI-01	Qz-diorite	56.03	0.72	17.07	8.03	0.15	3.84	8.43	2.90	0.82	0.13	1.15	99.27	32.5	241	59.7	27.4	15	69	15	289

Table 2.2: Analyses of Igneous rocks of the Azuero Peninsula and the Río quema Formation.

Sample	Trace Elements (ppm) Y	Zr	Nb	Ta	Cs	Ba	La	Ce	Pr	Nd	Sm	Eu	Gd	Tb	Dy	Ho	Er	Tm	Yb	Lu	Hf	Th	U
AN-02	30	90	5	0.21		63	3.14	7.66	1.24	6.41	2.47	0.916	3.78	0.76	5.11	1.08	3.38	0.552	3.59	0.523	2.3	0.37	0.11
CW-04	23	77	4	0.66		31	3.17	8.9	1.41	7.51	2.63	0.973	3.42	0.67	4.42	0.89	2.62	0.387	2.65	0.424	1.7	0.27	0.09
GUE-5Bis	22	77	5.2	0.39		47	3.5	8.85	1.41	7.21	2.49	0.948	3.41	0.65	4.01	0.81	2.42	0.374	2.43	0.348	1.9	0.26	0.09
LS-12	32	186	16.7	0.85		63	10.5	25.9	3.93	18.9	5.49	1.86	6.26	1.05	6.18	1.16	3.26	0.486	2.92	0.402	4.4	0.8	0.27
RQ-102I	29	150	9.7	0.8		111	7.76	20.8	3.04	15.5	4.55	1.62	5.23	0.96	5.81	1.09	3.04	0.415	2.54	0.393	3.4	0.7	0.24
CE-1	19	86	6	0.63		156	8.85	19.6	2.55	12.1	3.45	1.21	3.79	0.68	4.12	0.79	2.32	0.334	2.12	0.331	2.1	1	0.32
DES-112	19	93	5.3	0.39		98	6.33	15.9	2.15	9.98	2.77	0.945	3.1	0.57	3.62	0.75	2.26	0.338	2.13	0.338	2	0.51	0.16
RJ-11	37	143	5	0.23		36	7.43	18.3	3.08	15.7	4.96	1.76	6.14	1.09	6.79	1.33	3.93	0.613	3.94	0.552	3.3	0.53	0.19
RJ-13B	29	114	3	0.33	0.2	134	4.03	10.8	1.9	10.1	3.51	1.29	4.49	0.85	5.16	1.02	3.07	0.488	3.14	0.443	2.6	0.22	0.08
RQ-09A	35	90	6.1	0.23	0.1	296	8.3	18.5	2.94	14.5	4.51	1.43	5.55	0.99	6.17	1.29	3.9	0.62	4.1	0.599	2.3	0.68	0.27
RQ-26	30	137	5.8	0.35		89	6.27	14.8	2.34	11.5	3.7	1.3	4.74	0.89	5.5	1.16	3.33	0.521	3.38	0.482	3.2	0.49	0.15
AC-04	15	48	2	0.5	0.2	373	5.29	11.5	1.67	7.97	2.09	0.737	2.31	0.41	2.62	0.54	1.57	0.235	1.57	0.263	1.1	0.96	0.3
AC-11	15	49	2.1	0.49	0.2	358	5.32	11.5	1.63	7.96	2.14	0.738	2.29	0.4	2.63	0.52	1.57	0.244	1.6	0.272	1.2	0.59	0.28
AN-04	21	104	7.1	0.29	0.2	1024	16.6	29.7	3.95	16.4	3.78	1.17	3.8	0.63	3.77	0.76	2.3	0.372	2.45	0.355	2.3	1.91	0.81
CE-3B	13	30	0.6	0.23	0.1	135	2.61	6	0.86	4.55	1.41	0.647	1.79	0.34	2.24	0.47	1.43	0.209	1.41	0.239	0.8	0.3	0.15
CE-11	13	42	2	0.26		112	4.31	7.62	1.21	5.86	1.59	0.523	1.82	0.33	2.11	0.43	1.32	0.197	1.32	0.221	1	0.59	0.33
CW-02	9	30	0.9	0.38	1	470	4.6	9.56	1.32	6.09	1.59	0.49	1.57	0.24	1.55	0.32	1	0.159	1.12	0.2	0.8	0.53	0.24
DES-03	8	62	1.3	0.17		64	6.87	14.3	1.76	7.34	1.73	0.461	1.5	0.22	1.35	0.29	0.86	0.139	1.02	0.184	1.5	0.94	0.39
LI-01	30	212	25.2	0.85	1.1	650	16.8	33.2	4.44	18.8	4.76	1.34	5.14	0.88	5.29	1.04	3.13	0.508	3.38	0.489	4.7	2.44	0.92
LP-111	5	54	2	0.08	0.1	170	3.48	6.68	0.98	4.17	1.11	0.315	1.03	0.18	1.06	0.22	0.7	0.121	0.85	0.127	1.3	0.45	0.21
LP-204	7	53	2.5	0.05	0.3	638	7.25	13.4	1.92	8.06	1.88	0.535	1.6	0.23	1.23	0.23	0.7	0.116	0.82	0.122	1.3	1.07	0.4
PA-01	36	199	12.7	1.26	0.3	412	14.2	29.2	4.03	17.1	4.49	1.06	5.12	0.91	5.54	1.11	3.34	0.525	3.43	0.493	4.7	2.4	0.78
PIT-02	6	44	1.5	1.05	0.4	197	3.78	7.43	1.12	4.8	1.24	0.365	1.33	0.23	1.42	0.3	0.97	0.166	1.21	0.189	1.1	0.59	0.22
PLA-06	8	51	0.8	0.13	0.8	349	5.91	12.9	1.76	8	1.82	0.542	1.52	0.23	1.34	0.26	0.81	0.124	0.85	0.156	1.3	0.78	0.32
PM-01	22	123	3.2	0.62	0.5	297	11.6	24.7	3.42	15.5	3.84	1.32	3.9	0.66	4.12	0.82	2.42	0.361	2.35	0.378	2.6	1.81	0.52
RQ-03	13	40	1.6	0.24	0.7	479	3.9	7.63	1.24	5.94	1.67	0.571	1.97	0.35	2.14	0.43	1.33	0.216	1.47	0.222	1	0.45	0.19
RQ-07	19	69	3.9	0.18	0.5	450	5.85	11.9	1.89	8.72	2.54	0.778	2.94	0.51	3.21	0.66	2.04	0.329	2.23	0.328	1.9	0.77	0.31
RQ-11	19	73	2.2	0.1	0.4	450	6.02	12.2	1.96	9.27	2.66	0.842	3.03	0.55	3.44	0.7	2.11	0.346	2.34	0.341	1.8	0.76	0.31
RQ-12	7	49	4.8	0.19	0.4	817	4.28	7.96	1.15	4.93	1.35	0.329	1.41	0.24	1.48	0.3	0.95	0.163	1.12	0.169	1.3	0.67	0.3
RQ-13	9	45	1.4	0.23	0.7	334	4.25	8.34	1.27	5.69	1.53	0.44	1.58	0.26	1.59	0.34	1.07	0.176	1.22	0.189	1.1	0.69	0.33
RQ-15 And	8	47	1.5	0.06	0.9	184	4.06	8.24	1.24	5.49	1.4	0.429	1.47	0.24	1.51	0.32	1.01	0.171	1.18	0.18	1.2	0.67	0.33
RQ-24	20	86	2	0.08	1	469	9.32	18.2	2.58	11.3	2.93	0.835	3.23	0.58	3.53	0.72	2.22	0.352	2.34	0.353	2.1	2.14	0.63
RQ-M	18	36	1.8	0.21	0.3	198	7.48	13.7	1.92	9	2.37	0.708	2.57	0.47	3.02	0.64	1.95	0.301	2.09	0.348	0.9	0.92	1.82
TRI-01	20	84	2.5	0.78	0.3	355	7.48	14.9	2.14	9.7	2.73	0.828	3.11	0.56	3.5	0.7	2.13	0.338	2.21	0.331	2.1	1.4	0.48

Table 2.2. (continued)

(Fig. 2.5A). Low-Fe to medium-Fe and medium-K differentiation trends, with some samples plotted in the high-K and low-K zones, define the calc-alkaline affinity of the group (Fig. 2.5B, 2.5C). In terms of incompatible elements, the arc group and the RQF, contrary to the AIB and APVA, display relatively large values and higher range of (La/Sm), and lower values of (Nb/La) (Fig. 2.5D). This group contains the most different trace element content of the studied units. The trace element content is characteristic of volcanic arc affinities, with variably enrichment in fluid mobile elements (e.g., Ba, Sr) and also in the most incompatible elements with flat and depleted heavy REE's with negative Nb-Ti anomalies (Fig. 2.6C and 2.6F).

The Azuero Arc Group and the Río Quema Formation rocks are in agreement in terms of composition and chemical affinities, with those described as Paleocene-Early Eocene Arc (Lissinna, 2005), Early Arc (Wörner *et al*., 2009), Sona-Azuero Arc (Wenger *et al*., 2011) and Azuero Arc Group (Buchs *et al*., 2010). Most of the analyzed samples correspond to andesite, dacite and basaltic to andesitte dikes of the RQF, a volcanosedimentary sequence deposited in a fore-arc basin. However there are few samples corresponding to diorite and quartz-diorite batholiths representing the arc related intrusives of El Montuoso (PIT-02), Valle Rico (TRI-01), Parita (Pa-01), and Valle Rico-like intrusions (CW-2, AC-4, AC-11, AN-04, PM-01). Valle Rico-like intrusions occur specially at the north of the Río Quema Formation (northern margin of the fore-arc basin), however some intrusions have been observed in the centrer and southern margin of the preserved fore-arc basin.

2.6. Discussion

This work has focused on the study of the tectonovolcanic environment of the Azuero Peninsula and the Río Quema Formation (Cerro Quema host rock). This fore-arc basin is limited to the North of Cerro Quema by arc-related intrusives (El Montuoso and Valle Rico batholiths, see Fig. 1 for location). The southern limit is not clear, though we infer that the basin was limited by the Cretaceous subduction trench, which has not been identified in the field yet, or that it was subducted during later stages.

The classical interpretation of the Ocú formation assumes limestone deposition before the initiation of arc magmatism (Del Giudice and Recchi, 1969; Weyl, 1980; Kolarsky *et al*., 1995; Buchs *et al*., 2010). Recent studies have defined a series of fossiliferous hemipelagic limestones interbedded with basalt flows and crosscut by basaltic dikes of Azuero Primitive Volcanic Arc affinity (Buchs *et al*., 2010). These limestones were enclosed in the Ocú Formation unit, and interpreted as deposited during the subduction initiation (~75-73 Ma).

In the Cerro Quema mining area, the existence of a fossiliferous limestone level (defined hera as Río Quema Formation, limestone unit) led to enclose this limestones in the Ocú Formation. However, in the study area, the cropping out limestones overlie early volcanic arc rocks whose deposition followed the initiation of island arc magmatism. Therefore, the Río Quema Formation limestones and equivalent calcareous layers observed at the Güera River (West of the mining area) do not belong to the Ocú Formation. Consequently, they are not indicative of the onset of subduction, being possibly a bit younger. Therefore we suggest the restriction of the so-called Ocú Formation to only the grayish foraminifera bearing hemipelagic limestones deposited on top of basaltic basement rocks and/or interbedded with the igneous rocks of Azuero Primitive Volcanic Arc geochemical affinity.

The Río Quema Formation is interpreted as a fore-arc basin infill sequence accumulated during the geochemical and geodynamic maturation of the volcanic arc (Upper Cretaceous to Eocene (?) times). The presence of andesites and dacites in the Río Quema Formation are indicative of magmatism of intermediate to acid composition. The abundance of hyaloclastites in dacites and andesites, the scarcity of vesiculation and the presence of turbidites grading up into fine beds of hemipelagic sedimentary rocks indicate a submarine environment. However, the emplacement of dacites acted as a paleo-barrier to sedimentation producing the compartmentalization of the forearc basin (Fig. 2.7). The facies found on the northern slopes of the dacitic

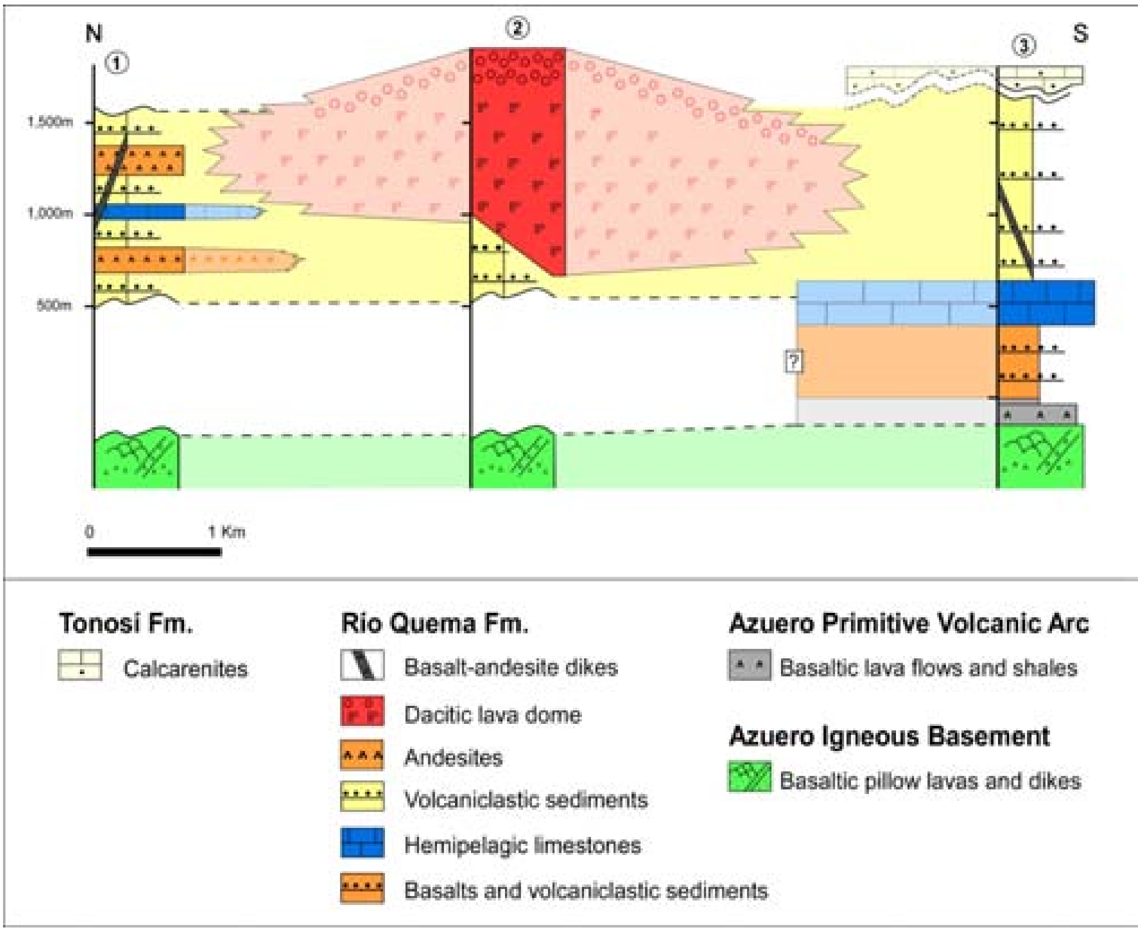

Figure 2.7: Schematic stratigraphic section across the Cerro Quema mining area. 1) North Cerro Quema area. 2) Central Cerro Quema area. 3) South Cerro Quema area.

domes are characterized by the presence of massive volcanic rocks, minor turbidites, limestone layers with wave imprints, and abundant basaltic-andesitic dikes. These features allow us to interpret this part of the series as proximal to the volcanic front, so that the northern volcano-sedimentary sequence defines the inner fore-arc basin. On the other hand, the facies observed on the southern slopes of the dacitic domes with a large fraction of volcanoclastic sediments, turbidites, shales and siltstones and a small presence of andesitic lava flows are interpreted as distal and deeper facies. Hence, the southern sedimentary sequence would define the outer section of the fore-arc basin, consistent with the SW to W paleocurrents observed in turbidite sediments, indicative of axial transport in the basin.

The main tectonic structures recognized in the mining area are the E-W Río Joaquín and Agua Clara fault zones, ENE-WSW folds and late sinistral NW-SE strike-slip faults. All these structures are compatible with a compressive and/or a transpressive tectonic regime. Since the Tonosí Formation unconformably overlies tectonic features and igneous rock units, we infer a minimum pre-Oligocene age for the main tectonic phase. However, additional field and geochronological data are required to better constrain the timing of tectonism.

Our geochemical data confirm that the Azuero Igneous Basement is chemically similar to the tholeiitic basalts of the Caribbean large igneous province (Goossens *et al*., 1977; Hauff *et al*., 2000; Hoernle *et al*., 2002; 2004). Therefore, the Azuero Igneous Basement cannot be interpreted as an accreted terrane (Goossens et al., 1977). Conversely, it represents the autochthonous basement of the upper plate (Caribbean Plate), uplifted and exhumed during convergence tectonics. The recognition of the autochthonous basement of the Río Quema Formation allows us to describe the depositional environment from the onset of intra-oceanic subduction to the geochemical and geodynamic maturation of the magmatic arc.

The Azuero Primitive Volcanic Arc is interpreted to have formed at the initial stages of the magmatic arc which developed on top of the Azuero igneous basement. Its voluminous sheet flows and pillowed non-vesicular basalts and andesites associated with cherts and shales indicate extrusion/deposition in a deep marine environment proximal to the volcanic centre. Its geochemical composition is unusual and its signature is intermediate between typical oceanic plateau and intra-oceanic island arc (i.e. variably enriched in fluid-mobile elements and depleted in heavy REEs). Our results are in agreement with those of Buchs *et al*. (2009, 2010), the Azuero Primitive Volcanic Arc rocks are true arc-related rocks, and could be associated to the initial magmatic arc generated at the onset of the Farallon plate subduction beneath the Caribbean Plate during Late Cretaceous Times.

The Azuero Arc Group and the Río Quema Formation is interpreted as the evolution of the Azuero Primitive Volcanic arc. The geochemical composition and affinities of its igneous rocks are in agreement with an evolved calc-alkaline volcanic arc. Our data is also in agreement with those from the Early arc of

Wörner *et al*. (2009), those from the Azuero arc of Buchs *et al*. (2010), and finally with those from Sona-Azuero arc of Wenger *et al*. (2011).

Basaltic dikes with Azuero Primitive Volcanic Arc affinity found crosscutting the Azuero Igneous Basement are interpreted as the conduits which feed the Azuero Primitive Volcanic Arc. However, the role of the dikes with Azuero Primitive Volcanic Arc affinity found crosscutting the Río Quema Formation, a well established calc-alkaline volcanic arc sequence, is not well understood so far.

In figure 2.8A we observe the Ta/Yb versus Th/Yb plot, were the effect of slab enrichment on depleted mantle source (e.g., MORB-source mantle), and on mantle sources enriched (e.g., OIB-source mantle) is shown (e.g., Lewis *et al*., 2002; Wenger *et al*., 2011). In this plot we can distinguish the magmas produced by subduction-related arc magmatism, in which the enrichment of a depleted mantle source occurs by the introduction of LILE-enriched fluids and sediments. This is noted by the enrichment in Th but not Ta, (e.g., higher Th/Yb ratio at constant Ta/Yb ratio).

The Azuero Igneous Basement rocks fall within the depleted mantle source field, whereas the Azuero Primitive Volcanic arc has higher values of the Th/Yb ratio for approximately the same Ta/Yb ratio. Moreover, the Azureo Arc and the rocks of the Río Quema Formation have even more higher values of the Th/Yb ratio than the AIB and the APVA for approximately the same value of the Ta/Yb ratio. This suggests that all groups are derived from a depleted mantle source, however the fluid enrichment is increasing from the initial stages of the subduction towards the late stages. As demonstrated by their trace element patterns (Fig. 2.6), the Azuero Arc and the Río Quema Formation rocks reflect a fluid modified but variable depleted mantle source, as is also documented by the difference in the values of the Th/Yb ratio. The Azuero Primitive Volcanic Arc can be interpreted as an intermediate evolutionary stage between the AIB and the Azuero Arc.

Figure 2.8B shows the effects of the wedge depletion and arc signature on the different studied rock groups. As noted, the arc signature is strongest for the

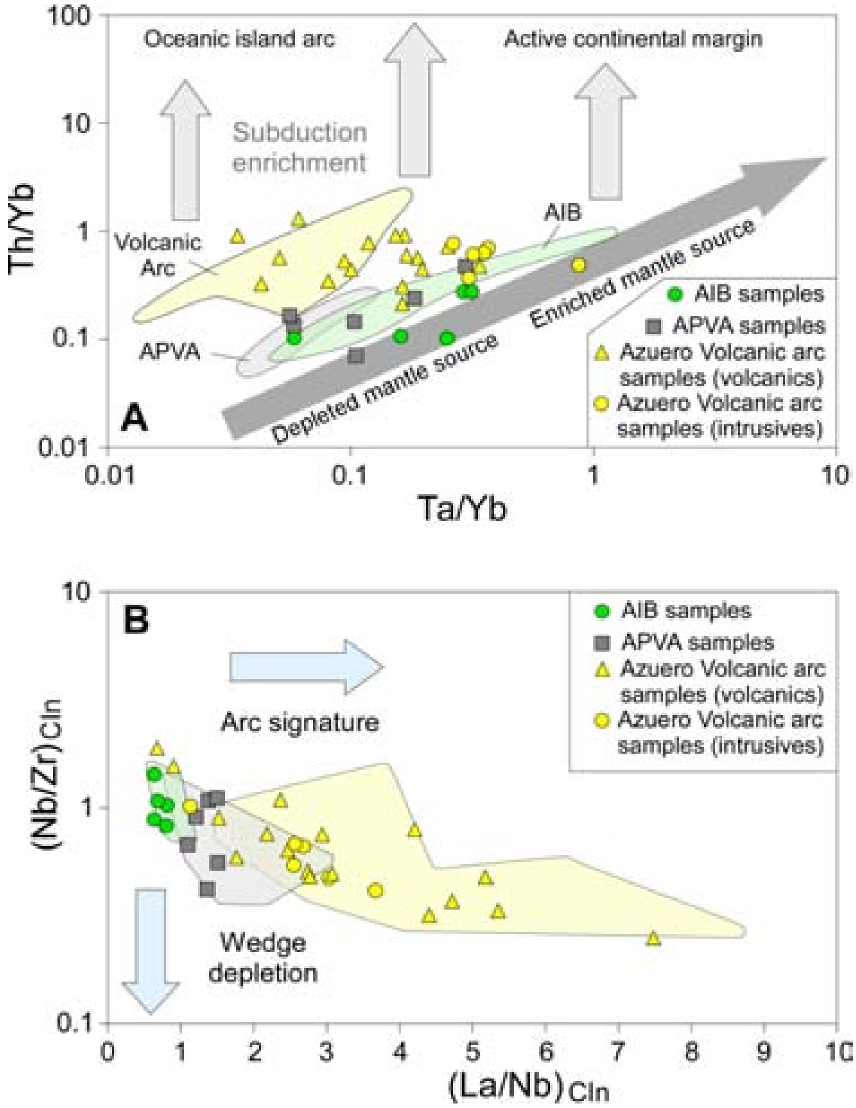

Figure 2.8: A) Plot of Ta/Yb versus Th/Yb (after Pearce, 1983), for igneous rokcs of the Azuero Peninsula and the Río Quema Formation. AIB field from Azuero CLIP of Lissina (2005), and CLIP Oceanic Basement of Wörner *et al*., (2009) and Wenger *et al*., (2011). APV field from some samples of the CLIP Oceanic Basement (Wörner *et al*., 2009; Wenger *et al*., 2011) with APVA affinity. Volcanic Arc field from Paleocene-Early Eocene Arc rocks from Lissinna (2005), Early Arc rocks from Wörner *et al*., (2009) and Sona-Azuero Arc rocks from Wenger *et al*., (2011). AIB: Azuero Igneous Basement, APVA: Azuero Primitive Volcanic Arc. B) Plot of Chondrite normalized ratios of La/Nb versus Nb/Zr. Chondrite abundances from McDonough and Sun (1995). AIB field from Azuero CLIP of Lissina (2005), CLIP Oceanic Basement of Wörner *et al*., (2009), Azuero Platau of Buchs *et al*., (2010), and CLIP Oceanic Basement of Wenger *et al*., (2011). APV field from Azuero Protoarc Group of Buchs *et al*., (2010), and some samples of the CLIP Oceanic Basement (Wörner *et al*., 2009; Wenger *et al*., 2011) with APVA affinity. Volcanic Arc field from Paleocene-Early Eocene Arc rocks from Lissinna (2005), Early Arc rocks from Wörner *et al*. (2009), Azuero Arc Group from Buchs *et al*. (2010), and Sona-Azuero Arc rocks from Wenger *et al*. (2011).

Azuero Volcanic Arc samples than for the Azuero Igneous Basement or for the Azuero Primitive Volcanic Arc. Nevertheless, the wedge depletion effect is more evident in the AIB and in the APVA than in the Azuero Volcanic Arc. As also noted in Figure 2.8A, the APVA is an intermediate evolutionary stage between the AIB and the Azuero Arc. This fact reflects the effect of the slab derived fluids in the arc evolution. Trace element patterns (Fig. 2.6), and ratios of Figure 2.5D and 2.8, document a systematic temporal evolution in magma composition.

2.7. Evolution of the Panamanian volcanic arc

According to our results, the Azuero Igneous Basement formation is compatible with the presence of a mantle plume under the Panamanian block, approximately between Turonian to Santonian times, generating massive, agglomerated and pillowed basaltic lavas and gabbros which are locally interlayered with hemipelagic sediments. This basement has a Tholeiitic character with plateau-like affinities, corresponding to the Caribbean Large Igneous Province (CLIP).

During Late Campanian times (~75- 73Ma) the Nazca plate started to subduct beneath the Caribbean plate, generating massive and pillowed basaltic lavas interlayered with shales and cherts. Because of the influence of the subducting slab derived fluids the composition of the AIB changed to the Azuyero Primitive Volcanic Arc, with Tholeiitic character and slightly enriched fluidmobile elements and depleted in Nb and Ti.

Once the arc matured, it generated more acidic rocks such as andesites, dacites, quartz-diorites, and the chemistry changed to Calc-alkaline character with volcanic arc affinities, denoting the strong influence of the subducting slab derived fluids.

2.8. Conclusions

1) The stratigraphy and petrology of the volcanosedimentary rocks of the central Azuero Peninsula and the Cerro Quema area denote a submarine

depositional environment. The tectonic setting corresponds to the fore-arc basin associated to a Late Cretaceous intra-oceanic volcanic arc.

2) A new lithostratigraphic unit, the Río Quema Formation, is proposed to describe the volcano-sedimentary sequence that crops out in the central Azuero Peninsula. The Río Quema Formation which hosts the Cerro Quema deposit is composed of volcanic and volcaniclastic sediments interbedded with hemipelagic limestones, dacite lava domes and intruded by basaltic to andesitic dikes. The Río Quema Formation has been divided into three units, a) Lower Unit, B) Limestone Unit, and C) Upper Unit. The total thickness of the sequence is approximately 1,700 m. The Río Quema Formation is overlying both, The Azuero Igneous Basement and the Azuero Primitive Volcanic Arc, and is discordantly overlapped by the Tonosí Formation.

3) The Río Joaquín fault zone, a major regional scale fault zone with broad E-W orientation and reverse-sense motion, has been recognized in the Cerro Quema mining area, and mapped with a slightly different trend from that proposed by Buchs (2008). Other regional structures such as the Agua Clara Fault, parallel to the Río Joaquín Fault Zone has been found affecting the distribution of the Río Quema Formation in the Central Azuero Peninsula. Along the Río Joaquín Fault Zone, the Azuero Igneous Basement is in direct contact with the Upper Unit of the Río Quema Formation. In addition, kilometric to decametric ENE-WSW folds and late sinistral NW-SE strike-slip faults have also been identified in the mining area. These structures suggest a compressive and/or transpressive tectonic regime, at least during Late Cretaceous–Oligocene times.

4) The Azuero Igneous Basement is composed by Upper Cretaceous (Aptian to Santonian) basalts and pillow basalts interbedded with pelagic sediments such as limestones and radiolarite. The igneous rocks of the Azuero Igneous Basement have tholeiitic character. Trace element content has flat or slightly enriched pattern, typical of plateau-like affinities. The Azuero Igneous Basement has geochemical affinities similar to the Caribbean Large Igneous Province (CLIP), and is interpreted as the western edge of the Caribbean Plate, forming the Azuero arc basement.

5) The Azuero Primitive Volcanic Arc is constituted by basalts and volcaniclastic rocks with tholeiitic character, locally interbedded with Late Campanian-Maastrichtian hemipelagic limestones. Trace elements indicate a signature between an oceanic plateau and a volcanic arc. Incompatible elements show that the slab derived fluids start to interact with the depleted mantle during the APVA deposition. The Azuero Primitive Volcanic Arc, develops on top of the Azuero Igneous Basement, and is interpreted as the initial stages of the Azuero volcanic arc.

6) The Azuero Arc Group, where the Río Quema Formation is enclosed, is constituted by volcano-sedimentary, volcanic and arc-related intrusive rocks, with a clear calc-alkaline character. The trace element content of the Azuero Arc Group is characteristic of volcanic arc affinities, with variably enrichment in fluid mobile elements (e.g., Ba, Sr) and also in the most incompatible elements with flat and depleted heavy REE's with negative Nb-Ti anomalies. Although this group derived from a depleted mantle source, it is strongly influenced by the enrichment produced by the subducting slab-derived fluids. The Azuero Arc Group developes on top of the Azuero Igneous Basement as well as on top of the Azuero Primitive Volcanic Arc, and is interpreted as the expression of the well developed and matured volcanic arc.

7) Geochemical evolution of the igneous rocks cropping out in the Azuero Peninsula indicates that a primitive tholeiitic volcanic arc (Azuero Primitive Volcanic Arc) was developed on an oceanic plateau (Azuero Igneous Basement) of also tholeiitic character, and evolved over time to a calc-alkaline volcanic arc (Azuero Arc Group).

2.9. References

Adamek, S., Frohlich, C., Pennington, W.D., 1988. Seismicity of the Caribbean-Nazca boundary; constraints on microplate tectonics of the Panama region. Journal of Geophysical Research, 93, 2053-2075.

Arculus, R. J., 2003. Use and abuse of the terms calcalkaline and calcalkalic. Journal of Petrology, 44, 929-935.

Bourgois, J., Azema, J., Tournon, J., Bellon, H., Calle, B., Parra, E., Toussaint, J.F., Glacon, G., Feinberg, H., Dewever, P., Origlia, I. 1982. Ages and Structures of the Basic and Ultrabasic Complexes of the Pacific Coast between 3-Degrees-N and 12-Degrees-N (Colombia, Panama and Costa-Rica). Bulletin De La Société Géologiques De France, 24, 545-554.

Buchs, D.M., 2008. Late Cretaceous to Eocene geology of the South Central American fore-arc area (southern Costa Rica and western Panama): Initiation and evolution of an intra-oceanic convergent margin. Doctoral Thesis. Université de Lausanne, Switzerland, 230pp.

Buchs, D.M., Baumgartner, P.O., Baumgartner-Mora, C., Bandini, A., Jackett, S-J., Diserens, M-O., Stucki, J. 2009. Seamount accretion and melange formation of the Osa Peninsula (southern Costa Rica): Eocene–Miocene mass wasting and tectonic processes along the Middle American Trench. In: James, K., Lorente, M.A., Pindell, J. (eds.). *The geology and evolution of the region between North and South America.* Geological Society of London, Special Publications, 411-456.

Buchs, D.M., Arculus, R.J., Baumgartner, P.O., Baumgartner-Mora, C., Ulianov, A., 2010. Late Cretaceous Arc Development on the SW margin of the Caribbean Plate: Insights from the Golfito (Costa Rica) and Azuero (Panama) Complexes. Geochemistry Geophysics Geosystems, 11, 7, 35pp.

Coates, A.G., Collins, L.S., Aubry, M.-P., Berggren, W.A., 2004. The Geology of the Darien, Panama, and the late Miocene-Pliocene collision of the Panama arc with northwestern South America. Geological Society of America Bulletin, 116, 1327-1344.

Corral, I., 2008. El dipòsit d'Au-Cu de "La Pava" (Península d'Azuero, Panamà): caracterització geològica i mineralògica. MSc. thesis. Universitat Autònoma de Barcelona, Barcelona, 31pp.

Cowan, H., Machette, M. N., Haller, K. M., Dart, R. L., 1998. Map and database of Quaternary faults and folds in Costa Rica and its offshore regions, U.S. Geological Survey Open File Reports, 98-779, 41pp.

de Boer, J.Z., Drummond, M.S., Bordelon, M.J., Defant, M.J., Bellon, H., Maury, R.C., 1995. Cenozoic magmatic phases of the Costa Rican island arc (Cordillera de Talamanca). Geological Society of America, 295, 35-55.

del Giudice, D., Recchi, G., 1969. Geologia del area del Proyecto Minero de Azuero. Informe técnico preparado para el gobierno de la Republica de Panama por las Naciones Unidas. Gobierno de la República de Panamá, Panama City, Panama, 48pp.

Denyer, P., Alvarado, G.E., 2007. Mapa Geológico de Costa Rica 1:400.000. Librería Francesa S.A. San José, Costa Rica.

Dirección General de Recursos Minerales., 1976. Panama Geologic Map (Mapa geológico de la República de Panamá), scale 1:250.000. Panama City, Panama.

Di Marco, G., Baumgartner, P.O., Channell, J.E.T., 1995. Late Cretaceous-early Tertiary paleomagnetic data and a revised tectonostratigraphic subdivision of Costa Rica and western Panama. Geological Society of America, 295, 1-27.

Duque-Caro, H., 1990. Neogene stratigraphy, paleoceanography and paleobiogeography in Northwest South America and the evolution of the Panama Seaway. Palaeogeography, Palaeoclimatology, Palaeoecology, 77, 203-234.

Escalante, G., 1990. The geology of southern Central America and western Colombia In: Dengo, G., Case, J.E. (eds.). The Caribbean Region. Boulder, Colorado, Geological Society of America, The Geology of North America, H, 201-230.

Ferencic, A., 1970. Porphyry copper mineralization in panama. Mineralium Deposita, 5, 383-389.

Ferencic, A., 1971. Metallogenic provinces and epochs in southern Central America. Mineralium Deposita, 6, 77-88.

Fisher, D.M., Gardner, T.W., Marshall, J.S., Sak, P.B., Protti, M., 1998. Effect of subducting sea-floor roughness on fore-arc kinematics, Pacific coast, Costa Rica. Geology, 26, 467-470.

Gardner, T., Marshall, J., Merritts, D., Bee, B., Burgette, R., Burton, E., Cooke, J., Kehrwald, N., Protti, M., Fisher, D., Sak, P., 2001. Holocene fore-arc block rotation in response to seamount subduction, southeastern Peninsula de Nicoya, Costa Rica. Geology, 29, 151-154.

Goossens, P.J., Rose, W.I.J., Flores, D., 1977. Geochemistry of tholeiites of the Basic Igneous Complex of northwestern South America. Geological Society of America Bulletin, 88, 1711-1720.

Harmon, R.S., 2005. Geological development of Panama. Water Science and Technology Library, 52, 45-62.

Hauff, F., Hoernle, K., van den Bogaard, P., Alvarado, G., Garbe-Schoenberg, D., 2000. Age and geochemistry of basaltic complexes in western Costa Rica; contributions to the geotectonic evolution of Central America. Geochemistry Geophysics Geosystems, 1, 5, 41pp.

Hoernle, K., Hauff, F., 2007. Oceanic Igneous Complexes. Central America, geology, resources, hazards, 1, 523-548.

Hoernle, K., Hauff, F., van den Bogaard, P., 2004. 70 m.y. history (139-69 Ma) for the Caribbean large igneous province. Geology, 32, 697-700.

Hoernle, K., van den Bogaard, P., Werner, R., Lissinna, B., Hauff, F., Alvarado, G., Garbe-Schonberg, D., 2002. Missing history (16-71 Ma) of the Galapagos hotspot: Implications for the tectonic and biological evolution of the Americas. Geology, 30, 795-798.

Horlacher, C.F., Lehmann, J.H., 1993. Regional Geology, Geochemistry and Exploration potential of the central Cerro Quema concession, Panamá. Unpublished report, 36pp.

Kellogg, J.N., Vega, V., Stallings, T.C., Aiken, C.L.V., 1995. Tectonic development of Panama, Costa Rica, and the Colombian Andes; constraints from Global Positioning System geodetic studies and gravity. Geological Society of America Special Paper, 295, 75-90.

Kerr, A.C., Marriner, G.F., Tarney, J., Nivia, A., Saunders, A.D., Thirlwall, M.F., Sinton, C.W., 1997. Cretaceous basaltic terranes in western Colombia: Elemental, chronological and Sr-Nd isotopic constraints on petrogenesis. Journal of Petrology, 38, 677-702.

Kesler, S.E., Sutter, J.F., Issigonis, M.J., Jones, L.M., Walker, R.L., 1977. Evolution of porphyry copper mineralization in an oceanic island arc; Panama. Economic Geology, 72, 1142-1153.

Kolarsky, R.A., Mann, P., Monechi, S., Meyerhoff-Hull, D., Pessagno, E.A., 1995. Stratigraphic development of southwestern Panama as determined from integration of marine seismic data and onshore geology. Geological Society of America Special Paper, 295, 159-200.

Kolarsky, R.A., Mann, P., 1995. Structure and neotectonics of an oblique-subduction margin, southwestern Panama. Geological Society of America Special Paper, 295, 131-157.

Krawinkel, H., Wozazek, S., Krawinkel, J., Hellmann, W., 1999. Heavy-mineral analysis and clinopyroxene geochemistry applied to provenance analysis of lithic sandstones from the Azuero-Soná Complex (NW Panama). Sedimentary Geology, 124, 149-168.

Krawinkel, J., and Seyfried, H., 1994. Struktur und Kinematik im Fore-arc der suedlichen zentralamerikanischen Landbruecke. Bonn, Terra Nostra, 2(94), 47-48.

Le Maitre, R.W., Bateman, P., Dudek, A., Keller, J., Lemeyre, J., Le Bas, M.J., Sabine, P.A., Schmid, R., Sorensen, H., Streckeisen, A., Wooley, A.R., Zanettin, B., 1989. A classification of igneous rocks and glossary of terms. Blackwell Scientific, Oxford, 193pp.

Leach, T.M., 1992. Petrological Evaluation of the High Sulphidation Systems in the La Pava and Cerro Quema Prospect Areas, Panama, for Cyprus Gold Company. Unpublished report, 55pp.

Lewis, J. F., Escuder-Viruerte, J., Hernaiz-Huerta, P. P., Gutierrez, G., Draper, G., Pérez-Estaún., 2002. Geochemical subdivisión of the Circum-Caribbean Island Arc, Dominican Cordillera Central: Implications for crustal formation, accretion and growth within an intra-oceanic setting. Acta Geologica Hispanica, 37, 2-3, 81-122.

Lissinna, B., Hoernle, K., van den bogaard, P., 2002. Northern migration of arc volcanism in western Panama: evidence for subduction erosion? Eos Transactions, American Geophysical Union, 83, 1463-1464.

Lissinna, B., 2005. A profile through the Central American Landbridge in western Panama: 115 Ma Interplay between the Galápagos Hotspot and the Central American Subduction Zone. Doctoral Thesis. Christian-Albrechts-Universität zu Kiel, Germany, 102pp.

Lissinna, B., Hoernle, F., Hauff, P., van den Bogaard, P., Sadofsky, S., 2006. The Panamanian island arc and Galápagos hotspot: A case study for the long-term evolution of arc/hotspot interaction. Geophysical Research Abstracts, 8, 05106.

Mann, P., Kolarsky, R.A., 1995. East Panama deformed belt; structure, age, and neotectonic significance. Geological Society of America Special Paper, 295, 111-130.

Mann, P., Corrigan, J., 1990. Model for late Neogene deformation in Panama. Geology, 18, 558-562.

Marshall, J.S., Idleman, B.D., Gardner, T.W., Fisher, D.M., 2003. Landscape evolution within a retreating volcanic arc, Costa Rica, Central America. Geology, 31, 5, 419-422.

Maury, R.C., Defant, M.J., Bellon, H., De Boer, J.Z., Stewart, R.H., Coten, J., 1995. Early Tertiary arc volcanic from eastern Panama. Geological Society of America Special Paper, 295, 30-34.

McDonough, W. F., Sun, S. S., 1995. The composition of the Earth: Chemical evolution of the mantle. Chemical Geology, 120, 223-253.

Metti, A., Recchi, G., 1976. Geología de la Península de Sona e Isla de Coiba. Boletín de Geología Publicación Especial, 541-553.

Metti, A., Recchi, G., Esquivel, D., 1972. Mapa geológico Sona-Isla de Coiba: Ministerio de Comercio e Industrias, Republica de Panamá, scale 1:250.000. Panama City, Panama.

Montero, W., Denyer, P., Barquero, R., Alvarado, G. E., Cowan, H., Machette, M. N., Haller, K. M., Dart, R. L., 1998. Map and database of Quaternary faults and folds in Costa rica and its offshore regions, U.S. Geological Survey Open File Reports, 98-481, 63pp.

Nelson, C.E., 2007. Metallic mineral resources. In: Bundschuh, J., Alvarado, G.E. (eds.). Central America. Geology, Resources and Hazards. The Netherlands, Taylor & Francis, 32(Chapter), 885-915.

Pearce, J. A., 1983. The role of sub-continental lithosphere in magma genesis at destructive plate margins. In C. J. Hawkesworth, M. J. Norry (eds.). Continental Basalts and Mantle Xenoliths. Nantwich, Shiva, 230-249.

Pindell, J., Kennan, L., 2009. Tectonic evolution of the Gulf of Mexico, Caribbean and northern South America in the mantle reference frame: an update. In: James, K., Lorente, M.A., Pindell, J. (eds.). The geology and evolution of the region between North and South America. Geological Society of London, 328(Special Publication), 1-55.

Recchi, G., Miranda, R., 1977. Calizas de los Planes-Guaniquito (Tonosí). Unpublished report, Panama City, Dirección General de Recursos Minerales, 27pp.

Révillon, S., Hallot, E., Arndt, N.T., Chauvel, C., Duncan, R.A., 2000. A complex history for the Caribbean plateau: Petrology, geochemistry and geochronology of the Beata Ridge, South Hispaniola. Journal of Geology, 108, 641-661.

Paris, G., Machette, M. N., Dart, R. L., Haller, K. M., 2000. Map and database of Quaternary faults and folds in Colombia and its offshore regions, U.S. Geological Survey Open File Reports, 00-0284, 60pp.

Puritch, E. J., Sutcliffe, R. H., Wu, Y., Armstrong, T., Yassa, A., 2012. Technical report and mineral resource estimate on the Cerro Quema Project, Los Santos Province, Panama, Prepared for Preshimco Resources Inc., by P&E Mining Consultants Inc. 123pp.

Sak, P.B., Fisher, D.M., Gardner, T.W., 2004. Effects of subducting seafloor roughness on upper plate vertical tectonism: Osa Peninsula, Costa Rica. Tectonics, 23, 16pp.

Silver, E.A., Reed, D.L., Tagudin, J.E., Heil, D.J., 1990. Implications of the North and South Panama thrust belts for the origin of the Panama Orocline. Tectonics, 9, 261-281.

Sinton, C.W., Duncan, R.A., Denyer, P., 1997. Nicoya Peninsula, Costa Rica; a single suite of Caribbean oceanic plateau magmas. Journal of Geophysical Research, 102, B7, 15.507-15.520.

Sinton, C.W., Duncan, R.A., Storey, M., Lewis, J., Estrada, J.J., 1998. An oceanic flood basalt province within the Caribbean Plate. Earth and Planetary Science Letters, 155, 221-235.

Smith, W. H. F., Sandwell, D. T., 1997. Global sea flor topography form satellite altimetry and ship depth soundings. Science, 277, 1956-1962.

Taboada, A., Rivera, L.A., Fuenzalida, A., Cisternas, A., Philip, H., Bijwaard, H., Olaya, J., Rivera, C., 2000. Geodynamics of the Northern Andes; subductions and intracontinental deformation (Colombia). Tectonics, 19, 787-813.

Torrey, C., Keenan, J., 1994. Cerro Quema Project, Panama, Prospecting in tropical and arid terrains. Toronto, Ontario, Canada, Unpublished report, 23pp.

Trenkamp, R., Kellogg, J.N., Freymueller, J.T., Mora, H.P., 2002. Wide plate margin deformation, southern Central America and northwestern South America, CASA GPS observations. Journal of South American Earth Sciences, 15, 157-171.

Tournon, J., Triboulet, C., Azéma, J., 1989. Amphibolites from Panama: anticlockwise P-T paths from a Preuper Cretaceous metamorphic basement in Istmian Central America. Journal of Metamorphic Geology, 7, 539-546.

Valiant, W. W., Collins, S. E., and Krutzelmann, H., 2011. Technical report on the Cerro Quema Project, Panama, Prepared for Preshimco Resources Inc., by Scott Wilson roscoe Postle Associates Inc., 109pp.

Weyl, R., 1980. Geology of Central America. Berlin, Gebrueder Borntraeger, 2nd edition, 371pp.

Wegner, W., Wörner, G., Harmon, R.S., Jicha, B.R., 2011. Magmatic history and evolution of the Central American Land Bridge in Panama since Cretaceous times. Geological Society of America Bulletin, 123, 703-724.

Wörner, G., Harmon, R.S., Wegner, W., 2009. Geochemical evolution of igneous rocks and changing magma sources during the formation and closure of the Central American land bridge of Panama: Backbone of the Americas: Shallow Subduction, Plateau Uplift, and Ridge Terrane Collision. Geological Society of America Memoir, 204, 183-196.

Wörner, G., Harmon, R.S., Hartmann, G., Simon, K., 2005. Igneous Geology and Geochemistry of the Upper Río Chagres Basin. In: Singh, V.P., Harmon, R.S. (eds.). The Río chagres, Panama: A Multidisciplinary Profile of a Tropical Watershed. Springer, 65-81.

Wörner, G., Harmon, R.S., Wegner, W., Singer, G., 2006. Linking America's backbone: Geological development and basement rocks of central Panama. Mendoza (Argentina), 2-7 April 2006, Geological Society of America Conference "Backbone of the Americas", Boulder (Colorado), Geological Society of America, Abstrstracts with Programs, 60.

CHAPTER

3

Sedimentation and volcanism in the Panamanian Cretaceous intra-oceanic arc and fore-arc: New insights from the Azuero Peninsula (SW Panama)

3.1. Introduction

The Panamanian microplate (Southern Central America) lies at the junction of four tectonic plates: the Caribbean plate to the north, the South American plate to the east and the Cocos and Nazca plates to the west and south, respectively (Fig. 3.1A). The southern edge of Panama is characterized by a long-lived intra-oceanic subduction zone. Volcanic arcs developed in the Late Cretaceous as a result of the subduction of the ancient Farallon plate beneath the Caribbean plate, and continued until the Miocene (~23 Ma) breakup of the Farallon plate (Barckhausen *et al*., 2001; Werner *et al*., 2003; Lonsdale, 2005; Buchs *et al*., 2009, 2010; Wörner *et al*., 2009; Pindell and Kennan, 2009). Episodic accretion of island arcs and oceanic plateau occurred since the early stages of subduction until Middle Eocene times (Lissinna, 2005; Buchs *et al*., 2011). During the Middle to Late Miocene, the collision of the Panamanian arc with Colombia (Keigwin, 1978; Wadge and Burke, 1983; Pindell *et* al., 1998; Trenkamp *et al*., 2002; Coates *et* al., 2004; Kennan and Pindell, 2009) produced a lateral escape of the Panamanian microplate towards the NW (e.g., Wadge and Bruke, 1983; Mann and Corrigan, 1990; Pindell, 1993; Kolarsky *et al*., 1995a) and was accommodated by left-lateral strike slip faults (e.g., Soná-Azuero Fault Zone). As a consequence, the subduction direction changed, causing the migration of the volcanic arc towards the North (Lissinna *et* al., 2002; Lissinna, 2005), where it remains active in the Cordillera Central.

The study of ancient intraoceanic subduction zones is handicapped by the lack of preservation of the rocks formed during the initial stages due to erosion, or because arcs are located in areas of difficult access (e.g., actual slope of the subduction trench) or because the arcs are overlain by modern arc materials. For example, subduction of relatively buoyant plates with irregular topography causes uplift in the fore-arc area and exposes it along the subduction margin (Fisher *et al.,* 1998; Gardner *et al*., 2001; Sak *et al*., 2004). The Azuero Peninsula, located on the Pacific side of SW Panama (Fig. 3.1B), is a rare example of a fore-arc where a complete section of the volcanic arc is still preserved. Such exposures provide the opportunity to study deep sections of the usually inaccessible inner and outer fore-arc margin. Migration of the volcanic arc towards the north during Middle to Late Miocene contributed to the preservation of the nascent volcanic arc.

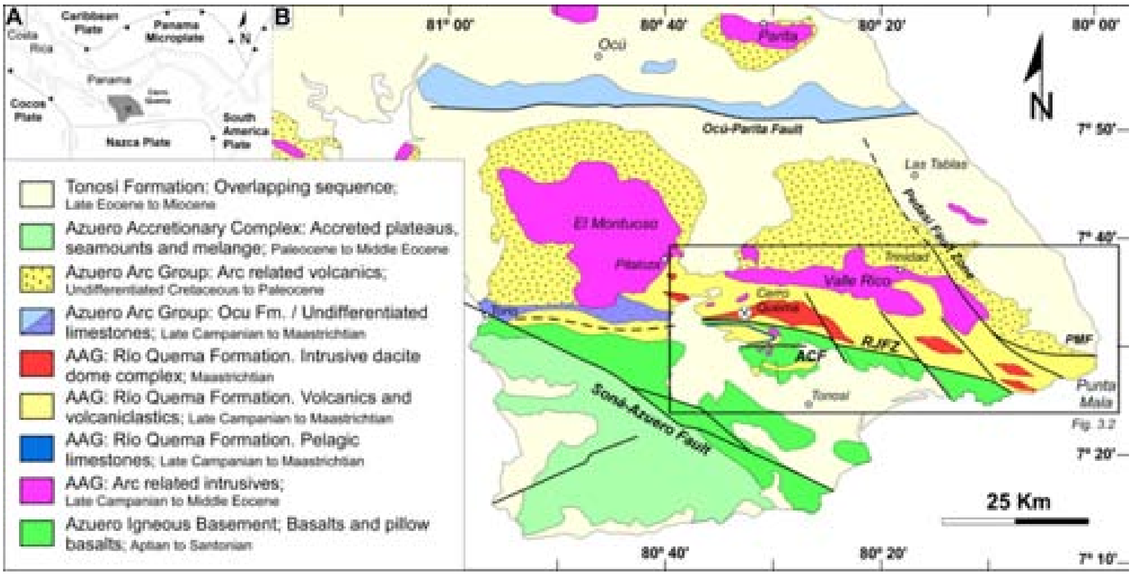

Figure 3.1: A) Present-day tectonic setting of South Central America. B) Simplified geological map of the Azuero Peninsula. AAG: Azuero Arc Group, RJFZ: Río Joaquín Fault Zone, ACF: Auga Clara Fault, PMF: Punta Mala Fault (After DGRM, 1976; Buchs *et al*., 2011b; Corral *et al*., 2011).

Fore-arc basins have long been recognized as repositories of volcanic material from the adjacent arc (e.g., Dickinson, 1974a, 1974b), making their sedimentary history potentially ideal for reconstructing temporal arc evolution. The excellent exposure of the arc basement, fore-arc basin, volcanic arc rocks and arc-related intrusive rocks offer the chance to study the relationship between volcanism, sedimentation and magmatism during the arc development and reconstruct its evolution. Although studies of stratigraphy, geochemistry, petrology and geochronology of the Azuero Peninsula have already been done (e.g., Del Giudice and Recchi, 1969; Kolarsky *et al*., 1995b; Hauff *et al*., 2000; Hoernle *et al*., 2002; Lissinna *et al.,* 2005; Wörner *et al.,* 2009; Buchs *et al*., 2010; Wegner *et al.,* 2011; Corral et al, 2011), some aspects remain to be addressed, such as a clear and detailed description of the volcanosedimentary sequences. Description and distribution of the volcanic facies, interpretation of depositional environment and paleogeographic reconstruction has not been carried out to date.

The aim of this study is to describe the lithofacies and stratigraphic relationships between the volcanic apron and the sedimentation (terrigenous and pelagic sediments) observed in the Azuero Peninsula. The depositional environment and volcanic processes are also addressed. Field and laboratory studies are complemented with new biostratigraphic data, which allow us to constrain the timing of the volcanic arc. The results are integrated in a paleoenvironmental model for the Upper Cretaceous volcanic arc. The model relates to offshore studies of arc successions, improving our understanding of the setting, origin, and history of sediment and rock recovered in drill cores (Allen *et al*., 2007).

3.2. Geologic setting

The Azuero Peninsula consists of volcanic, plutonic, sedimentary and volcanosedimentary rocks ranging in age from ~71Ma to ~40Ma (Del Giudice and Recchi, 1969; Bourgois *et* al., 1982; Kolarsky *et al*., 1995b; Lissinna *et al.,* 2002, 2006; Wörner *et al.,* 2005, 2006, 2009; Buchs *et al*., 2009, 2010; Wegner *et al.,* 2011; Corral *et al*., 2011). The main tectonic structures in the Azureo Peninsula are several regional subvertical faults delimiting variously uplifted blocks (Fig. 3.1B), such as the Soná-Azuero fault zone which strikes NW-SE or the Ocú-Parita (Kolarsky *et al*., 1995b), the Río Joaquín fault zone (Buchs, 2008; Corral *et al*., 2011), and the Agua Clara Fault, with broad E-W orientation.

The Azuero Peninsula can be divided into five major units as described below and shown in figure 3.1B (Buchs *et al*., 2010; Corral *et al*., 2011):

(1) The Azuero Igneous Basement of basalts and pillow basalts of tholeiitic character and plateau-like affinity (Hauff *et al*., 2000; Hoernle *et al*., 2002, 2004), which correspond to the arc basement.

(2) The Azuero Primitive Volcanic Arc, with tholeiitic character and an affinity between oceanic plateau and volcanic arc, corresponding to the initial stages of the volcanic arc.

(3) The Azuero Arc Group, composed of volcano-sedimentary rocks and arc-related magmatic rocks of calc-alkaline character and volcanic arc affinity.

(4) The Tonosí Formation (Recchi and Miranda, 1977; Kolarsky *et al*., 1995b; Krawinkel *et al*., 1999), a sedimentary sequence overlapping all the previous units.

(5) The Azuero Accretionary Complex (Buchs *et al*., 2011) that corresponds to seamounts and oceanic plateaus, accreted to the paleo-subduction trench.

The present work investigates the central and southeastern part of the Azuero Peninsula (Fig. 3.2) where the relationship between tectonic, sedimentological and volcanic processes associated to the arc evolution can be observed. In this setting, the Río Quema Formation (RQF) is a volcanosedimentary sequence of the Azuero Arc Group that records all these processes.

3.3. Tectonics

The main tectonic structure affecting the Río Quema Formation is the Río Joaquín Fault zone (RJFZ), an E-W trending regional fault zone (Fig. 3.2). Along it, the Azuero Igneous Basement is directly in contact with the RQF. A complex tectonic history is inferred for the RJFZ involving mesoscale and minor tectonic structures and neotectonic data. Left-lateral strike slip motion is deduced using focal mechanism data (Kolarsky *et al*., 1995a). However, mesoscale ENE-WSW folds and asymmetry of minor structures (e.g., network of tension gashes, cataclasites, etc.) suggest a dextral transpression with dominant reverse, dip-slip motion at least during Paleogene times (Corral *et al*., 2011). The inferred minimum vertical offset is 300-400 m, with the southern block uplifted with respect to the northern block. The Pedasí Fault Zone (PFZ) is

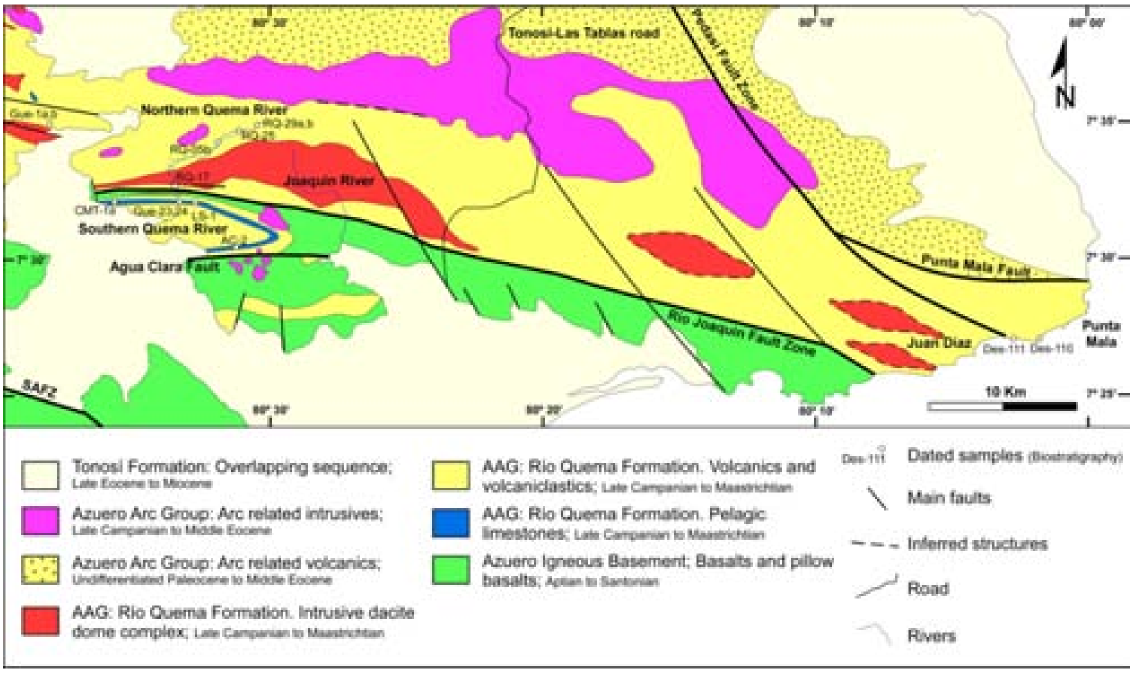

Figure 3.2: Detailed geological map of the Central and Southeastern Azuero peninsula. AAG: Azuero Arc Group, SAFZ: Soná-Azuero Fault Zone.

a secondary, regional structure, with NW-SE orientation affecting the eastern Azuero Peninsula (Fig. 3.2). A sinistral strike-slip motion is inferred for the PFZ, according to new neotectonic data from Rockwell *et al*, (2010) and also in concordance to the relative orientation with respect to the main regional faults of the area (e.g., Soná-Azuero Fault Zone; Cowan *et al*., 1998; Mann and Corrigan, 1990). Finally, several smaller Neogene transtensional normal faults, with NW-SE orientation, cut across the RQF, producing minor displacements (Fig. 3.2).

3.4. Facies analysis

Volcanic aprons comprise a complex assemblage of primary volcanic, resedimented volcaniclastic, and volcanogenic sedimentary facies that are governed by the interaction between volcanism, tectonics and surface processes, involving erosion, transport, and deposition (e.g., Mitchell, 1970; Sigurdsson *et al*., 1980; Houghton and Landis, 1989; McPhie, 1995).

Submarine volcaniclastic aprons are particularly informative because of their proximity to the volcanic source (Allen *et al*., 2007). These successions commonly provide the only record of volcanic activity, particularly with regard to "fragile" stratovolcanoes and composite cones, otherwise prone to erosion and mass wasting.

In the Azuero Peninsula (Fig. 3.2), this volcanic apron is represented by the Río Quema Formation, characterized by a volcanosedimentary sequence composed of volcanic and volcaniclastic sediments interbedded with hemipelagic limestones, submarine dacite lava domes and intruded by basaltic to andesitic dikes. The RQF represents the fore-arc basin sequence that unconformably lies on top of the Azuero Igneous Basement as well as on top of the Azuero Primitive Volcanic Arc. The RQF crops out extensively from the central to the southeastern Azuero Peninsula (Fig. 3.2), and allows the study of facies along the volcanic arc margin as well as towards the trench.

In order to reconstruct the paleoenvironmental model, we have followed the criteria used in previous works on volcanic sedimentology (e.g., Walton, 1979; Palmer and Walton, 1990; Nehlig *et al*., 2001; Allen, 2007; Manville *et al*., 2009). Accordingly, in the Río Quema Formation we have distinguished three different facies associations (Fig. 3.3):

1) The **Proximal apron** is a sequence dominated by lava flows, interbedded with breccias, debris flows and channel infilling sediments, crosscut by basaltic dikes. Lavas are andesites and basalts, 50 to 200 cm thick. Hyaloclastitic textures and autobrecciation are observed in those lavas. Debris flows are layers, 50 to 100 cm thick, of andesitic, basaltic and sedimentary angular pebbles in a fine grained matrix. The pebbles range from 5 to 40 cm in diameter. In the Punta Mala area, two types of breccias are identified, matrix-supported breccias with andesitic and basaltic subangular pebbles of 3 to 40 cm (Fig. 3.4A), and clast-supported breccias with basaltic angular pebbles of 10 to 70 cm in diameter. Moreover, we have also observed coarse crystal-rich sandstones and very thick turbidites with incomplete Bouma sequence, interpreted as channel fill. Finally, a swarm of basaltic dikes (50 to 100 cm thick) intruded the sequence. A synthetic stratigraphic section of proximal apron facies

could not be performed because most exposed rocks are disrupted by faults and covered by modern sediments.

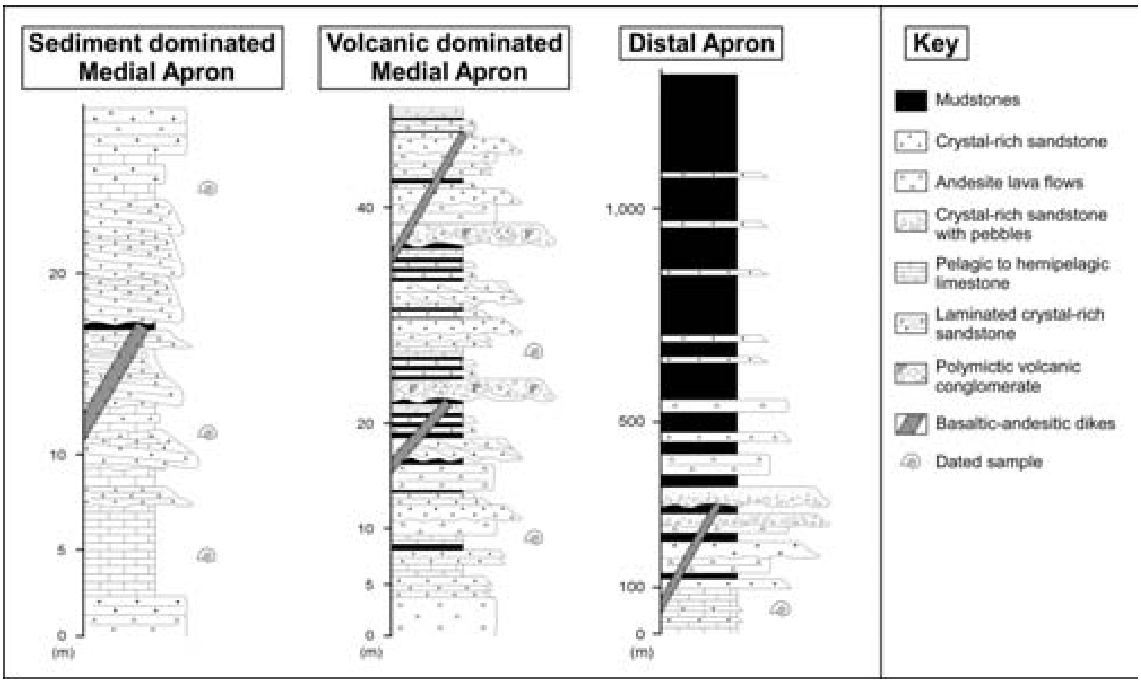

Figure 3.3: Synthetic stratigraphyc sections of the sediment dominated Medial Apron, volcanic dominated Medial Apron and Distal Apron facies of the Río Quema Formation.

2) The **Medial apron** is characterized by a volcanosedimentary succession dominated by andesitic lavas, polymictic volcanic conglomerates and crystal-rich sandstones with minor pelagic sediments and turbidites. Basaltic and andesitic dikes intruded the entire sequence. Facies of the Medial apron are best exposed in the Northern Quema River area. This part of the apron is usually dominated by volcanic rocks, but due to the volcanism heterogeneity there are intervals where the presence of volcanic rocks is not dominant. These zones are characterized by pelagic sediments and medium to coarse-grained crystal-rich sandstones with minor volcanic rocks. Therefore, in the Medial apron, we propose to distinguish between two types of depositional environment: a) the sediment-dominated medial apron and b) the volcanic-dominated medial apron (Fig. 3.3).

The sediment-dominated medial apron consists of a sequence of crystal-rich sandstones interlayered with pelagic-hemipelagic sediments, mainly limestones and mudrocks, as well as interbedded andesitic lava flows (Fig. 3.4B). Crystal-rich sandstone beds range from 60 to 200 cm thick, are very coarse to medium-grained, and grade upward to fine-grained. These beds often show cross bedding, parallel flow lamination and erosive bases. The crystal-rich sandstones are composed of lithic fragments, quartz, plagioclase, augite and epidote. Pelagic-hemipelagic limestones are thin-bedded fossiliferous micritic mudstones with very thin interbedded ash layers. These limestone layers range in thickness from 60 to 900 cm. Andesite lavas vary from equigranular to porphyritic and are 70 cm thick. The mineralogical components are quartz, plagioclase, augite, chlorite, epidote and pyrite, suggesting an incipient spilitization process.

The volcanic-dominated medial apron is composed of andesitic lavas and volcanic conglomerates with interbedded sedimentary rocks (e.g., crystal-rich sandstones, turbidites and pelagic sediments) (Fig. 3.4C). Andesitic lava flows are 50 to 200 cm thick, are mostly porphyritic, although some equigranular andesite lavas have also been observed. Lavas are composed of quartz, plagioclase, augite, chlorite, epidote and pyrite. In the case of the porphyritic lavas, phenocrysts occur in a microcrystalline quartz-feldspar matrix. Volcanic conglomerates are polymictic, with dacite pebbles (containing phenocrysts of hornblende and quartz), and pebbles of andesite, containing augite and plagioclase crystals. Pebbles size ranges from 5 to 40 cm. Conglomerate layers are up to 3 m thick and have sharp erosional bases. Crystal-rich sandstones are composed of lithic fragments, quartz, augite, plagioclase and epidote. Sandstone layers are usually 50 to 100 cm thick, but in some cases reach up to 250 cm in thickness. Turbiditic deposits consist of an alternation of thin bedded (5 to 10cm) sandstones and mudstones, showing complete Bouma sequences. Turbiditic layers usually range from 1 to 3 m thick. Pelagic sediments are represented by very thin fossiliferous pelagic limestone beds, typically on top of the turbiditic layers. Finally, a series of basaltic to andesitic dikes, 50 to 100cm thick, intruded the whole sequence.

3) The **Distal apron** comprises a thick succession (more than 1000 m) of sandy and muddy volcaniclastic facies, interbedded with pelagic limestones and

Figure 3.4: A) Matrix-supported basaltic-andesitic breccias, cropping out in Punta Mala area, corresponding to the Proximal Apron facies. B) Pelagic limestone interbedded with volcaniclastic crystal-rich sandstone, cropping out in Northern Quema River area, corresponding to the Sediment dominated Medial Apron facies. C) Polymictic conglomerate showing the andesitic and dacitic pebbles lithology, cropping out in Northern Quema River area, corresponding to the Volcanic dominated Medial Apron facies. D) Well bedded volcanic mudstones and very fine grained turbiditic layers, cropping out tin Southern Quema River area, corresponding to the Distal Apron facies.

andesitic lavas. Dacite domes and crosscutting basaltic to andesitic dikes have also been observed (Fig. 3.3). Facies of the Distal apron are extensively exposed in the Southern Quema river area, along the Joaquín river, at the Tonosí-Las Tablas road and near the Juan Díaz locality.

The base of the distal apron sequence is characterized by the presence of well bedded ~100 m thick pelagic limestone strata, a fossiliferous micritic limestone characterized by the presence of planktonic microfossils, and by some interbedded thin ash layers. Distal sediments consist of thin- to medium-bedded volcaniclastic sandstones, interbedded with 5 to 60 cm thick, mudstone layers. The sandstone beds are composed of sub-rounded lithic fragments, quartz crystals, augite, plagioclase and epidote in a fine grained chloritized matrix. Most sandstone beds are plane-parallel, commonly showing sharp-bases, incomplete Bouma sequences and mudstone tops or even lime-mudstone tops (Fig. 3.4D). Moreover, we have observed some layers of very coarse crystal-rich sandstones of 50 to 100 cm thickness, with erosional bases. Composition of these sandstones is similar to that of the thin bedded turbidites.

Lavas vary from equigranular to porphyritic andesites of 50 to 150 cm thickness, composed of quartz, augite, plagioclase, epidote, chlorite and pyrite. The andesitic lavas are also characterized by an incipient to well developed spilitization.

Dacites belong to a dome complex intruded in the transition zone between the distal and medial apron (not shown in Fig. 3.3). Dacite domes appear most conformably with the volcano-sedimentary sequence, although in some places they cut across the sequence. Dacite domes are up to 300-400 m thick and sometimes show flow lamination and hialoclastitic textures. Quartz and hornblende occur as phenocrysts (up to 5 cm in the case of hornblende) and smaller plagioclase crystals are observed in a microcrystalline quartz-feldspar matrix. Basaltic to andesitic dikes of 50 to 150 cm thick commonly intrude perpendicular to the stratification, but a few sills have been also found.

3.5. Biostratigraphy

The age of the Río Quema Formation is not well constrained despite of the amount of radiometric and biostratigraphic dating performed in the Azuero Peninsula (e.g., Del Giudice and Recchi, 1969; Kesler *et al*., 1977; Bourgois *et al*., 1982; Kolarsky *et al*., 1995b; Lissinna, 2005; Buchs *et al*., 2010). The RQF is enclosed within the Azuero Arc Group, where the Cretaceous and Paleogene volcanic arcs have not been differentiated so far. However, Corral *et al*. (2011) postulated the age of the RQF as Late Cretaceous, therefore, the Río Quema Formation could be part of the initial stages of the Azuero Arc Group.

In order to better constrain the age of the Río Quema Formation, as well as to understand the initial stages of the Panamanian Cretaceous Volcanic Arc, a biostratigraphical study was carried out. Sixteen thin sections of pelagic-hemipelagic limestones and mudstones from different depositional environments and localities of the Azuero Peninsula have been studied (see Fig. 3.2 for location and Table 3.1). A summary of the identified pelagic foraminifera and radiolarian is presented in Table 3.2 and in figure 3.5.

Based on the presence of the planctonic foraminifera *Globigerinelloides* cf. *prairiehillensis* Pessagno, *Heterohelix globulosa, Globotruncana* cf. *linneiana* and *Rugoglobigerina rugosa*, and the radiolarians *Pseudoaulophacus lenticulatus*, *Archaeodictyomitra lamellicostata* and *Pseudoaulophacus* sp., the age of our samples range from Late Campanian (e.g., OCU-01 and QUE-24) to Maastrichtian (e.g., RT-01 and RQ-17). These data represent a well constrained age for the Río Quema Formation as well as for the Panamanian Cretaceous volcanic arc, from Late Campanian to Maastrichtian.

Sample	Rock	Locality	Coordinates (UTM,WGS 84)		Age
AC-2	100 m thick pelagic limestone level of the RQF	Agua Clara	552858.00	829707.00	Campanian-Maastrichtian
CMT-01A	100 m thick pelagic limestone level of the RQF	Tonosi-Macaracas road	544526.21	832995.47	Campanian-Maastrichtian
DES-110	Mudstone interbedded with basaltic flow	Destiladeros beach	607085.00	823633.00	Upper Cretaceous
DES-111	Mudstone interbedded with basaltic flow	Destiladeros beach	605391.00	823726.00	Upper Cretaceous
GUE-1A	Pelagic limestone	Cerro Corazón del Mundo	541921.09	837826.41	Lower Maastrichtian
GUE-1B	Pelagic limestone	Cerro Corazón del Mundo	541921.09	837826.41	Lower Maastrichtian
LS-01	100 m thick pelagic limestone level of the RQF	Filo Jagüe	551392.98	832286.04	Lower Maastrichtian
OCU-01	Pelagic limestone	Ocu Quarry	525919.00	873264.00	Upper Campanian
QUE-23	100 m thick pelagic limestone level of the RQF	Southern Quema River	549004.38	832957.88	Campanian-Maastrichtian
QUE-24	100 m thick pelagic limestone level of the RQF	Southern Quema River	549004.38	832957.88	Upper Campanian
RQ-05B	Pelagic limestone interbedded with volcaniclastic sediments	Northern Quema River	551690.68	837052.49	Maastrichtian
RQ-17	Pelagic limestone interbedded with dacite lava dome	Southern Quema River	548685.19	834240.99	Maastrichtian
RQ-25	Pelagic limestone interbedded with volcaniclastic sediments	Northern Quema River	552990.67	837676.83	Campanian-Maastrichtian
RQ-29A	Hemipelagic limestone affected by wave ripples	Northern Quema River	554164.86	837945.59	Lower Maastrichtian
RQ-29B	Hemipelagic limestone affected by wave ripples	Northern Quema River	554164.86	837945.59	Lower Maastrichtian
RT-01	Pelagic limestone interbedded with basaltic flow	Torio River	507690.00	835052.00	Maastrichtian

Table 3.1: Description, location and age of the biostratigraphical study samples.

		AC-2	CMT-01A	LS-01	QUE-23	QUE-24	RQ-25	RQ-05B	RQ-29A	RQ-29B	RQ-17	GUE-1A	GUE-1B	RT-01	OCU-01	DES-110	DES-111
Foraminifera	*Globotruncana* cf. *ventricosa*	x															
	Globotruncanella cf. *petaloidea*	x												x			
	Globotruncana sp.		x			x					x						
	Globigerinelloides cf. *prairiehillensis* Pessagno		x	x								x			x		
	Globigerinelloides prairiehillensis Pessagno				x	x								x			
	Globigerinelloides cf. *Subcarinata*		x	x								x	x				
	Rugoglobigerina sp.		x			x						x					
	Globotruncana cf. *arca*		x														
	Heterohelix globulosa		x		x	x			x					x	x		
	Globotruncanita cf. *conica*			x		x			x			x	x				
	Globotruncana cf. *linneiana*			x								x	x				
	Rugoglobigerina rugosa			x	x	x		x			x				x		
	Globotruncana cf. *lapparenti* Brotzen			x	x												
	Rugoglobigerina sp. cf. *R. macrocephala* Brönnimann														x		
	Globotruncanita stuarti														x		
	Globotruncanita suartiformis														x		
	Globotruncanita calcarata					x									x		
	Globotruncanella sp.							x	x								
	Abattomphalus cf. *mayaroensis*							x			x						
	Archeoglobigerina sp.							x									
	Globotruncanella cf. *citae*										x						
	Globotruncana cf. *aegyptiaca* Nakkady								x	x				x			
Radiolaria	*Arqueoglobigerina* cf. *blowi* Pessagno													x			
	Ganserina cf. *ganseri*													x			
	Pseudoaulophacus lenticulatus	x	x	x			x	x				x	x		x		
	Archaeodictyomitra lamellicostata		x	x	x	x	x	x	x	x		x	x	x	x		
	Pseudoaulophacus sp.															x	x
	Theocampe sp.											x					
	Dictyomitra sp. cf. *D. koslovae* Foreman				x												
	Theocampe salillum Foreman					x				x	x						
	Cryptamphorella conara							x			x			x			

Table 3.2: Planktonic foraminifera and radiolarian found in the studied samples.

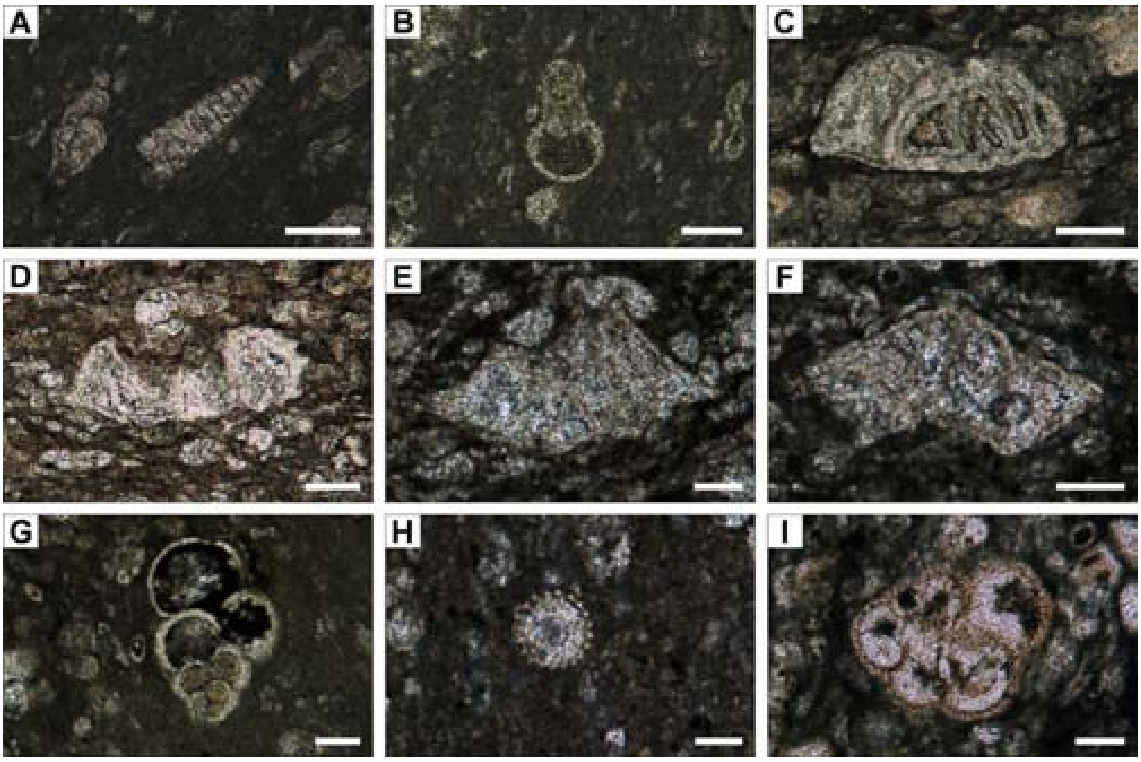

Figure 3.5: Planktonic foraminifera and radiolarian in samples from the Rio Quema Formation. Bar is equivalent to 100 µm. A: *Archaeodictyomitra lamellicostata*, B: *Globigerinelloides prairiehillensis* Pessagno, C: *Globotruncana* cf. *aegyptiaca* Nakkady, D: *Globotruncana* cf. *lapparenti* Brotzen, E: *Globotruncanita calcarata,* F: *Globotruncanita stuarti,* G: *Heterohelix globulosa,* H: *Pseudoaulophacus lenticulatus,* I: *Rugoglobigerina rugosa.*

3.6. Discussion

Oceanic volcanic arcs (and emergent oceanic island volcanoes) are typically surrounded by large aprons of volcaniclastic material (Manville *et al*., 2009). In the Azuero Peninsula the volcaniclastic apron of the Cretaceous volcanic arc is represented by the Río Quema Formation, interpreted as the fore-arc depositional sequence (Corral *et al*., 2011).

During the Cretaceous, Panama was part of the intra-oceanic subduction zone of the Farallon plate (a thin oceanic crust) beneath the Caribbean plate (a thick oceanic plateau). According to the models of Stern and Bloomer (1992) and Stern (2010), the initial intra-oceanic subduction is characterized by extension of the overriding plate. In the Azuero peninsula, this extension controlled the morphology and the evolution of the volcanic arc, generating a narrow fore-arc basin which was limited to the south by a topographyc hig that

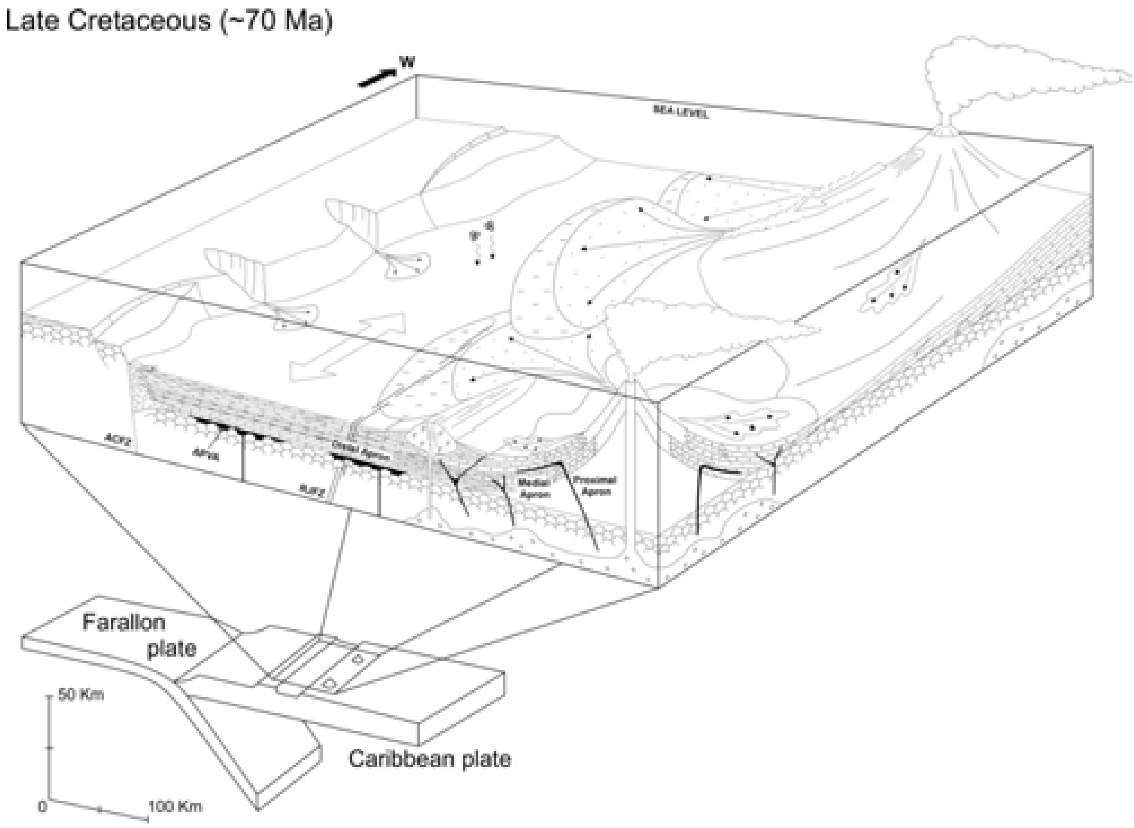

Figure 3.6: Paleoenvironmental reconstruction of the Panamanian Cretaceous intra-oceanic volcanic arc in the Late Campanian-Maastrichtian times (~70 Ma). RJFZ: Río Joaquín Fault Zone, ACFZ: Agua Clara Fault Zones, APVA: Azuero Primitive Volcanic Arc.

corresponded to the fore-bulge, affected by several E-W trending faults (e.g., Agua Clara and Río Joaquín Fault Zones) and limited in the North by the volcanic arc front.

Once volcanism started, volcanic aprons began to fill the fore-arc basin, recording volcanic events, tectonic pulses and sedimentary processes (Fig. 3.6). The detailed study of the Río Quema Formation shows coarsening from the south (Distal apron) towards the north (Proximal apron) of the fore-arc basin. Southern facies are dominated by mudstones, fine grained turbidites and pelagic limestone layers. Northern facies are dominated by basaltic and andesitic breccias and lava flows, polymictic volcanic conglomerates and are intruded by dike swarms (Fig. 3.6).

The Proximal apron reflects coarse sediment supply in a similar environment to the gravel-rich fan deltas and submarine slopes (e.g., Heller and Dickinson, 1985; Reading, 1991; Allen *et al*., 2007).

The Medial volcaniclastic apron consists of coarse-grained crystal-rich sandstones, polymictic conglomerates and andesitic lava flows, with a contribution of pelagic and turbiditic deposits. These sediments were most likely deposited from high-density turbidity currents and debris flows, derived directly from erupted material and from mass wasting of the unstable volcanic edifice or volcaniclastic apron (e.g., Houghton and Landis, 1989). The lavas, dikes and breccias within the Medial apron mark locations of contemporaneous submarine vents.

The Distal volcaniclastic apron is characterized by sandy and muddy facies interbedded with pelagic limestones with minor contribution of andesitic lavas. Bedforms and fossil evidence suggest a quiet, relatively deep-water bathyal environment in which suspension settling and dilute turbidity currents carried reworked volcaniclastic detritus (e.g., Allen *et al*., 2007). Despite the relatively quiet environment, tool marks, cross bedding and ripple marks locally show paleocurrents in the E-W direction, suggesting axial transport in a narrow fore-arc basin.

A dacite dome complex intruded in the interface between the distal and medial volcaniclastic apron. The intrusion produced volcaniclastic material through explosive magma-water interaction, autobrecciation and resedimentation of the dacite dome complex as mass flows, turbidites, and water-settled fallout (Cas *et al*., 1990; Kano *et al*., 1991; Cashman and Fiske, 1991; Fiske *et al*., 1998) contributing to the coarse sediment found in the distal apron.

Based on our biostratigraphic data, the age of Río Quema Formation and the formation of the volcaniclastic apron is Late Campanian to Maastirchtian. This age is in good agreement with previous studies carried out in the north and west of the Azuero Peninsula, corresponding to the limestones exposed in the Ocú quarry and Torio river (Del Giudice and Recchi, 1969; Weyl, 1980 and Buchs *et al*., 2010).

3.7. Conclusions

1) The Río Quema Formation represents the Proximal, Medial and Distal apron of an active island arc, which filled the fore-arc basin. The formation records the initial stages of the Panamanian volcanic arc.

2) Facies distribution shows lateral changes with coarser sediments in the north (Proximal apron) and finer sediments in the south (Distal apron) of the fore-arc basin. This suggests that the main sediment source is in the north, corresponding to the volcanic arc front, while a minor sediment contribution occurs in the south, providing from the fore-bulge erosion. Moreover, some indicators (e.g., ripples and tool marks) suggest an axial transport in a narrow fore-arc basin.

3) Our biostratigraphic data indicates an age from Late Campanian to Maastrichtian for the Río Quema Formation, constraining the age of the first volcanic arc developed on the Caribbean plate in the Panamanian region.

3.8. References

ALLEN S. R., HAYWARD B. W. & MATHEWS E. (2007). – A facies model for a submarine volcaniclastic apron: The Miocene Manukau Subgroup, New Zealand. – *Geol. Soc. Am. Bull.,* **119**, 725-742.

BARCKHAUSEN U., RANERO C. R., VON HUENE R., CANDE S. C. & ROESER H. A. (2001). – Revised tectonic boundaries in the Cocos Plate off Costa Rica; implications for the segmentation of the convergent margin and for plate tectonic models. – *J. Geophys. Res.,* **106**, 19,207-19,220.

BOURGOIS J., AZE´MA, J., TOURNON, J., BELLON, H., CALLE, B., PARRA, E., TOUSSAINT, J.-F., GLAC¸ON, G., FEINBERG, H., DE WEVER, P., ORGILIA, I. (1982). – Age et structures des complexes basiques et ultrabasiques de la facade pacifique entre 3ºN et 12ºN (Colombie, Panama et Costa Rica). – *B. Soc. Geol. Fr.,* **24**, 545-554.

BUCHS D. M. (2008). – Late Cretaceous to Eocene geology of the South Central American forearc area (southern Costa Rica and western Panama): Initiation and evolution of an intra-oceanic convergent margin. – Thesis, University of Lausanne, 230 p.

BUCHS D. M., BAUMGARTNER P. O., BAUMGARTNER MORA C., BANDINI A. N., JACKETT S.-J., DISERENS M.-O. & STUCKI J. (2009). – Late Cretaceous to Miocene seamount accretion and melange formation in the Osa and Burica Peninsulas (southern Costa Rica);

episodic growth of a convergent margin. – *In:* JAMES K. H., LORENTE M. A., & PINDELL J. L., Eds., The origin and evolution of the Caribbean plate. – *Geol. Soc.,* Sp. Publ., **328**, 411-456.

BUCHS D. M., ARCULUS R. J., BAUMGARTNER P. O., BAUMGARTNER-MORA C. & ULIANOV A. (2010). – Late Cretaceous arc development on the SW margin of the Caribbean Plate: Insights from the Golfito, Costa Rica, and Azuero, Panama, complexes. – *Geochem. Geophy. Geosy.,* **11**, Q07S24.

BUCHS D. M., ARCULUS R. J., BAUMGARTNER P. O. & ULIANOV A. (2011). – Oceanic intraplate volcanoes exposed: Example from seamounts accreted in Panama. – *Geology*, **39**, 335-338.

CAS R. A. F., ALLEN R. L., BULL S. W., CLIFFORD B. A. & WRIGHT J. V. (1990). – Subaqueous, rhyolitic dome-tome tuff cones; a model based on the Devonian Bunga Beds, southeastern Australia and a modern analogue. – *B. Volcanol.,* **52**, 159-174.

CASHMAN K. V. & FISKE R. S. (1991). – Fallout of pyroclastic debris from submarine volcanic eruptions. – *Science*, **253**, 275-280.

COATES A. G., COLLINS L. S., AUBRY M.-P. & BERGGREN W. A. (2004). – The Geology of the Darien, Panama, and the late Miocene-Pliocene collision of the Panama arc with northwestern South America. – *Geol. Soc. Am. Bull.,* **116**, 1327-1344.

CORRAL I., GRIERA A., GÓMEZ-GRAS D., CORBELLA M., CANALS À., PINEDA-FALCONETT M. & CARDELLACH E. (2011). – Geology of the Cerro Quema Au-Cu deposit (Azuero Peninsula, Panama). – *Geol. Acta.,* **9**, 481-498.

COWAN H., DART R. L. & MACHETTE M. N. (1998). – Map of Quaternary faults and folds of Panama and its offshore regions, scale 1:250,000. – *Open-File Rep. - U. S. Geol. Surv*.

DEL GIUDICE D. & RECCHI G. (1969). – Geología del área del Proyecto Minero de Azuero. – Informe técnico preparado para el gobierno de la Republica de Panama por las Naciones Unidas. Panamá City (Panamá), Gobierno de la República de Panamá, 48 p.

DICKINSON W. R. (1974a). – Plate tectonics and sedimentation. Sp. Publ. – *Soc. Econ. Paleontol. Mineral*., *Sp. Publ.*, **22**, 1-27.

DICKINSON W. R. (1974b). – Sedimentation within and beside ancient and modern magmatic arcs. – *Soc. Econ. Paleontol. Mineral*., *Sp. Publ.*, **19**, 230-239.

DIRECCIÓN GENERAL DE RECURSOS MINERALES. (1976). Panama Geologic Map 1:250,000. Panama City, Panama.

FISHER D. M., GARDNER T. W., MARSHALL J. S., SAK P. B. & PROTTI M. (1998). – Effect of subducting sea-floor roughness on fore-arc kinematics, Pacific coast, Costa Rica. – *Geology*, **26**, 467-470.

FISKE R. S., CASHMAN K. V., SHIBATA A. & WATANABE K. (1998). – Tephra dispersal from Myojinsho, Japan, during its shallow submarine eruption of 1952-1953. – *B. Volcanol.,* **59**, 262-275.

GARDNER T., MARSHALL J., MERRITTS D., BEE B., BURGETTE R., BURTON E., COOKE J., KEHRWALD N., PROTTI M., FISHER D. & SAK P. (2001). – Holocene forearc block rotation in response to seamount subduction, southeastern Peninsula de Nicoya, Costa Rica. – *Geology*, **29**, 151-154.

HAUFF F., HOERNLE K., VAN DEN BOGAARD P., ALVARADO G. & GARBE-SCHOENBERG D. (2000). – Age and geochemistry of basaltic complexes in western Costa Rica; contributions to the geotectonic evolution of Central America. – *Geochem. Geophy. Geosy.,* **1**.

HELLER P. L. & DICKINSON W. R. (1985). – Submarine ramp facies model for delta-fed, sand-rich turbidite systems. – *AAPG Bull.*, **69**, 960-976.

HOERNLE K., VAN DEN BOGAARD P., WERNER R., LISSINNA B., HAUFF F., ALVARADO G. & GARBE-SCHONBERG D. (2002). – Missing history (16-71 Ma) of the Galapagos hotspot: Implications for the tectonic and biological evolution of the Americas. – *Geology*, **30**, 795-798.

HOERNLE K., HAUFF F. & VAN DEN BOGAARD P. (2004). – 70 m.y. history (139-69 Ma) for the Caribbean large igneous province. – *Geology*, **32**, 697-700.

HOUGHTON B. F. & LANDIS C. A. (1989). – Sedimentation and volcanism in a Permian arc-related basin, southern New Zealand. – *B. Volcanol.,* **51,** 433-450.

KANO K. (1991). – Volcaniclastic sedimentation in a shallow-water marginal basin; the early Miocene Koura Formation, SW Japan. – *Sediment. Geol.*, **74**, 309-321.

KEIGWIN L. D., JR. (1978). – Pliocene closing of the Isthmus of Panama, based on biostratigraphic evidence from nearby Pacific Ocean and Caribbean Sea cores. – *Geology*, **6**, 630-634.

KENNAN L. & PINDELL J. L. 2009. – Dextral shear, terrane accretion and basin formation in the Northern Andes; best explained by interaction with a Pacific-derived Caribbean Plate? – *Geol. Soc., Sp. Publ.,* **328,** 487-531.

KESLER S. E., SUTTER J. F., ISSIGONIS M. J., JONES L. M. & WALKER R. L. (1977). – Evolution of porphyry copper mineralization in an oceanic island arc; Panama. – *Econ. Geol.,* **72**, 1142-1153.

KOLARSKY R. A. & MANN P. (1995a). – Structure and neotectonics of an oblique-subduction margin, southwestern Panama. – *Geol. Soc. Am. Bull. Sp. Publ.,* **295**, 131-157.

KOLARSKY R. A., MANN P., MONECHI S., MEYERHOFF-HULL D. & PESSAGNO E. A. (1995b). – Stratigraphic development of southwestern Panama as determined from integration of marine seismic data and onshore geology. – *Geol. Soc. Am. Bull. Sp. Publ.,* **295**, 159-200.

KRAWINKEL H., WOZAZEK S., KRAWINKEL J. & HELLMANN W. (1999). – Heavy-mineral analysis and clinopyroxene geochemistry applied to provenance analysis of lithic sandstones from the Azuero-Soná Complex (NW Panama). – *Sediment. Geol.,* **124**, 149-168.

LISSINNA B., HOERNLE K. & VAN DEN BOGAARD P. (2002). – Northern migration of arc volcanism in western Panama; evidence for subduction erosion? – *Eos. Trans. AGU*, **83**, 1463-1464.

LISSINNA B. (2005). – A profile through the Central American Landbridge in western Panama: 115 Ma Interplay between the Galápagos Hotspot and the Central American Subduction Zone. – Thesis, Christian-Albrechts-Universität zu Kiel, 102 p.

LISSINNA B., HOERNLE K., HAUFF P., VAN DEN BOGAARD P. & SADOFSKY S. (2006). – The Panamanian island arc and Galápagos hotspot: A case study for the long-term evolution of arc/hotspot interaction. – *Geophysical Research* (Abst.) **8**, 05106.

LONSDALE P. (2005). – Creation of the Cocos and Nazca plates by fission of the Farallon Plate. *Tectonophysics*, **404**, 237-264.

MANN P. & CORRIGAN J. (1990). – Model for late Neogene deformation in Panama. – *Geology*, **18**, 558-562.

MANVILLE V., NEMETH K. & KANO K. (2009). – Source to sink; a review of three decades of progress in the understanding of volcaniclastic processes, deposits, and hazards. – *Sediment. Geol.,* **220**, 136-161.

MCPHIE J. (1995). – A Pliocene shoaling basaltic seamount; Ba Volcanic Group at Rakiraki, Fiji. – *J. Volcanol. Geoth. Res.,* **64**, 193-210.

MITCHELL A. H. G. (1970). – Facies of an early Miocene volcanic arc, Malekula island, New Hebrides. – *Sedimentology*, **14**, 201-243.

NEHLIG P., LEYRIT H., DARDON A., FREOUR G., DE GOER DE HERVE A., HUGUET D. & THIEBLEMONT D. (2001). – Constructions et destructions du stratovolcan du Cantal. – *B. Soc. Geol. Fr.,* **172**, 295-308.

PALMER B. A. & WALTON A. W. (1990). – Accumulation of volcaniclastic aprons in the Mount Dutton Formation (Oligocene-Miocene), Marysvale volcanic field, Utah. – *Geol. Soc. Am. Bull.,* **102**, 734-748.

PINDELL J. L. (1993). – Regional synopsis of Gulf of Mexico and Caribbean evolution. – *Soc. Econ. Paleontol.* (Abst.), **13**, 251-274.

PINDEL J. L., HIGGS R. & DEWEY J. F. (1998). – Cenozoic palinspastic reconstruction, paleogeographic evolution, and hydrocarbon setting of the northern margin of South America. *In:* PINDELL J. L. & DRAKE C. L. Eds. – Paleogeographic Evolution and Non-glacial Eustasy, northern South America. – *Soc. Sediment. Geol.,* Sp. Publ., **58**, 45-86.

PINDELL J. L. & KENNAN L. (2009). – Tectonic evolution of the Gulf of Mexico, Caribbean and northern South America in the mantle reference frame; an update. *In:* JAMES K. H., LORENTE M. A., & PINDELL J. L., Eds., The origin and evolution of the Caribbean plate. – *Geol. Soc.,* Sp. Publ., **328**, 1-55.

READING H. G. (1991). – The classification of deep-sea depositional systems by sediment caliber and feeder system. – *J. Geol. Soc. London.,* **148**, 427-430.

RECCHI G. & MIRANDA R. (1977). – Calizas de los Planes-Guaniquito (Tonosí). Unpublished report, Panama City, Dirección General de Recursos Minerales, 27 p.

ROCKWELL T. K., BENNETT R. A., GATH E. & FRANCESCHI P (2010). – Unhinging an indenter: A new tectonic model for the internal deformation of Panama. – *Tectonics,* **29**.

SAK P. B., FISHER D. M. & GARDNER T. W. (2004). – Effects of subducting seafloor roughness on upper plate vertical tectonism; Osa Peninsula, Costa Rica. – *Tectonics*, **23**.

SIGURDSSON H., SPARKS R. S. G., CAREY S. N. & HUANG T. C. (1980). – Volcanogenic sedimentation in the Lesser Antilles. – *J. Geol.,* **88**, 523-540.

STERN R. J. & BLOOMER S. H. (1992). – Subduction zone infancy: Examples from the Eocene Izu-Bonin-Mariana and Jurassic California arcs. – *Geol. Soc. Am. Bull.,* **104**, 1621-1636.

STERN R. J. (2010). – The anatomy and ontogeny of modern intra-oceanic arc systems. – *In:* KUSKY T. M., ZHAI M. G. & XIAO W., Eds., – The evolving continents: Understanding Processes of Continental Growth. – *Geol. Soc.,* Sp. Publ., **338**, 7-34.

TRENKAMP R., KELLOGG J. N., FREYMUELLER J. T. & MORA H. P. (2002). – Wide plate margin deformation, southern Central America and northwestern South America, CASA GPS observations. – *J. S. Am. Earth. Sci.,* **15**, 157-171.

WADGE G. & BURKE K. (1983). – Neogene Caribbean plate rotation and associated Central American tectonic evolution. – *Tectonics*, **2**, 633-643.

WALTON A. W. (1979). – Volcanic sediment apron in the Tascotal Formation (Oligocene?), Trans-Pecos Texas. – *J. Sediment. Res.,* **49**, 303-314.

WEGNER W., WORNER G., HARMON R. S. & JICHA B. R. (2011). – Magmatic history and evolution of the Central American Land Bridge in Panama since Cretaceous times. – *Geol. Soc. Am. Bull.,* **123**, 703-724.

WERNER R., HOERNLE K., BARCKHAUSEN U. & HAUFF F. (2003). – Geodynamic evolution of the Galapagos hot spot system (central East Pacific) over the past 20 m.y.; constraints from morphology, geochemistry, and magnetic anomalies. – *Geochem. Geophy. Geosy.,* **4**.

WEYL R. (1980). Geology of Central America (2nd Ed), Gebrueder Borntraeger, Berlin.

WÖRNER G., HARMON R. S., HARTMANN G. & SIMON K. (2005). – Igneous geology and geochemistry of the upper Rio Chagres basin. *In:* HARMON R.S., Ed., The Río Chagres, Panama, Water Science and Technology Library, **52**, 65-82.

WÖRNER G., HARMON R. S., WEGNER W. & SINGER G. (2006). – Linking America's backbone: Geological development and basement rocks of central Panama. Abstrstracts with Programs. – *In:* Backbone of the Americas; shallow subduction, plateaus uplift, and ridge and terrane collision. – *Memoir. Geol. Soc. Am.,* **204**, 183 - 196.

WÖRNER G., HARMON R. S. & WEGNER W. (2009). – Geochemical evolution of igneous rocks and changing magma sources during the formation and closure of the Central American land bridge of Panama. *In:* KAY S. M., RAMOS V.A., & DICKINSON W. R., Eds., – Backbone of the Americas: Shallow Subduction, Plateau Uplift, and Ridge Terrane Collision, – *Geol. Soc. Am.,* **204**, 183-196.

CHAPTER 4

Volcanism and gold mineralization at the Cerro Quema Au-Cu deposit (Azuero Peninsula, Panama): Mineralization, hydrothermal alteration, geochemistry and geochronology

4.1. Introduction

Epithermal ore deposits were firstly defined by Lindgren (1922, 1923) as deposits formed from aqueous fluids charged with igneous emanations at shallow depth, including a broad range of precious metal, base metal, mercury and stibnite deposits. This definition, initially based on geologic reconstructions, ore mineralogy and related textures, was later completed by Berger and Eimon (1983) with fluid inclusion data, suggesting that epithermal ores formed over a temperature range of <150ºC to ~300ºC, from the surface to 1-2 km in depth. According to mineralogy and associated hydrothermal alteration, several classification schemes have been proposed: enargite-gold, Ashley (1982); high sulfur and low sulfur, Bonham (1984, 1986); acid sulfate and adularia-sericite, Hayba *et al*, (1985) and Heald *et al*, (1987); alunite-kaolinite and adularia-sericite, Berger and Henley (1989), among others. In the present work, the classification of Hedenquist (1987) and Hedenquist *et al*, (2000) is used: high sulfidation, intermediate sulfidation and low sulfidation, referring to the redox state of the sulfur present in the mineralizing fluid.

Epithermal precious metal deposits are commonly hosted by subaereal, calc-alkaline volcanic rocks that formed at convergent margins, island or continental arcs (Sillitoe, 1993; Arribas and Tosdal, 1994; Cooke and Simmons, 2000), as direct result of plate subduction. Epithermal deposits are scarce or absent in extensional tectonic regimes (Sillitoe *et al*., 1996), although submarine high sufidation epithermal Au-Cu deposits have been reported (e. g., Valu Fa Ridge, Lau basin, Southwest Pacific; Hannington and Herzig, 1993; Fouquet *et al*., 1993; Herzig *et al*., 1993; Pual Ridge, Conical seamount and Ladolam gold deposits, Papua New Guinea; Binns and Scott, 1993; Herzig *et al*., 1999; Petersen *et al*., 2002; Gemmell *et al*., 2004; Binns *et al*., 2007). This typology has been defined as high sulfidation epithermal deposits in the volcanogenic massive sulfide environment (Sillitoe *et al*., 1996).

Central America hosts a variety of metallic mineral resources including gold, copper, silver, lead, zinc, nickel, cobalt, antimony, tungsten and aluminum, spanning a broad range of deposit types (Nelson and Nietzen, 2000; Nelson, 2007). From a geodynamic point of view, South Central America is a region characterized by a long lived intra-oceanic subduction zone and by a volcanic arc activity since the Late Cretaceous, displaying the characteristics of zones where epithermal deposits can be potentially found. Gold and copper are the most economically important metals in Panama, and are mainly related to epithermal (e.g., Cana, Woakes, 1923; Nelson, 1995; Santa Rosa, Wleklinski, 1969; White, 1993; Nelson, 2001; Cerro Quema, Nelson, 1995, 2007; Corral *et al*., 2011a) and to porphyry copper systems (e.g., Petaquilla and Cerro Colorado, Kesler *et al*., 1977; Kesler, 1978; Nelson, 1995; Speidel, 2001), respectively.

The present study focuses on the Cerro Quema deposit (Azuero Peninsula, SW Panama), considered to be one of the most promising Au-Cu prospects in the country. Essentially, Cerro Quema is a composite structurally and lithologically controlled high sulfidation epithermal system, hosted by dacite domes, in a calc-alkaline volcanic arc environment (Corral *et al*., 2011a). Estimated gold resources are 7.23 Mt with an average gold grade of 1.10 g/T, containing 256,000 oz of Au in La Pava ore body (Valiant *et al*., 2011; Puritch, *et al*., 2012). Cerro Quema has also an economic potential for copper (Nelson, 2007; Corral *et al*., 2011a), but it has not been estimated so far.

Although hypogenic sulfides in the Cerro Quema deposit (e.g., pyrite, enargite, tennantite) and associated hydrothermal alteration minerals (e.g., alunite, kaolinite, pyrophyllite) are diagnostic of a high sulfidation state and acidic conditions of the fluids, the tectono-magmatic setting and depositional environment are different from those usually related to the classical high sulfidation deposits. Cerro Quema is associated to arc magmatisim, but in contrast with the classical high sulfidation epithermal models (e.g., Hedenquist, 1987; Sillitoe, 1989; White, 1991; Hedenquist and Lowenstern, 1994; Arribas, 1995), where these deposits are related to a volcanic edifice of the volcanic arc, Cerro Quema is located in the fore-arc basin.

Epithermal style mineralization, high-level porphyry systems and volcanogenic massive sulfide deposits may be end-members of a continuum (Hannington, 1997). From the geological and mineralogical characteristics, Cerro Quema has been considered as a high sulfidation epithermal system related to a underlying porphyry copper intrusion (Leach, 1992; Nelson, 1995), and as an oxidized Au-Cu deposit that shares characteristics of epithermal and VMS deposits (Nelson and Nietzen, 2000; Nelson, 2007). Thus, the definition of the deposit type for Cerro Quema is still a matter of debate.

In order to unravel the processes and conditions during ore deposition we first present the geological setting of the study area, followed by the description and discussion of new mineralogical, geochemical and geochronological (Ar/Ar) data. Finally, a conceptual genetic model is developed as a contribution to the understanding and exploration of high sulfidation Au-Cu deposits in ancient and modern terranes, with similar geological features.

4.2. Geologic setting

4.2.1. Regional geology

Panama is located in South Central America (Fig. 4.1A), an area geologically characterized by a long-lived intra-oceanic subduction zone. Panama represents the youngest segment of the land bridge between the North and South American plates, and is considered to be a tectonic block that lies at the junction of four tectonic plates, namely the Caribbean, South American, Cocos, and Nazca plates. A volcanic arc was developed since the Late Cretaceous as a result of the subduction of the ancient Farallon plate beneath the Caribbean plate. Volcanic arc magmatism continued until the Miocene (~23 Ma) (Barckhausen *et al*., 2001; Werner *et al*., 2003; Lonsdale, 2005; Buchs *et al*., 2009, 2010; Wörner *et al*., 2009; Pindell and Kennan, 2009). The accretion of sea mounts and oceanic plateaus to the subduction trench (Middle Eocene; Buchs *et al*., 2010), and the collision of the Panamanian volcanic arc with Colombia during Middle to Late Miocene (Keigwin, 1978; Wadge and Burke, 1983; Pindell *et al*., 1998; Trenkamp *et al*., 2002; Coates *et al*., 2004; Kennan and Pindell, 2009), produced a change of the subduction direction and migration of the volcanic arc towards the north (Lissinna, *et al*., 2002; Lissina, 2005). The Cordillera Central in north Panama is the present-day expression of the active Panamanian volcanic arc.

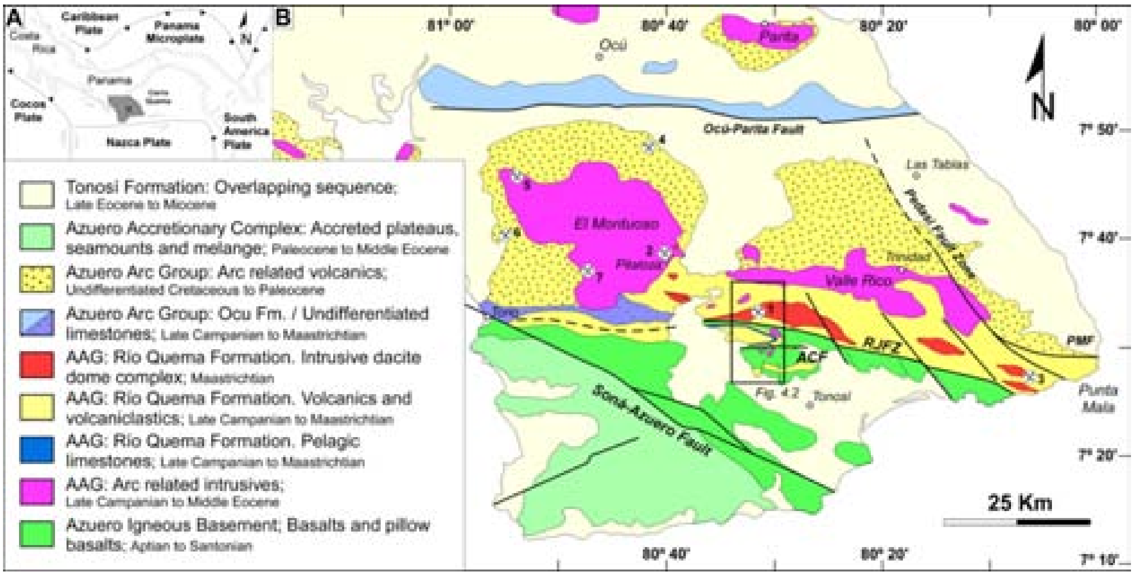

Figure 4.1: A) Plate tectonic setting of South Central America. B) Simplified geological map of the Azuero Peninsula with the main epithermal deposits. AAG: Azuero Arc Group, RJFZ: Río Joaquín Fault Zone, ACF: Auga Clara Fault, PMF: Punta Mala Fault (after Dirección General de Recursos Minerales, 1976; Buchs *et al*., 2011b; Corral *et al*., 2011a, 2013). Mineral deposits: 1) Cerro Quema, 2) Pitaloza, 3) Juan Díaz, 4) Las Minas, 5) Quebrada Barro, 6) Quebrada Iguana, 7) Cerro Viejo.

4.2.2. Geology of the Azuero Peninsula and the Cerro Quema deposit

Situated in SW Panama, the Azuero Peninsula is a region which host several epithermal deposits and prospects (e.g., Juan Diaz, Pitaloza, Las Minas, Cerro Viejo, see Fig. 4.1B). This high gold potential makes this region attractive for mining companies.

Geologically, the Azuero Peninsula is essentially composed by an igneous basement overlain by fore-arc sediments. It is constituted by volcanic, plutonic, sedimentary and volcanosedimentary rocks ranging in age from ~98 Ma to ~40 Ma (Del Giudice and Recchi, 1969; Bourgois *et al*., 1982; Kolarsky *et al*., 1995; Lissinna *et al*., 2002, 2006; Lissinna, 2005; Wörner *et al*., 2005, 2006, 2009; Buchs *et al*., 2010, 2011b; Wegner *et al*., 2011; Corral *et al*., 2011a, 2013).

Five distinct rock associations have been recognized in the Azuero Peninsula (Fig. 4.1B): 1) The Azuero Igneous Basement (AIB), composed by Upper Cretaceous (Aptian to Santonian) basalts and pillow basalts with geochemical affinities similar to the Caribbean Large Igneous Province (CLIP), and interpreted as the arc basement (Del Giudice and Recchi, 1969; Kolarsky *et al*., 1995; Hauff *et al*., 2000; Hoernle *et al*., 2002, 2004; Lissinna, 2005; Buchs *et al*., 2009, 2010; Corral *et al*., 2011a). 2) The Azuero Primitive Volcanic Arc (APVA), a non mapable unit constituted by basalts and volcaniclastic rocks with tholeiitic character, locally interbedded with late Campanian-Maastrichtian hemipelagic limestones, equivalent to the proto-arc defined by Buchs *et al*, (2010), and corresponding to the initial stages of the volcanic arc. 3) The Azuero Arc Group (AAG), constituted by volcano-sedimentary, volcanic and arc-related intrusive rocks (e.g., the Valle Rico and the El Montuoso batholiths; Fig. 4.1B) with calc-alkaline character, representing the Cretaceous and Paleogene volcanic arcs (Lissinna, 2005; Wörner *et al*., 2009; Buchs *et al*., 2010, 2011b; Wegner *et al*., 2011; Corral *et al*., 2011a, 2013). 4) The Tonosí Formation, a Middle Eocene to Early Miocene sedimentary sequence unconformably overlapping all the previously described units (Recchi and Miranda, 1977; Kolarsky *et al*., 1995; Krawinkel *et al*., 1999). 5) The Azuero Accretionary Complex, corresponding to Paleocene to Middle Eocene seamounts, oceanic plateaus and mélanges accreted along the ancient subduction trench (Hoernle *et al*., 2002; Lissinna, 2005; Hoernle and Hauff, 2007; Buchs *et al*., 2011a).

The tectonic setting of the Azuero Peninsula is characterized by several regional subvertical faults with dominant E-W and NW-SE direction (Fig. 4.1B). The main regional faults are the Soná-Azuero Fault zone (SAFZ) which strikes NW-SE, the Ocú-Parita fault, striking E-W and the Río Joaquín Fault Zone (RJFZ), with a broad E-W orientation (Kolarsky *et al*., 1995; Buchs, 2008; Corral *et al*., 2011a; 2013). The Río Joaquín Fault Zone (RJFZ) is a 30Km regional scale E-W trending fault zone, with a reverse dip-slip motion. Along this fault, the Azuero Igneous Basement is directly in contact with the Azuero Arc Group (Río Quema Formation). Secondary regional structures with NW-SE orientation are affecting the eastern Azuero Peninsula, as the Pedasí Fault Zone (PFZ) and the Punta Mala Fault (PMF), both with a sinistral strike-slip motion (Corral *et al*., 2013). At local scale, the center of the Azuero Peninsula is affected by a large network of faults with a predominantly NW-SE and NE-SW trend, showing subvertical dip and normal sense of offset and occasionally strike slip motion (Fig. 4.2). Moreover, mesoscale ENE-WSW open folds, with moderate limb dips

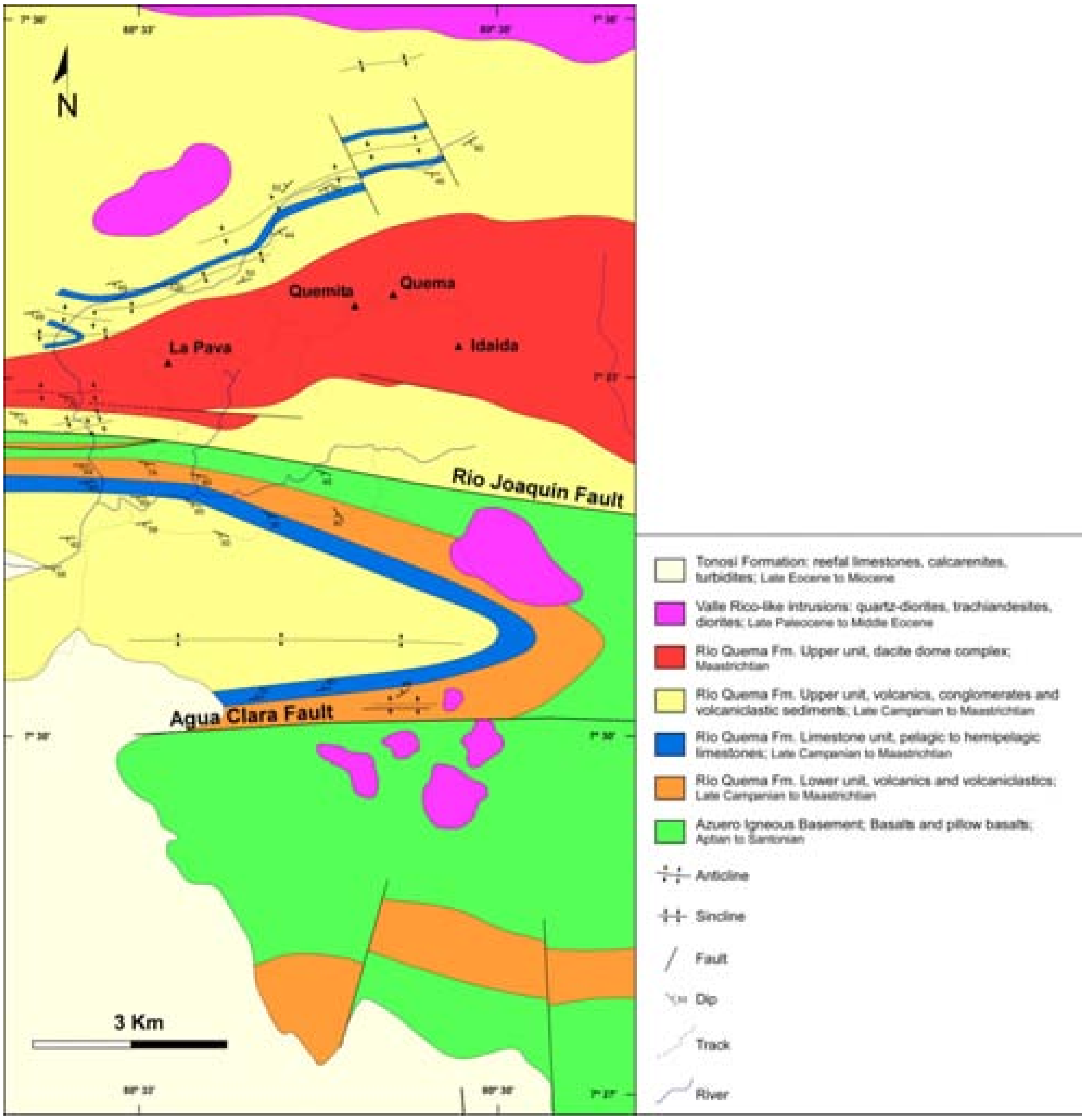

Figure 4.2: Simplified geologic map of Central Azuero Peninsula, and location of the Cerro Quema Au-Cu deposit (After Corral *et al*., 2011a, 2013).

and fold axes gently plunging to the SW are also characteristic of this area. All the previously described structures suggest a dextral transpression with dominant reverse dip-slip motion (Corral *et al*., 2011a, 2013).

Previous field-based studies on the stratigraphy of the mining area were carried out by Horlacher and Lehmann (1993) who differentiated two main units, 1) The Ocú Formation, composed of limestones and volcanosedimentary rocks, and 2) The Quema Formation made up of dacites and massive andesites. Recent works (Corral *et al*., 2011a, 2013) based on new field and geochemical data, and biostratigraphic correlations, defined a new litostratigraphic unit named Río Quema Formation (RQF), grouping the units defined by Horlacher and Lehmann (1993). The RQF constraints better the tectonic setting and the environment of deposition, facilitating the understanding of the geodynamic context.

The Río Quema Formation, which hosts the Cerro Quema deposit, is a volcanosedimentary sequence enclosed within the Azuero Arc Group. It is interpreted as the volcaniclastic apron of the Panamanian Cretaceous volcanic arc. This fore-arc sequence crops out from the central to the southeastern Azuero Peninsula, and based on biostratigraphic data is Late Campanian to Maastrichtian in age (Corral *et al*., 2013). The Río Quema Formation is composed of volcanic and volcaniclastic sediments interbedded with hemipelagic limestones, dacite lava domes and is intruded by basaltic to andesitic dikes. The total thickness of the Río Quema Formation is approximately 1,700 m, and is overlying both, the Azuero Igneous Basement and the Azuero Primitive Volcanic Arc, and discordantly overlapped by the Tonosí Formation. According to Corral *et al*, (2011a) the Río Quema Formation is constituted by three units (Fig. 4.3):

1) Lower Unit, constituted by andesitic lava flows and well bedded crystal-rich sandstone to siltstone turbidites, interbedded with hemipelagic thin limestone beds. 2) Limestone Unit, a thick light grey biomicritic hemipelagic limestone, interlayered with well bedded cherts, thin bedded turbidites and fine ash layers. 3) Upper Unit, composed of volcaniclastic sediments interlayered with massive to laminar andesitic lava flows, dacite domes, dacite hyaloclastites and polymictic conglomerates. Moreover, volcaniclastic turbidites, crystal-rich sandstones, siltstones and thin pelagic limestones beds have also been observed in the upper unit. Dacite domes appear mostly conformabe with the volcano-sedimentary sequence, although in some places they cut across the sequence. Dacite domes are up to 300-400 m thick and sometimes show flow lamination and hialoclastitic textures. Dacites from the lava domes are characterized by quartz and hornblende phenocrysts (up to 5 cm in hornblende) and smaller plagioclase crystals in a microcrystalline quartz-feldspar matrix. Inclusions of apatite in the hornblende phenochrysts are also characteristic of

dacites. Finally basaltic to andesitic dikes intrude the entire Río Quema Formation.

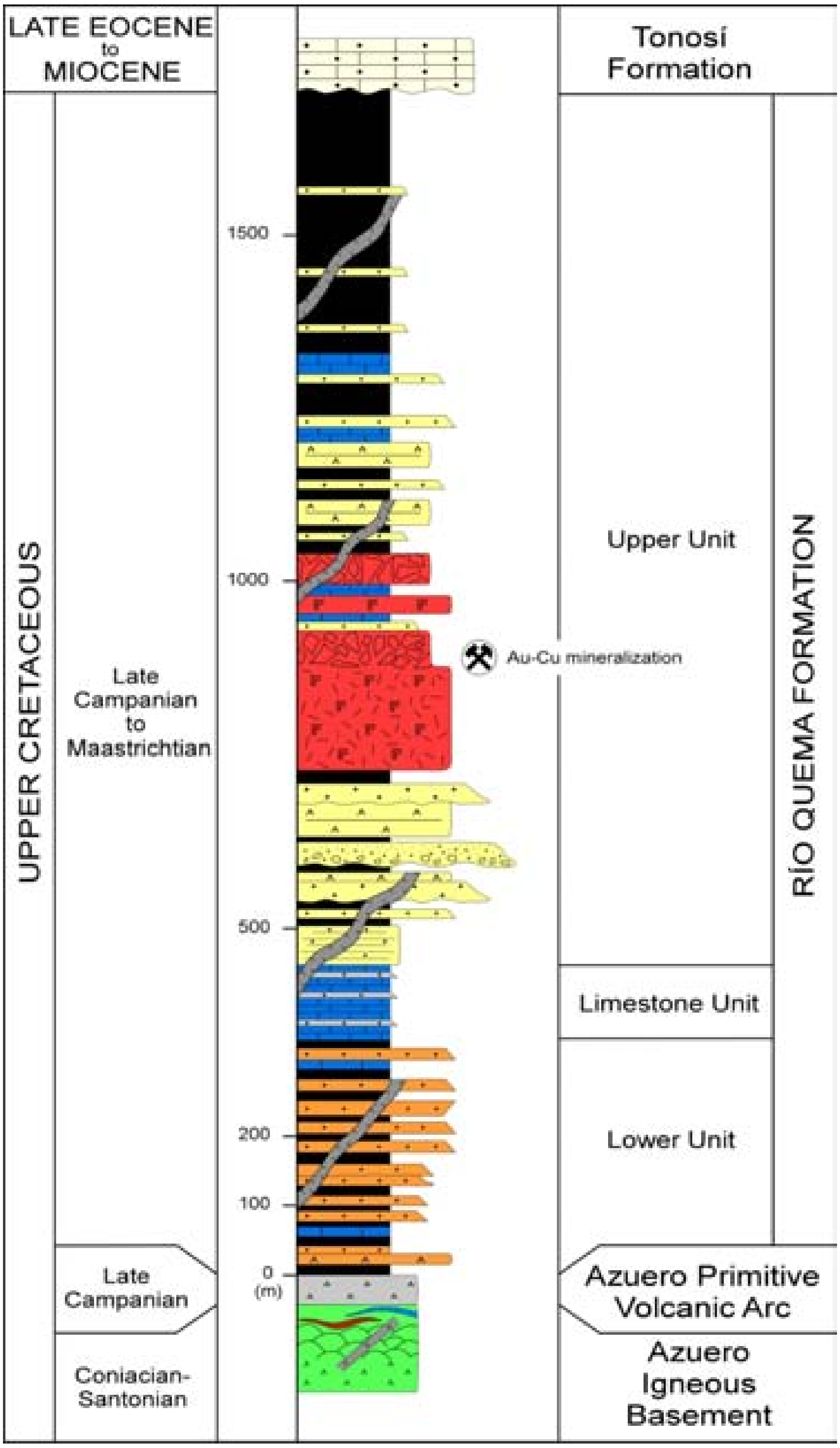

Figure 4.3: Stratigraphic section of the Río Quema Formation indicating emplacement of the Cerro Quema Au-Cu deposit (After Corral *et al.*, 2011a).

The Cerro Quema deposit is located in the center of the Azuero Peninsula, and covers an area of ~20 Km^2 (Fig 4.1B and Fig 4.2). It is related to an E-W trending regional fault system, parallel to the Rio Joaquín Fault Zone (Corral *et al*., 2011a). The deposit is constituted by several ore bodies, named, from E to W, Cerro Quema, Cerro Quemita and La Pava (Fig. 4.4). Although mineralization and hydrothermal alteration continue towards the east (e.g., Cerro Idaida, Pelona and Peloncita), the economic gold-copper potential of this eastern zone has not been evaluated so far. However, data from Cerro Idaida are used in this study in order to complement the geological characterization of the Cerro Quema deposit.

Figure 4.4: Overview of the Cerro Quema deposit where the studied ore bodies are shown.

4.3. Hydrothermal and supergene alterations

Wall-rock alteration at Cerro Quema was previously described by Leach (1992), Torrey and Keenan (1994) and Corral *et al*, (2011a). Here we present new data on the hydrothermal alteration mineralogy and zoning, deduced from the study of surface and drill core samples.

The hydrothermal alteration at Cerro Quema is mainly restricted to the dacite domes of the Río Quema Formation (Fig. 4.5), and displays an E-W trend parallel to secondary faults of the RJFZ. However, volcaniclastic sediments and andesite lava flows also affected by E-W trending faults, and located to the east and to the west of the Cerro Quema deposit, also show weakly hydrothermal alteration. Hydrothermally altered dacites are easily distinguishable due its characteristic texture of hornblende and quartz phenocrystals with minor plagioclase crystals enclosed by a quartz-feldspar matrix (Fig. 4.6A and Fig. 4.7A). Although alteration is structurally controlled, lithological control can be also recognized as shown by mushrooming at shallow levels (e.g., La Pava; Leach, 1992) due to the circulation of hydrothermal fluids through high permeability zones such as hyaloclastites and fractures.

The Cerro Quema alteration pattern consists of an inner zone of nearly pure quartz (vuggy silica), with local quartz-alunite and pyrophyllite alteration (advanced argillic alteration), enclosed by a kaolinite, illite and illite/smectite-bearing zone (argillic alteration) (Fig. 4.5). Propylitic alteration has been only observed in some drill-core samples, but not in surface, and seems to form an external halo surrounding the argillic alteration zone.

Intense weathering typical of tropical latitudes have affected the Cerro Quema deposit, including fresh and hydrothermally altered rocks. Therefore, a supergene alteration overprints the hydrothermal alteration producing changes in the mineral association and masking the hypogene alteration zones. The next section describes the mineralogy and distribution of the hypogene and supergene alteration zones developed at Cerro Quema, which is summarized in Figure 4.8.

4.3.1. Vuggy silica alteration

The vuggy silica constitutes the inner alteration zone (Fig. 4.5), and is made up of a groundmass of microcrystalline anhedral quartz grains, disseminated pyrite, barite and minor rutile, with traces of sphalerite. At depth, it is characterized by a dissemination of pyrite, chalcopyrite, enargite and tennantite. Vuggy silica texture is characterized by voids preserving the crystal morphology of hornblende and plagioclase (Fig. 4.6B and 4.7B). Commonly drusy quartz, pyrite and rutile are found filling the void spaces. Dacite quartz phenocrystals remain preserved and contain secondary fluid inclusions, presumably recording the hydrothermal alteration and mineralization events (Corral *et al*., 2011b).

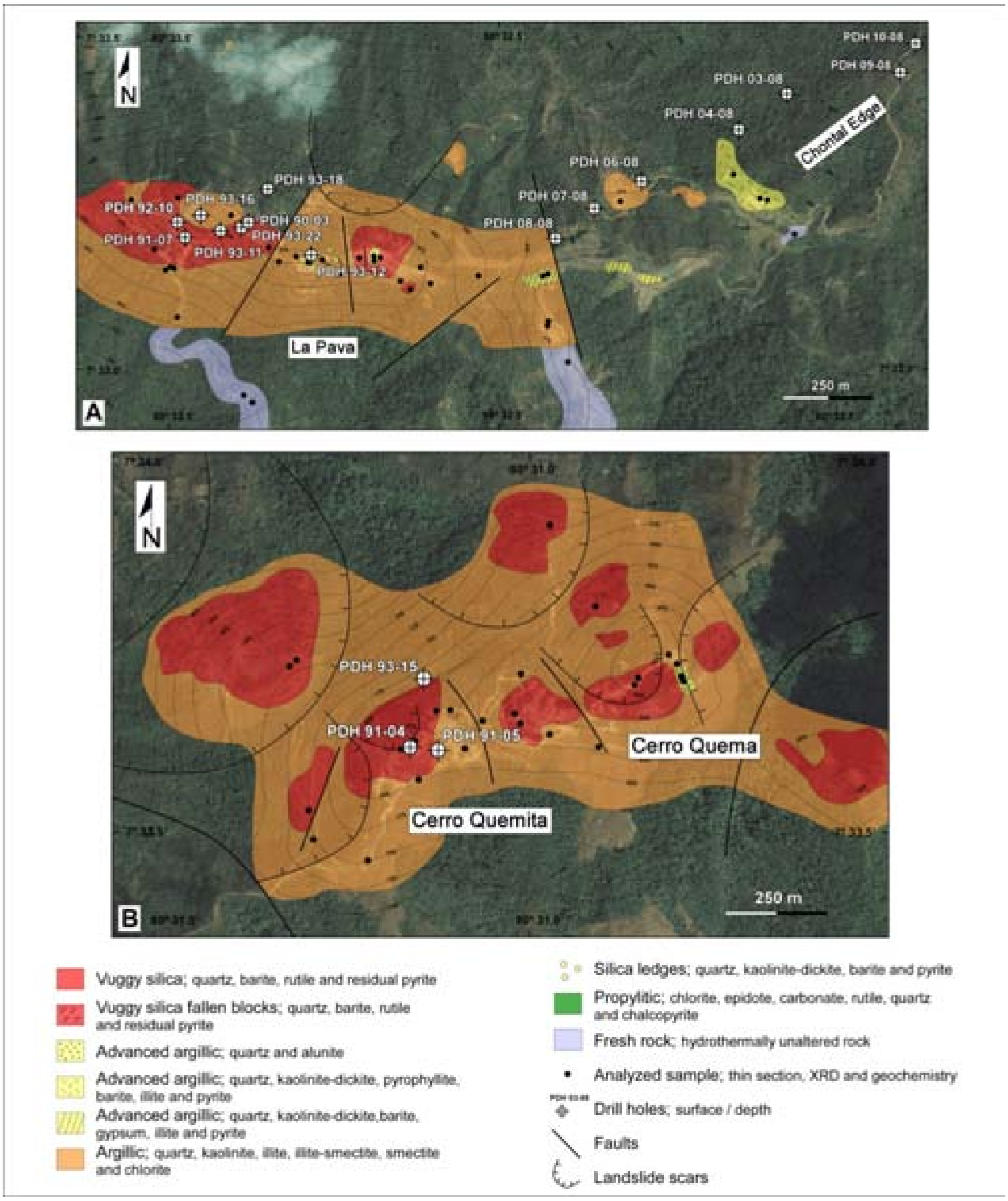

Figure 4.5: Cerro Quema deposit hydrothermal alteration maps; A) La Pava orebody and Chontal Edge. B) Cerro Quemita and Cerro Quema orebodies. Topographic map has been extracted from a 90 m SRTM (Shuttle Radar Topography Mission) digital elevation model (DEM).

Vuggy silica occurs as irregular funnel and tabular-shaped bodies, with prominent vertical development, and is commonly found on top of mineralized zones. Associated to the vuggy, patches of massive silica and silicificated breccias are also present.

4.3.2. Advanced argillic alteration

The advanced argillic alteration zone develops irregularly around the vuggy silica, and seems to partially enclose the inner alteration zone of the deposit (Fig. 4.5). This alteration zone has different expressions, in surface and in subsurface samples. Surface samples are characterized by the presence of quartz-alunite at La Pava ore body while by the presence of quartz, dickite, pyrophyllite, barite and illite at Cerro Quema, La Pava and in the Chontal Edge (see Fig. 4.5 for location).

At La Pava, the quartz-alunite assemblage occurs in a massive silica breccia zone (Fig 4.6C). Alunite is very fine grained, and is found as a minor component (only identifiable by XRD) associated to the breccia matrix.

Advanced argillic alteration characterized by quartz, dickite, pyrophyllite, barite, illite and minor diaspore is found widespread in the study area, affecting massive and brecciated dacites (Fig. 4.6D). Dacites are highly silicificated and clay minerals (e.g., dickite, pyrophyllite, illite) are found replacing hornblende and plagioclase as well as in the breccias matrix (Fig. 4.7C). Barite is found in fractures and as part of breccia matrix. Disseminated pyrite is also characteristic of this alteration zone. At depth, the advanced argillic alteration contains quartz, alunite-natroalunite, aluminum-phosphate-sulfate minerals (APS), dickite, pyrophyllite, barite and rutile. This assemblage has only been observed in drill-core samples, associated to hydraulic breccias (Fig. 4.7D). Pyrite and chalcopyrite are disseminated in both, vuggy silica fragments and more intensively, in the breccia matrix. Veins of pyrite, enargite and tennantite are found crosscutting the hydrothermal breccias. Traces of bornite and secondary sulfide minerals (supergene), such as covellite and chalcocite have also been found in this alteration zone.

4.3.3. Argillic alteration

The argillic alteration forms an external halo surrounding the vuggy silica and advanced argillic alteration zones (Fig. 4.5). The argillic envelope bounds the vuggy silica generally with a sharp contact. On the contrary, the contact between the advanced argillic and the argillic zone is gradational. The argillic halo is made up of quartz, kaolinite, illite and illite-smectite with minor chlorite, replacing hornblende and plagioclase crystals (Fig. 4.7E). Locally, disseminated pyrite is also found associated to the argillic alteration. The hydrothermally altered rock is weakly silicified, of whitish-grayish color, and frequently preserves the original volcanic rock texture (Fig. 4.6E).

Clay minerals distribution in the argillic alteration zone show zoning from the center to the external zone. Kaolinite dominates in the inner zone, whereas in the distal zones mineral assemblages grade to kaolinite ± illite, and to kaolinite ± illite ± illite-smectite. Moreover, in some samples from the most distal zones, kaolinite ± smectite ± chlorite-smectite, and chlorite have been recognized. Moreover, at La Pava, subvertical pipe-like structures composed of quartz, dickite, barite and pyrite (silica ledges; Fig. 4.6F), have been observed crosscutting the argillic alteration.

4.3.4. Propylitic alteration

The propylitic alteration zone constitutes the distal alteration halo, affecting dacites, andesites and volcaniclastic sediments (e.g., turbidites and debris flows; Fig. 4.6G). Propylitic alteration does not crop out in surface. Identification and characterization of this alteration zone has been performed with data obtained from drill-core samples.

This alteration is characterized by the presence of chlorite, epidote, carbonate, rutile, pyrite and chalcopyrite, with minor hematite and magnetite. Moreover, traces of sphalerite, chalcocite and covellite are also characteristic of this alteration halo. Propylitic zone shows a transitional contact with the argillic alteration zone, characterized by the presence of clay minerals mixed with propylitic alteration minerals.

Propylitically altered rocks are weakly silicified and chloritized, hornblende is replaced by chlorite and epidote, and plagioclase is replaced by carbonate (Fig.

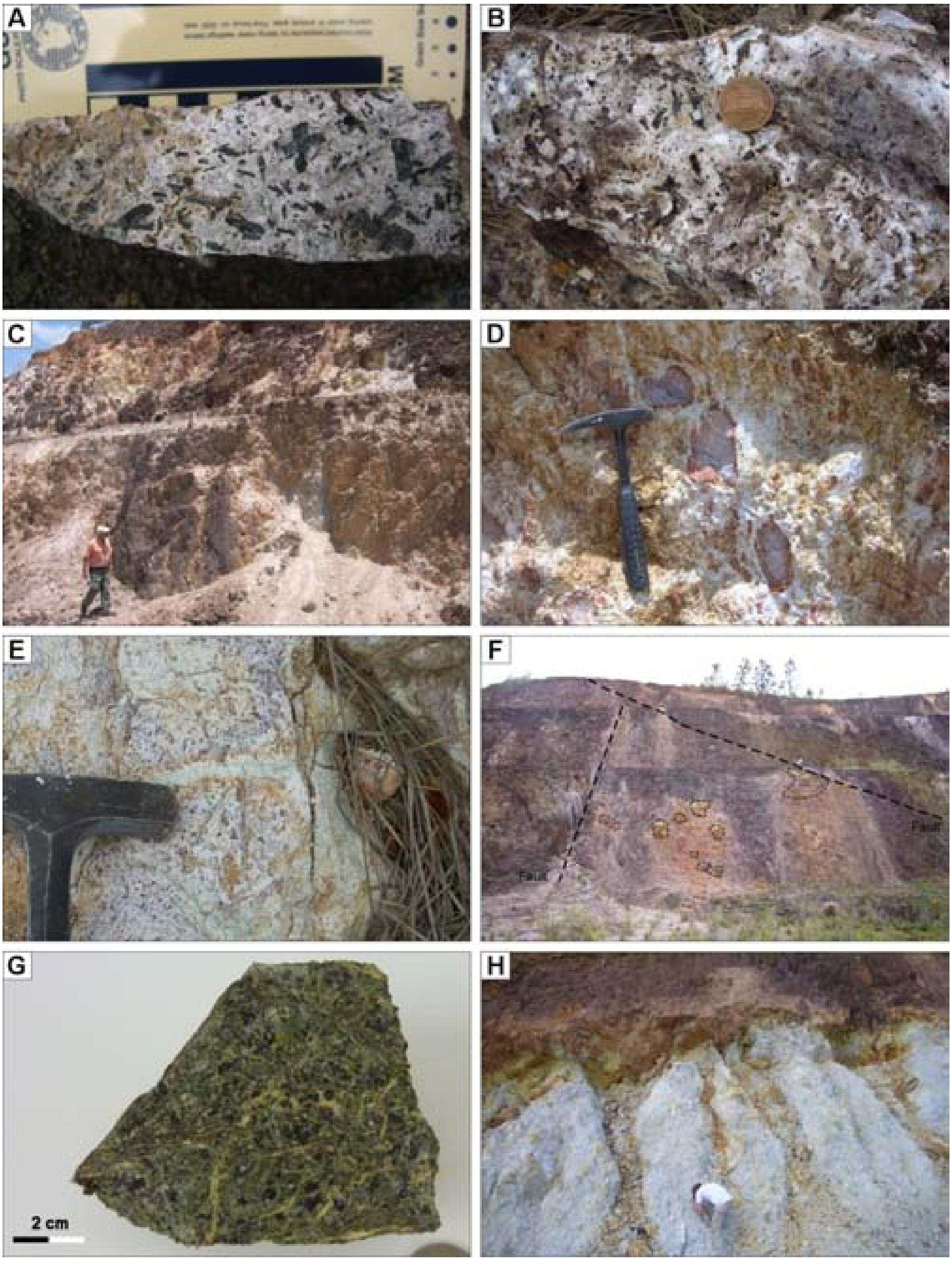

Figure 4.6: Hydrothermal alteration at Cerro Quema. A) Fresh dacite (dacite dome complex), of the Río Quema Formation, showing the characteristic porphyritic texture (hornblende and quartz phenocrysts with smaller plagioclase crystals, in a quartz-feldspar matrix). B) Vuggy silica at Cerro Quemita ore body. The rock preserves the original texture. Voids correspond to hornblende and plagioclase crystals now filled by Fe-oxides. Matrix has been totally replaced by microcrystalline quartz. C) Advancded argillic alteration: quartz-alunite zone. Strongly silicified and brecciated dacite with a fine grained quartz-alunite matrix at La Pava. D) Advanced argillic

alteration: quartz, dickite, pyrophyllite, barite and illite zone. Breccia composed by clasts of dacite affected by argillic alteration (quartz, kaolinite, illite) in a matrix presenting an advanced argillic alteration (quartz, dickite, pyrophyllite and illite), at Cerro Quema ore body. E) Argillic alteration: kaolinite, illite and illite/smectite zone. Dacite is totally replaced by clay minerals preserving the original rock texture at Cerro Quemita. F) Silica ledges, subvertical pipe-like structures composed of quartz, dickite, barite and pyrite enclosed in a quartz-kaolinite altered rock at La Pava. Image width is approximately 20 m. G) Propylitic alteration of a drill core sample (PDH 10-08; see Fig. 4.5 for location) showing a propylitized sedimentary breccia or microconglomerate. Matrix is silicified, pyritized and chloritized, hornblende is epidotized and pyritized. The rock is crosscut by carbonate veins. H) Redox boundary at Chontal edge. Oxidation is affecting an advanced argillic alteration zone (quartz, dickite, pyrophillite, barite, illite and pyrite).

4.7F), which occurs as patches and veinlets. Pyrite and chalcopyrite are found disseminated and in fractures. Minor amounts of rutile, magnetite and hematite occur replacing hornblende and as disseminations. Residual apatite after hornblende alteration is also observed.

4.3.5. Supergene alteration

Sulfide oxidation in high sulfidation systems is markedly controlled by rock permeability (Sillitoe, 1999). At Cerro Quema it is provided by the vuggy silica, hydrothermal breccias, fracture zones as well as hyaloclastite textures. Oxidation reaches up to 150 m in depth (e.g. La Pava ore body; Torrey and Kennan, 1994). Although the redox boundary is irregular, it is commonly subhoritzontal at the district scale (Fig. 4.6H).

Supergene alteration developed a thick silica- and iron oxide-rich lithocap above the primary sulfide-bearing zone. This lithocap is characterized by vuggy silica rich in hematite and goethite, with minor barite, jarosite, halloysite and kaolinite. Traces of pyrite are still present.

Below the oxidation zone (redox boundary), within the primary sulfide-bearing zone, secondary copper sulfides such as chalcocite and covellite are precipitated producing the enrichment zone.

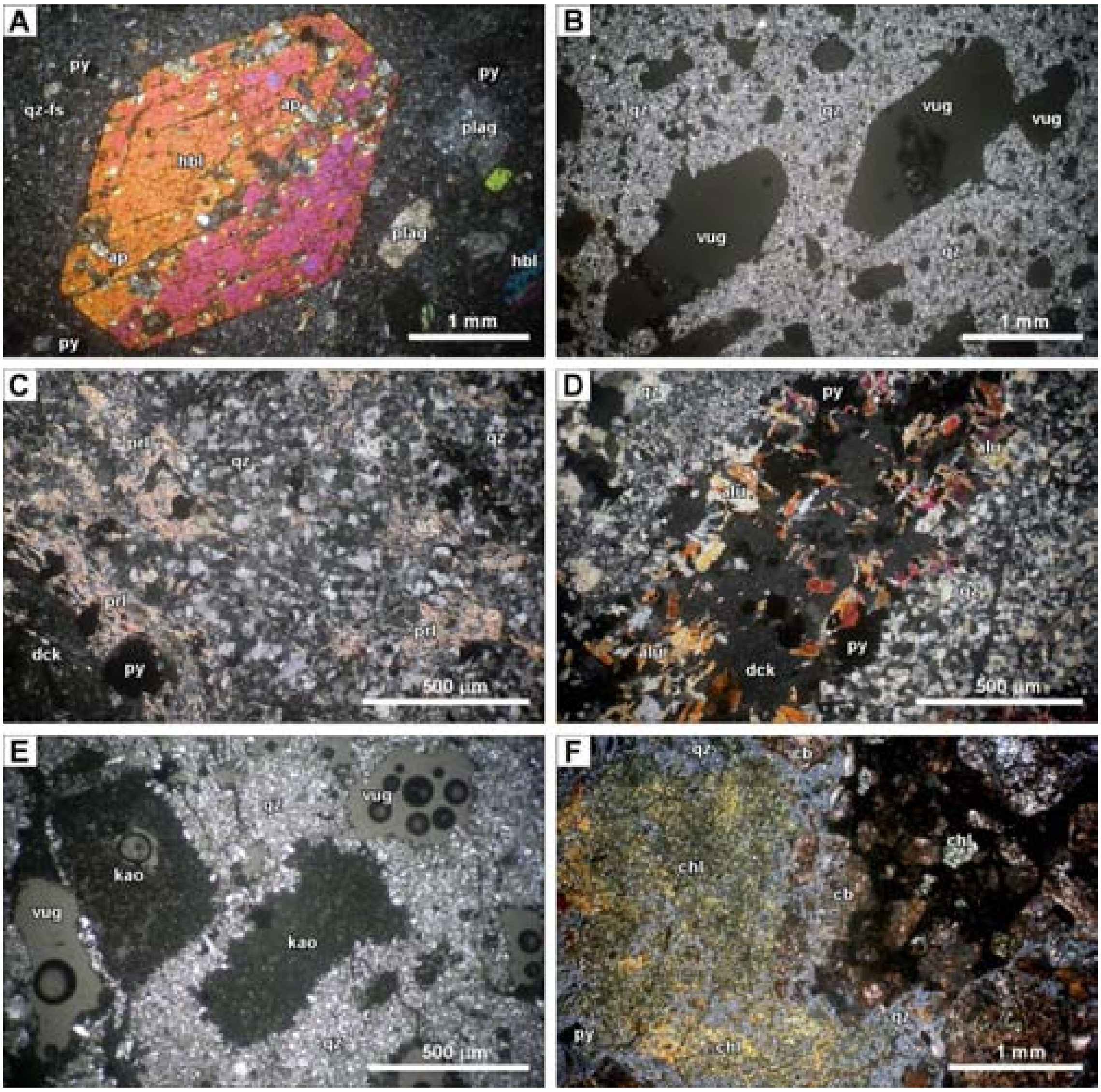

Figure 4.7: Hydrothermal alteration at Cerro Quema. A) Relatively fresh dacite showing honrnblende phenocrystals and partially carbonated plagioclase crystals in a slightly silicified quartz-feldspar matrix (crossed polarized light). Note the presence of apatite inclusions in hornblende (also recognizable in the propylitic alteration zone). B) Hornblende and plagioclase crystal morphologies are preserved within the vuggy silica (crossed polarized light). Dacite matrix has been totally replaced by microcrystalline quartz. C) Dacite with a quartz, dickite, pyrophyllite, and pyrite assemblage, typical of the advanced argillic alteration (crossed polarized light). D) Hydraulic breccia in dacite, constituted by fragments of vuggy silica with a matrix composed of alunite-natroaluinte, pyrite and dickite (crossed polarized light). E) Dacite affected by argillic alteration (crossed polarized light). Matrix has been replaced by microcrystalline quartz and plagioclase voids have been filled by kaolinite. F) Crossed polarized light image of a sedimentary breccia affected by propylitic alteration. Breccia matrix is slightly silicified, chloritized, carbonated and pyritized. Breccia clasts (volcanic rock) show also carbonatization of feldspars and chloritization of hornblendes. ap: apatite; alu: alunite; cb: carbonate; chl: chlorite; dck: dickite; hbl: hornblende; kao: kaolinte; qz-fs: quartz-feldspar matrix; plag: plagioclase; prl: pyrophyllite; py: pyrite; qz: quartz.

4.4. Mineralization

Gold occurs as disseminated submicroscopic grains and as "invisible gold" within the pyrite lattice (Corral *et al.*, 2011a). Copper is associated to Cu-bearing phases such as chalcopyrite, enargite, bornite and tennantite (hypogene) as well as to secondary copper sulfides such as covellite and chalcocite (supergene). Gold and copper (enargite-tennantite) are mainly concentrated in the vuggy silica and advanced argillic alteration zones. However, minor copper, gold and sulfide mineralization have been also found in the argillic and propylitic alteration zones.

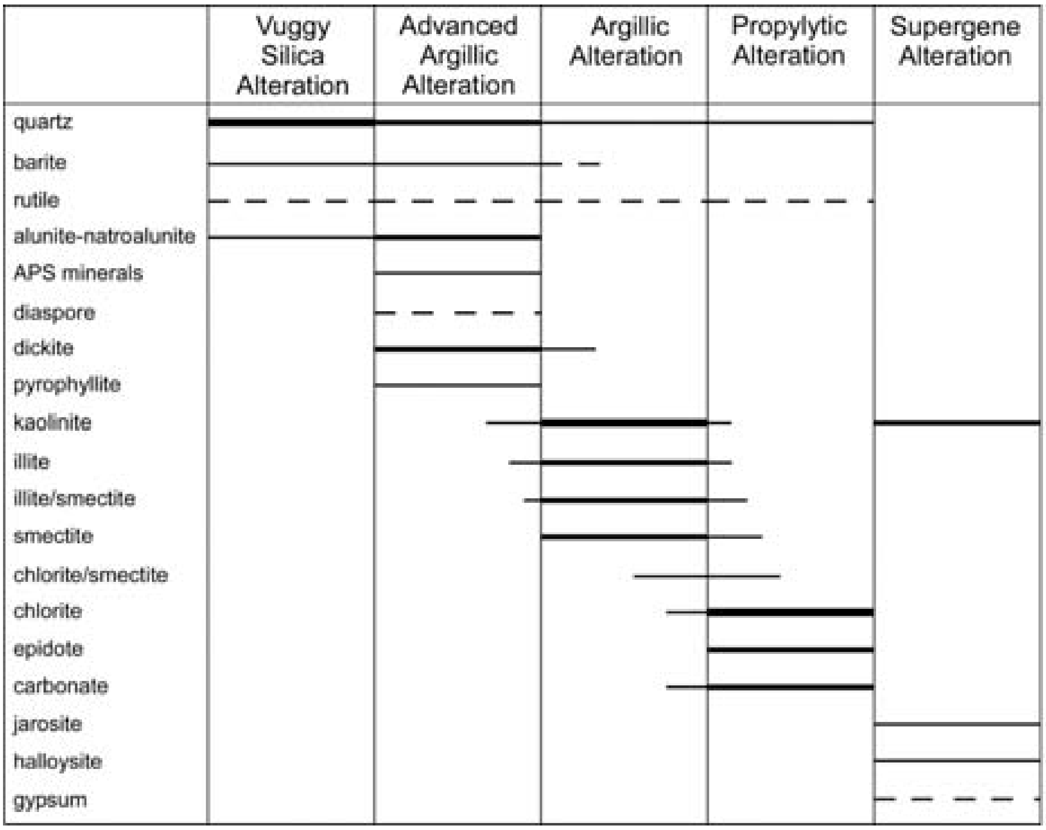

Figure 4.8: Paragenetic sequence of hydrothermal alteration minerals recognized at Cerro Quema deposit.

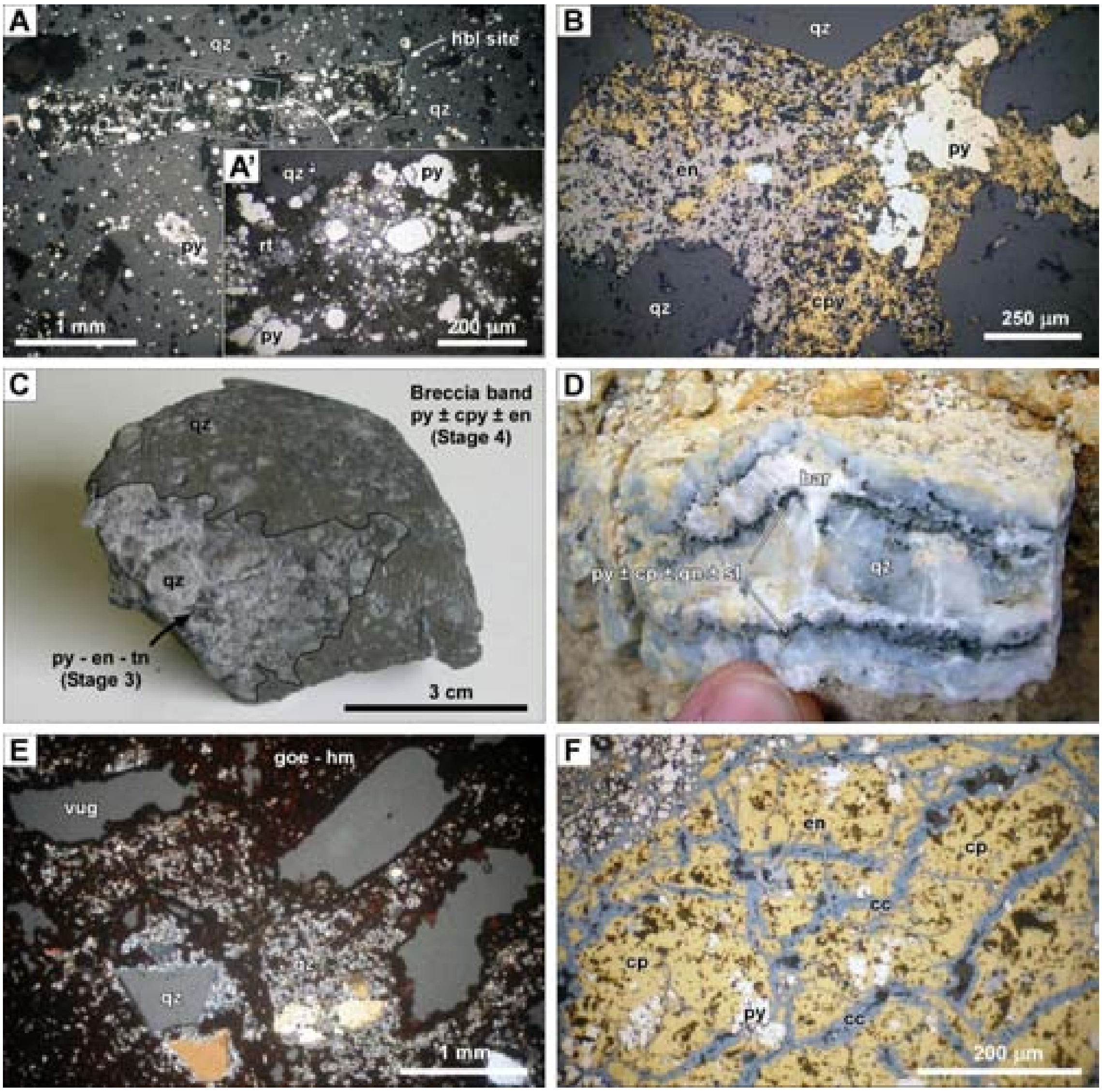

Figure 4.9: Mineral assemblages of the hypogene and supergene mineralization at Cerro Quema. A) Vuggy silica with disseminated pyrite and replacement of hornblende by pyrite and rutile (reflected polarized light). B) Mineralization stage 3: veinlets of enargite, pyrite and chalcopyrite crosscutting a vuggy silica altered dacite (reflected polarized light). C) Veinlets of mineralization stage 3 with pyrite, enargite and tennantite crosscut by breccia bands of the mineralization stage 4, made of pyrite, chalcopyrite and enargite. D) Intermediate sulfidation base metal veins composed of pyrite, quartz and barite with traces of sphalerite and galena. E) Supergene oxidation developed on a previous hypogenically altered dacite. Iron oxides and hydroxides (hematite and goethite) are disseminated in the groundmass, however they are also found filling vugs and replacing the hydraulic breccia matrix. Part of the original rock texture is still preserved (polarized light). F) Breccia band of the supergene enrichment zone, constituted by pyrite, chalcopyrite ± enargite showing replacement textures of chalcopyrite by chalcocite (reflected polarized light). bar: barite, cc: chalcocite, cp: chalcopyrite, en: enargite, gn: galena, goe: goethinte, hm: hematite, py: pyrite, qz: quartz, rt: rutile, sl: sphalerite, tn: tennantite.

4.4.1 Hypogene mineralization

Hypogene mineralization is generally found below the oxidized zone (up to 150m depth), however some small outcrops are found at surface. Although pyrite is the most abundant sulfide at Cerro Quema deposit, there is a group of accompanying sulfides also related with the Au-Cu mineralization.

Pyrite is commonly found as fine disseminated crystals (idiomorphic, subidiomorphic and framboidal) in the hydrothermally altered rock. However, it also appears associated with rutile filling voids after hornblende leaching (Fig. 4.9A), in microveinlets (associated with chalcopyrite, enargite and tennantite), as matrix material in hydraulic breccias (intergrown with alunite-natroalunite and dickite), in breccia bands (intergrown with chalcopyrite and enargite) and in intermediate sulfidation base metal veins (associated with chalcopyrite, sphalerite and galena).

Chalcopyrite appears as dissemination in the deeper zones of the system, but also in microveinlets associated with pyrite, enargite and tennantite (Fig. 4.9B), and in the breccia bands, intergrown with pyrite and enargite. Chalcopyrite associated with pyrite, sphalerite and galena is also a minor component of the intermediate sulfidation base metal veins.

Enargite and tennantite are mainly found in microveinlets, associated with pyrite and chalcopyrite (Fig. 4.9C). and as disseminations associated with chalcopyrite in the deeper zones of the system. Enargite has also been found in breccia band associated with pyrite and chalcopyrite.

Bornite, galena and sphalerite are present as trace minerals. Bornite and sphalerite are mainly found disseminated in the groundmass, while galena is only found in the intermediate sulfidation base metal veins, associated with pyrite, chalcopyrite and sphalerite (Fig. 4.9D).

Hypogene mineralization has been divided into five stages (Fig. 4.10). Stage 1 consists of a dissemination of fine grained idiomorphic pyrite with minor enargite, tennantite and chalcopyrite at depth (Fig. 4.9A). Stage 1 is also characterized by the precipitation of rutile and barite in voids and in the groundmass. Stage 2 is constituted by a dissemination of pyrite in a hydraulic breccia matrix, associated with alunite and dickite with traces of chalcopyrite.

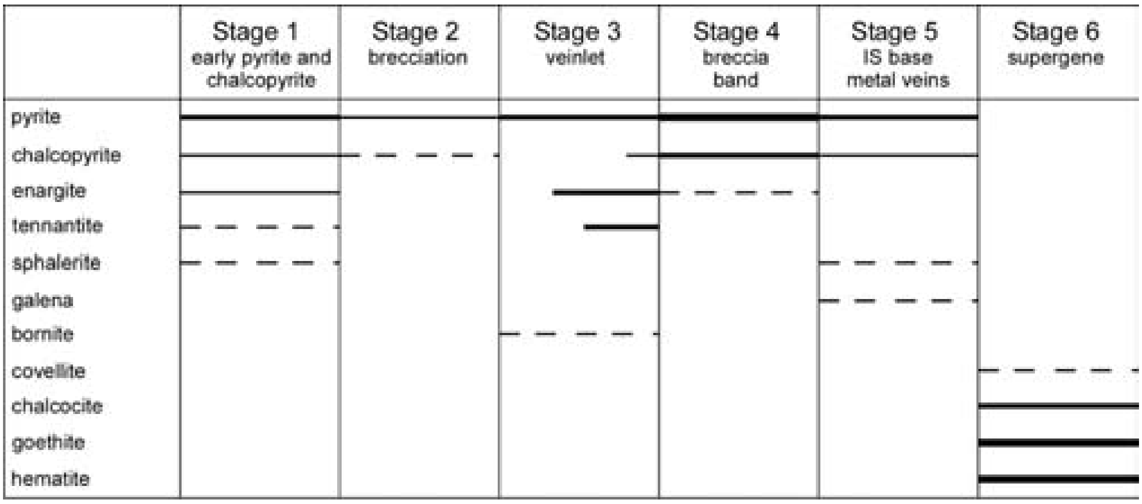

Figure 4.10: Paragenetic sequence of ore minerals recognized at Cerro Quema deposit.

Stage 3 consists of veinlets of pyrite, chalcopyrite, enargite and tenantite (Fig. 4.9B) crosscutting Stages 1 and 2. Replacement textures of pyrite by enargite, enargite by tennantite and tennantite by chalcopyrite are observed in the veinlets. Stage 4 is constituted by breccia bands of ~5 cm thick, mainly composed of pyrite, chalcopyrite with minor enargite. Breccia bands crosscut all the previous stages (Fig. 4.9C). Stage 5 corresponds to intermediate sulfidation, 5 to 10 cm thick base metal veins. These veins are composed of pyrite as the main sulfide species, quartz and barite as the main gangue minerals, with minor chalcopyrite, sphalerite and galena (Fig. 4.9D). Intermediate sulfidation base metal veins are usually related to the late stages of a high sulfidation epithermal system, and should crosscut all the previously described mineralization stages. However, here we only have crosscutting evidences up to Stage 3.

4.4.2. Supergene mineralization

Supergene oxidation affects the Cerro Quema deposit and is best developed in the upper part of mineralized bodies. It is characterized by the presence of hematite and goethite filling voids in the vuggy silica zone, disseminated within the groundmass and replacing the matrix of hydrothermal breccias (Fig. 4.9E). Supergene jarosite, kaolinite, halloysite and gypsum are also found in fractures, vuggs and breccia matrix. Hypogene pyrite, barite and rutile remain as trace minerals in the oxidation zone.

Below the oxidation cap, the precipitation of secondary Cu-bearing minerals such as chalcocite and minor covellite produced a zone of supergene enrichment. The secondary Cu-sulfides are found replacing chalcopyrite, tennantite and enargite as well as filling small fractures (Fig. 4.9F).

4.5. Trace metal content

Trace element abundance and distribution in ore deposits is important because they may contain anomalies for many elements other than those which are mined (Kesler *et al*., 2003). These trace elements may help to understand the genetic processes and evolution of an ore deposit and can be used as an exploration tool as well.

High sulfidation deposits commonly contain economically important amounts of Au, Ag, and Cu, as well as significant amounts of As, Sb, Hg and Te (Kesler *et al*., 2005). Although these elements are probably of magmatic origin (e.g., Heinrich *et al*., 2004), they vary greatly in relative abundance between deposits, suggesting that the fluids varied in composition throughout the life of underlying magmas (Deditius *et al*., 2009).

Pyrite, a ubiquitous mineral in most hydrothermal ore deposits, can contain high levels of trace elements either as inclusions, or within the crystal lattice. Its chemistry can be used to distinguish between a hydrothermal and syn-sedimentary/diagenetic origin and can be also used as indicator of provenance (Koglin *et al*., 2010). The Co/Ni and S/Se ratios in pyrite have been used as empirical indicator of the depositional environment (e.g., Goldschmidt, 1954; Edwards and Carlos, 1954; Lofthus-Hills and Solomon, 1967; Bralia *et al*., 1979; Bajwah *et al*., 1987; Roberts, 1982; Clark *et al*., 2004). However, it must be emphasized that trace element concentrations of pyrite alone, cannot unequivocally characterize a deposit type.

Additionally, major- and trace-element contents of alunite- and APS-group minerals, which can be formed under acidic and oxidizing conditions (e.g., Knight, 1977) and/or during the weathering of sulfides, in porphyry Cu and epithermal Au deposits, may provide significant information to understand their origin (hypogene versus supergene). On the other hand, the presence of APS minerals in ore deposits is related in time and space to gold and silver concentrations and therefore can be used as an ore guide in mineral exploration (Bove, 1990; Dill, 2003).

Geochemical data of trace elements in high sulfidation epithermal deposits are not abundant (e.g., Nansatsu, Japan (Hedenquist *et al*., 1994); Rodalquilar, Spain (Hernandez *et al*., 1989); Pueblo Viejo, Dominican Republic (Kesler *et al*., 2003)). In this study we present trace element data, based on analyses of whole rock, sulifides (pyrite), and sulfates (alunite and APS minerals) in order to better understand the deposit enrichment, distribution and association of trace elements and mineral origin at Cerro Quema.

Whole rock analyses of Au, Ag, Cd, Cu, Pb, Zn, As, Ba, Sb, S and Hg were performed on 34 samples of the vuggy silica and advanced argillic alteration zones by INAA and ICP (at Activation Laboratories, Canada). S, Fe, Co, Ni, Cu, As, Se, Ag, Cd, Sb, Au and Hg have been analyzed by EMPA in 55 pyrites from six drill-hole samples of vuggy silica and advanced argillic alteration. Al, Fe, Ca, Na, K, P, F, S, Cu, As, Sr, Ba, Ce and Pb have been also analyzed by EMPA on 20 alunites and 21 APS minerals from two drill core samples of the advanced argillic alteration. EMPA analyses were performed at the Serveis Cientifico-tècnics of the University of Barcelona

4.5.1. *Whole rock*

Results of the whole rock analyses have been grouped into two different categories according to sample alteration: samples from the oxide zone (affected by supergene alteration) and samples of the sulfide zone (affected by hypogene alteration). Results are shown in Table 4.1 (see Appendix 1 for sample location).

As suggested by Kesler *et al*., (2003), an indication of the deposit enrichment degree is shown by comparing the average concentration of elements in the oxide zone and in the sulfide zone respect to the average concentration of those elements in country rocks (i.e., diorites and quartz diorites), with which the mineralization is probably genetically associated (Table 4.2). Because Ag, Cd, Pb, As and Hg are below the detection limit in the country rocks, they have not been considered for the enrichment calculations. The enrichment of the oxide zone respect to the sulfide zone has been calculated by comparing the concentration of elements in the oxide zone with respect to the sulfide zone (Table 4.2).

Although in the Cerro Quema deposit Au and Cu are the elements of mining interest, the highest enrichment degree respect to the country rock is shown by Sb, Ba and S. Other elements such as Zn and Ni are depleted respect to the country rock. In the oxide zone, elements such as Au and Sb are concentrated whereas Cu, Zn and Ba are depleted.

Correlation coefficients (Table 4.3) between element pairs were used to define element affinities and their mineral correlation. Because all elements showed highly skewed population, calculations for element correlation were performed after previous transformation to log values as suggested in Kesler *et al*. (2003). Correlation ranges have been defined as strongly correlated ($r > 0.90$), well correlated ($0.89 > r > 0.60$), and poorly correlated ($0.59 > r > 0.40$).

In the oxide zone, Cu is poorly correlated with Zn and Cd, and As is well correlated with Sb. In the sulfide zone, Au is well correlated with Ag, Pb and Ba, and poorly correlated with Sb. Ag is well correlated with Pb and poorly correlated with As and Ba. Cu is strongly correlated with Zn, well correlated with Cd and As, and poorly correlated with Pb. As is well correlated with Cd, Cu and Zn, and poorly correlated with Sb, and Ag. Zn is strongly correlated with Cu and Pb and well correlated with Cd and As. Ba is well correlated with Au and poorly correlated with Ag and Pb. Finally, Sb is poorly correlated with Au and As.

Sample	Alteration	oxide/sulfide	Au (ppb)	Ag	Cd	Cu	Mn	Mo	Ni	Pb	Zn	S (%)	As	Ba	Hg	Sb	W	Mass (g)
			Trace Elements (ppm)															
La Pava																		
9311-95	VS	oxide zone	317	bdl	0.8	1520	9	21	4	123	3	0.758	429	2500	bdl	33.2	173	33.5
9311-111	VS	sulfide zone	1680	0.8	bdl	36	bdl	2	bdl	57	1	0.042	72	360000	bdl	4.7	235	43.1
9311-153	VS	sulfide zone	908	1.1	bdl	10	bdl	3	bdl	98	bdl	0.039	20	13000	bdl	24.5	576	33.3
9210-37.50	VS	oxide zone	2070	0.9	1.7	1100	bdl	18	6	25	4	0.143	80	17000	bdl	8.5	159	41
9210-121	VS	oxide zone	2400	0.3	1.8	1880	bdl	60	6	15	3	0.362	221	1400	bdl	27.8	79	41.6
9210-136	VS	oxide zone	1250	0.5	1.2	571	bdl	7	2	10	3	0.19	23	530	bdl	3.6	203	49.2
9322-34	VS	oxide zone	683	0.4	1.5	635	bdl	23	4	147	2	0.085	495	21000	bdl	13	203	38.2
9322-96	VS	oxide zone	198	0.4	0.8	373	bdl	13	2	20	3	0.071	375	bdl	bdl	21.9	215	30.7
9322-121	VS	sulfide zone	91	0.8	0.9	338	bdl	bdl	1	12	2	0.095	20	1100	bdl	2.3	365	30.9
9003-20	VS	oxide zone	378	0.3	bdl	129	bdl	16	1	204	bdl	0.036	32	bdl	bdl	5.7	359	39.1
9003-56	VS	oxide zone	321	0.4	1.7	468	bdl	bdl	2	69	1	0.118	11	1300	bdl	1	184	33.9
LP-235	VS	sulfide zone	511	0.3	1.6	1140	bdl	8	4	92	2	0.107	829	bdl	bdl	32.3	119	36.5
LP-220	VS	sulfide zone	98	bdl	bdl	7	bdl	2	bdl	4	bdl	0.007	21	bdl	bdl	53	345	37.5
CLP-1	VS	oxide zone	666	0.3	1	1040	bdl	47	3	432	3	0.058	3700	bdl	bdl	129	53	40.1
LP-225	AA	oxide zone	bdl	bdl	1.3	48	bdl	bdl	1	34	8	0.368	28	bdl	bdl	1.7	68	32.8
Chontal Edge																		
0308-24.50	AA	oxide zone	31	0.3	0.8	251	bdl	135	2	41	2	0.096	636	9300	bdl	51.2	461	35
0308-65.80	AAA	sulfide zone	bdl	bdl	1.1	275	15	bdl	17	5	14	7.76	12	bdl	bdl	3.4	87	42.2
0308-111.60	AAA	sulfide zone	bdl	bdl	bdl	364	bdl	5	bdl	4	3	0.601	106	720	bdl	11.2	329	31
Cerro Quemita																		
9315-87	VS	oxide zone	291	0.6	1.4	1440	3	20	2	21	11	0.266	188	1200	bdl	8.6	228	40.4
9315-120	VS	sulfide zone	48	0.3	1.8	1090	26	bdl	23	186	74	9.54	77	280	bdl	6.1	279	38.2
9104-9.50	VS	oxide zone	721	0.8	0.9	312	bdl	4	2	74	2	0.034	810	300	bdl	18	196	41
9104-22.85	VS	oxide zone	768	0.6	1.9	1160	bdl	bdl	6	12	2	0.139	485	1100	bdl	4.3	115	40.5
9104-54.55	VS	oxide zone	242	0.8	0.6	83	bdl	5	bdl	18	2	0.025	98	bdl	bdl	5.7	683	34.4
9104-82	VS	oxide zone	865	0.5	0.6	135	bdl	4	bdl	64	2	0.114	681	220	bdl	17.3	304	41.8
Qt-01	VS	oxide zone	1470	0.4	1.2	959	bdl	17	4	139	1	0.032	1870	bdl	bdl	81	290	38.2
Qt-02	VS	oxide zone	572	0.4	1.1	597	bdl	bdl	3	64	2	0.082	797	17000	bdl	20.3	188	37.4
QA-10	VS	oxide zone	627	2	bdl	164	bdl	5	bdl	36	bdl	0.025	296	640	bdl	15.2	225	38.3
Cerro Quema																		
LP-104	VS	oxide zone	311	0.4	1.6	657	bdl	bdl	3	13	4	0.12	448	bdl	bdl	57.7	226	42.2
LP-107	VS	oxide zone	245	0.3	1.1	206	bdl	3	1	73	bdl	0.029	129	bdl	11	317	179	38.5
QA-17B	VS	sulfide zone	bdl	bdl	bdl	2	bdl	bdl	bdl	bdl	bdl	0.003	15	bdl	bdl	8.1	408	38.1
Cerro Idaida																		
9343-21.50	VS	oxide zone	884	1	bdl	1030	10	9	3	105	74	0.241	2470	540	bdl	58.4	400	41.9
9343-50	VS	oxide zone	227	0.2	1.4	1100	bdl	4	1	61	6	0.256	2490	530	6	7.2	230	42.8
9343-77	VS	sulfide zone	314	1.1	15.2	10000	6	14	17	65	403	10.12	27400	bdl	bdl	95.3	105	47.4
9343-80	VS	sulfide zone	39	bdl	0.8	1060	23	bdl	20	11	61	7.554	122	280	bdl	2.4	202	46.2

Table 4.1: Trace elements analyzed in the samples from the different ore bodies of the Cerro Quema deposit. VS: vuggy silica, AA: argillic alteration, AAA: advanced argillic alteration.

	Au	Cu	Ni	Zn	S	Ba	Sb
Country rock average (*n=6*)	7.93	125.43	16.00	68.43	0.01	351.71	0.19
Sulfide zone enrichment (*n= 23*)	36.55	9.59	0.46	0.75	582.06	97.06	104.12
Oxide zone enrichment (*n= 11*)	88.00	5.88	0.17	0.08	26.10	9.24	219.58
Oxide/Sulfide zone enrichment	2.41	0.61	0.37	0.11	0.04	0.10	2.11

Table 4.2: Calculated enrichment factors for the oxide and sulfide zones with respect to the country rocks, and enrichment factor of the oxide zone with respect to the sulfide zone. Element concentration is expressed in ppm except for Au which is expressed in ppb.

	Au	Ag	Cd	Cu	Pb	Zn	As	Ba	Sb
Oxide zone									
Au	1.00	0.31	0.14	0.36	-0.02	0.10	0.00	0.07	-0.08
Ag		1.00	-0.34	-0.31	-0.32	0.09	-0.11	0.06	-0.22
Cd			1.00	0.57[c]	-0.30	0.01	-0.05	0.22	-0.10
Cu				1.00	-0.01	0.53[c]	0.32	0.30	0.10
Pb					1.00	0.31	0.37	-0.13	0.35
Zn						1.00	0.38	0.20	0.05
As							1.00	-0.07	0.60[b]
Ba								1.00	-0.32
Sb									1.00
Sulfide zone									
Au	1.00	0.82[b]	0.05	0.06	0.62[b]	-0.05	0.32	0.65[b]	0.40[c]
Ag		1.00	0.29	0.23	0.68[b]	0.07	0.40[c]	0.58[c]	0.31
Cd			1.00	0.79[b]	0.43[c]	0.89[b]	0.74[b]	-0.43	0.16
Cu				1.00	0.40[c]	0.90[a]	0.71[b]	-0.12	0.00
Pb					1.00	0.90[a]	0.38	0.43[c]	0.08
Zn						1.00	0.71[b]	-0.35	0.01
As							1.00	-0.11	0.52[c]
Ba								1.00	-0.14
Sb									1.00

Table 4.3: Correlation coefficients (r) of trace and major elements at Cerro Quema. Correlations were calculated for elements transformed to log values. Superindex indicates a: strongly correlated, b: well correlated, c: poorly correlated.

4.5.2. Pyrite

EMPA analyses have been performed in different pyrite types (e.g., idiomorphic, zoned and framboidal; Fig 4.11; Appendix 2) in order to infer the

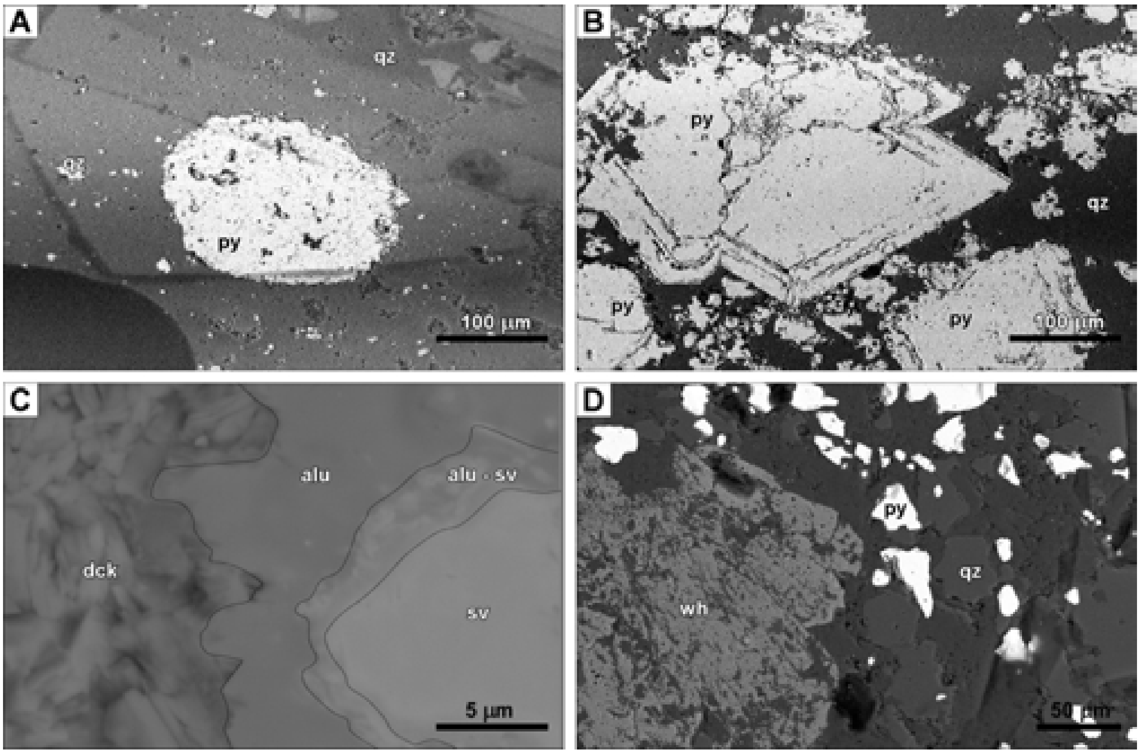

Figure 4.11: BSE images of analyzed pyrites and alunites. A) Framboidal pyrite. B) Idiomorphic and zoned pyrites. C) Alunite crystal showing an inner core of svanbergite with an intermediate zone of intergrown alunite-svanbergite in a matrix composed by dickite. D) Woodhauseite crystal in a quartz pyritized matrix. alu: alunite, dck: dickite, py: pyrite, qz: quartz, sv: svanbergite, wh: woodhauseite.

possible relationship between pyrite textures and chemical composition. Although all the analyzed pyrites show quite similar content in Fe, S, Ag, Cd, Sb and Se, some differences in their Cu, Co and Ni contents are observed (Table 4.4). Au, Hg and As are generally below the detection limit, therefore, their concentrations have not been considered. Values of the Co/Ni ratios (N= 11) range from 0.58 to 5.50, and S/Se ratios (N=21) are between 1050 and 2694.

4.5.3. Sulfates

Although more than 40 mineral species have the fundamental alunite crystal structure (Stoffregen and Alpers, 1987; Stoffregen el al., 2000), here, the general alunite formula $AB_3(XO_4)_2(OH)_6$, is used. In alunite, A site can be substituted by Na (alunite-natroalunite solid solution), Ca (alunite-minamiite solid solution), Ba (alunite-walthierite solid solution), Sr, REE, Pb, Ag, H_3O and NH_4 (Scott, 1990). B site is occupied by Al, but can be substituted by Fe (alunite-jarosite solid solution) and minor Cu and Zn (Dill, 2001). X site is dominantly occupied by S and is mainly substituted by P, however substitution for As and Sb could occur to form the large APS group minerals (Strunz and Tennyson, 1982; Scott, 1987; Jambor, 1999; Papike *et al.*, 2006).

At Cerro Quema, alunite and APS minerals occur in the matrix breccia associated to pyrite and dickite, disseminated and in voids of the vuggy silica altered rocks, and also replacing plagioclase crystals (Fig 4.11 C, D). In general, alunite is zoned, and often presents an inner core of APS minerals (woodhouseite and/or svanbergite; Fig 4.11 C). Representative chemical data for alunite and APS minerals from Cerro Quema are shown in table 4.5 and Appendix 3.

Alunites are Na-rich (2.26-4.79 wt% Na_2O), exhibiting the wide compositional range of the alunite-natroalunite solid solution. Ca is generally low (< 0.36 wt% CaO), Fe is also low (< 0.26 wt% Fe_2O_3) with the exception of one alunite exhibiting 2.16 wt% Fe_2O_3. P is generally present as a trace (< 0.56 wt% P_2O_5). A few alunite samples show P enrichment (1.23-3.20 wt% P_2O_5), which is correlated with an enrichment in Sr (3.28-3.39 wt% SrO) and in Ba (1.07-1.73 wt% BaO). In contrast, APS minerals show irregular trace-element (Na, Ca, Sr, Ba and Fe) content. S ranges from 14.65 to 23.86 wt% SO_3, and P ranges from 10.14 to 18.97 wt% P_2O_5. APS show enrichment in Sr (13.18-19.14 wt% SrO) and Ca (0.58-4.02 wt% CaO) with occasional Ba enrichment (1.04-1.45 wt% BaO), characteristic of the woodhouseite-svanbergite solid solution. Na and Fe are generally low (<0.94 wt% Na_2O and <0.94 wt% Fe_2O_3), with a few exceptions exhibiting up to 2.09 wt% Na_2O and up to 1.58 wt% Fe_2O_3.

4.6. $^{40}Ar/^{39}Ar$ Geochronology

The $^{40}Ar/^{39}Ar$ method for determining the radiometric age of earth materials has gained widespread acceptance in the geological community and has been

	9107-11.55	9343-66	9316-173.2	9316-236	0308-51.8	0308-73.6
Alteration	Vuggy silica	Vuggy silica	Vuggy silica	Vuggy silica	Advanced argillic	Advanced argillic
Location	La Pava	Cerro Idaida	La Pava	La Pava	Chontal Edge	Chontal Edge
Fe (wt %)	n=4	n=10	n=15	n=7	n=9	n=10
min-max	43.68-46.63	44.51-46.84	44.10-46.72	44.63-46.58	44.61-46.51	43.59-46.53
median	44.68	45.38	45.76	45.44	45.97	46.17
average (±sd)	44.92 (±1.48)	45.61 (±0.72)	45.61 (±0.69)	45.37 (±0.66)	45.72 (±0.64)	45.87 (±0.85)
S (wt%)	n=4	n=10	n=15	n=7	n=9	n=10
min-max	52.52-53.38	53.10-53.85	52.68-54.14	52.85-53.54	53.31-54.02	53.08-54.06
median	52.92	53.53	53.49	53.35	53.51	53.46
average (±sd)	52.94 (±0.48)	53.56 (±0.22)	53.54 (±0.37)	53.29 (±0.24)	53.57 (±0.22)	53.47 (±0.30)
Cu (wt%)	n=2	n=10	n=15	n=6	n=9	n=7
min-max	1.12-1.14	0.03-2.12	0.06-3.67	0.57-2.21	0.05-1.72	0.12-3.16
median	1.13	0.47	0.24	1.28	0.24	0.19
average (±sd)	1.13 (±0.01)	0.82 (±0.74)	0.56 (±0.94)	1.22 (±0.61)	0.48 (±0.57)	0.71 (±1.11)
Co (ppm)	n=3	n=0	n=2	n=4	n=3	n=1
min-max	500-17800	-	183-800	175-400	200-300	1100
median	17800	-	492	400	231.00	-
average (±sd)	12033 (±9988)	-	492 (±436)	344 (±113)	244 (±51)	-
Ni (ppm)	n=3	n=1	n=2	n=4	n=1	n=1
min-max	700-4300	300	200-700	200-600	300.00	200
median	4300	-	450	400	-	-
average (±sd)	3100 (±2078)	-	450 (±354)	400 (±183)	-	-
Se (ppm)	n=4	n=1	n=5	n=4	n=4	n=3
min-max	200-500	300	200	200	200-300	200-300
median	400	-	200	200	200.00	200
average (±sd)	375 (±150)	-	200 (±0)	200 (±0)	225 (±50)	233 (±58)
Ag (ppm)	n=1	n=5	n=5	n=5	n=3	n=0
min-max	400	300-300	300	300-400	300-400	-
median	-	300	300	300	300	-
average (±sd)	-	300 (±0)	300 (±0)	340 (±55)	333 (±58)	-
Cd (ppm)	n=4	n=2	n=1	n=0	n=2	n=1
min-max	300-311	300-300	300	-	300	300
median	306	300	-	-	300	-
average (±sd)	306 (±7.8)	300 (±0)	-	-	300 (±0)	-
Sb (ppm)	n=1	n=1	n=7	n=2	n=4	n=5
min-max	500	500	500-700	500	500-700	500-700
median	-	-	600.00	500.00	600.00	600.00
average (±sd)	-	-	600 (±100)	500 (±0)	600 (±82)	600 (±71)
Co/Ni	n=3	n=0	n=2	n=4	n=1	n=1
min-max	0.71-4.14	-	0.92-1.14	0.58-2.00	1.00	5.50
median	4.14	-	1.03	0.73	-	-
average (±sd)	3.00 (±4.81)	-	1.03 (±0.16)	1.01 (±0.66)	-	-
S/Se	n=4	n=1	n=5	n=4	n=4	n=3
min-max	1050-2669	1782	2634-2694	2658-2669	1801-2681	1779-2664
median	1414	-	2675	2665	2678	2654
average (±sd)	1637 (±769)	-	2671 (±25)	2664 (±5)	2459 (±439)	2365 (±508)

Table 4.4: Quantitative analyses, Co/Ni and S/Se ratios of pyrites from Cerro Quema.

Sample	1	2	3	4	5
Description	Natroalunite	Natroalunite	Natroalunite	APS	APS
Al_2O_3	35.86	33.43	33.6	32.53	31.83
FeO Total	0.05	0.14	2.16	0.00	0.26
CaO	0.02	0.17	0.23	0.77	2.49
Na_2O	4.22	3.77	4.62	0.92	0.52
K_2O	4.31	3.56	1.98	0.52	0.41
P_2O_5	0.25	2.42	3.20	12.33	17.53
F	0.33	0.06	0.55	0.45	0.62
SO_3	38.43	35.85	34.34	20.14	16.65
CuO	0.10	0.08	0.00	0.29	0.00
As_2O_5	0.04	0.00	0.02	0.05	0.04
SrO	0.51	3.39	3.28	16.44	15.81
BaO	0.42	0.38	1.73	0.41	0.22
CeO	0.00	0.27	0.59	0.29	0.22
PbO	0.10	0.16	0.26	0.00	0.25
$(H_2O)^*$	15.36	16.31	13.43	14.86	13.16
(Total)**	100	100	100	100	100
		Cations based on 14 oxygen atoms			
Al	2.83	2.65	2.78	2.81	2.80
Fe	0.00	0.01	0.13	0.00	0.02
Ca	0.00	0.01	0.02	0.06	0.20
Na	0.55	0.49	0.63	0.13	0.08
K	0.37	0.31	0.18	0.05	0.04
P	0.01	0.14	0.19	0.77	1.11
F	0.07	0.01	0.12	0.10	0.15
S	1.93	1.81	1.81	1.11	0.93
Cu	0.01	0.00	0.00	0.02	0.00
As	0.00	0.00	0.00	0.00	0.00
Sr	0.02	0.13	0.13	0.70	0.68
Ba	0.01	0.01	0.05	0.01	0.01
Ce	0.00	0.01	0.02	0.01	0.01
Pb	0.00	0.00	0.00	0.00	0.01
Calculated H	6.86	7.32	6.30	7.28	6.54
Total cations	12.66	12.91	12.36	13.05	12.55

Table 4.5: Representative analyses of alunites and APS minerals from Cerro Quema. Oxide content is expressed in wt %. * Calculated by difference. ** Assume 100% sum. 1: Na-rich alunite (Natroalunite). 2: Sr-rich Natroalunite. 3: Sr-, P- and Ba-rich Natrolaunite (Natroalunite-Svanbergite). 4: Sr-rich APS (Svanbergite). 5: Sr- and Ca-rich APS (Svanbergite-Woodhouseite).

applied to a host of problems including sedimentary provenance studies, paleomagnetism, thermal histories of metamorphic terranes and mantle, and atmospheric evolution (Lee *et al*., 1991). In particular, many studies have focused on hornblende because of its high retentivity of Ar and its presence in a large variety of rock types.

First geochronological studies of arc rocks in the Azuero Peninsula were carried out by Del Giudice and Recchi (1969) and Kesler *et al*, (1977). Their work was focused on dating (K/Ar) the Azuero Peninsula batholits (e.g., El Montuoso and Valle Rico, see Fig. 4.1 for location). Del Giudice and Recchi (1969) obtained an age of 69 ± 10 Ma for a quartz-diorite from El Montuoso batholith, and 53 ± 3 Ma for a quartz-diorite from the Valle Rico batholith. Later on, Kesler *et al*, (1977), obtained K/Ar ages on hornblende and plagioclase from a quartz-diorite from El Montuoso batholith, of 64.87 ± 1.34 Ma and 52.58 ± 0.63 Ma, respectively.

Lissina, (2005) reported Ar/Ar ages of eastern Azuero Peninsula arc rocks. Results from Punta Mala area were 52.0 ± 0.2 Ma (basalt matrix) and 50.7 ± 0.1 Ma (granite plagioclase), and 60.9 ± 0.5 Ma (basalt matrix) from NE Azuero Peninsula. Granodiorites and granites from the Valle Rico batholith gave ages of 49.5 ± 0.2 Ma (plagioclase) and 50.6 ± 0.3 Ma (plagioclase), respectively.

A recent study by Wegner *et al*, (2011) provided new hornblende Ar/Ar ages of arc rocks from the central Azuero Peninsula, obtaining an age of 67.5 ± 1.9 Ma and of 71.0 ± 2.0 Ma for a dacite. Montes *et al*, (2012) reported three U/Pb ages on zircons from El Montuoso batholith (67.7 ± 1.4 Ma, 66.0 ± 1.0 Ma and, 67.6 ± 1.0 Ma), an age from the Valle Rico batholith (49.2 ± 0.9 Ma) and two ages from the Parita batholith (48.1 ± 1.2 Ma and 41.1 ± 0.7Ma; see Fig. 4.1B for location).

All the previously described radiometric ages, togwther with the Ar/Ar ages obtained in the present study, allowed to reconstruct the geological history of the Azuero Peninsula, as well as to constrain the age of the Cerro Quema deposit.

Sample	UTM Coordinates		Rock	Mineral	Plateau	N
	Easting	Northing			Age (Ma) ± σ	
El Montuoso batholith						
PIT 01	538993	844948	Quartz-diorite	Amphibole	65.7 ± 1.4	4 of 8
			Quartz-diorite	Amphibole	65.5 ± 0.7^a	9 of 9
Dacite (Río Quema fm.)						
LP 204	552352	833906	Dacite	Amphibole	67.9 ± 1.3	5 of 9
			Dacite	Amphibole	69.7 ± 1.2^a	7 of 7
			Dacite	Amphibole	66.0 ± 1.1	5 of 7
			Dacite	Amphibole	65.6 ± 1.3	3 of 6
Valle Rico batholith						
TRI 01	577143	842439	Quartz-diorite	Amphibole	54.8 ± 1.2^a	11 of 11
Parita batholith						
PA 01	525135	890665	Diorite	Amphibole	40.8 ± 1.4	4 of 12

Table 4.6: Summary of $^{39}Ar/^{40}Ar$ incremental-heating experiments. a: integrated age.

In the present study, eight hornblende phenocrystals were selected for laser step-heating $^{40}Ar/^{39}Ar$ analysis, following the method of Merrihue (1965). These analyses allow us to determine the age of four different country rocks related with the Cerro Quema deposit. Results are shown in Table 4.6 and in Figure 4.12.

Mineral separates were prepared by crushing 1 Kg of rock, sieving, washing and finally handpicking to obtain 100 mg of optically pure mineral. The $^{40}Ar/^{39}Ar$ analyses were performed at the U. S. Geological Survey (Denver, Colorado) on samples irradiated at the US Geological Survey TRIGA reactor in Denver, Colorado (Dalrymple *et al.*, 1981). Sample PIT-1 was collected near Pitaloza village, and corresponds to the El Montuoso batholit. Sample TRI-1 was collected near Trinidad village and represents the Valle Rico batholith. Sample LP204 is a dacite of the dome complex of the Río Quema Formation, collected in the mining area, representing the Cerro Quema host rock. Sample PA-01 was collected near the Parita village, N of the Ocú-Parita fault, and corresponds to the Parita batholiths, an intrusive stock of the Azuero Arc Group. Sample location is summarized in Table 4.6.

An attempt to date the volcaniclastic sediments of the Río Quema Formation was made in order to get an age of all the volcanic, volcaniclastic and plutonic rocks of the Azuero Arc Group. Unfortunately no plateau ages could be obtained and the integrated ages (143 ± 11 Ma and 98 ± 7 Ma) have no geologic sense within the geologic framework of the Azuero Peninsula.

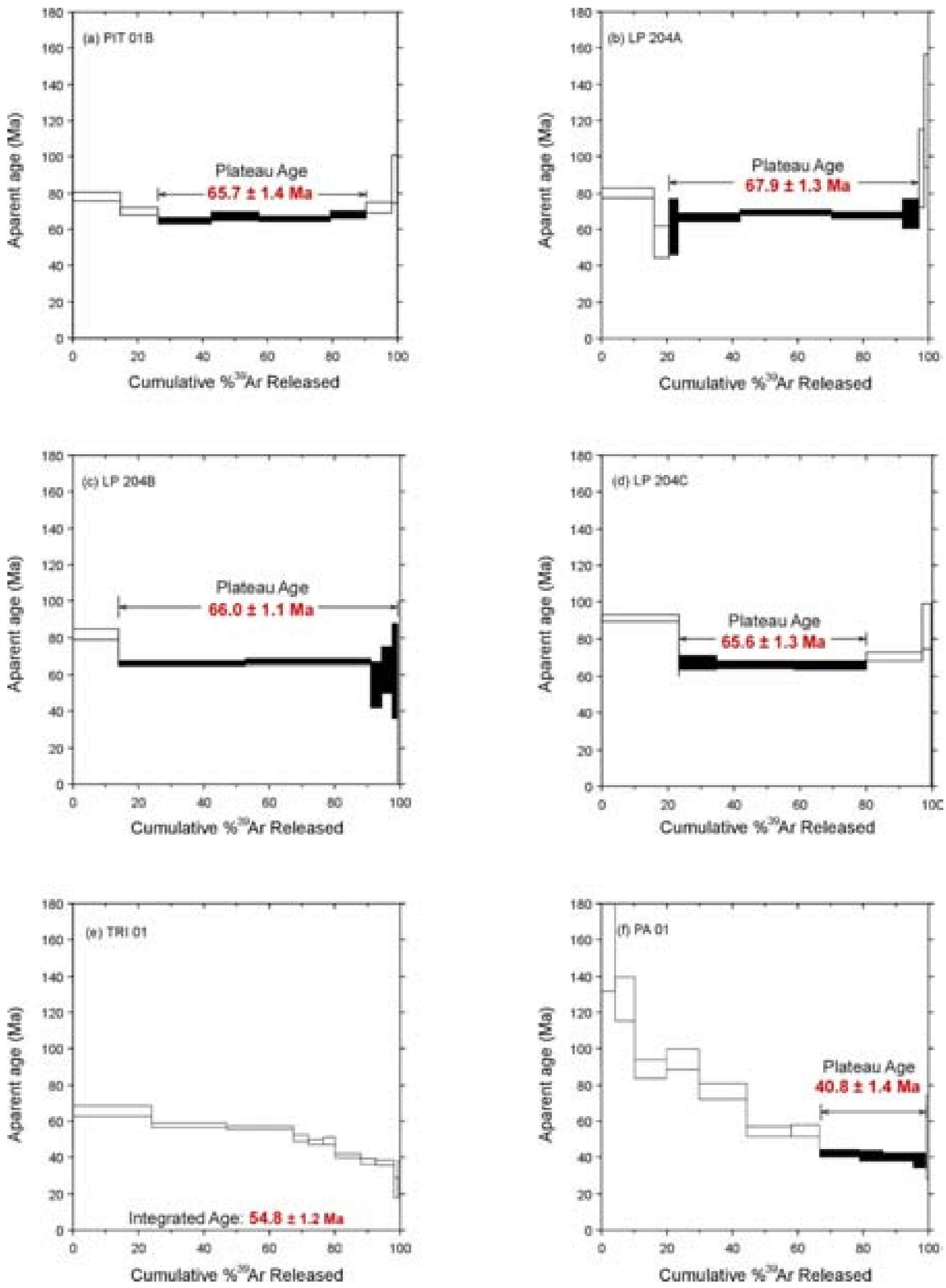

Figure 4.12: Hornblende argon age spectra of the dated rocks related with the Cerro Quema deposit. All diagrams are plotted using the same age scale for comparison. Arrows indicate the steps used for plateau ages.

4.7. Discussion

4.7.1. Deposit classification

According to the previously described spatial distribution of the hydrothermal alteration (e.g., vuggy silica grading to advanced argillic and to argillic), and its mineralogy (e.g., alunite, APS minerals, barite, kaolinite, dickite, pyrophyllite), together with the mineralization style (e.g., dissemination and veinlets of pyrite, enargite, tennantite, chalcopyrite), Cerro Quema fit well within the classical high sulfidation epithermal model described by Hedenquist, (1987), Berger and Henley (1989), White (1991), Hedenquist and Lowenstern (1994), and Arribas *et al*. (1995b). And consequently, its hydrothermal alteration and mineralization could be related to the circulation of acidic fluids of magmatic origin derived from the emplacement of an underlying porphyry copper intrusion.

Field observations suggest that the model based on an oxidized Au-Cu deposit that shares characteristics of both, epithermal and volcanogenic massive sulfide (VMS) deposits (Nelson and Nietzen, 2000; Nelson, 2007) can be discarded, as no signs of lenses or bedded massive sulfides were found in surface outcrops nor in drill holes. Thus, our work are in agreement and confirms the hypothesis proposed by Leach (1992), Cerro Quema is a high sulfidation epithermal Au-Cu deposit.

4.7.2. Trace element distribution

Hypogene mineralization was the first hydrothermal process affecting the host rock, developing the sulfide zone. Later, weathering of the hypogenically altered rock caused the dissolution and oxidation of hypogene minerals developing the oxide zone.

In the sulfide zone Au is well correlated with Ag, Pb and Ba (Table 4.3; Fig. 4.13A, 4.13B). Assuming that Au is present as invisible gold associated to the pyrite lattice (Corral *et al*., 2011a), Au-Ba correlation suggests that Au-bearing pyrite is associated to the presence of barite. Au and Ag are also well correlated suggesting the presence of both elements within the pyrite lattice. As the Ag content in whole rock is up to 1 ppm, and up to 400 ppm in pyrites (see table 4.4), the Ag content in the mineralized rock seems to be related to the presence of disseminated pyrite. Correlation of Au with Pb is not well understood, however Pb could be related to the presence of Pb-bearing minerals and as sulfosalts. Cu is strongly correlated with Zn (Fig. 4.13C), well correlated with Cd and As (Fig. 4.13D), and poorly correlated with Pb, suggesting that Cu is associated to cupriferous pyrite and chalcopyrite, containing Zn traces or sphalerite inclusions. Correlation between Cu and As, and Cu and Sb, is explained by the presence of enargite and tennantite which could also explain the correlation of Cu and As with Zn and Ag and of Sb with As (Fig. 4.13E). The lack of correlation between Cu and Au (Figure 4.13F) may be due to the presence of Au within the pyrite lattice whereas Cu is associated to Cu-bearing minerals (chalcopyrite, enargite and tennantite). The strong correlation of Zn with Cu and Pb, could be due to the presence of a disseminated sphalerite in the sulfide zone and/or as sphalerite inclusions in pyrite, which could also explain the good correlation of Zn and Cd and As.

Trace element distribution and correlations in the oxide zone strongly differ from those in the sulfide zone. Oxidation produces dissolution of cupriferous pyrite, chalcopyrite, Ba-bearing minerals, enargite and tennantite, resulting in an enrichment of Au, Ag, Pb and Sb (inmobile elements), and a depletion of Cd, Cu, Zn, As and Ba (mobile elements).

In the oxide zone, Au and Ag are not well correlated with each other nor with other trace elements (see Table 4.3), which could be explained from the difference in element mobility during mineral dissolution. As and Sb are strongly correlated (Fig. 4.13E), and do not correlate well with other trace elements, suggesting that As and Sb could be present as oxides in this zone.

Only two analyzed samples have Hg contents above the detection limit (11 and 6 ppm, respectively). As Hg is commonly partitioned into a rising vapor phase by boiling (Barnes and Seward, 1997), such low concentration may suggest that the upper part of the system, where evidences of boiling usually occur, could have been eroded. Therefore, what we see today probably corresponds to the remaining deeper part of the hydrothermal system.

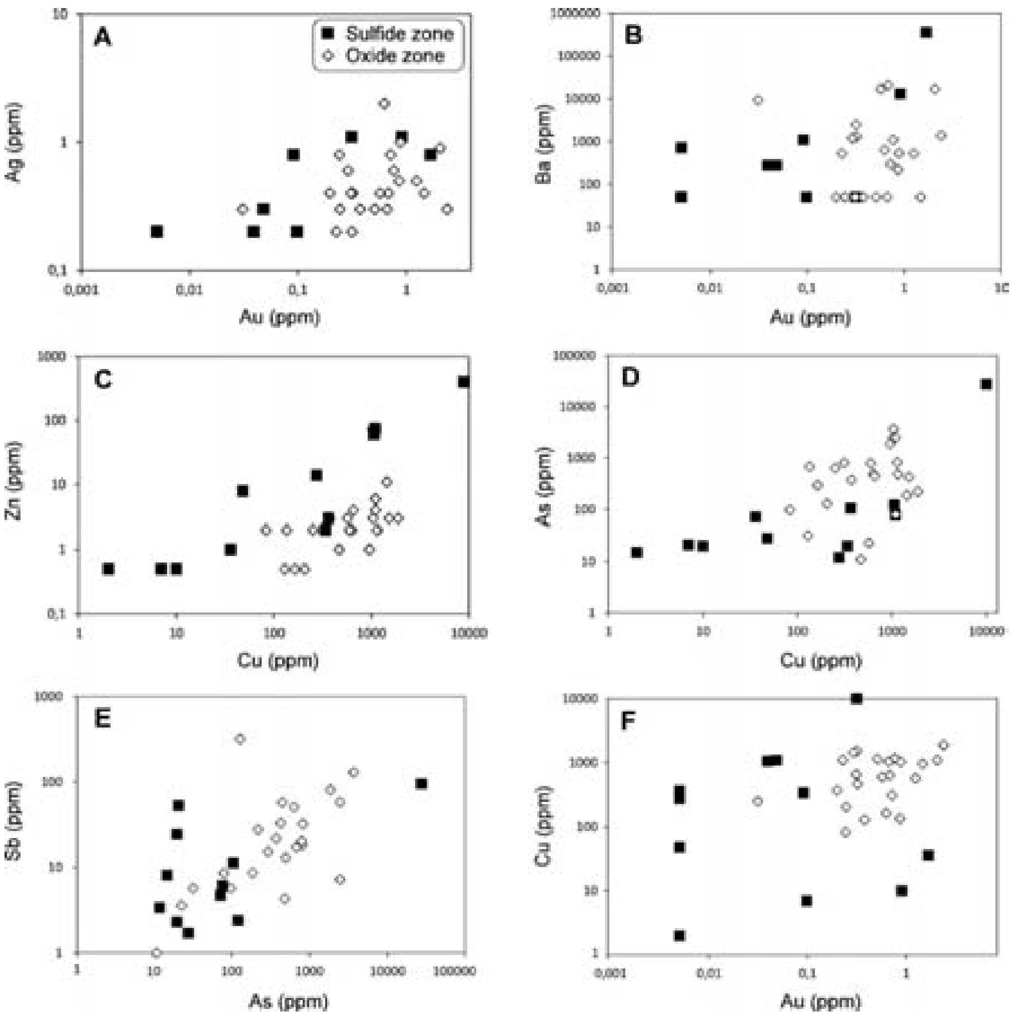

Figure 4.13: Correlation plots between element pairs. A: Au-Ag. B: Au-Ba. C: Cu-Zn. D: Cu-As. E: As-Sb. F: Au-Cu. All plots show good correlation whereas the Au-Cu plot (F) does not.

An important conclusion from trace element distribution and correlation is that Au exploration should be focused in the oxide zones in areas where the Ba anomaly is high. As usual in this type of deposits, Cu exploration should be centered in the sulfide zone, below the red-ox boundary, where primary copper sulfides such as enargite, bornite and tennantite, and secondary copper sulfides such as chalcocite and covellite are present.

4.7.3. Pyrite composition

Hydrothermal pyrites typically contain a host of minor and trace element, including: Ag, As, Au, Bi, Cd, Co, Cu, Hg, Mo, Ni, Pb, Pd, Ru, Sb, Se, Sb, Sn, Te, Tl and Zn (Abraitis *et al*., 2004). Trace element content in pyrites has been used as indicative of their origin (e.g., Loftus-hills and Solomon, 1967; Fintor *et al*., 2011). EMPA analyses of pyrite from Cerro Quema are reported in Table 4.4. No relationship between trace element content and pyrite texture (e.g., idiomorphic, zoned and framboidal; Fig. 4.11A, 4.11B), has been observed. Pyrites do not show significant differences in terms of major and trace elements, excepting for their Cu, Co and Ni content.

The Cu content in pyrites at Cerro Quema is especially high (up to 3.67 wt%). This Cu anomaly could be explained by the presence of submicroscopic inclusions of Cu-bearing mineral phases, such as chalcopyrite, enargite and tennantite and/or by the presence of Cu in the pyrite lattice (Huston *et al*., 1995; Abraitis *et al*., 2004).

Co/Ni ratio in pyrites has been used to distinguish between magmatic-hydrothermal and sedimentary origin of pyrites (e.g., Loftus-hills and Solomon, 1967; Price, 1972; Bralia *et al*., 1979; Bajwah *et al*., 1987; Brill, 1989; Raymond, 1996; Fintor *et al*., 2011), Co/Ni ratios from ~1 to 5 have been assigned to hydrothermal pyrites, whereas Co/Ni ratio values of < 1 are typical of pyrites of sedimentary or digenetic origin. Cerro Quema pyrites have Co/Ni ratios ranging from 0.58 to 5.50, with an average of 1.96, suggesting a hydrothermal origin irrespective of their textures (Fig. 4.14). Therefore, framboidal pyrite (Fig. 4.11) at Cerro Quema formed in a hydrothermal environment contrasting with similar textures typical of sedimentary-diagenetic environments.

S/Se ratios have also been used to discriminate between sedimentary and magmatic-hydrothermal origin of pyrites. S/Se values of < 15,000 correspond to magmatic-hydrothermal origin whereas those of sedimentary origin have values > 30,000 (Edwards and Carlos, 1954). S/Se ratio values of pyrites from Cerro Quema range from 1050 to 2694, pointing to a magmatic-hydrothermal origin, in agreement with the results from Co/Ni ratio.

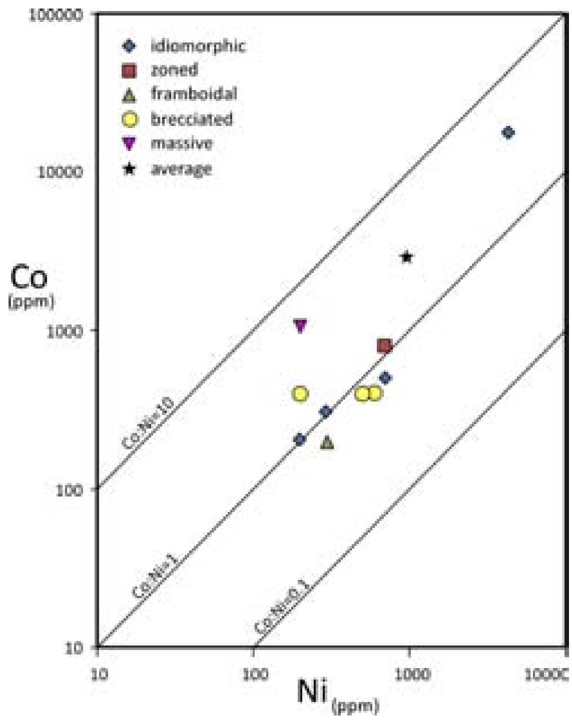

Figure 4.14: Distribution of cobalt and nickel contents of pyrites from the Cerro Quema deposit.

4.7.4. Sulfate composition

Analyzed alunites are Na-rich, covering the wide range of alunite-natroalunite solid solution. The core of alunite-natroalunites is constituted by Aluminum-Phosphate-Sulfate minerals (APS), which are also found as single crystals in the advanced argillic alteration zone. APS are Sr and Ca-rich, which correspond to the woodhouseite-svanbergite solid solution.

Studies focused on the alunite geochemistry (e.g., Stoffregen and Alpers, 1987; Arribas *et al*., 1995a; Deyell *et al*., 2005), showed that although trace-element concentrations are extremely variable, supergene alunite is generally K-rich in comparison with that of higher temperature occurrences. According to Stoffregen and Cygan (1990), the Na enrichment in alunite is due to the preferential incorporation of Na into the alunite structure at high temperatures, assuming a constant K/Na ratio in the solution. On the other hand, Aoki *et al*, (1993) suggested that the core of hypogene alunite is commonly enriched in PO_4 and multi-valent cations such as Ca (crandalite, woodhouseite), Sr (svanbergite) and Ba (groceixite). These complexes are usually rimmed by minamiite and rhythmic bands of alunite and natroalunite (Stoffregen and Alpers 1987, Aoki *et al*., 1993), as observed in the Cerro Quema alunites.

Texture and chemical characteristics of alunite-natroalunite and woodhouseite-svanbergite from Cerro Quema (see Fig. 4.11C, 4.11D and Table 4.5) present all the previously mentioned characteristics which indicate a magmatic hydrothermal origin, related to an intrusion-driven hydrothermal system.

4.7.5. Geochronology

Ar/Ar ages of this study complete the existing radiometric and biostratigraphic ages of the volcanic, volcaniclastic, sedimentary and plutonic rocks of the Azuero Peninsula and allow to constrain the age of the Cerro Quema deposit.

Quartz-diorites of the El Montuoso batholith belong to the Azuero Arc Group and represent the arc-related intrusives of the Cretaceous volcanic arc. Plateau and integrated Ar/Ar ages obtained from hornblendes of the El Montuoso batholith (65.7 ± 1.4 Ma and 65.5 ± 0.7 Ma) are in agreement with previous hornblende K/Ar ages (69 ± 10 Ma and 64.87 ± 1.34 Ma) of Del Giudice and Recchi (1969) and Kesler (1977), and also with recent zircon U/Pb ages (67.7 ± 1.4 Ma, 66.0 ± 1.0 Ma and, 67.6 ± 1.0 Ma) of Montes *et al*, (2012). Younger plagioclase K/Ar age (52.58 ± 0.63 Ma) was obtained by Kesler (1977) and it was interpreted as due to partial postcrystallization argon loss from the plagioclase.

Dacite dated in this study belongs to the syn-volcanic intrusion of the Cretaceous volcanic arc of the Azuero Arc Group. Obtained hornblende Ar/Ar ages (67.9 ± 1.3 Ma, 66.0 ± 1.1 Ma, 65.6 ± 1.3 Ma and 69.7 ± 1.2 Ma) correspond to the dacite dome complex of the Río Quema Formation (Corral *et al*., 2011a; 2013). A recent study of Wegner *et al*, (2011) reported two ages of 71.0 ± 2.0 and 67.5 ± 1.9 Ma for two dacite samples located in the central Azuero Peninsula.

Dating the volcaniclastic sediments of the Río Quema Formation by radiometric methods was not possible. However, a recent study by Corral *et al*. (2013) based on biostratigraphy, proposed a Late Campanian to Maastrichtian age for the limestone beds interbedded with the dacite domes, volcanic and volcanicalastic rocks of the Río Quema formation. This age represents the oldest arc-related volcanic rocks of the Azuero Arc Group, corresponding to a fore-arc basin sequence.

The Valle Rico quatz-diorite batholith belongs to the Azuero Arc Group and represents the arc-related intrusive of the Paleogene volcanic arc of the Azuero Peninsula. This batholith intruded following E-W trending regional faults, to the north of the Cretaceous volcanic arc (arc and fore-arc), producing thermal contact aureolas (Corral *et al*., 2011a, 2013). The obtained integrated Ar/Ar age, 54.8 ± 1.2 Ma is in agreement with a previous hornblende K/Ar age of 53 ±3 Ma (Del Giudice and Recchi, 1969). However, our hornblende age is older than plagioclase Ar/Ar ages of 49.5 ± 0.2 Ma and 50.6 ± 0.3 Ma, reported by Lissinna (2005) from the same batholith. This discrepancy could be caused by partial postcrystallization argon loss from the plagioclase, although recent zircon U/Pb dating by Montes *et al*. (2012) reported an age of 49.2 ± 0.9 Ma, similar to those obtained by Lissina (2005). The reasons for the discrepancy between our data and Lissina's are not still understood.

The Northernmost intrusive of the Azuero Peninsula is the Parita batholith, which corresponds to the youngest plutonic event in the area. Plateau age of this batholith is 40.8 ± 1.4 Ma, in agreement with the zircon U/Pb ages of (48.1 ± 1.2 Ma and 41.1 ± 0.7Ma) reported by Montes *et al*, (2012) for the same batholith. The Parita batholith is interpreted as the Paleogene expression of the Panamanian volcanic arc, which indicates the arc migration towards the North during Eocene times.

4.7.6. Age of the Cerro Quema deposit

Alunite is a common subject of isotopic and age measurements in the study of high suflidation epithermal deposits (e.g., Rye *et al*., 1992; Arribas *et al*., 1995b; Itaya *et al*., 1996; Rye, 2005). Unfortunately, in our case, the small size of the crystals and their fine intergrowth with kaolinite-dickite did not allow to obtain pure samples for dating. Therefore the age of the Cerro Quema deposit has been constrained from field evidences coupled with biostratigraphic data of sedimentary rocks of the Río Quema Formation (Corral *et al*., 2013) and geochronological data of the igneous rocks of the Azuero Peninsula. The estimated age of the deposit is based on the following observations:

1) Crystal-rich sandstones and turbidites of the Río Quema Formation, a volcano-sedimentary sequence of Campanian-Maastrichtian age (Corral *et al*., 2013), do not contain pebbles and/or fragments from the erosion of rocks affected by hydrothermal alteration. Therefore, hydrothermal alteration (and associated mineralization) shold be younger than the age of hese rocks. Also, dacite pebbles in conglomerates resulting from the erosion of the dacite dome complex, the Cerro Quema host rock (71-66 Ma; Wegner *et al*., 2011; this study), show no signs of hydrothermal alteration. Therefore, hydrothermal alteration and mineralization should be younger than 71-76 Ma, the age of the dacite dome complex.

2) According to Hedenquist and Lowernstein (1994) and Arribas (1995), high sulfidation epithermal deposits may be related to porphyry copper intrusions at depth. If this is the case, Cerro Quema should be related to a magmatic event. In the Azuero Peninsula, the first recorded magmatic event after the Cretaceous, occurred during the Lower Eocene (55-49 Ma; Del Giudice and Recchi, 1969; Kesler *et al*., 1977; Lissinna, 2005; Montes *et al*., 2012; this study), and corresponds to Valle Rico-like batholith intrusions. These intrusions occurred following E-W trending regional faults along the entire fore-arc basin, from North, where they produced thermal contact aureoles in the Río Quema Formation (Corral *et al*., 2011; 2013), to South, near the Agua Clara Fault (See Fig. 4.2 for location). Therefore, if mineralizing fluids derived from the emplacement of a porphyry copper-like intrusion at depth, associated to the Valle Rico batholith, the likely maximum age of the Cerro Quema deposit should be 55-49 Ma (Lower Eocene).

Our estimated age for Cerro Quema, deduced from geological constraints, contrasts with ages of other high sulfidation epithermal deposits in Central and South America, such as Pueblo Viejo (Dominican Republic; Kesler *et al*., 1981; Nelson, 2000), Yanacocha (Peru; Turner, 1997, 1998; Longo, 2005; Longo *et al*., 2010) and La Coipa (Chile; Oviedo *et al*., 1991), which are related to the emplacement of volcanic dome complexes, suggesting that mineralization and host rocks are contemporaneous. If Cerro Quema formed during the dome complex emplacement (although such a genetic relationship could not be demonstrated) the age of the deposit should be of Upper Cretaceous age (~70 – 66 Ma), the age of the dacite dome complex.

In any case, our estimated age should be confirmed from further dating (e.g., Ar/Ar in alunites, Re/Os in sulfides and/or U/Pb in hydrothermal rutiles). Meanwhile, the age of the Cerro Quema deposit remains as an open question.

4.8. Geologic evolution and epithermal mineralization

This section focuses on the different events that chronologically occurred from Late Cretaceous to present times in order to understand the geologic evolution of the Azuero Peninsula and the formation of the Cerro Quema deposit. Geologic evolution is synthesized in Figure 4.15.

4.8.1. Arc development

The Late Campanian (~75-73 Ma) marked the initiation of the Farallon plate subduction (Buchs *et al*., 2010), a thin oceanic crust, beneath the Caribbean plate, a thick oceanic plateau. According to the models of Stern and Bloomer (1992) and Stern (2010), the initial stages of an intra-oceanic subducion are characterized by extension of the overriding plate. In the Azuero Peninsula, this extension controlled the morphology and evolution of the volcanic arc. From Late Campanian to Maastrichtian (~71-65 Ma) the first stage of magmatism occurred on the Carribbean Plate. This stage is characterized by the intrusion of

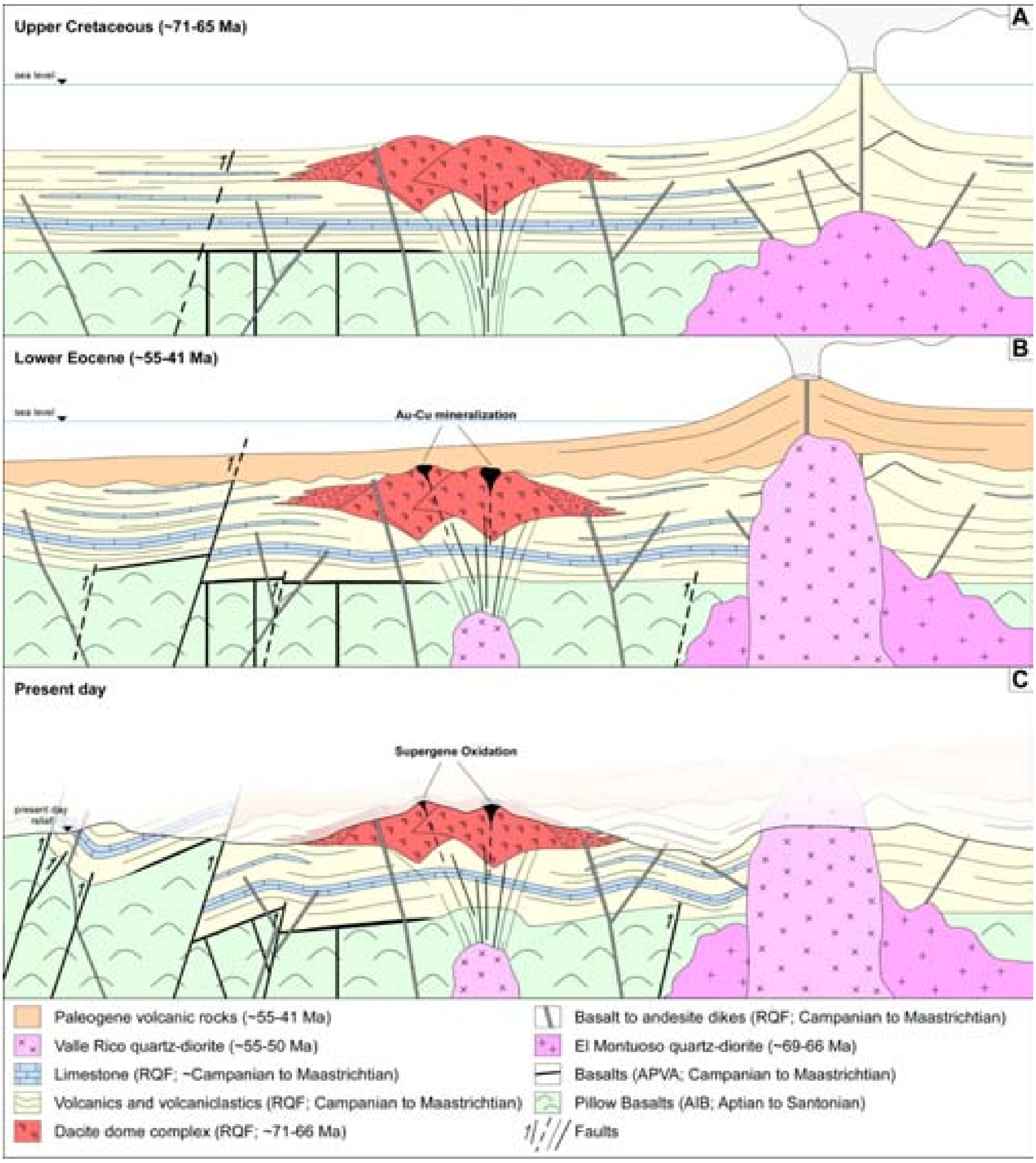

Figure 4.15: Geologic model of the Cerro Quema deposit and the Azuero Peninsula from Late Cretaceous to present. AIB: Azuero Igneous Basement, APVA: Azuero Primitive Volcanic Arc, RQF: Río Quema Formation.

the El Montuoso batholith and the development of the arc and fore-arc basin. The Río Quema Formation, of Late Campanian to Maastrichtian age, filled up the fore-arc basin and recorded the volcanic and sedimentary processes of Late Cretaceous volcanic arc. Contemporarily to the volcanism, a dacite dome complex (Cerro Quema host rock), intruded the Río Quema formation, being interstratified with the volcanic and sedimentary sequences of the fore-arc basin (Fig. 4.15A).

4.8.2. Arc maturation and emplacement of the Cerro Quema deposit

During lower Eocene (~55-49 Ma) a second stage of magmatism occurred (Fig. 4.15B). Valle Rico-like batholiths intruded along E-W trending regional faults mainly to the north of the Cretaceous fore-arc basin, where produced thermal contact aureoles. However some Valle Rico-like intrusions (quartz-diorites, diorites and trachiandesites) occurred in the central and southern limit of the fore-arc basin. Porphyry copper intrusion related with the Valle Rico batholith, intruded beneath the fore-arc basin, triggered the development of the Cerro Quema deposit in the dacite dome complex of the Río Quema Formation.

4.8.3. *Arc migration*

During the ~48-40 Ma span, the Azuero Peninsula suffered the accretion of intra-oceanic island arcs such as la Hoya and Punta Blanca islands (Buchs *et al.*, 2011a). Subduction erosion and possible slab flattening induced the migration of the arc front towards the Caribbean. The emplacement of the Parita batholith to the North of the Ocú-Parita Fault (See Fig. 4.1 for location) corroborates the front arc migration towards the North during this stage.

4.8.4. Erosion and supergene enrichment

Since the emplacement of the Cerro Quema Au-Cu deposit (~55-49 Ma) until present, erosion and supergene enrichment processes have been affecting the Panamanian volcanic arc as well as the Cerro Quema deposit (Fig 4.15C). In order to estimate the minimum depth of erosion, we used stability temperature ranges of mineral associations in the alteration zones (e.g., Stoffregen, 1987; Reyes, 1990, 1991; Reed and Barnes, 1997), and salinity data from fluid inclusions (Corral *et al.*, 2011b).

The main clay mineral association cropping out at Cerro Quema is kaolinite ± illite ± illite/smectite, indicating a temperature range of 180-220ºC during mineral precipitation. Assuming this temperature range and a fluid salinity of 2 wt% NaCl eq. (Corral *et al.*, 2011b), the minimum estimated depth of erosion is approximately 100 m. However, the presence of other clay mineral associations such as dickite ± pyrophyllite ± illite, indicate a temperature range of 200-250ºC. In this case, the estimated minimum depth of erosion would be approximately 250 m.

The erosion of 100-250 m produced the disappearance of the uppermost superficial expression of the Cerro Quema deposit. As a consequence, oxidation and intense weathering generated a thick Au-bearing, silica- and iron-rich lithocap of up to 150 m depth, below which a Cu-rich zone is developed (Fig. 4.15C). This supergene enrichment is the process which made the deposit to be economically profitable.

4.9. Summary and conclusions

In the present work, new data on the geology, mineralogy and geochemistry of the Cerro Quema Au-Cu deposit are presented, emphasizing the relationship between volcanism and gold mineralization. Based on field and geochronological data, a geologic model integrating the genesis of the Cerro Quema deposit within the geotectonic framework of the Azuero Peninsula is presented. The main conclusions are as follows:

1) Cerro Quema is a high sulfidation epithermal Au-Cu deposit, hosted by the dacite dome complex of the Río Quema Formation. It is a composite, structurally and lithologically controlled deposit, characterized by four hydrothermal alteration halos with vuggy silica in the inner zone, grading to advanced argillic, argillic and propyllitic alteration. Mineralization consists in a dissemination and microveinlets of pyrite with minor chalcopyrite, enargite and tennantite, with traces of sphalerite, crosscut by intermediate sulfidation base metal veins, composed of pyrite, quartz and barite with traces of sphalerite, chalcopyrite and galena.

2) Weathering and supergene oxidation processes affected the Cerro Quema deposit developing two different mineralized zones. An upper quartz and iron oxides lithocap, enriched in Au, Ag, Pb and Sb, and a lower supergene enrichment zone, where Cu, Cd, Zn, As and Ba are concentrated. Whole rock trace metal content and correlation coefficients between element pairs suggest that Au exploration should be focused in the oxide zone with high Ba anomaly. On the other hand, Cu exploration should be centered in the supergene enrichment zone, in places where primary and secondary Cu-sulfides are present.

3) Idiomorphic, zoned, framboidal and brecciated pyrites from the Cerro Quema deposit show similar trace element content despite of their different texture. Pyrites are especially rich in Cu, however significant concentrations in Co, Ni, Ag, Se and Sb have been also found. Co/Ni ratio values in pyrites (0.58 to 5.50) indicate that all are hydrothermal in origin, irrespective of their textures. S/Se ratio values in pyrite (1050 to 2694) suggest a magmatic-hydrothermal origin, in agreement with the Co/Ni ratio values.

4) The advanced argillic alteration of the Cerro Quema deposit is characterized by the occurrence of alunite associated to pyrite and dickite. Zoning is a characteristic feature of alunites which often present an inner core of APS minerals. Alunites are Na-rich, covering the range of alunite-natroalunite solid solution. APS minerals are related to the core of alunite-natroalunite, but they are also present as single crystals. APS minerals are Sr, Ca and Ba-rich, characteristics of the woodhouseite-svanbergite solid solution. Alunite-natroalunite and woodhouseite-svanbergite display textural and chemical characteristics suggesting a hypogene origin, probably magmatic-hydrothermal, related to an intrusion-driven hydrothermal system.

5) Geochronological data allow to differentiate at least three stages of volcanism and plutonism in the Azuero Peninsula, ranging from Late Cretaceous to Middle Eocene. The first stage is characterized by the Cretaceous volcanic arc and fore-arc development, represented by the dacite dome complex of the Río Quema Formation (~67-66 Ma) and by the quartz-diorite batholit of the El Montuoso (~66 Ma). The second stage corresponds to

the Lower Eocene volcanic arc, characterized by the intrusion of Valle Rico-like batholiths (~55 Ma). The third stage, denoting the arc migration towards the North, corresponds to Middle Eocene plutonism, recorded by the Parita batholith (~41 Ma).

6) Field observations coupled with geochronological and biostratigraphical data, allow to estimate a maximum age of the Cerro Quema deposit as Lower Eocene (~55-49 Ma). The formation of the deposit could be related with the second stage of volcanism and plutonism recorded in the Azuero Peninsula. Hydrothermalism and mineralization are probably related with fluids derived from the emplacement of a porphyry copper intrusion associated to the Valle Rico batholith intrusion, which occurred along the entire fore-arc basin following E-W trending regional faults.

7) The geologic model of the Cerro Quema deposit demonstrates that high sulfidation deposits are not exclusive of volcanic edifices or volcanic domes related to subduction zones. High sulfidation deposits can also occur in the fore-arc basin, related to acidic intrusions between the volcanic arc front and the subduction trench. These observations should be taken into account for exploration of high sulfidation epithermal deposits in geologically similar terranes.

4.10. References

Abraitis, P. K., Pattrick, R. A. D., and Vaughan, D. J., 2004, Variations in the compositional, textural and electrical properties of natural pyrite: a review: International Journal of Mineral Processing, v. 74, p. 41-59.

Aoki, M., Comsti, E. C., Lazo, F. B., and Matsuhisa, Y., 1993, Advanced argillic alteration and geochemistry of alunite in an evolving hydrothermal system at Baguio, northern Luzon, Philippines: Shigen Chishitsu, v. 43, p. 155-164.

Arribas, A., and Tosdal, R. M., 1994, Isotopic composition of Pb in ore deposits of the Betic Cordillera, Spain; origin and relationship to other European deposits: Economic Geology, v. 89, p. 1074-1093.

Arribas, A., 1995, Characteristics of high-sulfidation epithermal deposits, and their relation to magmatic fluid, *in* Thompson, J.F.H., ed., Magmas, Fluids, and Ore Deposits, Mineralogical Association of Canada Short Course, v. 23, p. 419-454.

Arribas, A., Cunningham, C. G., Rytuba, J. J., Rye, R. O., Kelly, W. C., Podwysocki, M. H., McKee, E. H., and Tosdal, R. M., 1995a, Geology, geochronology, fluid inclusions, and isotope geochemistry of the Rodalquilar gold alunite deposit, Spain: Economic Geology, v. 90, p. 795-822.

Arribas, A., Jr., Hedenquist, J. W., Itaya, T., Okada, T., Concepcion, R. A., and Garcia, J. S., Jr., 1995b, Contemporaneous formation of adjacent porphyry and epithermal Cu-Au deposits over 300 ka in northern Luzon, Philippines: Geology, v. 23, p. 337-340.

Ashley, R. P., 1982, Occurrence model for enargite-gold deposits: U. S. Geological Survey, Open-file Report, v. 82-795, p. 144-147.

Bajwah, Z. U., Seccombe, P. K., and Offler, R., 1987, Trace element distribution, Co:Ni ratios and genesis of the Big Cadia iron-copper deposit, New South Wales, Australia: Mineralium Deposita, v. 22, p. 292-300.

Barckhausen, U., Ranero, C. R., von Huene, R., Cande, S. C., and Roeser, H. A., 2001, Revised tectonic boundaries in the Cocos Plate off Costa Rica; implications for the segmentation of the convergent margin and for plate tectonic models: Journal of Geophysical Research, v. 106, p. 19,207-19,220.

Barnes, H. L., and Seward, T. M., 1997, Geothermal systems and mercury deposits, *in* Barnes, H. L., ed., Geochemistry of hydrothermal ore deposits, 3rd ed.: New York, Wiley, p. 699-736.

Berger, B. R., and Eimon, P. I., 1983, Conceptual models of epithermal precious metal deposits: *in* Shanks, W. C. ed., Cameron Volume on Unconventional Mineral Deposits. Society of Mining Engineers of AIME, p. 191-205.

Berger, B. R., and Henley, R. W., 1989, Advances in the understanding of epithermal gold-silver deposits, with special reference to the Western United States: Economic Geology Monographs, v. 6, p. 405-423.

Binns, R. A., Barriga, F. J. A. S., and Miller, D. J., 2007, Leg 193 Synthesis: Anatomy of an active felsic-hosted hydrothermal system, Eastern Manus Basin, Papua New Guinea, *in* Barriga, F. J. A. S., Binns, R. A., Miller, D. J., and Herzig, P. M. eds., Proceedings of the Ocean Drilling Program, Scientific Results, v. 193, p. 1-71.

Binns, R. A., and Scott, S. D., 1993, Actively forming polymetallic sulfide deposits associated with felsic volcanic rocks in the eastern Manus back-arc basin, Papua New Guinea: Economic Geology and the Bulletin of the Society of Economic Geologists, v. 88, p. 2226-2236.

Bonham, H. F., 1984, Three major types of epithermal precious-metal deposits: Abstracts with Programs - Geological Society of America, v. 16, p. 449.

Bonham, H. F., 1986, Models for volcanic-hosted epithermal precious metal deposits: a review, *in* Proceedings International Volcanological Congress, Symposium 5, p. 13-17.

Bourgois, J., Azéma, J., Tournon, J., Bellon, H., Calle, B., Parra, E., Toussaint, J.-F., Glaçon, G., Feinberg, H., De Wever, P., Orgilia, I., 1982, Age et structures des complexes basiques et ultrabasiques de la façade pacifique entre 3ºN et 12ºN (Colombie, Panamá et Costa Rica): Bulletin de la Société Géologique de France, v. 24, p. 545-554.

Bove, D. J., Rye, R. O., and Hon, K., 1990, Evolution of the Red Mountain alunite deposit, Lake City, Colorado: U. S. Geological Survey, Open-File Report, v. 90-0235, 29 pp.

Bralia, A., Sabatini, G., and Troja, F., 1979, A revaluation of the Co/Ni ratio in pyrite as geochemical tool in ore genesis problems; evidences from southern Tuscany pyritic deposits: Mineralium Deposita, v. 14, p. 353-374.

Brill, B. A., 1989, Trace-element contents and partitioning of elements in ore minerals from the CSA Cu-Pb-Zn Deposit, Australia, and implications for ore genesis: The Canadian Mineralogist, v. 27, p. 263-274.

Buchs, D. M., 2008, Late Cretaceous to Eocene geology of the South Central American forearc area (southern Costa Rica and western Panama): Initiation and evolution of an intra-oceanic convergent margin: Unpublished PhD thesis, Lausanne, Switzerland, Université de Lausanne, 230 pp.

Buchs, D. M., Baumgartner, P. O., Baumgartner Mora, C., Bandini, A. N., Jackett, S.-J., Diserens, M.-O., and Stucki, J., 2009, Late Cretaceous to Miocene seamount accretion and melange formation in the Osa and Burica Peninsulas (southern Costa Rica); episodic growth of a convergent margin: Geological Society Special Publications, v. 328, p. 411-456.

Buchs, D. M., Arculus, R. J., Baumgartner, P. O., Baumgartner-Mora, C., and Ulianov, A., 2010, Late Cretaceous arc development on the SW margin of the Caribbean Plate: Insights from the Golfito, Costa Rica, and Azuero, Panama, complexes: Geochemistry Geophysics Geosystems, v. 11, Q07S24.

Buchs, D. M., Arculus, R. J., Baumgartner, P. O., and Ulianov, A., 2011a, Oceanic intraplate volcanoes exposed: Example from seamounts accreted in Panama: Geology, v. 39, p. 335-338.

Buchs, D. M., Baumgartner, P. O., Baumgartner-Mora, C., Flores, K., and Bandini, A. N., 2011b, Upper Cretaceous to Miocene tectonostratigraphy of the Azuero area (Panama) and the discontinuous accretion and subduction erosion along the Middle American margin: Tectonophysics, v. 512, p. 31-46.

Clark, C., Grguric, B., and Mumm, A. S., 2004, Genetic implications of pyrite chemistry from the Palaeoproterozoic Olary Domain and overlying Neoproterozoic Adelaidean sequences, northeastern South Australia: Ore Geology Reviews, v. 25, p. 237-257.

Coates, A. G., Collins, L. S., Aubry, M.-P., and Berggren, W. A., 2004, The Geology of the Darien, Panama, and the late Miocene-Pliocene collision of the Panama arc with northwestern South America: Geological Society of America Bulletin, v. 116, p. 1327-1344.

Cooke, D. R., and Simmons, S. F., 2000, Characteristics and genesis of epithermal gold deposits: Reviews in Economic Geology, v. 13, p. 221-244.

Corral, I., Griera, A., Gómez-Gras, D., Corbella, M., Canals, À., Pineda-Falconett, M., and Cardellach, E., 2011a, Geology of the Cerro Quema Au-Cu deposit (Azuero Peninsula, Panama): Geologica Acta, v. 9, 3-4, p. 481-498.

Corral, I., Cardellach, E., Corbella, M., Canals, À., and Johnson, C. A., 2011b, Origin and evolution of fluids associated with the Cerro Quema Au-Cu deposit (Azuero Peninsula, Panama): evidence from microthermometry, O, H and S isotopes, *in* Barra, F., Reich, M., Campos, E., and Tornos, F., eds., Proceedings of the 11th Biennial Meeting of the Society for Geology Applied to Mineral Deposits, Antofagasta, Chile, Universidad Católica del Norte, p. 178-180.

Corral, I., Gómez-Gras, D., Griera, A., Corbella, M., and Cardellach, E., 2013, Sedimentation and volcanism in the Panamanian Cretaceous intra-oceanic arc and fore-arc: New insights from the Azuero Peninsula, (SW Panama): Bulletin de la Société Géologique de France, v.184, 1, p. 35-45.

Dalrymple, G. B., Alexander, E. C., Jr., Lanphere, M. A., and Kraker, G. P., 1981, Irradiation of samples for ^{40}Ar / ^{39}Ar dating using the Geological Survey TRIGA reactor: U. S. Geological Survey Professional Paper 1176, 55 pp.

Deditius, A. P., Utsunomiya, S., Ewing, R. C., Chryssoulis, S. L., Venter, D., and Kesler, S. E., 2009, Decoupled geochemical behavior of As and Cu in hydrothermal systems: Geology, v. 37, p. 707-710.

Del Giudice, D., and Recchi, G., 1969, Geología del área del Proyecto Minero de Azuero, Report for the Government of the Panamanian Republic, Programa para el desarrollo de las Naciones Unidas, Panama, 48 pp.

Deyell, C. L., Rye, R. O., Landis, G. P., and Bissig, T., 2005, Alunite and the role of magmatic fluids in the Tambo high-sulfidation deposit, El Indio-Pascua Belt, Chile: Chemical Geology, v. 215, p. 185-218.

Dill, H. G., 2001, The geology of aluminium phosphates and sulphates of the alunite group minerals; a review: Earth-Science Reviews, v. 53, p. 35-93.

Dill, H. G., 2003, A comparative study of APS minerals of the Pacific Rim fold belts with special reference to South American argillaceous deposits: Journal of South American Earth Sciences, v. 16, p. 301-320.

Direccion General de Rercursos Minerales, 1976, Mapa Geológico de Panamá. Escala 1:500,000. : Panama.

Edwards, A. B., and Carlos, G. C., 1954, The selenium content of some Australian sulphide deposits: Proceedings - Australasian Institute of Mining and Metallurgy, v. 172, p. 31-63.

Fintor, K., Tóth, T. M., and Schubert, F., 2011, Hydrothermal palaeofluid circulation in the fracture network of the Baksa Gneiss Complex of SW Pannonian Basin, Hungary: Geofluids, v. 11, p. 144-165.

Fouquet, Y., von Stackelberg, U., Charlou, J. L., Erzinger, J., Herzig, P. M., Muehe, R., and Wiedicke, M., 1993, Metallogenesis in back-arc environments; the Lau Basin example: Economic Geology and the Bulletin of the Society of Economic Geologists, v. 88, p. 2154-2181.

Gemmell, J. B., Sharpe, R., Jonasson, I. R., and Herzig, P. M., 2004, Sulfur Isotope Evidence for Magmatic Contributions to Submarine and Subaerial Gold Mineralization: Conical Seamount and the Ladolam Gold Deposit, Papua New Guinea: Economic Geology, v. 99, p. 1711-1725.

Goldschmidt, V. M., 1954, Geochemistry: Oxford University Press, London, 730 pp.

Hannington, M. D., 1997, The Porphyry-Epithermal-VMS transition: lessons from the Iskut River Area, British Columbia, and modern island arcs: SEG Newsletter, v. 29, p. 12-13.

Hannington, M. D., and Herzig, P. M., 1993, Shallow submarine hydrothermal systems in modern island arc settings: Program with Abstracts - Geological Association of Canada; Mineralogical Association of Canada: Joint Annual Meeting, Canada (CAN), 1993, 1993, p. 40-40.

Hauff, F., Hoernle, K., van den Bogaard, P., Alvarado, G., and Garbe-Schoenberg, D., 2000, Age and geochemistry of basaltic complexes in western Costa Rica; contributions to the geotectonic evolution of Central America: Geochemistry Geophysics Geosystems, v. 1, 1009.

Hayba, D. O., Bethke, P. M., Heald, P., and Foley, N. K., 1985, Geologic, mineralogic, and geochemical characteristics of volcanic-hosted epithermal precious-metal deposits: Reviews in Economic Geology, v. 2, p. 129-167.

Heald, P., Foley, N. K., and Hayba, D. O., 1987, Comparative anatomy of volcanic-hosted epithermal deposits; acid-sulfate and adularia-sericite types: Economic Geology, v. 82, p. 1-26.

Hedenquist, J. W., 1987, Mineralization associated with volcanic-related hydrothermal systems in the Circum-Pacific basin: Transactions of the Circum-Pacific Energy and Mineral Resources Conference, v. 4, p. 513-524.

Hedenquist, J. W., and Lowenstern, J. B., 1994, The role of magmas in the formation of hydrothermal ore deposits: Nature, v. 370, p. 519-527.

Hedenquist, J. W., Matsuhisa, Y., Izawa, E., White, N. C., Giggenbach, W. F., and Aoki, M., 1994, Geology, geochemistry, and origin of high sulfidation Cu-Au mineralization in the Nansatsu District, Japan: Economic Geology, v. 89, p. 1-30.

Hedenquist, J. W., Arribas R, A., and Gonzalez-Urien, E., 2000, Exploration for epithermal gold deposits: Reviews in Economic Geology, v. 13, p. 245-277.

Heinrich, C. A., Driesner, T., Stefansson, A., and Seward, T. M., 2004, Magmatic vapor contraction and the transport of gold from the porphyry environment to epithermal ore deposits: Geology, v. 32, p. 761-764.

Hernandez, P. A., Garcia-Estrada, P. A., Cowley, P. N., and Gallagher, M. J., 1989, Geological setting, alteration and lithogeochemistry of the Transacción epithermal gold deposit, Rodalquilar mining district, Southeast Spain: Institution of Mining and Metallurgy Transactions. Sec. B, v. 98, p. 78-80.

Herzig, P. M., Hannington, M. D., Fouquet, Y., von Stackelberg, U., and Petersen, S., 1993, Gold-rich polymetallic sulfides from the Lau back arc and implications for the geochemistry of gold in sea-floor hydrothermal systems of the Southwest Pacific: Economic Geology and the Bulletin of the Society of Economic Geologists, v. 88, p. 2182-2209.

Herzig, P. M., Peterson, S., and Hannington, M. D., 1999, Epithermal-type gold mineralization at Conical Seamount; a shallow submarine volcano south of Lihir Island, Papua New Guinea: Proceedings of the 5th Biennial SGA Meeting, v. 5, p. 527-530.

Hoernle, K., van den Bogaard, P., Werner, R., Lissinna, B., Hauff, F., Alvarado, G., and Garbe-Schonberg, D., 2002, Missing history (16-71 Ma) of the Galapagos hotspot: Implications for the tectonic and biological evolution of the Americas: Geology, v. 30, p. 795-798.

Hoernle, K., Hauff, F., and van den Bogaard, P., 2004, 70 m.y. history (139-69 Ma) for the Caribbean large igneous province: Geology, v. 32, p. 697-700.

Hoernle, K., and Hauff, F., 2007, Oceanic Igneous Complexes: *in* Bundschuh, J., and Alvarado, G., Central America, Geology, Resources, Hazards, v. 1, p. 523-548.

Horlacher, C. F., and Lehmann, J. H., 1993, Regional Geology, Geochemistry and Exploration potential of the central Cerro Quema concession, Unpublished report, Panamà. 36 pp.

Huston, D. L., Sie, S. H., Suter, G. F., Cooke, D. R., and Both, R. A., 1995, Trace elements in sulfide minerals from eastern Australian volcanic-hosted massive sulfide deposits; Part I, Proton microprobe analyses of pyrite, chalcopyrite, and sphalerite, and Part II, Selenium levels in pyrite; comparison with $\delta^{34}S$ values and implications for the source of sulfur in volcanogenic hydrothermal systems: Economic Geology, v. 90, p. 1167-1196.

Itaya, T., Arribas, A., and Okada, T., 1996, Argon release systematics of hypogene and supergene alunite based on progressive heating experiments from 100 to 1000 degrees C: Geochimica et Cosmochimica Acta, v. 60, p. 4525-4535.

Jambor, J. L., 1999, Nomenclature of the alunite supergroup: The Canadian Mineralogist, v. 37, p. 1323-1341.

Keigwin, L. D., Jr., 1978, Pliocene closing of the Isthmus of Panama, based on biostratigraphic evidence from nearby Pacific Ocean and Caribbean Sea cores: Geology, v. 6, p. 630-634.

Kennan, L., and Pindell, J. L., 2009, Dextral shear, terrane accretion and basin formation in the Northern Andes; best explained by interaction with a Pacific-derived Caribbean Plate?: Geological Society Special Publications, v. 328, p. 487-531.

Kesler, S. E., 1978, Metallogenesis of the Caribbean region: Journal of the Geological Society, v. 135, p. 429-441.

Kesler, S. E., Sutter, J. F., Issigonis, M. J., Jones, L. M., and Walker, R. L., 1977, Evolution of porphyry copper mineralization in an oceanic island arc; Panama: Economic Geology, v. 72, p. 1142-1153.

Kesler, S. E., Russell, N., Seaward, M., Rivera, J., McCurdy, K., Cumming, G. L., and Sutter, J. F., 1981, Geology and geochemistry of sulfide mineralization underlying the Pueblo Viejo gold-silver oxide deposit, Dominican Republic: Economic Geology, v. 76, p. 1096-1117.

Kesler, S. E., Russell, N., and McCurdy, K., 2003, Trace-metal content of the Pueblo Viejo precious-metal deposits and their relation to other high-sulfidation epithermal systems: Mineralium Deposita, v. 38, p. 668-682.

Kesler, S. E., Campbell, I. H., Smith, C. N., Hall, C. M., and Allen, C. M., 2005, Age of the Pueblo Viejo Gold-Silver Deposit and Its Significance to Models for High-Sulfidation Epithermal Mineralization: Economic Geology, v. 100, p. 253-272.

Knight, J. E., 1977, A thermochemical study of alunite, enargite, luzonite, and tennantite deposits: Economic Geology, v. 72, p. 1321-1336.

Koglin, N., Frimmel, H. E., Minter, W. E. L., and Braetz, H., 2010, Trace element characteristics of different pyrite types in Mesoarchaean to Palaeoproterozoic placer deposits: Mineralium Deposita, v. 45, p. 259-280.

Kolarsky, R. A., Mann, P., Monechi, S., Meyerhoff-Hull, D., and Pessagno, E. A., 1995, Stratigraphic development of southwestern Panama as determined from integration of marine seismic data and onshore geology: Geological Society of America Special Publication, v. 295, p. 159-200.

Krawinkel, H., Wozazek, S., Krawinkel, J., and Hellmann, W., 1999, Heavy-mineral analysis and clinopyroxene geochemistry applied to provenance analysis of lithic sandstones from the Azuero-Sona Complex (NW Panama): Sedimentary Geology, v. 124, p. 149-168.

Leach, T. M., 1992, Petrological Evaluation of the High Sulphidation Systems in the La Pava and Cerro Quema Prospect Areas, Panama, Unpublished report for Cyprus Gold Company. 55 pp.

Lee, J. K. W., Onstott, T. C., Cashman, K. V., Cumbest, R. J., and Johnson, D., 1991, Incremental heating of hornblende in vacuo: Implications for $^{40}Ar/^{39}Ar$ geochronology and the interpretation of thermal histories: Geology, v. 19, p. 872-876.

Lindgren, W., 1922, A suggestion for the terminology of certain mineral deposits: Economic Geology, v. 17, p. 292-294.

Lindgren, W., 1923, Concentration and circulation of the elements from the standpoint of economic geology: Economic Geology, v. 18, p. 419-442.

Lissinna, B., Hoernle, K., van den Bogaard, P., and Anonymous, 2002, Northern migration of arc volcanism in western Panama; evidence for subduction erosion?: Eos Transactions, American Geophysical Union, v. 83, p. 1463-1464.

Lissinna, B., 2005, A profile through the Central American Landbridge in western Panama: 115 Ma Interplay between the Galápagos Hotspot and the Central American Subduction Zone: Unpublished PhD. thesis, Kiel, Germany, Fakultät der Christian-Albrechts-Universität zu Kiel, 102 pp.

Lissinna, B., Hoernle, K., Hauff, P., Van den Bogaard, P., and Sadofsky, S., 2006, The Panamanian island arc and Galápagos hotspot: A case study for the long-term evolution of arc/hotspot interaction: Geophysical Research Abstracts, v. 8, p. 05106.

Loftus-Hills, G., and Solomon, M., 1967, Cobalt, nickel and selenium in sulphides as indicators of ore genesis: Mineralium Deposita, v. 2, p. 228-242.

Longo, A. A., 2005, Evolution of volcanism and hydrothermal activity in the Yanacocha mining district, northern Peru: Unpublished PhD. thesis, Oregon, USA, Oregon State University, 469 pp.

Longo, A. A., Dilles, J. H., Grunder, A. L., and Duncan, R., 2010, Evolution of Calc-Alkaline Volcanism and Associated Hydrothermal Gold Deposits at Yanacocha, Peru: Economic Geology, v. 105, p. 1191-1241.

Lonsdale, P., 2005, Creation of the Cocos and Nazca plates by fission of the Farallon Plate: Tectonophysics, v. 404, p. 237-264.

Merrihue, C., 1965, Trace-element determinations and potassium-argon dating by mass spectroscopy of neutron-irradiated samples: Eos Transactions, American Geophysical Union, v. 46, p. 125-125.

Montes, C., Bayona, G. A., Cardona, A., Buchs, D. M., Silva, C. A., Morón, S. E., Hoyos, N., Ramírez, D. A., Jaramillo, C. A., and Valencia, V., 2012, Arc-continent collision and orocline formation: Closing of the Central American seaway: Journal of Geophysical Research, v. 117, B04105, 25 pp.

Nelson, C. E., 1995, Porphyry copper deposits of southern Central America: Arizona Geological Society Digest, v. 20, p. 553-565.

Nelson, C. E., 2001, Gold mineralization in dome fields of the Veraguas Belt, Panama: Special Publication (Society of Economic Geologists (U. S.)), v. 8, p. 307-316.

Nelson, C. E., 2000, Volcanic domes and gold mineralization in the Pueblo Viejo District, Dominican Republic: Mineralium Deposita, v. 35, p. 511-525.

Nelson, C. E., 2007, Metallic mineral resources, *in* Bundschuh., J and Alvarado., G., Eds., Central America, Geology, Resources and Hazards. V. 1, p. 885-915.

Nelson, C. E., and Nietzen, F., 2000, Metalogenia del oro y cobre en américa central: Revista Geológica de América Central., v. 23, p. 25-41.

Oviedo, L., Fuster, N., Tschischow, N., Ribba, L., Zuccone, A., Grez, E., and Aguilar, A., 1991, General geology of La Coipa precious metal deposit, Atacama, Chile: Economic Geology, v. 86, p. 1287-1300.

Papike, J. J., Karner, J. M., Spilde, M. N., and Shearer, C. K., 2006, Terrestrial analogs of martian sulfates: Major and minor element systematics of alunite-jarosite from Goldfield, Nevada: American Mineralogist, v. 91, p. 1197-1200.

Petersen, S., Herzig, P. M., Hannington, M. D., Jonasson, I. R., and Arribas, A., 2002, Submarine Gold Mineralization Near Lihir Island, New Ireland Fore-Arc, Papua New Guinea: Economic Geology, v. 97, p. 1795-1813.

Pindell, J. L., Higgs, R., and Dewey, J. F., 1998, Cenozoic palinspastic reconstruction, paleogeographic evolution, and hydrocarbon setting of the northern margin of South America: *In* Pindell, J. L. & Drake, C. L. eds., Paleogeographic Evolution and Non-glacial Eustasy, northern South America. Society for Sedimentary Geology Special Publication, v. 58, p. 45-86.

Pindell, J. L., and Kennan, L., 2009, Tectonic evolution of the Gulf of Mexico, Caribbean and northern South America in the mantle reference frame; an update: Geological Society Special Publications, v. 328, p. 1-55.

Price, B. J., 1972, Minor elements in pyrites from the Smithers map area, B. C., and exploration applications of minor element studies: Report - Department of Geological Sciences, University of British Columbia, v. 13, p. 32-33.

Puritch, E. J., Sutcliffe, R. H., Wu, Y., Armstrong, T., and Yassa, A., 2012 , W. Technical report and mineral resource estimate on the Cerro Quema Project, Los Santos province, Panama, Prepared for Preshimco Resources Inc., by P&E Mining Consultants Inc., 123 pp.

Raymond, O. L., 1996, Pyrite composition and ore genesis in the Prince Lyell copper deposit, Mt Lyell mineral field, western Tasmania, Australia: Ore Geology Reviews, v. 10, p. 231-250.

Recchi, G., and Miranda, R., 1977, Calizas de los Planes-Guaniquito (Tonosí): Unpublished report, Panama, Dirección General de Recursos Minerales (DGRM), 27 pp.

Reed, M. H., and Barnes, H. L., 1997, Hydrothermal alteration and its relationship to ore field composition, *in* Barnes, H. L., ed., Geochemistry of hydrothermal ore deposits, 3rd ed.: New York, Wiley, p.303-365.

Reyes, A. G., 1990, Petrology of Philippine geothermal systems and the application of alteration mineralogy to their assessment: Journal of Volcanology and Geothermal Research, v. 43, p. 279-309.

Reyes, A. G., 1991, Mineralogy, distribution and origin of acid alteration in Philippine geothermal systems: Geological Survey of Japan Report 227, p. 59-65.

Roberts, F. I., 1982, Trace element chemistry of pyrite; a useful guide to the occurrence of sulfide base metal mineralization: Journal of Geochemical Exploration, v. 17, p. 49-62.

Rye, R. O., Bethke, P. M., and Wasserman, M. D., 1992, The stable isotope geochemistry of acid sulfate alteration: Economic Geology, v. 87, p. 225-262.

Rye, R. O., 2005, A review of the stable-isotope geochemistry of sulfate minerals in selected igneous environments and related hydrothermal systems: Chemical Geology, v. 215, p. 5-36.

Scott, K. M., 1987, Solid solution in, and classification of, gossan-derived members of the alunite-jarosite family, Northwest Queensland, Australia: American Mineralogist, v. 72, p. 178-187.

Scott, K. M., 1990, Origin of alunite- and jarosite-group minerals in the Mt. Leyshon epithermal gold deposit, Northeast Queensland, Australia: American Mineralogist, v. 75, p. 1176-1181.

Sillitoe, R. H., 1989, Gold deposits in western Pacific island arcs; the magmatic connection: Economic Geology Monographs, v. 6, p. 274-291.

Sillitoe, R. H., 1993, Epithermal models; genetic types, geometrical controls and shallow features: Geological Association of Canada Special Paper, v. 40, p. 403-417.

Sillitoe, R. H., 1999, Styles of high-sulphidation gold, silver and copper mineralisation in porphyry and epithermal environments: Australasian Institute of Mining and Metallurgy, v. 4-99, p. 29-44.

Sillitoe, R. H., Hannington, M. D., and Thompson, J. F. H., 1996, High sulfidation deposits in the volcanogenic massive sulfide environment: Economic Geology, v. 91, p. 204-212.

Speidel, F., Faure, S., Smith, M. T., and McArthur, G. F., 2001, Exploration and discovery at the Petaquilla copper-gold concession, Panama: Society of Economic Geologists Special Publication, v. 8, p. 349-362.

Stern, R. J., and Bloomer, S. H., 1992, Subduction zone infancy: Examples from the Eocene Izu-Bonin-Mariana and Jurassic California arcs: Geological Society of America Bulletin, v. 104, p. 1621-1636.

Stern, R. J., 2010, The anatomy and ontogeny of modern intra-oceanic arc systems: Geological Society Special Publications, v. 338, p. 7-34.

Stoffregen, R. E., 1987, Genesis of acid-sulfate alteration and Au-Cu-Ag mineralization at Summitville, Colorado: Economic Geology, v. 82, p. 1575-1591.

Stoffregen, R. E., and Alpers, C. N., 1987, Woodhouseite and svanbergite in hydrothermal ore deposits; products of apatite destruction during advanced argillic alteration: The Canadian Mineralogist, v. 25, Part 2, p. 201-211.

Stoffregen, R. E., and Cygan, G. L., 1990, An experimental study of Na-K exchange between alunite and aqueous sulfate solutions: American Mineralogist, v. 75, p. 209-220.

Stoffregen, R. E., Alpers, C. N., and Jambor, J. L., 2000, Alunite-Jarosite Crystallography, Thermodynamics, and Geochronology: Reviews in Mineralogy and Geochemistry, v. 40, p. 453-479.

Strunz, H., and Tennyson, C., 1982, Mineralogische Tabellen. Mineral tables; a classification of minerals according to crystal chemical principles, with an introduction to crystal chemistry, ed. 5: Federal Republic of Germany, Akademische Verlagsgesellschaft Geest & Portig, 621 pp.

Torrey, C., and Keenan, J., 1994, Cerro Quema Project, Panama, Prospecting in tropical and arid terrains: Unpublished report, Toronto, Ontario, Canada. 23 pp.

Trenkamp, R., Kellogg, J. N., Freymueller, J. T., and Mora, H. P., 2002, Wide plate margin deformation, southern Central America and northwestern South America, CASA GPS observations: Journal of South American Earth Sciences, v. 15, p. 157-171.

Turner, S. J., 1997, The Yanacocha epithermal gold depoists, northern Peru: High sulfidation mineralization in a flow dome setting: Unpublished PhD. thesis, Colorado, USA, Colorado School of Mines, 342 pp.

Turner, S. J., 1998, Discovery and gological setting of high-sulfidation Au mineralization in the Yanacocha district, northern Peru, *In* Walton, G., and Jambor, J. (Eds.), Pathways '98 Extended abstracts volume (British Columbia and Yukon Chamber of Mines: Vancouver), p. 90.

Valiant, W. W., Collins, S. E., and Krutzelmann, H., 2011, Unpublished Technical report on the Cerro Quema Project, Panama, Prepared for Preshimco Resources Inc., by Scott Wilson Roscoe Postle Associates Inc., 109 pp.

Wadge, G., and Burke, K., 1983, Neogene Caribbean plate rotation and associated Central American tectonic evolution: Tectonics, v. 2, p. 633-643.

Wegner, W., Worner, G., Harmon, R. S., and Jicha, B. R., 2011, Magmatic history and evolution of the Central American Land Bridge in Panama since Cretaceous times: Geological Society of America Bulletin, v. 123, p. 703-724.

Werner, R., Hoernle, K., Barckhausen, U., and Hauff, F., 2003, Geodynamic evolution of the Galapagos hot spot system (central East Pacific) over the past 20 m.y.; constraints from morphology, geochemistry, and magnetic anomalies: Geochemistry Geophysics Geosystems, v. 4. 1108.

White, N. C., 1991, High sulfidation epithermal gold deposits; characteristics and a model for their origin: Geological Survey of Japan Report 227, p. 9-20.

White, N. C., 1993, Geology and Mineralization of the Santa Rosa gold deposits, Panama: Society of Mining Engineers, v. Preprint Series, p. 5.

Woakes, E. R., 1923, The Darien gold mine, Panama: Mining Magazine, v. 29, p. 270-278.

Wörner, G., Harmon, R. S., Hartmann, G., and Simon, K., 2005, Igneous geology and geochemistry of the upper Rio Chagres basin: *in* Harmon, R. S., ed., The Río Chagres, Panama, A multidisciplinary profile of a tropical watershed, The Netherlands, Springer, p. 65-82.

Wörner, G., Harmon, R. S., Wegner, W., and Singer, G., 2006, Linking America's backbone: Geological development and basement rocks of central Panama: Abstrstracts with Programs, Geological Society of America Conference "Backbone of the Americas" Mendoza, Argentina, Geological Society of America, p. 60.

Wörner, G., Harmon, R. S., and Wegner, W., 2009, Geochemical evolution of igneous rocks and changing magma sources during the formation and closure of the Central American land bridge of Panama: Backbone of the Americas: Shallow Subduction, Plateau Uplift, and Ridge Terrane Collision, Geological Society of America Memoir 204, p. 183-196.

CHAPTER 5

Fluid inclusions and Stable isotope geochemistry of the Cerro Quema high sulfidation Au-Cu deposit (Azuero Peninsula, Panama): Origin and evolution of mineralizing fluids

5.1. Introduction

The high sulfidation Au-Cu epithermal-type deposit of Cerro Quema (Azuero Peninsula, SW Panama; Fig. 5.1) is considered one of the most promising Au prospects in Panama. It was discovered in 1988 by the Compañía de Exploración Minera S. A. (CEMSA), based on the results of the geological and metallogenetic study carried out in Panama by the United Nations Development Program (UNDP) in 1965. The Cerro Quema deposit is constituted by several mineable bodies, named from East to West, Cerro Quema, Cerro Quemita and La Pava (Fig. 5.2). The estimated total resources are 7.23 Mt with an average gold grade of 1.10 g/t, containing 256,000 oz of Au concentrated in La Pava ore body (Valiant *et al*., 2011; Puritch, *et al*., 2012). Although more mineralized bodies are found towards the east (e.g., Cerro Idaida, East Quema Jungle, Cerro Pelona), their Au and Cu content have not been evaluated up to date.

First geological studies carried out in the Azuero Peninsula (e.g., Del Giudice and Recchi, 1969; Ferencic, 1970; Kesler *et al*., 1977) noted the metallogenic potential of Au and Cu in this region. Later works centered on the Cerro Quema deposit were focused on the geology (e.g., Horlacher and Lehmann, 1993; Nelson, 1995; Corral *et al*., 2011a, 2013), the metallogeny (e.g., Leach, 1992; Corral *et al*., 2011b; this study, Chapter 4) and the economic potential for gold mining (e.g., Torrey and Keenan, 1994; Valiant *et al*., 2011; Puritch, *et al*., 2012). Although Cerro Quema has economic potential for copper (Nelson, 2007; Corral *et al*., 2011a; this study, Chapter 4), the exploitation of this metal has not been considered so far.

Up to date, no study has been focused on the genesis of the deposit, and therefore, the origin and evolution of fluids related to ore deposition remain unclear for the Cerro Quema deposit. In the present work we present the results of the first fluid inclusion and stable isotope study in order to understand the origin and evolution of mineralizing fluids responsible for ore deposition. Finally, a conceptual model integrating the geochemical and geological data is presented.

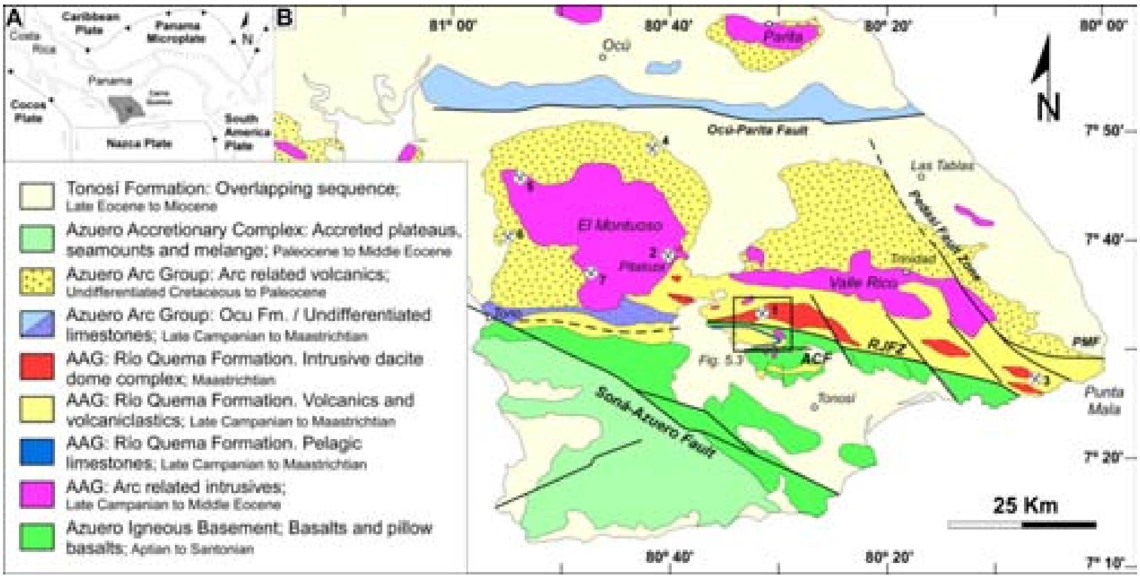

Figure 5.1: Simplified geological map of the Azuero Peninsula. AAG: Azuero Arc Group, RJFZ: Río Joaquín Fault Zone, ACF: Agua Clara Fault, PMF: Punta Mala Fault (After Dirección General de Recursos Minerales, 1976; Buchs *et al*., 2010; Corral *et al*., 2011a; 2013). Mineral deposits: 1) Cerro Quema, 2) Pitaloza, 3) Juan Díaz, 4) Las Minas, 5) Quebrada Barro, 6) Quebrada Iguana, 7) Cerro Viejo.

5.2. Geological setting

The Cerro Quema deposit, located in the central Azuero Peninsula (Fig. 5.1), is enclosed in the Azuero Arc Group, a sequence of volcanic, plutonic, volcanosedimentary and sedimentary rocks, representing the Panamanian Cretaceous-Paleogene volcanic arc (Buchs *et al*., 2010, 2011; Corral *et al*., 2011a, 2013). The Panamanian volcanic arc is an intra-oceanic arc, developed on top of the western edge of the Caribbean plate, as a consequence of the ancient Farallon plate subduction beneath the Caribbean plate.

Mineralization is hosted by dacitic volcanic domes of the Río Quema Formation (RQF), a volcanosedimentary sequence interpreted as a fore-arc basin sequence (Corral *et al*., 2011a, 2013). The RQF crops out in the central Azuero Peninsula, expanding form East to West. It is limited to the North by a series of diorite and quatz-diorite batholits (e.g., El Montuoso and Valle Rico), and by the Azuero Igneous Basement to the South (Fig. 5.1). The main regional tectonic structures affecting the distribution of the Río Quema Formation are E-

W trending regional faults such as the Agua Clara and the Rio Joaquin Fault Zone.

Figure 5.2: Overview of the Cerro Quema deposit where the studied ore bodies are shown.

In order to constrain the timing of volcanism and plutonism of the Panamanian volcanic arc, recent works have been focused in dating the main lithostratigraphic units of the Azuero Peninsula. Based on biostratigraphic data Corral *et al*. (2013) obtained an age from Late Campanian to Maastrichtian for the Río Quema Formation. Dacite domes of the Rio Quema Formation have been dated by Ar/Ar in hornblendes, obtaining an age range of ~ 71 to 66 Ma (Wegner *et al*., 2011; this study, Chapter 4). The El Montuoso batholith has been dated by K/Ar and Ar/Ar in hornblendes and by U/Pb in zircons, obtaining an age range of ~ 69 to 65 Ma (Del Giudice and Recchi, 1969; Kesler *et al*., 1977; Montes *et al*., 2012; this study, Chapter 4). Thus, according to geochronological data, the Río Quema Formation and the El Montuoso batholith constitute the Cretaceous volcanic arc, representing the arc related volcanics and the arc related intrusives, respectively. On the other hand, the Valle Rico batholith which crops out to the North of the Río Quema Formation, producing thermal aureolas (Corral *et al*., 2011a; 2013), has been dated by Ar/Ar on hornbled and plagioclase, and by U/Pb (zircon), obtaining an age range from ~55 to 49 Ma (Del Giudice and Recchi, 1969; Lissinna, 2005; Montes *et al*., 2012; this study, Chapter 4). Therefore, the Valle Rico batholith is interpreted to represent the arc related intrusive of the Paleogene volcanic arc. Both volcanic arcs (Cretaceous and Paleogene) were developed on top of the Azuero Igneous Basement, which represents the arc basement of Coniacian - early Santonian age (~89-85 Ma; Kolarsky *et al*., 1995; Lissinna, 2005; Buchs *et al*., 2009).

Based on field evidences, biostratigraphy, and geochronology (this study, Chapter 4), a lower Eocene age (55-49 Ma) has been inferred for the Cerro Quema deposit, relating the mineralization with the hydrothermal fluids derived from the emplacement of porphyry copper stocks with Valle Rico-like affinity. Intrusions similar to Valle Rico batholith occurred along the entire fore-arc basin, from N to S, following E-W trending regional faults parallel to the Río Joaquin Fault Zone and the Agua Clara Fault (Corral *et al*., 2011a, 2013; this study, Chapter 4).

5.3. Geology of the deposit

The Cerro Quema deposit, which covers an area of ~20 Km^2, is a composite structurally and lithologically controlled high sulfidation epithermal system (Corral *et al*., 2011a, this study, Chapter 4). The 1,700 m thick volcanosedimentary sequence of the Río Quema Formation, which hosts the Au-Cu mineralization, overlays the Azuero Igneous Basement and is discordantly overlapped by the Tonosí Formation. Tectonically, the RQF is affected by a large network of faults with a predominantly NW-SE and NE-SW trend, showing subvertical dip and normal sense of offset and occasionally strike slip motion. Moreover, mesoscale ENE-WSW open folds, with moderate limb dips and fold axes gently plunging to the SW are observed in the area (Fig. 5.3). Deformation indicators (e.g., tension gashes, cataclasites, etc.) are observed mostly in the northern area, whereas a kilometer-scale E-W trending syncline characterizes the southern area (Fig. 5.3). All these structures suggest a dextral transpression with dominant reverse dip-slip motion (Corral *et al*., 2011a, 2013).

Cerro Quema deposit is characterized by a widespread hydrothermal alteration which develops concentric alteration halos in the host rock (Fig. 5.4). Mineralization and hidrothermal alteration at Cerro Quema is strongly controlled

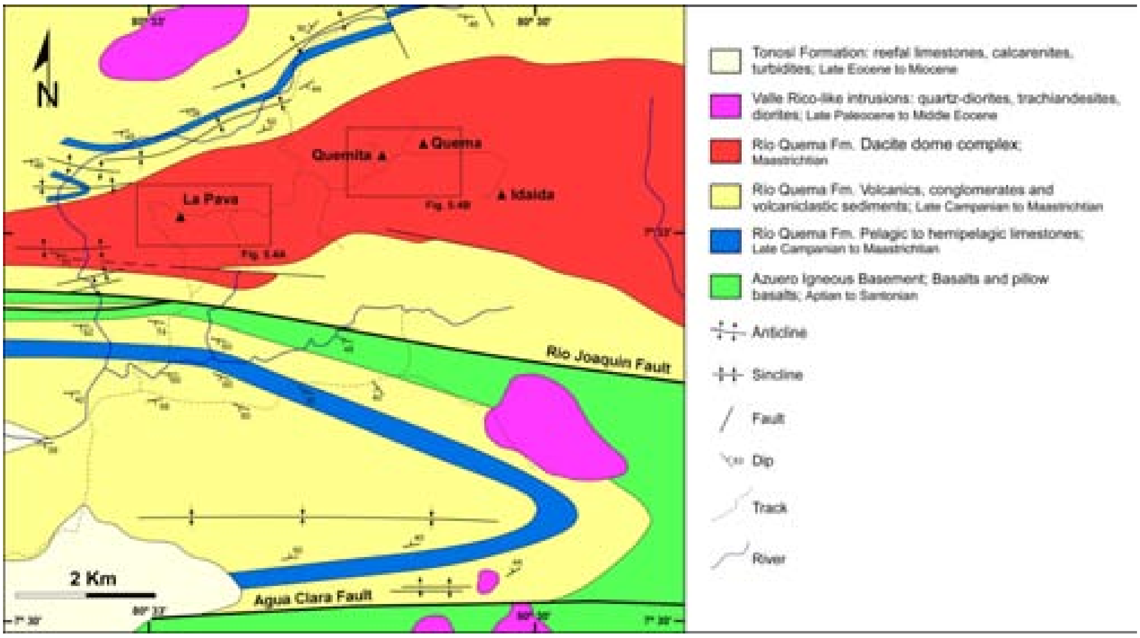

Figure 5.3: Geologic map of the central Azuero Peninsula, including the Cerro Quema deposit (Modified from Corral *et al*., 2011a, 2013; this study, Chapter 4).

by E-W trending regional faults parallel to the Rio Joaquín Fault zone (Corral *et al*., 2011a; this study, Chapter 4). However the lithological control plays an important role on the development of the hydrothermal alteration zones at deposit scale, as noted by mushrooming at shallow levels (e.g., La Pava; Leach, 1992). Additionally, surrounding rocks such as, andesites and volcaniclastic sediments of the RQF and also affected by the E-W trending faults, show a weak hydrothermal alteration.

Previous studies on the Cerro Quema deposit (e.g., Leach, 1992; Corral *et al*., 2011a; this study, Chapter 4) reported three distinct hydrothermal alteration zones (Fig. 5.4). An inner zone of vuggy silica made up of a groundmass of intergrown microcrystalline anhedral quartz grains, pyrite, chalcopyrite, enargite, tennantite, barite and minor rutile with sphalerite traces. A zone of advanced argillic alteration developing near and/or enclosing the inner vuggy silica alteration, characterized by quartz, alunite, natroalunite, aluminium-phosphate-sulfate minerals (APS), dickite, pyrophyllite, barite, illite and minor diaspore and rutile, and by sulfides (pyrite, chalcopyrite, enargite and tennantite).

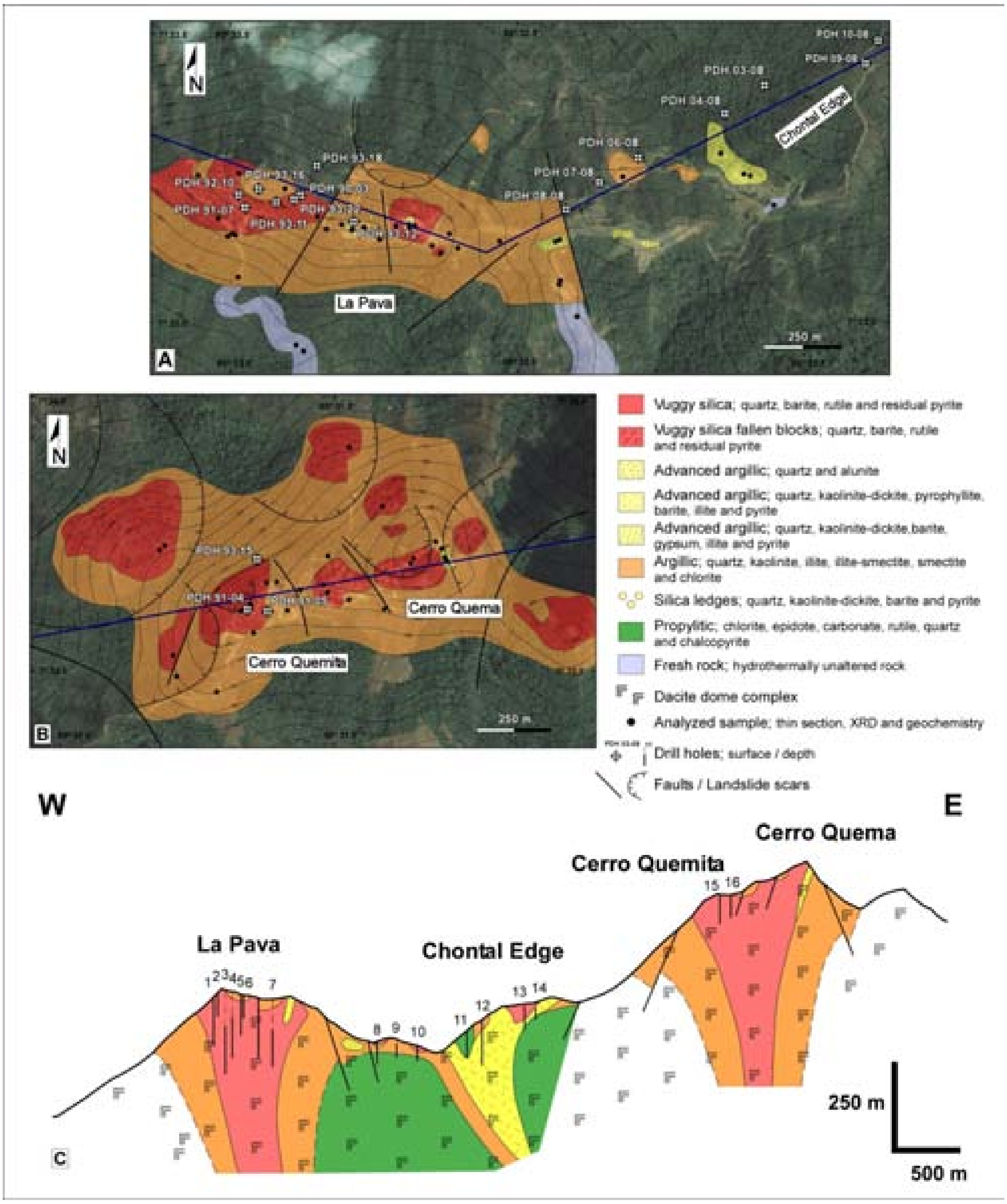

Figure 5.4: Hydrothermal alteration maps and geologic section of the Cerro Quema deposit. A) Hydrothermal map of La Pava and Chontal edge. B) Hydrothermal alteration map of Cerro Quemita and Cerro Quema ore bodies. C) Geologic section (W-E) of the hydrothermal alteration at the Cerro Quema deposit. Drill holes; 1: PDH 92-10, 2: PDH 91-07, 3: PDH 93-16, 4: PDH 93-11, 5: PDH 93-22, 6: PDH 90-03, 7: PDH 93-12, 8: PDH 08-08, 9: PDH 07-08, 10: PDH 06-08, 11: PDH 04-08, 12: PDH 03-08, 13: PDH 09-08, 14: PDH 10-08, 15: PDH 91-04, 16: PDH 93-15.

Finally, an argillic alteration zone, bounds the vuggy silica generally with a sharp contact, and has gradational contact with the advanced argillic alteration.

This argillic alteration is characterized by quartz, kaolinite, illite, illite-smectite, smectite, chlorite-smectite and chlorite with minor disseminated pyrite. A propylitic alteration, which is only observable in drill core samples, constitutes the distal alteration zone and shows a transitional contact with the argillic alteration zone. It is constituted by chlorite, epidote, carbonate, rutile, pyrite and chalcopyrite, with minor hematite and magnetite and traces of sphalerite, chalcocite and covellite. Moreover, intense weathering typical of tropical latitudes affected the Cerro Quema deposit, producing a quartz and iron oxide-rich lithocap and a supergene enrichment zone. The supergene alteration overprints the primary hydrothermal alteration, producing changes on the mineralogy. Gold occurs as disseminated submicroscopic grains and as "invisible gold" within the pyrite lattice (Corral *et al.*, 2011a). Copper is associated to Cu-bearing minerals such as chalcopyrite, enargite, bornite and tennantite as well as to secondary copper sulfides such as covellite and chalcocite (this study, Chapter 4). Gold and copper occur especially in the vuggy silica and advanced argillic alteration zones.

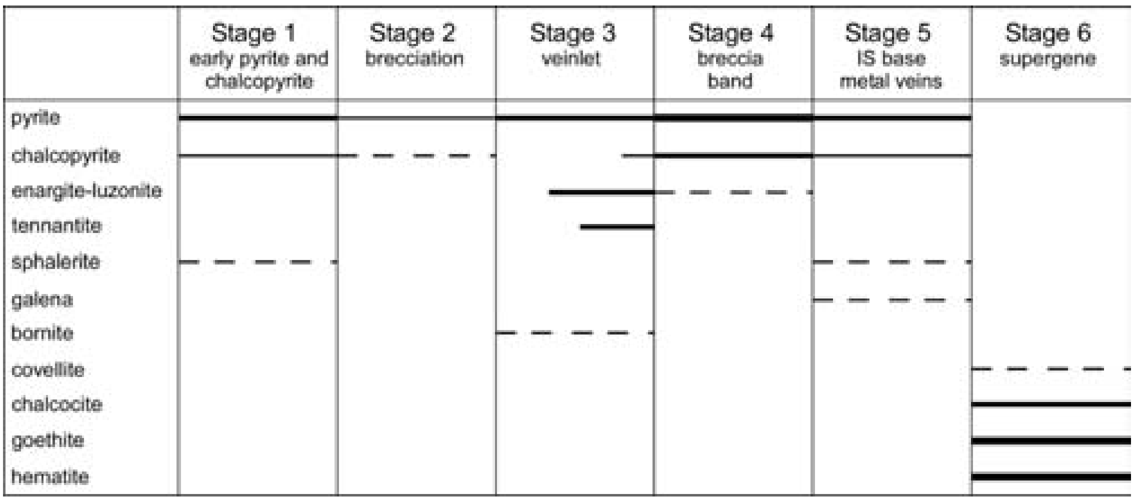

Figure 5.5: Paragenetic sequence of ore minerals recognized at Cerro Quema deposit, adapted from (this study, Chapter 4).

Mineralization has been divided into six stages (this study, Chapter 4; Fig. 5.5). The first stage consists in a dissemination of pyrite, chalcopyrite and enargite with traces of sphalerite (Fig. 5.6A). Stage two consists in a dissemination of pyrite and chalcopyrite in a hydraulic breccia matrix, associated with alunite and dickite, which are also present in the rock hosting the breccia (Fig. 5.6B). Stage three is constituted by veinlets of pyrite, chalcopyrite, enargite and tennantite crosscutting stages one and two (Fig. 5.6C).

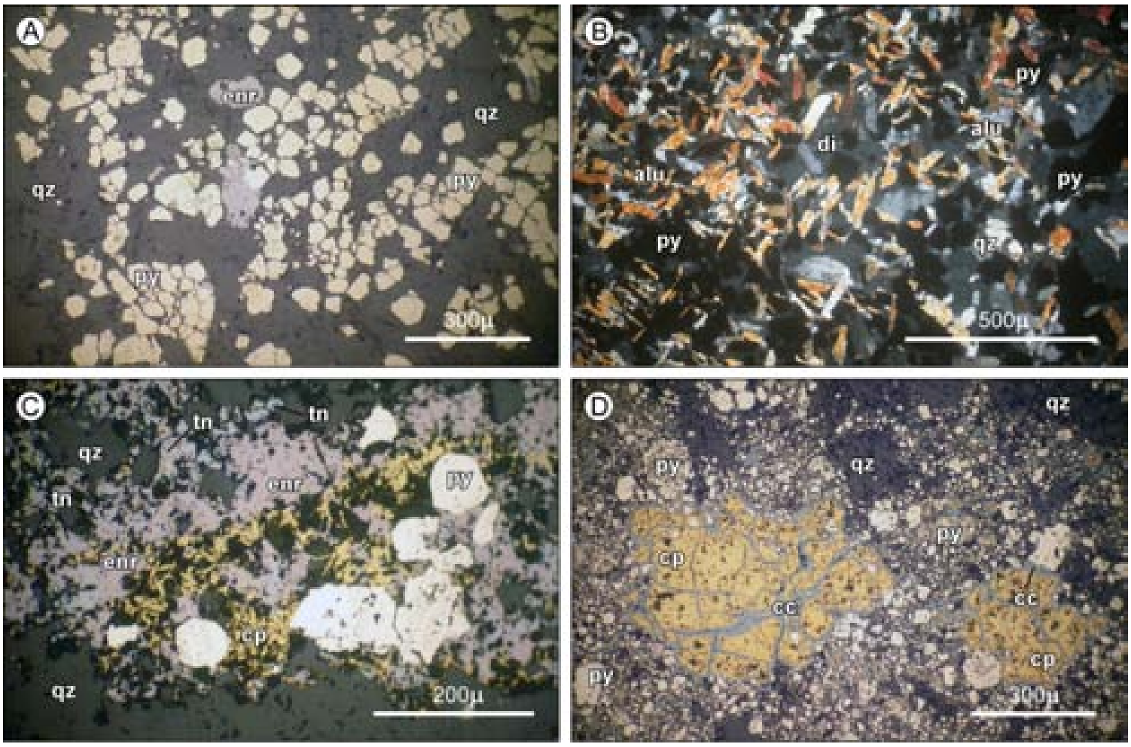

Figure 5.6: Mineralization at Cerro Quema deposit. A) Mineralization Stage 1, dissemination of pyrite and minor enargite in the vuggy silica groundmass. B) Mineralization Stage 2, dissemination of pyrite in a hydraulic breccias matrix, associated with quartz, alunite-natroalunite and dickite. C) Mineralization Stage 3, veinlet of pyrite, chalcopyrite, enargite and rennantite. Note the replacement textures of pyrites by enargite, enargite by tennantite and enargite-tennantite by chalcopyrite. D) Mineralization Stage 4, breccia band composed of pyrite, chalcopyrite, minor enargite and secondary copper-sulfides (chalcocite). Note the vuggy silica clasts incorporation in the breccias band. All images are reflected polarized light, excepting B, which corresponds to an image of transmitted crossed polarized light. alu: alunite, cc: chalcocite, cp: chalcopyrite, di: dickite, enr: enargite, py: pyrite, qz: quartz, tn: tennantite.

Replacement textures of pyrite by enargite, enargite by tennantite, and tennantite by chalcopyrite are observed in the stage three veinlets. Stage four is characterized by breccia bands composed of pyrite and minor chalcopyrite and enargite crosscutting the previous mineralization stages (Fig. 5.6D). Stage five corresponds to intermediate sulfidation base metal, up to 10 cm thick, veins composed of quartz, pyrite, barite and minor chalcopyrite, sphalerite and galena. Stage six is represented by the supergene alteration, developing an oxide zone and an enrichment zone. The oxidation zone is characterized by the presence of hematite and goethite filling voids of vuggy silica, in the groundmass, and within the matrix of hydrothermal breccias. Supergene jarosite, kaolinite and halloysite are found in fractures, vuggs and in the breccia matrix. Hypogene pyrite, barite and rutile remain as trace minerals in the oxidation zone. Below the oxidation zone, secondary Cu-bearing minerals such as chalcocite and minor covellite, replacing chalcopyrite and enargite, and filling small voids, constitute the supergene enrichment zone.

Ore stages at Cerro Quema are syn- and post- hydrothermal alteration, as indicated by; 1) the occurrence of disseminated sulfides in the groundmass of hydrothermally altered rocks. 2) The coexistence of sulfides and hydrothermal alteration minerals in the matrix of hydraulic breccias. 3) The occurrence of sulfide mineralization filling fissures, disseminated, in stockworks and in voids of the vuggy silica alteration zone.

5.4. Fluid inclusion study

5.4.1. Sampling and analytical methods

Fluid inclusion studies were carried out on samples selected from the different hydrothermal alteration zones developed on the Cerro Quema deposit, at surface and subsurface (drill core samples). Microthermometrical analyses were performed on secondary fluid inclusions, hosted in primary igneous quartz phenocrysts from dacites of the RQF (Fig. 5.7A). A few measurements could be also done on calcite from a vein crosscutting a dacite affected by propylitic alteration. Secondary fluid inclusions are assumed to be trapped during the hydrothermal event related to mineralization (Corral *et al*., 2011b; this study, Chapter 4).

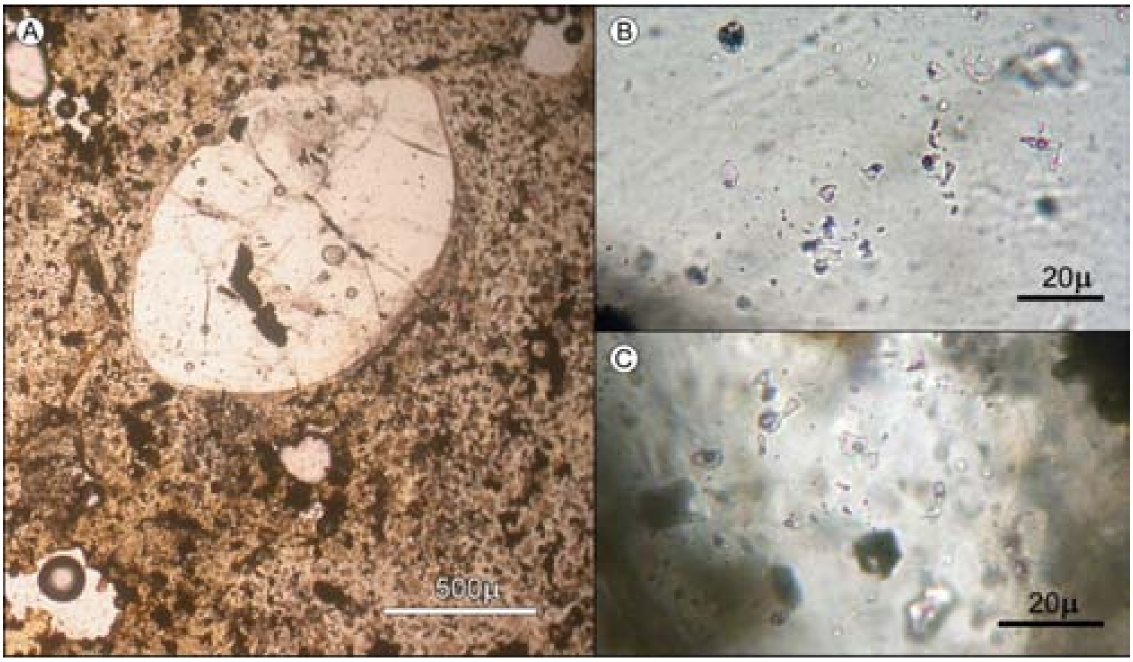

Figure 5.7: Fluid inclusions types and occurrences. A) Igneous quartz phenocryst of a dacite affected by vuggy silica alteration. All the fluid inclusion measurements were performed in this type of quartz crystals, affected by different hydrothermal alteration. B) Two-phase (L>V) fluid inclusion in trails within a quartz phenocryst. C) Two-phase (L>V) fluid inclusions randomly distributed in a quartz phenocryst. All images are taken with transmitted polarized light.

The microthermometrical study was carried out at the Universitat Autònoma de Barcelona fluid inclusion laboratory. Measurements were made on doubly polished thin sections (about 100 µm thick) using a Linkam THMSG-600 heating-freezing stage. The equipment was previously calibrated with synthetic standards. The data are reproducible to ± 0.5 ºC for the freezing runs and ± 5ºC for the heating runs. A total of 213 fluid inclusions were analyzed by cycles of freezing down to – 180 ºC and heating up to the appropriate temperature of total homogenization to ensure stability of the inclusions and representativeness of the determinations. These cycles were generally repeated several times in order to avoid nucleation problems during freezing runs.

Homogenization (*Th*) took place by bubble disappearance to liquid (V→L). Salinities are expressed as wt. % NaCl equivalent and were estimated from the melting temperatures (*Tmi*) of the last crystal of ice for two-phase fluid inclusions (Bodnar, 1993). Due to the fluid inclusions size, eutectic temperature (Te), were difficult to observe and no measurements were possible.

5.4.2. Fluid inclusion types and occurrence

The fluid inclusion study was carried out on samples affected by the different hydrothermal alteration types present throughout the deposit (Fig. 5.4): vuggy silica at Cerro Quemita, La Pava, Cerro Idaida and Chontal edge, and advanced argillic and propylitic alteration at Chontal edge.

From the petrographic study, only one type of fluid inclusions has been identified on the basis of number of phases and liquid to vapor ratios at room temperature. Fluid inclusions are biphasic (L+V), characterized by a dark vapor bubble, generally less than 50% of the inclusion volume, and were classified following the criteria of Shepherd *et al*. (1985), as two-phase liquid-rich (L>V). They show a variety of shapes: rounded, elongate or irregular, only a few of them show a negative crystal shape (Fig. 5.7B and 5.7C). Fluid inclusions are typically of small size (between 5 and 15 μm), making difficult the observation of phase changes during heating-freeezing runs.

All the studied fluid inclusions are considered secondary, occurring randomly distributed (Fig. 5.7C), isolated, in clusters and following trails (Fig. 5.7B) within igneous quartz phenocrysts.

5.4.3. Microthermometrical data

The microthermometrical results are summarized in Table 5.1 and Figure 5.8. Heterogenous trapping and postentrapment phenomena (necking down) are common features in fluid inclusions from epithermal systems (Bodnar *et al*., 1985). Hence, in an attempt to avoid collection of erroneous data, we only studied fluid inclusion trails, groups and clusters where all inclusions showed similar liquid-vapor phase ratios.

Salinity is used to represent the content of dissolved chlorides, principally NaCl but including KCl, $CaCl_2$, etc., (e.g., Roedder, 1963; Hedenquist *et al*., 1992). Hydrothermal fluids are therefore commonly discussed with reference to the experimentally well-studied phase relations in the binary system NaCl-H_2O (Bodnar, 1993; Bodnar and Vityk, 1994). Salinity was calculated using the program *Aqso5e*, included in the package FLUIDS (Bakker, 2003). This program is based on the method of Potter *et al*. (1978), for salinity calculations in NaCl bearing aqueous solutions at low temperatures and low salinities.

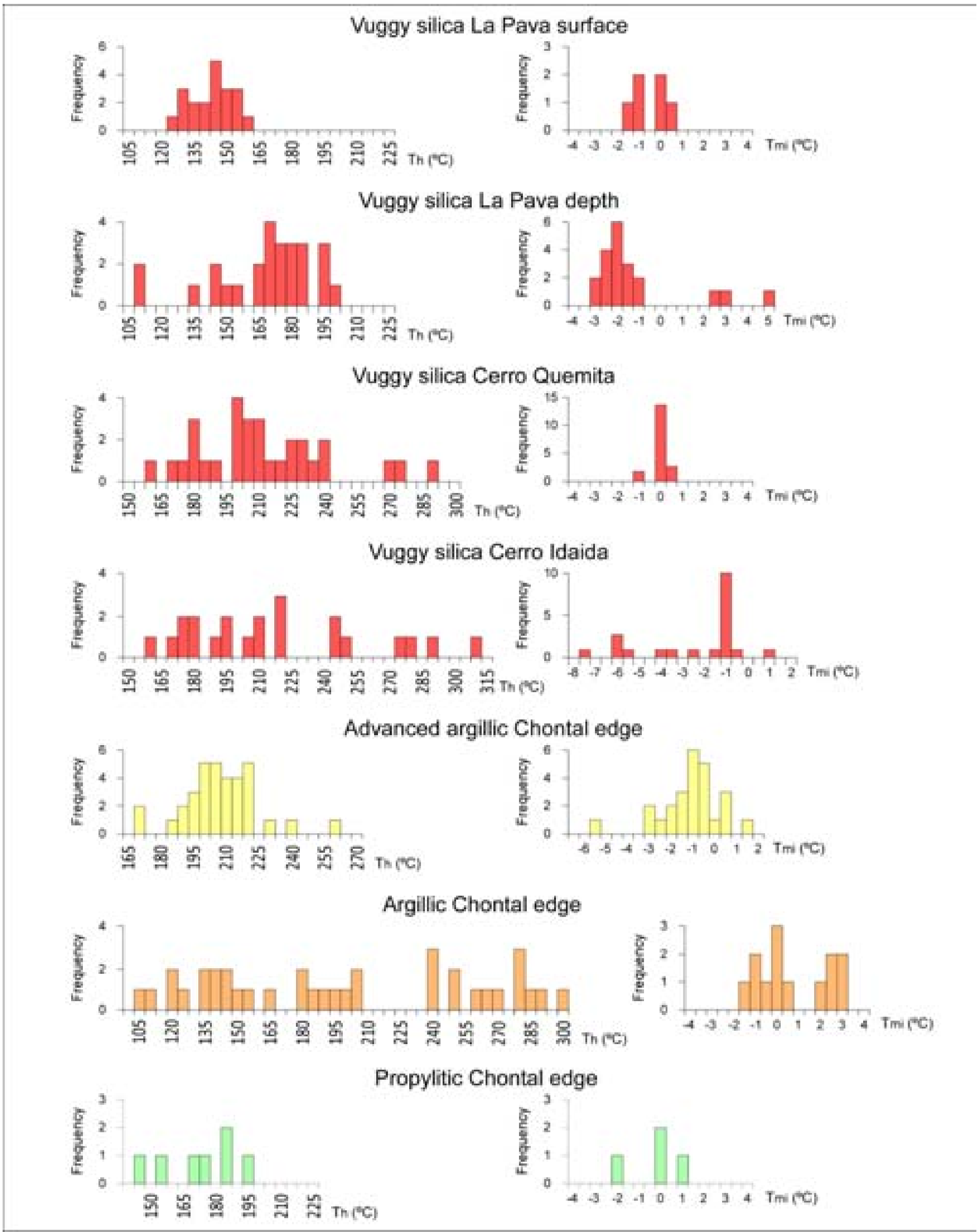

Figure 5.8: Representative frequency histograms of the homogenization temperature (*Th*) and melting ice temperature (*Tmi*) of fluid inclusions from the different alteration zones of the Cerro Quema deposit.

Sample	Deposit	Alteration zone	F.I.	Coordinates (ºWGS84) Longitude	Latitude	Elevation (asl)	*Th* (ºC) range (N)	*Tmi* (ºC) range (N)	wt % NaCl eq. range (N)
LP05	La Pava	VS	S	7.552843	-80.545937	520 m	123 - 156 (21)	-1.5 - +0.4 (6)	0.5 - 2.6 (5)
9311	La Pava	VS	S	7.553654	-80.548764	359 m	148 - 199 (27)	-3.3 - +4.6 (21)	2.2 - 5.4 (18)
0608	Chontal Edge	VS	S	7.554922	-80.537961	297 m	132 - 264 (23)	-1.1 - -0.2 (2)	0.4 - 1.9 (2)
9104	Cerro Quemita	VS	S	7.560327	-80.519231	791 m	160 - 286 (31)	-1.3 - +0.5 (20)	0.0 - 2.2 (16)
9343	Cerro Idaida	VS	S	7.555226	-80.507060	666 m	148 - 311 (24)	-7.8 - +0.6 (21)	1.0 - 11.5 (20)
0308	Chontal Edge	AAA	S	7.557230	-80.534429	341 m	166 - 256 (35)	-5.9 - +1.1 (26)	0.2 - 9.5 (22)
0908	Chontal Edge	AA	S	7.557644	-80.531515	492 m	132 - 299 (11)	-0.1 (1)	0.2 (1)
1008	Chontal Edge	AA	S	7.558298	-80.531266	490 m	103 - 277 (25)	-1.6 - +3.0 (12)	0.2 - 2.2 (6)
0808-23	Chontal Edge	Prop	S	7.553488	-80.540223	374 m	145 - 181 (4)	-2.0 - +0.9 (4)	0.4 - 3.4 (3)
0808-31	Chontal Edge	Prop	P	7.553488	-80.540223	353 m	173 - 190 (3)	-	-

Table 5.1: Summary of microthermometric results for fluid inclusions of the Cerro Quema deposit. All measurements were performed in quartz, excepting those of sample 0808-31 which were performed in calcite. Salinity has been calculated for fluid inclusions with *Tmi* ≤ 0 ºC. Th: homogenization temperature, *Tmi*: melting ice temperature, VS: vuggy silica, AAA: advanced argillic alteration, AA: argillic alteration, P: propylitic alteration, S: secondary, P: primary, (q): quartz, (cc): calcite.

5.4.3.1. CO_2 content in fluid inclusions

During the petrographic study and the microthermometrical measurements, phase transitions characteristic of the presence of volatiles (melting of CO_2 around -56.6 ºC or presence of CO_2 hydrates) have not been observed, pointing to the absence of significant amounts of volatiles. However, some melting ice temperatures were observed above 0ºC, between 0.1 and 4.6 ºC (19 of 213), which could indicate the presence of small quantities of CO_2 in the hydrothermal fluid, less than 2.2 molar (Hedenquist and Henley, 1985). According to Bodnar *et al*. (1985), low concentrations of CO_2 are typical of many ore deposits, particularly those forming in epithermal and magmatic-hydrothermal environments, like the Cerro Quema deposit. Therefore, calculated salinities should be considered as maximum values, as the possible presence of CO_2 depresses the melting ice temperature (Hedenquist and Henley, 1985; Fall *et al*., 2011).

5.4.3.2. Vuggy silica

Secondary fluid inclusions in quartz phenocrysts from La Pava vuggy silica alteration zone at surface (520 masl; Fig. 5.8) are characterized by an average *Th* of 140 ºC (σ=10 ºC) and by an average *Tmi* of -0.7 ºC (σ= 0.7ºC). Calculated salinity has an average of 1.6 wt% NaCl eq. (σ= 0.9 wt% NaCl eq.) However, at depth (359 masl; Fig. 5.8), vuggy silica shows an average *Th* of 166 ºC (σ=24ºC) and an average *Tmi* of -1.4 ºC (σ= 2.0ºC). Calculated salinity has an average of 3.7 wt% NaCl eq. (σ= 0.8 wt% NaCl eq.). Therefore, these data indicate that at La Pava orebody fluids responsible for the vuggy silica alteration were hotter and more saline at depth, and colder and more diluted at surface.

At the Chontal edge, fluid inclusions of vuggy silica at depth (341 masl) shows an average *Th* of 191 ºC (σ=32 ºC) and an average *Tmi* of -0.7 ºC (σ=0.6ºC). Calculated salinity has an average of 1.1 wt% NaCl eq. (σ=1.0 wt% NaCl eq.). This suggests an increase at depth of the homogenization temperature respect to the vuggy silica at La Pava. Salinity is not comparable due to the scarcity and spread of data from the vuggy silica of the Chontal edge.

On the other hand, the vuggy silica from Cerro Quemita at depth (791 masl; Fig. 5.8) is characterized by an average *Th* of 209 ºC (σ=31 ºC) and by an average *Tmi* of -0.2 ºC (σ= 0.4ºC). Calculated salinity has an average of 0.5 wt% NaCl eq. (σ= 0.5 wt% NaCl eq.). These data denote an increase in temperature, and a decrease in salinity, with respect to the vuggy silica present at depth at La Pava.

Finally, the vuggy silica from Cerrro Idaida at depth (666 masl; Fig. 5.8), is characterized by an average *Th* of 216 ºC (σ=46 ºC) and by an average *Tmi* of -2.7 ºC (σ= 2.4 ºC). Calculated salinity has an average of 4.5 wt% NaCl eq. (σ=3.4 wt% NaCl eq.). This shows an increase in *Th* with respect to the vuggy silica at La Pava, Chontal edge and Cerro Quemita. A precise distribution of fluid salinity within n the vuggy silica alteration zone is difficult to estimate due to the scarcity of data and the elevated standard deviation values. However, a trend increasing from surface to depth (e.g., La Pava orebody) and from West to East of the Cerro Quema deposit (e.g., La Pava – Cerro Idaida), can be envisaged.

5.4.3.3. Advanced argillic alteration

The scarcity of igneous quartz phenocrysts with secondary fluid inclusions in advanced argillic alteration samples precluded systematic measurements. Only one sample from the Chontal edge collected in a drill hole, at 341 masl could be studied (Fig. 5.8). Fluid inclusions in quartz from this sample geve an average *Th* of 206 ºC (σ=18 ºC), and an average *Tmi* of -1.3 ºC (σ=1.4ºC), which corresponds to a salinity average of 2.7 wt% NaCl eq. (σ=2.0 wt% NaCl eq.).

5.4.3.4. Argillic alteration

Two drill core samples located at the Chontal edge zone, affected by argillic alteration were studied (Fig. 5.4; Table 5.1). Unfortunately, the small size of the fluid inclusions and the opacity of the igneous quartz phenocrysts resulted in a small number of measurements. In order to facilitate the interpretation of the data, and as both samples are close each other, *Th* and *Tmi* measurements have been plotted together (Fig. 5.8).

Sample 0908 is characterized by an average *Th* of 243 ºC (σ=53 ºC). Only one measurement of *Tmi* was possible, giving a temperature of -0.1 ºC, which corresponds to a salinity of 0.2 wt% NaCl eq.

Sample 1008 is characterized by an average *Th* of 176 ºC (σ=54 ºC), and by an average *Tmi* of 0.6 ºC (σ=2 ºC). Calculated salinity has an average of 1.4 wt% NaCl eq. (σ= 1.4 wt% NaCl eq.).

5.4.3.5. Propylitic alteration

Microthermometrical measurements were done on two samples: a hypogene calcite, and a quartz phenocryst. Although data come from different minerals, they are represented in a single *Th* and *Tmi* frequency histograms (Fig. 5.8).

Fluid inclusions in quartz gave an average *Th* of 162 ºC (σ=17 ºC), and an average *Tmi* of -0.4 ºC (σ=1.2 ºC). Calculated salinity has an average of 2.2 wt% NaCl eq. (σ=2.3 wt% NaCl eq.). Fluid inclusions in calcite show an average *Th* of 182 ºC (σ=9 ºC). Unfortunately, no melting ice temperature could be measured. Although microthermometrical data from quartz and calcite are scarce, they are in good agreement.

5.5. Stable Isotopes

5.5.1. Sampling and analytical methods

Stable isotope analyses (O, H and S) were performed on surface and drill core samples from the mineralized bodies of the Cerro Quema deposit (Cerro Quema, Cerro Quemita, La Pava and Cerro Idaida; Appendix 4), at the USGS laboratories in Denver (USA). Sulfides and quartz were handpicked from crushed and sieved samples. Kaolinite-dickite and alunite were separated by decantation methods to obtain the clay particle size and then by centrifugation to separate the different minerals. After these processes, each sample was X-rayed to check the mineralogy and purity of clays.

Sulfates and sulfides were combined with V_2O_5 and combusted in an elemental analyzer. The resulting SO_2 followed directly into a Thermo Delta mass spectrometer for sulfur isotope measurement ($\delta^{34}S$) according to the method of Giesemann *et al*. (1994), with a precision of ± 0.5 ‰ (1σ). Oxygen isotope analyses of sulfates were performed by online high-temperature carbon reduction, with a precission of ± 1.0 ‰ (2σ). Silicates were reacted with BrF_5 (Clayton and Mayeda, 1963) and the resulting CO_2 gas was analyzed using a FinniganMAT252 mass spectrometer, with a precision of ± 3 ‰ (2σ) for $\delta^{18}O$. H ratios of kaolinite-dickite were determined with a FinniganMAT252 mass spectrometer, using the method of Vennemann and O'Neil (1993), with a precision of ± 6 ‰ (2σ) for δD. Analytical precision was based on replicate analyses. The $\delta^{18}O$ and δD analyses are reported in per mil relative to V-SMOW, and the $\delta^{34}S$ values are reported relative to the Canyon Diablo Troilite standard.

5.5.2 Sulfur isotopes

Sulfur isotope data were obtained on pyrite (*n=22*), enargite (*n=8*), chalcopyrite (*n=1*), barite (*n=5*) and alunite (*n=6*), (Table 5.2 and Fig. 5.9). $\delta^{34}S$ of pyrite range between -4.8 and -12.7‰, and enargite from -5.0 and -12.1‰. A chalcopyrite sample has a value of -5.5‰. $\delta^{34}S$ of alunite range from +15.0 to +17.4‰, and barite from +14.1 to +17.0‰. Comparing the different orebodies of the Cerro Quema deposit, no significant variability of $\delta^{34}S$ can be observed, suggesting a homogeneous sulfur source at deposit scale. However, sulfate $\delta^{34}S$ shows a small variability, being lighter from the East to the West, from -14.1‰ at Cerro Quemita to -17.0‰ at La Pava. $\delta^{34}S$ values for pyrite-alunite coexisting pairs (Table 5.2 and Fig. 5.9) are consistent with isotopic equilibrium between these minerals at the homogenization temperatures obtained from fluid inclusions. $\delta^{34}S$ values of sulfides and sulfates (Fig. 5.9) are similar to those reported in other high sulfidation epitermal deposits such as Summitville (USA:

Rye *et al*., 1990, 1992; Bethke *et al*., 2005), Lepanto (Phillipines; Hedenquist and Garcia, 1990) and Pueblo Viejo (Dominican Republic; Kesler *et al*., 1981; Vennemann *et al*., 1993).

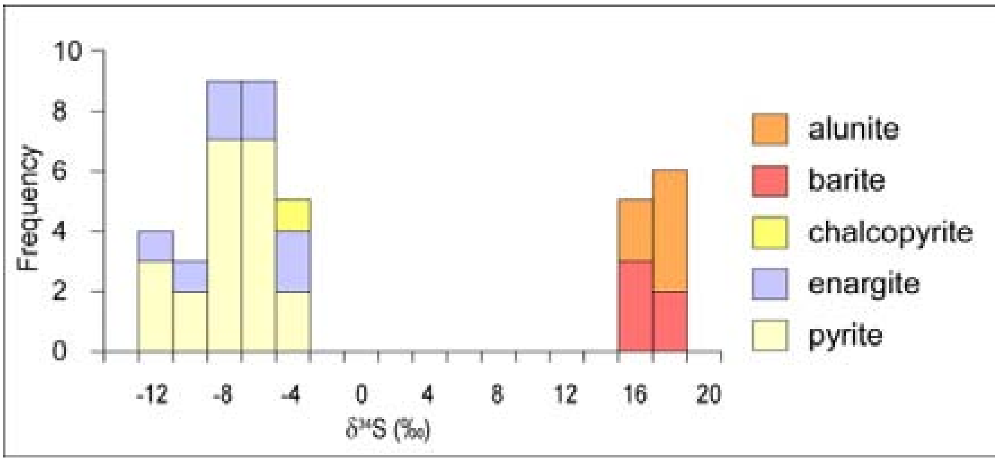

Figure 5.9: Frequency histogram of $\delta^{34}S$ in sulfides and sulfates from the Cerro Quema deposit.

5.5.3 Oxygen and hydrogen isotopes

Oxygen isotope analyses were performed on vuggy quartz (*n=24*), kaolinite (*n=19*) dickite (*n=4*), alunite (*n=6*) and barite (*n=5*). Hydrogen isotope analysis were performed on kaolinite (*n=19*) and dickite (*n=4*). In addition to vuggy quartz, oxygen isotope analyses were also performed on dacite quartz phenocrysts from the RQF (Cerro Quema host rock) (*n=3*). Results are shown in Table 5.3 and Table 5.4.

The $\delta^{18}O$ values of vuggy quartz, (+9.0 to +17.5‰) are heavier than those quartz phenocrysts of the Cerro Quema host rock (Dacite; +8.6 to +8.8‰). In general, quartz phenocrysts in altered igneous rocks retain their primary isotopic compositions (Taylor, 1968), implying that acid leaching and vuggy quartz development resulted in a ~ 0.5 to 8.9 ‰ $\delta^{18}O$ enrichment. $\delta^{18}O$ values of vuggy quartz show an important variability throughout the Cerro Quema area, becoming heavier from East to West in surface samples (e.g., 11.8% at Cerro

Quema surface to 17.5% at La Pava surface) and lighter from surface to depth (e.g., 17.5% at La Pava surface to 12.5% at La Pava at depth).

$\delta^{18}O$ values of kaolinite range from +12.7 to 18.1‰ and δD from -103.3 to -35.2‰, whereas $\delta^{18}O$ in dickite vary between +12.7 and +16.3‰ and δD from -44 to -30‰. Although δD values of kaolinite and dickite are highly variable throughout the Cerro Quema deposit, $\delta^{18}O$ values, show a trend from higher values in the East to lower in the West (from +18‰ at Cerro Quema to +16‰ at La Pava). Finally, $\delta^{18}O$ of alunite and barite show a wide range, from -1.6 to +9.8‰ in alunite and from +2.7 to +11.6‰ in barite.

5.6. Discussion

5.6.1 Characteristics of the hydrothermal fluid

In the study of a hydrothermal system it is essential to determine the thermal history, as this relates to the fluid flow characteristics and geochemical structure of the system (Hedenquist *et al*., 1992). Two of the principal physical processes occurring in the epithermal environment are boiling and mixing (Giggenbach and Stewart, 1982). Fluid inclusion data (*Th* and *Tmi*) allowed the recognition of these processes at Cerro Quema.

Results of microthermometrical measurements on secondary fluid inclusions from the Cerro Quema deposit are shown on a *Tmi* vs. *Th* plot (Fig. 5.10). In Figure 5.10A, where all the measurements are plotted together, two different trends can be distinguished: one from high *Tmi* and *Th* to lower *Tmi* and *Th* (a), and another formed by fluid inclusions characterized by low *Tmi* and high *Th* evolving to moderate *Tmi* and low *Th* (b). In any case, the relationship between homogenization and melting ice temperatures is not straightforward, probably reflecting a complex sequence of fluid events, such as cooling, mixing, and boiling. Only the study of individual samples or a group of samples with the same characteristics may help to understand the processes recorded by the fluid inclusions.

Sample	$\delta^{34}S$ (al)	$\delta^{34}S$ (ba)	$\delta^{34}S$ (cpy)	$\delta^{34}S$ (enr)	$\delta^{34}S$ (py)
			Chontal edge		
0308-51	17.4				-8.2
0308-60	15.6				-8.2
0308-60					-8.4
0308-65				-9.3	-8.3
0308-73					-8
0308-95	17.3				-8.5
0308-98				-11.2	-7.2
0308-104	17.2				-8.4
0308-104	17.2				
0308-105					-11.7
0308-111	15.0			-12.1	-7.2
0308-111					-7.2
0308-131					
0308-134					-9
QUE-51			-5.5		-4.8
QUE-51					-5.2
QUE KAN		15.4			
QUE KAN		15.5			
			La Pava		
9316-182		16.9			
9316-190		17.1			
9210-16					-12.7
LP225					-12.6
LP225					-7.6
			Cerro Quemita		
QT-02		14.1			
9315-130					-10.7
			Cerro Idaida		
9343-36				-7.5	-12.1
9343-56				-7.9	-6.7
9343-56				-8.6	-6
9343-66				-5.3	
9343-66				-5.0	
			El Montuoso batholith		
Pit-02				-5.0	

Table 5.2: Sulfur isotope composition ($\delta^{34}S_{CDT}$ ‰) for sulfides and sulfates of the Cerro Quema deposit. al: alunite, ba: barite, cpy: chalcopyrite, enr: enargite, py:pyrite.

When fluid inclusions from the advanced argillic alteration zone of the Chontal edge and from the vuggy silica from La Pava (surface and drill core samples) are plotted together (Fig. 5.10B), a trend evolving from high *Tmi* and low *Th* towards low *Tmi* and *Th* can be recognized. In a *Th* vs. *Tmi* plot, such trends may be indicative of a boiling process with slightly cooling (Sheppard *et al*., 1985; Hedenquist and Henley, 1985), although coexistence of vapor-rich and liquid-rich fluid inclusions in the same sample has not been observed.

Sample	$\delta^{18}O$ (al)	$\delta^{18}O$ (ba)	δD (di)	$\delta^{18}O$ (di)	δD (kaol)	$\delta^{18}O$ (kaol)	$\delta^{18}O$ (qz)
Chontal edge							
0308-29			-30	14.6			
0308-51	9.8						10.4
0308-60	6.7						
0308-60	6.6						
0308-65			-44	12.7			
0308-95	4.2						9.0
0308-104	-1.6						10.7
0308-105			-39	12.7			
0308-111	4.9						
0308-131			-36	16.3			
QUE-51							16.6
QUE-51							13.5
QUE KAN		10.8					
QUE KAN		10.8					
La Pava							
9210-16							16.2
9322-78							15.5
9311-106							12.9
9311-153							12.5
9316-182		11.6					
9316-190		10.9					
LP04					-47	17.9	
LP211					-41	15.2	
LP212A					-46	17.6	
LP213B					-35	17.7	
LP213B					-36	17.7	
LP215					-77	16.6	
LP216					-66	17.1	
LP218							17.5
LP220							16.6
LP222					-40	15.4	
LP223					-42	15.5	
LP225						14.6	16.8
LP226					-80	15.6	
LP226					-81	15.6	
LP228					-57	18.1	
CLP4					-38	16.9	
CLP4					-42	16.9	
Cerro Quemita, Cerro Quema and Cerro Idaida							
914-59							11.7
914-82							12.5
9315-130							12.1
QT02		2.7					
QA05					-103	14.3	
QA10							12.9
QA15A					-50	17.4	
QA17B							11.8
QA24					-39	18.0	
QA29					-52	17.4	
QA30					-48	17.1	
QA32							12.3
9343-36							13.7
9343-56							11.9
9343-66							11.4

Table 5.3: Oxygen and Hydrogen isotope composition of the hydrothermally altered rocks of the Cerro Quema Deposit. al: alunite, ba: barite, di:dickite, kaol: kaolinite, qz: quartz.

Sample	Rock	Location	Unit	$\delta^{18}O$ (quartz)
LP204	dacite	La Pava	Río Quema Formation	8.7
LP218	dacite	La Pava	Río Quema Formation	8.8
QA32	dacite	Cerro Quema	Río Quema Formation	8.6

Table 5.4: Oxygen isotope composition ($\delta^{18}O_{VSMOW}$ ‰) of the Cerro Quema host rock.

On the other hand, in Figure 5.10C where fluid inclusions of the vuggy silica from Cerro Idaida and Cerro Quemita are plotted, two different trends can be distinguished. A first trend is characterized by fluid inclusions with low *Tmi* and high *Th* evolving towards a low *Th* at *Tmi* almost constant (a).The second trend is depicted by fluid inclusions with high *Tmi* and high *Th* evolving towards low *Tmi* and *Th* (b). According to Sheppard *et al*. (1985) and Hedenquist and Henley (1985), these trends would be indicative of simple cooling (a) and mixing or dilution of the fluid with cooler and a less saline fluid (b).

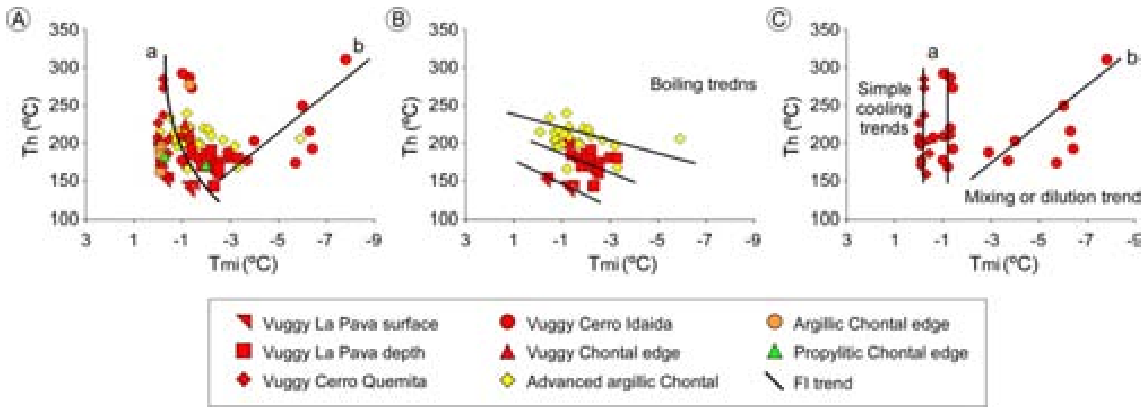

Figure 5.10: Homogenization temperature (*Th*) – Melting ice temperature (*Tmi*) plots showing the different fluid inclusion trends observed in the measured microthermometric data. A) *Th-Tmi* plot of all the measured fluid inclusions. B) *Th-Tmi* plot with data from measurements of the fluid inclusions of the vuggy silica form La Pava (at surface and subsurface) and of the fluid inclusions of the advanced argillic alteration from the Chontal edge. C) *Th-Tmi* plot with data from measured fluid inclusions in the vuggy silica from Cerro Quemita and Cerro Idaida.

At Cerro Quema deposit, mineralizing fluids were of variable temperature, ranging from 140 to 243 ºC (average temperatures), and low salinity (from < 1 to ~ 11 wt % NaCl, although most data are below 5 wt % NaCl). *Th* vs. *Tmi* plots (Fig. 5.10) of the advanced argillic alteration (Chontal edge), vuggy silica (La

Pava, Cerro Idaida and Cerro Quemita), indicate boiling, and mixing of magmatic and meteoric fluids. Our observations are consistent with data documented in several high sulfidation deposits (e.g., Arribas, 1995).

Some information on pressure conditions during the formation of the Cerro Quema deposit may be obtained from fluid inclusion data. Most pressures estimated from fluid inclusions are stated to represent lithostatic or hydrostatic pressures, or some intermediate value. According to Roedder and Bodnar, (1980), the local pressure at the site of the inclusion at the time of trapping, is actually hydrostatic in any case, because it is a fluid pressure.

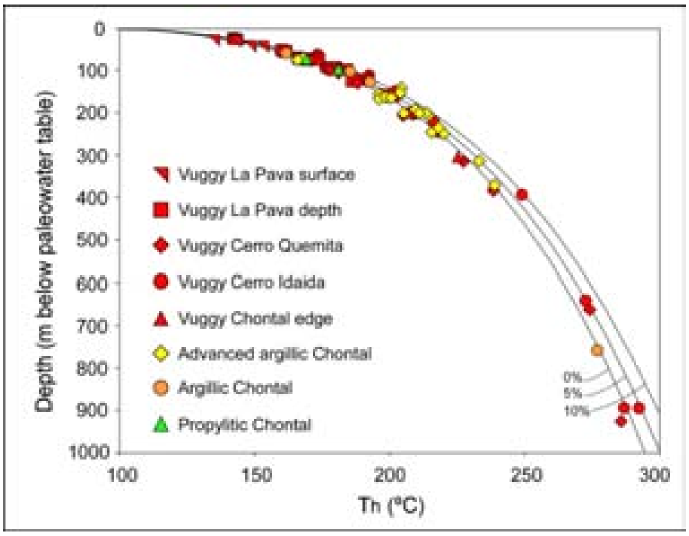

Figure 5.11: Elevation versus temperature (*Th*) plot of measured fluid inclusions at the Cerro Quema deposit. Boiling point curves of Haas (1971) for fluids with different salinities (0%, 5% and 10%), are also represented.

Assuming that fluid inclusions in the studied samples were trapped under boiling conditions, the *P-T* entrapment conditions can be estimated using the boiling point curves of Haas (1971). *Th* data of the different hydrothermal alteration zones are represented in Figure 5.11, plotted against the elevation and referenced with the boiling point curves for pure water (0 wt% NaCl), and for water containing 5 wt% NaCl and 10 wt% NaCl, respectively. As observed, most of samples plot between 30 and 400 m below the paleowater table, mainly in the upper zone (30-250m), which corresponds to a pressure of 4 to 37 bars under hydrostatic conditions (Haas, 1971). These observations suggest a shallow depth of emplacement for the Cerro Quema deposit, which is in agreement with a minimum depth of emplacement of 150-250 m below the paleowater table reported in Chapter 3 based on geological observations.

5.6.2 Sulfur source and geothermometry

The isotopic composition and evolution of total sulfur ($\delta^{34}S_{\Sigma S}$) in a hydrothermal fluid may provide insights as to the provenance of sulfur and the conditions of mineral formation. Coexisting sulfides and sulfates may in turn, be useful for thermometrical measurements. Alunite is an important mineral component of the advanced argillic alteration assemblage and is abundantly present in the drill core samples from the Chontal edge. Textural and mineralogical relationships indicate that alunite is paragenetically contemporaneous with associated pyrite.

According to Field and Gustafson (1976), Kusakabe *et al*. (1984) and Field *et al*. (1983; 2005), the use of $\delta^{34}S$ of sulfide and sulfate vs. $\Delta^{34}S_{sulfate\text{-}sulfide}$ plot, is a powerful tool to estimate the $\delta^{34}S_{\Sigma S}$, $X_{SO_4^{2-}}$ and X_{H_2S} of the mineralizing fluid (assuming isotopic equilibrium between sulfate and sulfide). The $\delta^{34}S$ of coexisting pyrite and alunite of samples from the Chontal edge (Table 5.2) have been represented in a $\delta^{34}S$-$\Delta^{34}S_{sulfate\text{-}sulfide}$ plot (Fig. 5.12A). Regression analyses of alunite-pyrite pairs form two linear and converging trend lines. The point of convergence of these two lines on the *y* axis ($\delta^{34}S$), defines the value for $\delta^{34}S_{\Sigma S}$, and the slopes of the upper and lower regression lines approximate the $X_{SO_4^{2-}}$ and X_{H_2S} of the system, respectively.

As observed in Figure 5.12A, the obtained $\delta^{34}S_{\Sigma S}$ of the mineralizing fluid responsible for the Cerro Quema deposit is -0.5‰, and calculated $X_{SO_4^{2-}}$ and X_{H_2S} are 0.31 and 0.69 respectively, with a H_2S/SO_4^{2-} (R) ratio of 2.23. These data indicate that: 1) sulfur in the deposit is of magmatic origin, with a $\delta^{34}S_{\Sigma S}$ value similar to that reported in other world class high sulfidation epithermal deposits and porphyry copper deposits associated with I-type granites (Ohmoto and Goldhaber, 1997; Hedenquist and Lowenstern, 1994; Arribas, 1995).

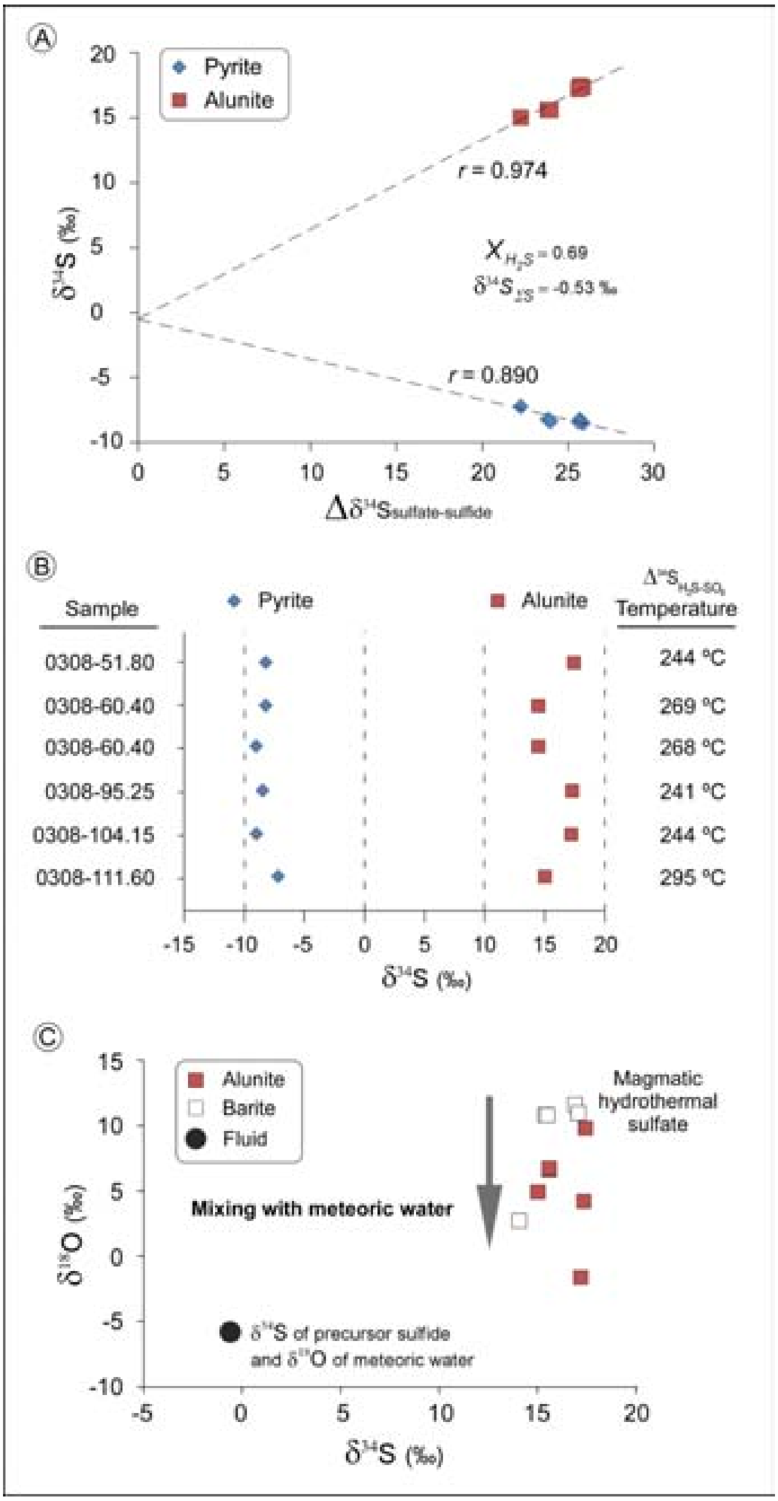

Figure 5.12: Summary of $\delta^{34}S$ and $\delta^{18}O$ data on alunite, barite, pyrite and vuggy quartz. A) $\delta^{34}S$‰ plot of sulfate (alunite) and sulfide (pyrite) pairs vs. delta (Δ) value. The convergence and slope of the two regression lines is an approximation of the bulk sulfur isotopic composition ($\delta^{34}S_{\Sigma S}$) and the proportion of oxidized to reduced sulfur species ($X_{SO_4^{2-}}$ and X_{H_2S}) in the hydrothermal fluid. B) $\delta^{34}S$‰ values of sulfides and sulfates from the advanced argillic alteration zone. Also shown is the temperature determined from sulfide-sulfate mineral pairs. C) $\delta^{34}S$ and $\delta^{18}O$ of barite and alunite showing a vertical trend, indicating a mixing between magmatic sulfate and meteoric waters (see text for explanation).

2) fluids responsible of the of hydrothermal alteration stage characterized by the presence of pyrite and alunite are are potentially mineralizing fluids as R values are in between the range of hydrothermal ore-forming fluids (R= 4 ±2; Rye *et al*., 1992; Hedenquist *et al*., 1994 Nansatsu, Arribas *et al*., 1995 Rodalquilar;

Arribas, 1995). 3) Mineralization at Cerro Quema was produced by a sulfide dominant hydrothermal fluid.

δ^{34}S values of sulfides coexisting with sulfates reflect isotopic equilibrium between H_2S and SO_4^{2-} in the hydrothermal fluid (see Fig. 5.9). This equilibrium is typical of magmatic-hydrothermal deposits (Rye *et al*., 2005), and has also been shown in world class high sulfidation epithermal deposits (e.g., Field and Fifarek, 1985; Arribas, 1995). Therefore, δ^{34}S values of sulfides and sulfates can be used as geothermometer. Using the equation of Ohmoto and Rye (1979), calculated equilibrium temperatures for alunite-pyrite pairs range between 241 and 295 ºC (*n=6* pairs; Fig. 5.12B), consistent with the disproportionation temperature of magmatic SO_2 to H_2S + SO_4^{2-} in the hydrothermal solution, which occurs below 400 ºC (Sakai and Matsubaya, 1977; Bethke, 1984; Stoffregen, 1987; Rye *et al*., 1992).

5.6.3 δ^{34}S / δ^{18}O *of alunite and barite*

δ^{34}S and $\delta^{18}O_{SO_4^{2-}}$ values of alunite and barite from the advanced argillic alteration zone at Cerro Quema are shown in Figure 5.12C. Both minerals present a narrow range of δ^{34}S values (+14.1 to +17.4‰), but variable δ^{18}O values, ranging from -1.6 to +11.6‰. According to these isotopic characteristics, sulfates from Cerro Quema fall within the magmatic-hydrothermal field defined by Rye *et al*., (1992; 2005). The high δ^{34}S values of alunites and barites are consistent with sulfate derived from sulfuric acid produced after disproportionation of magmatic SO_2, which reacted with the wall rocks producing the acid-sulfate alteration (Holland, 1965; Stoffregen, 1987). However, the variable values of δ^{18}O, which draw a vertical trend, suggest that disproportionation of some SO_2 may have occurred in mixures of magmatic and meteoric waters. The effect of mixing between magmatic and meteoric waters is to decrease the δ^{18}O by an amount dependent on the δ^{18}O and the degree of involvement of meteoric waters (Rye *et al*., 1992). This interpretation is in agreement with the fluid inclusion data obtained in the vuggy silica and the advanced argillic alteration zone, which suggest the boiling of a hydrothermal fluid with slightly cooling, and a mixing or dilution of a hydrothermal fluid with cooler and less saline fluids (e.g., meteoric waters).

5.6.4 H and O isotope composition of hydrothermal fluids

Studies of fluid-mineral isotopic equilibria in geothermal systems have shown that quartz is very resistant to isotopic exchange, preserving the original isotopic signature (Clayton *et al.*, 1968; Blattner, 1975; Clayton and Steiner, 1975). As previously noted, at Cerro Quema, vuggy silica is enriched in $\delta^{18}O$ relative to quartz phenocrysts of the unaltered host rock (avg. values of +13.3‰ and +8.7‰, respectively). Assuming a fluid with a constant oxygen isotopic composition, the increase in $\delta^{18}O_{quartz}$ would reflect progressively lower temperatures of deposition from W to E, in agreement with the decrease in the homogenization temperatures obtained from fluid inclusions. On the other hand, $\delta^{18}O_{quartz}$ values decrease with depth, suggesting an increase in temperature towards the deeper parts of the system, a characteristic observed in other high sulfidation epithermal deposits such as Summitville (Colorado, USA; Larson and Taylor, 1987; Bethke *et al.*, 2005).

Assuming a temperature of quartz formation based on the of fluid inclusion data (153ºC for samples from La Pava, 206ºC for samples from the Chontal edge, 209ºC for samples from Cerro Quemita, 216ºC for samples from Cerro Quema and 216ºC for samples from Cerro Idaida), $\delta^{18}O$ composition of water in equilibrium with vuggy quartz ranges from -2.6 to +3.0‰ (using the quartz-water fractionation equation of Matsuhisha *et al.*, 1979). As shown in Figure 5.13, the $\delta^{18}O$ values of quartz of the Cerro Quema deposit, overlap those reported by Larson and Taylor (1987) and Bethke *et al.* (2005) for quartz from Summitville (Colorado, USA), and those from other high sulfidation epithermal deposits such as Pueblo Viejo (Dominican Republic; Vennemann *et al.*, 1993), Pierina (Peru; Fifarek and Rye, 2005), Nansatsu (Japan; Hedenquist *et al.*, 1994) and Rodalquirar (Spain; Arribas *et al.*, 1995).

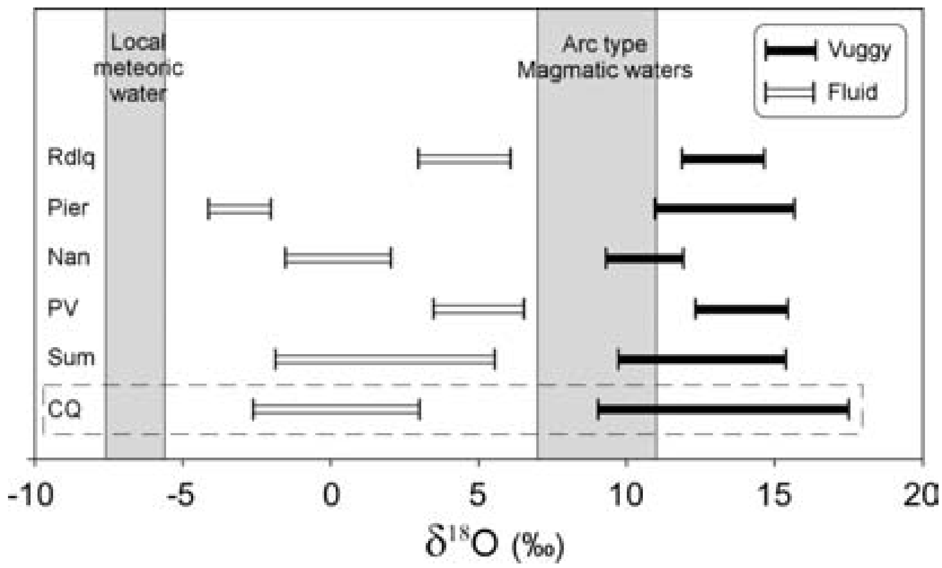

Figure 5.13: Diagram showing the range of mineral $\delta^{18}O$ values and calculated $\delta^{18}O$ values of fluids in equilibrium with vuggy quartz (see text for temperatures). Also shown a comparison with data from Rodalquilar (Arribas *et al*., 1995), Pierina (Fifarek and Rye, 2005), Nansatsu (Hedenquist *et al*., 1994), Pueblo Viejo (Vennemann *et al*., 1993), and Summitville (Larson and Taylor, 1987; Bethke *et al*., 2005). Local meteoric waters field from Caballero (2010); arc type magmatic waters field from Taylor (1986) and Giggenbach (1992). Rdl: Rodalquilar, Pier: Pierina, Nan: Nansatsu, PV: Pueblo Viejo, Sum: Summitville.

Calculated $\delta^{18}O$ values of the parental fluid in equilibrium with quartz at Cerro Quema plot in the field between the arc type magmatic waters (Taylor, 1986; Giggenbach, 1992) and the present day meteoric water (Caballero, 2010), and is similar to other high sulfidation systems such as Summitville, Pierina and Nansatsu. In these deposits, as in Cerro Quema, hydrothermal waters are isotopically closer to the composition of local meteoric waters, indicating that vuggy quartz was precipitated from magmatic fluids mixed with variable amounts of meteoric water at different temperatures. This obervations are in agreement with the high grade pockets found in the vuggy silica lateration zone, because fluid mixing is an important process for ore formation (e.g., Ohmoto *et al*., 1983; Hofstra *et al*., 1991; Plumlee, 1994; Cooke and Simmons, 2000).

Kaolinite and dickite are widespread found within the advanced argillic and the argillic ateration zones at Cerro Quema, and their isotopic composition ($\delta^{18}O$

and δD) may reflect the geological conditions during the mineral deposition (Savin and Lee, 1988). For instance, δ^{18}O values of kaolinite of sedimentary origin usually vary from +19 to +23‰, whereas those of kaolinite from residual deposits (primary) range from +15 to +19‰ (Murray and Janssen, 1984).

δ^{18}O and δD values of dickite and kaolinite from Cerro Quema range from +12.7 to +18.1‰, and from -30 to -103‰, respectively, and are shown in Table 5.3 and plotted on δ^{18}O/δD diagram in Figure 5.14.

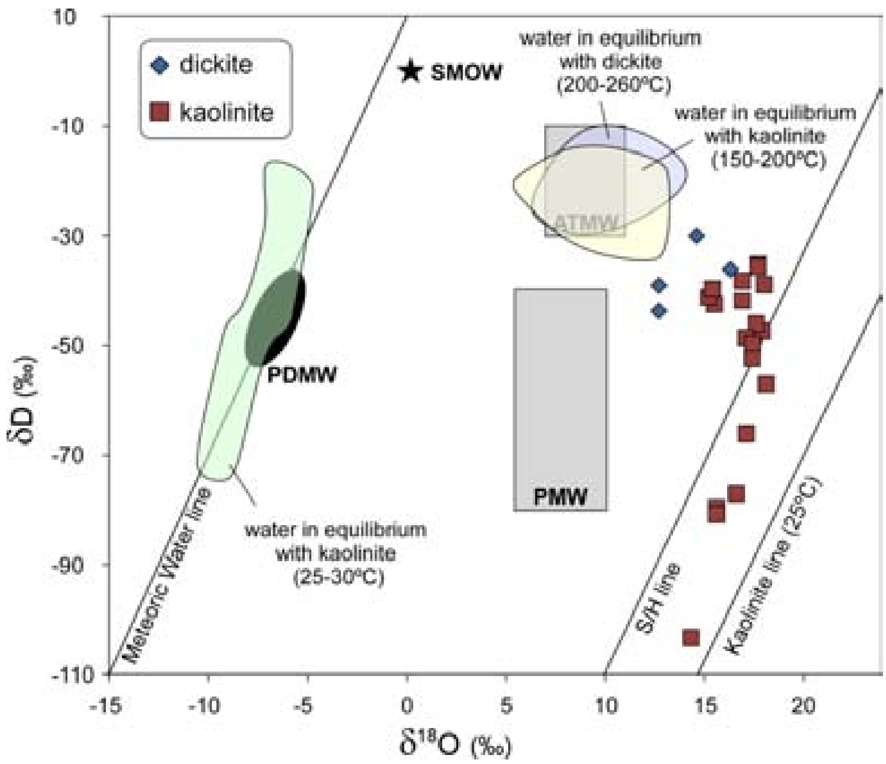

Figure 5.14: Plot of δ^{18}O and δD values of kaolinite and dickite minerals, and the water in equilibrium with these kaolinites and dickites. PDMW: Present day meteoric water (Caballero, 2010), PMW: Primary magmatic waters (Taylor, 1974; Sheppard, 1986), ATMW: Arc-type magmatic waters (Taylor, 1986; Giggenbach, 1992), S/H line: Supergene/Hypogene line (Sheppard *et al*., 1969), Kaolinite line (25ºC; Savin and Epstein, 1970; Sheppard and Gilg, 1996).

In Figure 5.14, two groups of kaolinite/dickite can be distinguished: a group of samples plotting between the supergene/hypogene (S/H; Sheppard *et al*., 1969), and the kaolinite line at 25ºC (Savin and Epstein, 1970; Sheppard and Gilg, 1996), corresponding to kaolinites/dickites of supergene origin. A second group, plotting between the S/H line and the Arc Type Magmatic Waters box (ATMW), which are considered to be of hydrothermal origin. Therefore, kaolinite/dickite of meteoric and hydrothermal origin coexist in the deposit, only distinguishable from their $\delta^{18}O$ and δD values.

In order to estimate the isotopic composition of fluids responsible for the kaolinite and dickite precipitation, a temperature range based on fluid inclusion data, mineral paragenesis and isotope geothermometry was used. The assumed temperatures were: 200 to 260ºC for hypogene dickites; 150 to 200ºC for hypogene kaolinites; and 25 to 30ºC for kaolinites of supergene origin. Calculations have been performed using the fractionation equations of Gilg and Sheppard (1996), and Sheppard and Gilg (1996) for oxygen and hydrogen, respectively.

Results show that δD and $\delta^{18}O$ of fluid in equilibrium with hypogene dickite range from -28 to -13‰ and from +7.1 to +13.3‰, respectively. δD and $\delta^{18}O$ of fluid in equilibrium with hypogene kaolinite range from -32 to -15‰ and from +6.5 to +12.4‰, respectively. These values are compatible with an origin related to the arc-type magmatic waters (ATMW) defined by Taylor (1986) and Giggenbach (1992).

On the other hand, D and $\delta^{18}O$ of the fluid in equilibrium with kaolinite of supergene origin, range from -72 to -20‰ and from -10.0 to -5.2‰, respectively. These calculated values are clearly consistent with kaolinite formation at low temperature in equilibrium with water having an isotopic composition close to the present-day meteoric water in the area (PDMW; Caballero, 2010).

5.7. Conclusions

Several conclusions arise from our study of the Cerro Quema high sulfidation epithermal Au-Cu deposit. Some of the background of the previous discussion is summarized in this section and represented in Figure 5.15, which is an overview of the geochemistry of the hydrothermal fluid and their relationship with the Au-Cu mineralization. Based on stable isotope (O, H, and S), and on fluid inclusion data, the main conclusion are as follows:

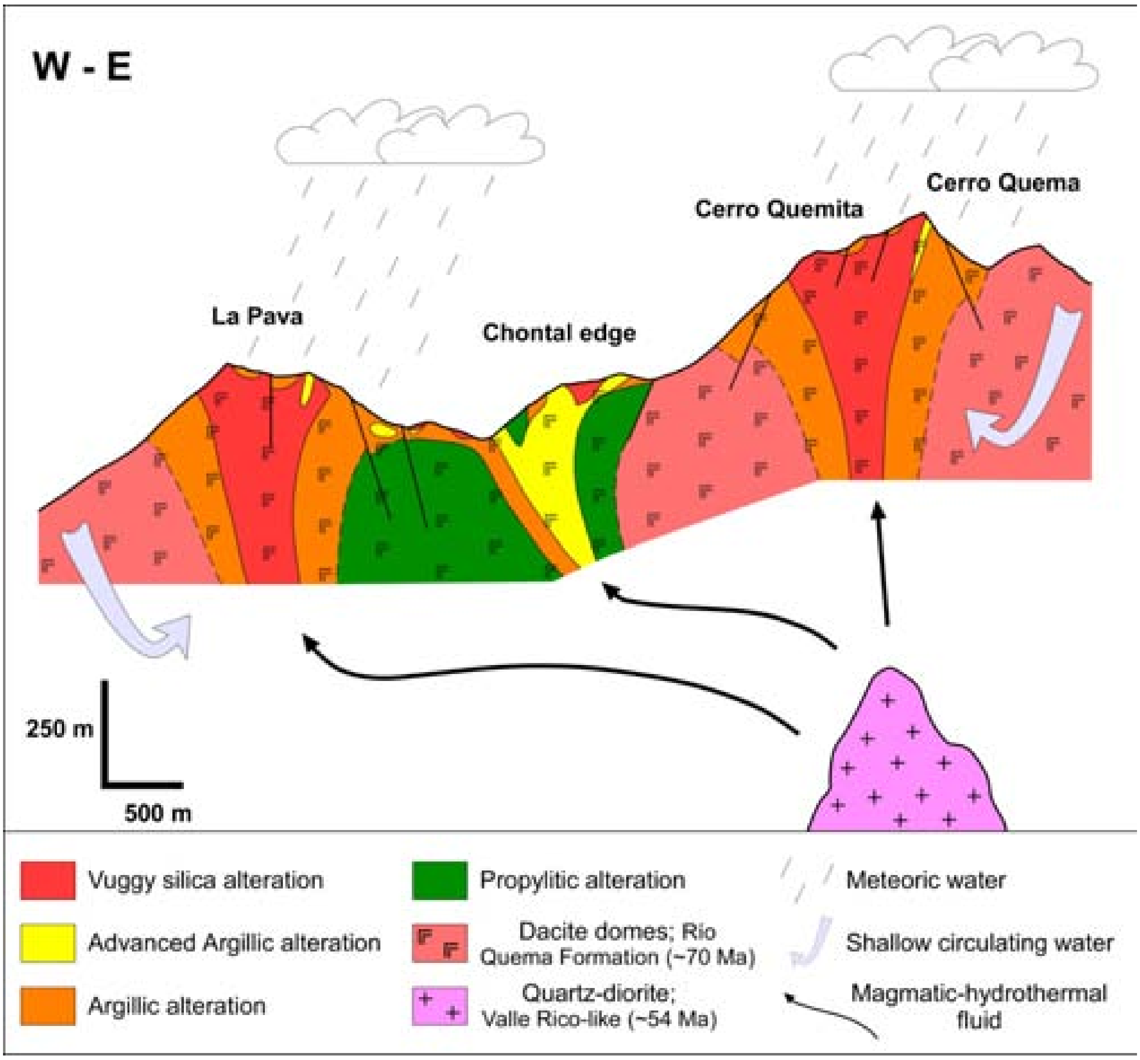

Figure 5.15: Genetic model for the Cerro Quema Au-Cu deposit based on the isotope and fluid inclusion data. The magmatic-hydrothermal mineralizing fluid of intermediate temperature and low salinity comes from the emplacement of Valle Rico-like intrusions and migrates towards the W interacting with surface waters and the host rock (dacite dome complex of the RQF). This interaction produced the development of a widespread hydrothermal alteration and the precipitation of Au and Cu.

1) Fluid inclusions data characterize a fluid with variable temperature, ranging from 140 to 243 ºC, and low salinity (< 5 wt % NaCl). This fluid was cooler in the W (La Pava) and hotter in the E (Cerro Quema), indicating the

proximity to the fluid source and heat, which is presumably located to the E (see Fig. 5.15).

2) Boiling, mixing and cooling processes deduced from fluid inclusion data (*Th*/*Tmi* plot), indicate the interaction of the mineralizing hydrothermal fluid with a cooler and less saline fluid, probably of meteoric origin.

3) Calculated fluid pressure during mineralization was up to 37 bars under hydrostatic conditions, corresponding to a range between 30 to 250 m below the paleowater table. This indicates that the deposit was emplaced at shallow depth.

4) The mineralizing hydrothermal fluid was characterized by $\delta^{34}S_{\Sigma S}$ values of -0.5‰, where $X_{SO_4^{2-}}$ and X_{H_2S} are 0.31 and 0.69 respectively, with a H_2S/SO_4^{2-} (R) ratio of 2.23. These values are compatible with a sulfide dominant hydrothermal fluid of magmatic origin. However, variable $\delta^{18}O$ with constant $\delta^{34}S$ of alunite and barite (Fig. 5.12C), suggests a contribution of meteoric waters.

5) Sulfur isotope geothermometry from coexisting alunite and pyrite pairs, gave equilibrium temperatures ranging from 241 to 295 ºC. Calculated temperatures are in agreement with microthermometrical measurements from fluid inclusions of the advanced argillic alteration zone.

6) $\delta^{18}O$ values of vuggy silica decrease from W (La Pava) to E (Cerro Quema) of the deposit and from surface to depth. These successive enrichments in ^{18}O reflect progressively lower temperatures of deposition, indicating the relative distance to the fluid and heat source. The variation in $\delta^{18}O$ of vuggy silica is in agreement with the temperature gradients deduced from fluid inclusion measurements, suggesting that the fluid and heat source was situated to the E of Cerro Quema (see Fig. 5.15).

7) $\delta^{18}O$ values of fluids in equilibrium with vuggy silica, from -2.6 to +3.0‰, suggest that the hydrothermal fluid during vuggy silica precipitation was a mixture of magmatic and meteoric waters.

8) According to $\delta^{18}O$ and δD values of fluids in equilibrium with kaolinite and dickite, two origins for these minerals can be distinguished: hypogene kaolinite and dickite with $\delta^{18}O$ and δD values ranging from +6.5 to +13.3‰ and from -32 to -15‰ respectively, and supergene kaolinite with $\delta^{18}O$ and δD values from -10.0 to -5.2‰ and from -72 to -20‰, respectively. The origin of kaolinite and dickite is only distinguishable from their $\delta^{18}O$ and δD values.

5.8. References

Arribas, A., 1995. Characteristics of high-sulfidation epithermal deposits, and their relation to magmatic fluid. In: Thompson, J. F. H. (Ed.), Magmas, Fluids, and Ore Deposits, Mineralogical Association of Canada Short Course 23, 419-454.

Arribas, A. Cunningham, C. G., Rytuba, J. J., Rye, R. O., Kelly, W., Podwysocky, M. H., McKee, E. H., Tosdal, R. M., 1995. Geology, geochronology, fluid inclusions, and isotope geochemistry of the Rodalquilar gold alunite deposit, Spain. Economic Geology 90 (4), 795-822.

Bakker, R. J., 2003. Package FLUIDS 1. Computer programs for analysis of fluid inclusion data and for modelling bulk fluid properties. Chemical Geology 194 (1-3), 3-23.

Bethke, P. M., 1984. Controls on base- and precious-metal mineralization in deeper epithermal environments. U. S. Geological Survey Open-File Report 84-890, 84-890.

Bethke, P. M., Rye, R. O., Stoffregen, R. E. and Vikre, P. G., 2005. Evolution of the magmatic-hydrothermal acid-sulfate system at Summitville, Colorado; integration of geological, stable isotope, and fluid inclusion evidence. Chemical Geology 215 (1-4), 281-315.

Bodnar, R. J., 1993. Revised equation and table for determining the freezing point depression of H2O-NaCl solutions. Geochimica et Cosmochimica Acta 57 (3), 683-684.

Bodnar, R. J., Reynolds, T. J. and Kuehn, C. A., 1985. Fluid inclusion systematics in epithermal systems. In: Berger, B. R., Bethke, P. M. (Eds.), Geology and Geochemistry of Epithermal Systems. Reviews in Economic Geology 2, 73-97.

Bodnar, R. J. and Vityk, M. O., 1994. Interpretation of microthermometric data for H2O-NaCl fluid inclusions. In: De Vivo, B., and Frezzotti, M. L. (Eds.), Fluid inclusions in Minerals, Methods and Applications, 117-130.

Buchs, D. M., Arculus, R. J., Baumgartner, P. O., Baumgartner-Mora, C. and Ulianov, A., 2010. Late Cretaceous arc development on the SW margin of the Caribbean Plate: Insights from the Golfito, Costa Rica, and Azuero, Panama, complexes. Geochemistry, Geophysics, Geosystems 11 (7), Q07S24.

Buchs, D. M., Baumgartner, P. O., Baumgartner-Mora, C., Bandini, A. N., Jackett, S. J., Diswrens, M. O., Stucki, J., 2009. Late Cretaceous to Miocene seamount accretion and melange formation in the Osa and Burica Peninsulas (southern Costa Rica); episodic growth of a convergent margin. Geological Society Special Publications 328, 411-456.

Buchs, D. M., Baumgartner, P. O., Baumgartner-Mora, C., Flores, K. and Bandini, A. N., 2011. Upper Cretaceous to Miocene tectonostratigraphy of the Azuero area (Panama) and the discontinuous accretion and subduction erosion along the Middle American margin. Tectonophysics 512 (1-4), 31-46.

Caballero, A., 2010. Exploración de aguas subterráneas en el arco seco de Panamá (Sector de Las Tablas) mediante métodos geofísicos. Thesis. Universitat de Barcelona, 271 pp.

Clayton, R. N. and Mayeda, T. K., 1963. The use of bromine pentafluoride in the extraction of oxygen from oxides and silicates for isotopic analysis. Geochimica et Cosmochimica Acta 27, 43-52

Clayton, R. N. and Steiner, A., 1975. Oxygen isotope studies of the geothermal system at Wairakei, New Zealand. Geochimica et Cosmochimica Acta 39 (8), 1179-1186.

Cooke, D. R. and Simmons, S.F., 2000. Characteristics and genesis of epithermal gold deposits. Reviews in Economic Geology 13, 221-244.

Corral, I., Cardellach, E., Corbella, M., Canals, À. and Johnson, C.A., 2011. Origin and evolution of fluids associated with the Cerro Quema Au-Cu deposit (Azuero Peninsula, Panama): evidence from microthermometry, O, H and S isotopes. Proceedings of the 11th SGA Biennial Meeting. Let's talk ore deposits. Published by: Ediciones Universidad Católica del Norte, Antofagasta, Chile: 178-180.

Corral, I., Gómez-Gras, D., Griera, A., Corbella, M. and Cardellach, E., 2013. Sedimentation and volcanism in the Panamanian Cretaceous intra-oceanic arc and fore-arc: New insights from the Azuero Peninsula, (SW Panama). Bulletin de la Société Géologique de France 184 (1), 35-45.

Corral, I. Griera, A., Gómez-Gras, d., Corbella, M., Canals, À., Pineda-Falconett, M., Cardellach, E., 2011. Geology of the Cerro Quema Au-Cu deposit (Azuero Peninsula, Panama). Geologica Acta, 9 (3-4), 481-498.

Del Giudice, D. and Recchi, G., 1969. Geologia del area del Proyecto Minero de Azuero. Informe técnico preparado para el gobierno de la Republica de Panama por las Naciones Unidas, actuando y participando como agencia ejecutora.

Dirección General de Rercursos Minerales (DGRM), 1976. Mapa Geológico de Panamá. Escala 1:500,000. , Panamá.

Fall, A. S., Tattitch, B., and Bodnar, R.J., 2011. Combined microthermometric and Raman spectroscopic technique to determine the salinity of H_2O-CO_2-NaCl fluid inclusions based on clathrate melting. Geochimica et Cosmochimica Acta 75 (4), 951-964.

Ferencic, A., 1970. Porphyry copper mineralization in panama. Mineralium Deposita 5 (4), 383-389.

Field, C. W. and Fifarek, R. H., 1985. Light stable-isotope systematics in the epithermal environment. In: Berger, B. R., Bethke, P. M. (Eds.), Geology and Geochemistry of Epithermal Systems, Reviews in Economic Geology 2, 99-128.

Field, C. W. and Gustafson, L. B., 1976. Sulfur isotopes in the porphyry copper deposit at El Salvador, Chile. Economic Geology 71 (8), 1533-1548.

Field, C. W., Rye, R. O., Dymond, J. R., Whelan, J. F. and Senechal, R. G., 1983. Metalliferous sediments of the East Pacific. In: Shanks III, W. C. (Ed.), Cameron Volume on Unconventional Mineral Deposits. Society of Mining engineers of the American Institute of Mining, Metallurgical, and Petroleum Engineers, 133-156.

Field, C. W., Zhang, L., Dilles, J. H., Rye, R. O. and Reed, M. H., 2005. Sulfur and oxygen isotopic record in sulfate and sulfide minerals of early, deep, pre-main stage porphyry Cu-Mo and late main stage base-metal mineral deposits, Butte district, Montana. Chemical Geology 215 (1-4), 61-93.

Fifarek, R. H. and Rye, R. O., 2005. Stable isotope geochemistry of the Pierina high-sulfidation Au-Ag deposit, Peru; influence of hydrodynamics on SO_4^{2-}- H_2S sulfur isotopic exchange in magmatic-steam and steam-heated environments. Chemical Geology 215 (1-4), 253-279.

Giesemann, A., Jager, H. J., Norman, A. L., Krouse, H. R. and Brand, W. A., 1994. On-line sulfur isotope determination using an elemental analyzer coupled to a mass spectrometer. Analytical Chemistry 66, 2816-2819.

Giggenbach, W. F., 1992. Magma degassing and mineral deposition in hydrothermal systems along convergent plate boundaries. Economic Geology 87 (7), 1927-1944.

Giggenbach, W. F. and Stewart, M. K., 1982. Processes controlling the isotopic composition of steam and water discharges from steam vents and steam-heated pools in geothermal areas. Geothermics 11 (2), 71-80.

Gilg, H. A. and Sheppard, S. M. F., 1996. Hydrogen isotope fractionation between kaolinite and water revisited. Geochimica et Cosmochimica Acta 60 (3), 529-533.

Haas, J. L., 1971. The effect of salinity on the maximum thermal gradient of a hydrothermal system at hydrostatic pressure. Economic Geology 66 (6), 940-946.

Hedenquist, J. W. and Garcia, J. S., 1990. Sulfur isotope systematics in the Lepanto mining district, northern Luzon, Phillippines. Mining Geology 40, 67.

Hedenquist, J. W. and Henley, R. W., 1985. The importance of CO_2 on freezing point measurements of fluid inclusions; evidence from active geothermal systems and implications for epithermal ore deposition. Economic Geology 80 (5), 1379-1406.

Hedenquist, J. W. and Lowenstern, J. B., 1994. The role of magmas in the formation of hydrothermal ore deposits. Nature 370 (6490), 519-527.

Hedenquist, J. W., Matsuhisa, Y., Izawa, E., White, N. C., Giggenbach, W. F., Aoki, M., 1994. Geology, geochemistry, and origin of high sulfidation Cu-Au mineralization in the Nansatsu District, Japan. Economic Geology 89 (1), 1-30.

Hedenquist, J. W., Reyes, A.G., Simmons, S. F. and Taguchi, S., 1992. The thermal and geochemical structure of geothermal and epithermal systems; a framework for interpreting fluid inclusion data. European Journal of Mineralogy 4 (5), 989-1015.

Hofstra, A. H. leventhal, J. S., Northrop, H. R., Landis, G. P., Rye, R. O., Birak, D. J., Dahl, A. R., 1991. Genesis of sediment-hosted disseminated-gold deposits by fluid mixing and sulfidization: Chemical-reaction-path modeling of ore-depositional processes documented in the Jerritt Canyon district, Nevada. Geology 19 (1), 36-40.

Holland, H. D., 1965. Some applications of thermochemical data to problems of ore deposits; [Part] 2, Mineral assemblages and the composition of ore forming fluids. Economic Geology 60 (6), 1101-1166.

Horlacher, C. F. and Lehmann, J. H., 1993. Regional Geology, Geochemistry and Exploration potential of the central Cerro Quema concession, Panamà. Unpublished report, 36 pp.

Kesler, S. E. Russell, N., Seaward, M., Rivera, J., McCurdy, K., Cumming, G. L., Sutter, J. F., 1981. Geology and geochemistry of sulfide mineralization underlying the Pueblo Viejo gold-silver oxide deposit, Dominican Republic. Economic Geology 76 (5), 1096-1117.

Kesler, S. E., Sutter, J. F., Issigonis, M. J., Jones, L. M. and Walker, R. L., 1977. Evolution of porphyry copper mineralization in an oceanic island arc; Panama. Economic Geology 72 (6), 1142-1153.

Kolarsky, R. A., Mann, P., Monechi, S., Meyerhoff-Hull, D. and Pessagno, E. A., 1995. Stratigraphic development of southwestern Panama as determined from integration of marine seismic data and onshore geology. Special Paper - Geological Society of America 295, 159-200.

Kusakabe, M. Nakagawa, S., Hori, S., Matsuhisa, Y., jeda, J. M., Serrano, L., 1984. Oxygen and sulfur isotopic composition of quartz, anhydrite, and sulfide minerals from the El Teniente and Rio Blanco porphyry copper deposits, Chile. Bulletin - Geological Survey of Japan 35, 583-614.

Larson, P. B. and Taylor, H. P., 1987. Solfataric alteration in the San Juan Mountains, Colorado; oxygen isotope variations in a boiling hydrothermal environment. Economic Geology 82 (4), 1019-1036.

Leach, T. M., 1992. Petrological Evaluation of the High Sulphidation Systems in the La Pava and Cerro Quema Prospect Areas, Panama. Unpublished report, 55 pp.

Lissinna, B., 2005. A profile through the Central American Landbridge in western Panama: 115 Ma Interplay between the Galápagos Hotspot and the Central American Subduction Zone. Thesis. Christian-Albrechts Universität zu Kiel, 102 pp.

Montes, C., Bayona, G. A., Cardona, A., Buchs, D. M., Silva, C. A., Morón, S. E., Hoyos, N., Ramírez, D. A., Jaramillo, C. A., Valencia, V., 2012. Arc-continent collision and orocline formation: Closing of the Central American seaway. Journal of Geophysical Research 117 (B04105), 25.

Murray, H. and Janssen, J., 1984. Oxygen isotopes - indicators of kaolin genesis? Procedings of the 27th International Geological Congress 15, 287-303.

Nelson, C. E., 1995. Porphyry copper deposits of southern Central America. Arizona Geological Society Digest 20, 553-565.

Nelson, C. E., 2007. Metallic mineral resources. In: Jochen Bundschuh and Guillermo E. Alvarado (Eds.), Central America: Geology, Resources and Hazards. The Netherlands, Taylor & Francis, Chapter 32, 885-915.

Ohmoto, H. and Goldhaber, M. B., 1997. Sulfur and carbon isotopes. In: Barnes, H. L. (Ed.), Geochemistry of hydrothermal ore deposits. Wiley, New York, 517-612.

Ohmoto, H., Mizukami, M., Drummond, S. E., Eldrige, C. S., Pisutha-Arnond, V., and Lenagh, T. C., 1983. Chemical processes of kuroko formation. Economic Geology Monographs 5, 570-604.

Ohmoto, H. and Rye, R. O., 1979. Isotopes of sulfur and carbon. In Barnes. H. L. (Ed.), Geochemistry of hydrothermal ore deposits. John Wiley & Sons, New York, 509-567.

Plumlee, G. S., 1994. Fluid chemistry evolution and mineral deposition in the main-stage Creede epithermal system. Economic Geology 89 (8), 1860-1882.

Potter, R. W., Clynne, M. A. and Brown, D. L., 1978. Freezing point depression of aqueous sodium chloride solutions. Economic Geology 73, 284-285.

Puritch, E. J., Sutcliffe, R. H., Wu, Y., Armstrong, T. and Yassa, A., 2012. Technical report and mineral resource estimate on the Cerro Quema Project, Los Santos province, Panama, Prepared for Preshimco Resources Inc., by P&E Mining Consultants Inc., 123 pp.

Roedder, E., 1963. Studies of fluid inclusions; [Part] 2, Freezing data and their interpretation. Economic Geology 58 (2), 167-211.

Roedder, E. and Bodnar, R. J., 1980. Geologic Pressure Determinations from Fluid Inclusion Studies. Annual Review of Earth and Planetary Sciences 8 (1), 263-301.

Rye, R. O., 2005. A review of the stable-isotope geochemistry of sulfate minerals in selected igneous environments and related hydrothermal systems. Chemical Geology 215 (1-4), 5-36.

Rye, R. O., Bethke, P. M. and Wasserman, M. D., 1992. The stable isotope geochemistry of acid sulfate alteration. Economic Geology 87 (2), 225-262.

Rye, R. O., Stoffregen, R. E. and Bethke, P. M., 1990. Stable isotope systematics and magmatic hydrothermal processes in the Summitville, CO, gold deposit. U. S. Geological Survey Open-File Report 90-626, 31.

Sakai, H. and Matsubaya, O., 1977. Stable isotopic studies of japanese geothermal systems. Geothermics 5 (1-4), 97-124.

Savin, S. M. and Epstein, S., 1970. The oxygen and hydrogen isotope geochemistry of clay minerals. Geochimica et Cosmochimica Acta 34 (1), 25-42.

Savin, S. M. and Lee, M., 1988. Isotopic studies of phyllosilicates. Reviews in Mineralogy and Geochemistry 19 (1), 189-223.

Shepherd, T. J., Rankin, A. H. and Alderton, D. H. M., 1985. A practical guide to fluid inclusion studies. Blackie & Son, Glasgow, United Kingdom (GBR), 239 pp.

Sheppard, S. M. F., 1986. Characterization and isotopic variations in natural waters. Reviews in Mineralogy 16, 165-183.

Sheppard, S. M. F. and Gilg, H. A., 1996. Stable isotope geochemistry of clay minerals; The story of sloppy, sticky, lumpy and tough, Cairns-Smith (1971). Clay Minerals 31 (1), 1-24.

Sheppard, S. M. F., Nielsen, R. L. and Taylor, H. P., 1969. Oxygen and hydrogen isotope ratios of clay minerals from porphyry copper deposits. Economic Geology 64 (7), 755-777.

Stoffregen, R. E., 1987. Genesis of acid-sulfate alteration and Au-Cu-Ag mineralization at Summitville, Colorado. Economic Geology 82 (6), 1575-1591.

Taylor, B. E., 1986. Magmatic volatiles; isotopic variation of C, H, and S. Reviews in Mineralogy and Geochemistry 16 (1), 185-225.

Taylor, H. P., 1968. The oxygen isotope geochemistry of igneous rocks. Contributions to Mineralogy and Petrology 19 (1), 1-71.

Taylor, H. P., 1974. The Application of Oxygen and Hydrogen Isotope Studies to Problems of Hydrothermal Alteration and Ore Deposition. Economic Geology 69 (6), 843-883.

Torrey, C. and Keenan, J., 1994. Cerro Quema Project, Panama, Prospecting in tropical and arid terrains, Toronto, Ontario, Canada. Unpublished report, 23 pp.

Valiant, W. W., Collins, S. E. and Krutzelmann, H., 2011. Technical report on the Cerro Quema Project, Panama., Prepared for Preshimco Resources Inc., by Scott Wilson Roscoe Postle Associates Inc., 109 pp.

Vennemann, T. W., Muntean, J. L., Kesler, S. E., O’Neil, J. R., Valley, J. W., and Russell, N., 1993. Stable isotope evidence for magmatic fluids in the Pueblo Viejo epithermal acid sulfate Au-Ag deposit, Dominican Republic. Economic Geology 88 (1), 55-71.

Vennemann, T. W. and O'Neil, J. R., 1993. A simple and inexpensive method of hydrogen isotope and water analyses of minerals and rocks based on zinc reagent. Chemical Geology 103 (1-4): 227-234.

Wegner, W., Worner, G., Harmon, R. S. and Jicha, B. R., 2011. Magmatic history and evolution of the Central American Land Bridge in Panama since Cretaceous times. Geological Society of America Bulletin 123 (3-4), 703-724.

CHAPTER 6

Conclusions

6.1. On the tectonostratigraphy and geochemistry of the Azuero Peninsula and the Río Quema Formation

6.2. On the sedimentation and volcanism in the Panamanian Cretaceous intra-oceanic arc and fore-arc

6.3. On the dome volcanism and gold mineralization

6.4. On the fluid inclusions and stable isotopes

6.5. Guidelines for exploration of high sulfidation epithermal deposits in the Azuero Peninsula

6.6. Future work

6.1. On the tectonostratigraphy and geochemistry of the Azuero Peninsula and the Río Quema Formation

- The stratigraphy and petrology of the volcanosedimentary rocks of the central Azuero Peninsula and the Cerro Quema area denote a submarine depositional environment. The tectonic setting corresponds to the fore-arc basin associated to a Late Cretaceous intra-oceanic volcanic arc.

- A new lithostratigraphic unit, the Río Quema Formation, is proposed to describe the volcano-sedimentary sequence that crops out in the central Azuero Peninsula. The Río Quema Formation, which hosts the Cerro Quema deposit, is composed of volcanic and volcaniclastic sediments interbedded with hemipelagic limestones, dacite lava domes and intruded by basaltic to andesitic dikes. The Río Quema Formation has been divided into three units, a) Lower Unit, B) Limestone Unit, and C) Upper Unit. The total thickness of the sequence is approximately 1,700 m. The Río Quema Formation is overlying both, The Azuero Igneous Basement and the Azuero Primitive Volcanic Arc, and is discordantly overlapped by the Tonosí Formation.

- The Río Joaquín fault zone, a major regional scale fault zone with broad E-W orientation and reverse-sense motion, has been recognized in the Cerro Quema mining area, and mapped with a slightly different trend from that proposed by Buchs (2008). Other regional structures such as the Agua Clara Fault, parallel to the Río Joaquín Fault Zone has been found affecting the distribution of the Río Quema Formation in the Central Azuero Peninsula. Along the Río Joaquín Fault Zone, the Azuero Igneous Basement is in direct contact with the Upper Unit of the Río Quema Formation. In addition, kilometric to decametric ENE-WSW folds and late sinistral NW-SE strike-slip faults have also been identified in the mining area. These structures suggest a compressive and/or transpressive tectonic regime, at least during Late Cretaceous–Oligocene times.

- The Azuero Igneous Basement is composed by Upper Cretaceous (Aptian to Santonian) basalts and pillow basalts interbedded with pelagic sediments such as limestones and radiolarite. The igneous rocks of the Azuero Igneous Basement have tholeiitic character. Trace element content has flat or slightly enriched pattern, typical of plateau-like affinities. The Azuero Igneous Basement has geochemical affinities similar to the Caribbean Large Igneous Province (CLIP), and is interpreted as the western edge of the Caribbean Plate, forming the Azuero arc basement.

- The Azuero Primitive Volcanic Arc is constituted by basalts and volcaniclastic rocks with tholeiitic character, locally interbedded with Late Campanian-Maastrichtian hemipelagic limestones. Trace elements indicate a signature between an oceanic plateau and a volcanic arc. Incompatible elements show that the slab derived fluids start to interact with the depleted mantle during the APVA deposition. The Azuero Primitive Volcanic Arc, develops on top of the Azuero Igneous Basement, and is interpreted as the initial stages of the Azuero volcanic arc.

- The Azuero Arc Group, where the Río Quema Formation is enclosed, is constituted by volcano-sedimentary, volcanic and arc-related intrusive rocks, with a clear calc-alkaline character. The trace element content of the Azuero Arc Group is characteristic of volcanic arc affinities, with variably enrichment in fluid mobile elements (e.g., Ba, Sr) and also in the most incompatible elements with flat and depleted heavy REE's with negative Nb-Ti anomalies. Although this group derived from a depleted mantle source, it is strongly influenced by the enrichment produced by the subducting slab-derived fluids. The Azuero Arc Group developes on top of the Azuero Igneous Basement as well as on top of the Azuero Primitive Volcanic Arc, and is interpreted as the expression of the well developed and matured volcanic arc.

- Geochemical evolution of the igneous rocks cropping out in the Azuero Peninsula indicates that a primitive tholeiitic volcanic arc (Azuero Primitive Volcanic Arc) was developed on an oceanic plateau (Azuero Igneous Basement) of also tholeiitic character, and evolved over time to a calc-alkaline volcanic arc (Azuero Arc Group).

6.2. On the sedimentation and volcanism of the Panamanian Cretaceous intra-oceanic arc and fore-arc

- The Río Quema Formation represents the Proximal, Medial and Distal apron of an active island arc, which filled the fore-arc basin. The formation records the initial stages of the Panamanian volcanic arc.

- Facies distribution shows lateral changes with coarser sediments in the north (Proximal apron) and finer sediments in the south of the fore-arc basin (Distal apron). This suggests that the main sediment source is in the north, corresponding to the volcanic arc front, while a minor sediment contribution occurs in the south, providing from the fore-bulge erosion. Moreover, some indicators (e.g., ripples and tool marks) suggest an axial transport in a narrow fore-arc basin.

- Our biostratigraphic data indicates an age which range from Late Campanian to Maastrichtian for the Río Quema Formation, constraining the age of the first volcanic arc developed on the Caribbean plate in the Panamanian region.

6.3. On the volcanism and gold mineralization

- Cerro Quema is a high sulfidation epithermal Au-Cu deposit, hosted by the dacite dome complex of the Río Quema Formation. It is a composite, structurally and lithologically controlled deposit, characterized by four hydrothermal alteration halos with vuggy silica in the inner zone, grading to advanced argillic, argillic and propylitic alteration. Mineralization consists in a dissemination and microveinlets of pyrite with minor chalcopyrite, enargite and tennantite, with traces of sphalerite, crosscut by intermediate sulfidation base metal veins, composed of pyrite, quartz and barite with traces of sphalerite, chalcopyrite and galena.

- Weathering and supergene oxidation processes affected the Cerro Quema deposit developing two different mineralized zones. An upper quartz and iron oxides lithocap, enriched in Au, Ag, Pb and Sb, and a lower supergene enrichment zone, where Cu, Cd, Zn, As and Ba are concentrated. Whole rock trace element data and correlation coefficients between element pairs suggest that Au exploration should be focused in the oxide zone with high Ba anomaly. On the other hand, Cu exploration should be centered in the supergene enrichment zone, in places where primary and secondary Cu-sulfides are present.

- Idiomorphic, zoned, framboidal and brecciated pyrites from the Cerro Quema deposit show similar trace element content despite of their different texture. Pyrites are especially rich in Cu, however significant concentrations in Co, Ni, Ag, Se and Sb have been also found. Co/Ni ratio values in pyrites (0.58 to 5.50) indicate that all are hydrothermal in origin, irrespective of their textures. S/Se ratio values in pyrite (1050 to 2694) suggest a magmatic-hydrothermal origin, in agreement with the Co/Ni ratio values.

- The advanced argillic alteration of the Cerro Quema deposit is characterized by the occurrence of alunite associated to pyrite and dickite. Zoning is a characteristic feature of alunites which often present an inner core of APS minerals. Alunites are Na-rich, covering the range of alunite-natroalunite solid solution. APS minerals are related to the core of alunite-natroalunite, but they are also present as single crystals. APS minerals are Sr, Ca and Ba-rich, characteristics of the woodhouseite-svanbergite solid solution. Alunite-natroalunite and woodhouseite-svanbergite display textural and chemical characteristics suggesting a hypogene origin, probably magmatic-hydrothermal, related to an intrusion-driven hydrothermal system.

- Geochronological data allow to differentiate at least three stages of volcanism and plutonism in the Azuero Peninsula, ranging from Late Cretaceous to Middle Eocene. The first stage is characterized by the Cretaceous volcanic arc and fore-arc development, represented by the dacite dome complex of the Río Quema Formation (~67-66 Ma) and by the quartz-diorite batholit of the El Montuoso (~66 Ma). The second stage corresponds to the Lower Eocene volcanic arc, characterized by the intrusion of batholiths such as the Valle Rico quartz-diorite (~55 Ma). The third stage, denoting the arc migration towards the North, corresponds to Middle Eocene plutonism, recorded by the Parita batholith (~41 Ma).

- Field observations coupled with geochronological and biostratigraphical data, allow to estimate a maximum age of the Cerro Quema deposit as Lower Eocene (~55-49 Ma). The formation of the deposit could be related with the second stage of volcanism and plutonism recorded in the Azuero Peninsula. Hydrothermalism and mineralization are probably related with fluids derived from the emplacement of a porphyry copper intrusion associated to the Valle Rico batholith intrusion, which occurred along the entire fore-arc basin following E-W trending regional faults.

- The geologic model of the Cerro Quema deposit demonstrates that high sulfidation deposits are not exclusive of volcanic edifices or volcanic domes related to subduction zones. High sulfidation deposits can also occur in the fore-arc basin, related to acidic intrusions between the volcanic arc front and the subduction trench. These observations should be taken into account for exploration of high sulfidation epithermal deposits in geologically similar terranes.

6.4. On the fluid inclusions and stable isotopes

- Fluid inclusions data characterize a fluid with variable temperature, ranging from 140 to 243 ºC, and low salinity (< 5 wt % NaCl). This fluid was cooler in the W (La Pava) and hotter in the E (Cerro Quema), indicating the proximity to the fluid source and heat, which is presumably located to the E.

- Boiling, mixing and cooling processes deduced from fluid inclusion data (*Th*/*Tmi* plot), indicate the interaction of the mineralizing hydrothermal fluid with a cooler and less saline fluid, probably of meteoric origin.

- Calculated fluid pressure during mineralization was up to 37 bars under hydrostatic conditions, corresponding to a range between 30 to 250 m below the paleowater table. This indicates that the deposit was emplaced at shallow depth.

- The mineralizing hydrothermal fluid was characterized by $\delta^{34}S_{\Sigma S}$ values of -0.5‰, where $X_{SO_4^{2-}}$ and X_{H_2S} are 0.31 and 0.69 respectively, with a H_2S/SO_4^{2-} (R) ratio of 2.23. These values are compatible with a sulfide dominant hydrothermal fluid of magmatic origin. However, variable $\delta^{18}O$ with constant $\delta^{34}S$ of alunite and barite suggests a contribution of meteoric waters.

- Sulfur isotope geothermometry from coexisting alunite and pyrite pairs, gave equilibrium temperatures ranging from 241 to 295 ºC. Calculated temperatures are in agreement with microthermometrical measurements from fluid inclusions of the advanced argillic alteration zone.

- $\delta^{18}O$ values of vuggy silica decrease from W (La Pava) to E (Cerro Quema) of the deposit and from surface to depth. These successive enrichments in ^{18}O reflect progressively lower temperatures of deposition, indicating the relative distance to the fluid and heat source. The variation in $\delta^{18}O$ of vuggy silica is in agreement with the temperature gradients deduced from fluid inclusion measurements, suggesting that the fluid and heat source was situated to the E of Cerro Quema.

- $\delta^{18}O$ values of fluids in equilibrium with vuggy silica, from -2.6 to +3.0‰, suggest that the hydrothermal fluid during vuggy silica precipitation was a mixture of magmatic and meteoric waters.

- According to $\delta^{18}O$ and δD values of fluids in equilibrium with kaolinite and dickite, two origins for these minerals can be distinguished: hypogene kaolinite and dickite with $\delta^{18}O$ and δD values ranging from +6.5 to +13.3‰ and from -32 to -15‰ respectively, and supergene kaolinite with $\delta^{18}O$ and δD values from -10.0 to -5.2‰ and from -72 to -20‰, respectively. The origin of kaolinite and dickite is only distinguishable from their $\delta^{18}O$ and δD values.

6.5. Guidelines for exploration of high sulfidation epithermal deposits in the Azuero Peninsula

- High sulfidation epithermal deposits in the Azuero Peninsula are not exclusively related to volcanic edifices or volcanic domes. Field differentiation between the arc units (arc-related intrusives, arc-related volcanics, and the fore- and back-arc basins) is the first step in selecting favorable areas.

- Au-Cu mineralization is related with fluids derived from the emplacement of an acidic intrusion associated to the Valle Rico batholith (~55-49 Ma). Identification of country rocks affected by the Lower Eocene plutonic event may be an additional guide.

- Cerro Quema is controlled by E-W trending regional faults parallels to the Río Joaquín Fault zone. From the tectonic point of view, the exploration should be focused in the identification of these regional faults.

- Identification of hydrothermal alteration zones (vuggy silica, grading to advanced argillic, argillic and finally to propylitic alteration) in volcanic rocks, mainly in dacites.

- Weathering and supergene oxidation processes affected Cerro Quema. Au exploration should be focused in the oxide zone were Ba anomaly is also high, and Cu exploration should be centered in the supergene enrichment zone.

6.6. Future work

- As geological and geochronological data has only allowed to constrain the age of the minralization, further effort shoud be made in dating minerals related with the hydrothermal alteration and/or mineralization such as Ar/Ar on alunite, U/Pb on rutile and, Re/Os on pyrite.

- Integration of aeromagnetic and field geological mapping is usually used to differenciate tectonic terranes with distinctive lithologies, structural styles and metamorphic grade. Processing of the aeromagnetic data obtained by the UNDP in the 60's and integration with our regional geologic data, might help to differentiate the lithostratigraphic units and hydrothermally altered from unaltered rocks, providing information of probable mineralized areas.

- Due to the difficult acces to certain zones of the Azuero Peninsula, remote sensing processing could help the exploration of epithermal deposits in the area. Results from remote sensing processing on the Cerro Quema deposit could be applied to areas with potential to host Au-Cu deposits.

- Numerical simulations of heat, fluid mass and solutes transport as well as chemical reactions could be used in order to understand the gold and sulfides/sulfates deposition. These numerical simulations should facilitate the exploration of similar gold deposits in the Azuero Peninsula.

Acknowledgements / Agraïments / Agradecimientos

Arribat a aquest punt, on tota la feina "està feta", només em queda agrair a totes les persones que m'han ajudat de manera directa o indirecta a la realització d'aquest treball. Aquestes línies estan dedicades a totes aquestes persones, i també a totes aquelles que de manera involuntària hagi pogut oblidar. A totes elles gràcies de tot cor.

En primer lloc vull donar el meu sincer agraïment al meu director de tesi, l'Esteve Cardellach, per donar-me la oportunitat de formar part d'aquest projecte de recerca, per dirigir aquest estudi i posar al meu abast tots els mitjans necessaris per a tirar endavant aquest treball, i per tenir sempre ganes d'ensenyar i explicar les coses una vegada i una altra tranquil·lament. Sense ell, aquesta memòria no hagués estat possible. Però, sobre tot vull agrair-li tot el que m'ha cuidat durant aquests anys. Realment treballant amb ell, m'he sentit tant a gust com a casa.

En segon lloc haig de senyalar a un grup de persones que han estat també importants en la realització d'aquesta tesi. A l'Albert Griera, en David Gómez i la Mercè Corbella els hi haig d'agrair moltíssimes coses, entre elles el seu suport en les campanyes de camp, el seu ajut davant dels problemes (geològics i no geològics), la seva implicació en aquest projecte, la revisió dels treballs presentats en congressos i revistes (i també d'alguns capítols de la tesi), però sobre tot, la seva empenta i motivació per que aquesta tesi tirés endavant. A tots ells mil milions de gràcies, heu estat fonamentals, i he après moltíssim de vosaltres.

També vull donar-li les gràcies a l'Àngels Canals, per la seva disponibilitat sempre que ha estat necessària, tant al camp com al laboratori, especialment en la fase d'estudi de les inclusions fluides. La seva revisió critica ha permès donar un salt de qualitat als capítols que ha revisat.

Otras personas a las que les quiero agradecer de todo corazón su ayuda y colaboración, son los profesores Mario Pineda y Rosario Domínguez (y a toda su familia de Bajo Corral). Me acogieron en su casita de Chitré y Bajo Corral durante gran parte de mis estancias en Panamá, e hicieron que me sintiera como uno más de la familia. Me gustaría también resaltar la gran ayuda ofrecida por Mario, tanto en la organización de las campañas de campo como sobre el terreno. Mario es el único panameño que se conoce todas las carreteras, carreterillas y caminos habidos y por haber de la Península de Azuero. Gracias por todo, y sobre todo por dejarme ser vuestro hermano "fulito".

Me gustaría agradecer a Bellhaven Copper and Gold Inc. el acceso a la propiedad minera y a las muestras y testimonios de sondeo utilizados en este estudio, y también a los geólogos de Cerro Quema, Thomas Baxter y Abel J. Castillo. Además, gracias también a todos los macheteros (acompañantes) que nos asignaron como guías en las campañas de cartografía y muestreo, especialmente a los señores Félix, Sixto, Popi, Fidel, Euri, Benigno, Dungo, Dungito, Luis y Eustaquio. Gracias a todos por conseguir que nuestro trabajo en la "selva" fuera totalmente seguro, y sobre todo, gracias por brindarme su amistad.

I would like to show my gratitude to Carl Nelson and Stewart Redwood for the discussions, comments and recommendations during the development of the Thesis. I learned a lot about Cerro Quema, and about high sulfidation epithermal deposits and the possible link with other type of deposits.

I would also like to thank David Buchs and Peter O. Baumgartner as they introduced me and our research group into the geology of the Caribbean and the Azuero Peninsula. Their comments, explanations and field support were fundamental in the initial stages the Thesis.

Quiero agradecer también el apoyo y ayuda de Elena Vindel y Tomás Martín. Muchas gracias también por los buenos momentos vividos en Rodalquilar y Madrid.

A José Fernández Barrenechea y Belén Soutullo les quiero agradecer su ayuda durante mi estancia en la Universidad Complutense de Madrid. A ellos les debo el conocimiento de las técnicas de separación de arcillas y la preparación de agregados orientados para difracción de rayos-X.

Durante mi estancia en la Universidad de Huelva, disfruté de la compañía y de las enseñanzas de Felipe González. A él le debo todo lo que sé de métodos de teledetección aplicados a yacimientos minerales. Muchas gracias Felipe, por acogerme en tu casa y tu familia. Gracias también a Reinaldo Sáez, que participó muy amablemente en mi aprendizaje durante la estancia, y también por su buen saber, paciencia y liderazgo en la salida de campo de Rodalquilar.

During my stay at the U. S. Geological Survey (Denver, CO) I appreciated the lessons and help of Craig A. Johnson and Cayce A. Gulbransen in the understanding of the stable isotope analytical techniques, of George Breit in the alunite separation and analytical techniques, and of Michael Cosca and John Lee in the Ar/Ar dating. I also thank Richard Moscati for their happy moments and also for his implication in the revision of a scientific paper derived from this thesis. Finally I would also express my gratitude to the entire "USGS soccer team".

També vull agrair la participació en aquesta tesis de l'Esmeralda Caus, la Gumer Galán i de la Linda Daniele, del Departament de Geologia de la UAB i del Juan Diego Martín, de la Facultat de Geologia de la UB, ja que si be no estàn relacionats amb el projecte, han aportat també el seu granet de sorra.

Moltes gràcies a tots els integrants del "Coffe time team", Pini, Linda, Esteve, Mercè Corbella, Reche, Geneta, Paco, David, Mercè Rullán, María Luisa, Teixell i Grigri, per totes les vegades que hem arreglat i desarreglat el món, per totes les clatellades que m'heu fotut cada dilluns durant aquests últims quatre anys degut a la "tertulia deportiva", i per simplement ser allà i compartir una bona estona.

Al Dr. Àlvar Pastor, el meu inseparable amic i company de promoció, "curro", doctorat i espero que de moltes aventures més. Gràcies a tu he tingut sempre una visió alternativa de la realitat, i m'has fet veure el costat bo de les coses. Junts hem passat els millors i pitjors moments de les nostres tesis i ens hem donat suport l'un a l'altre, ets un crack! De tot cor, GRÀCIES.

A la Dra. Àfrica Pitarch, també amiga i companya de promoció i doctorat. Tu sempre has anat un pas endavant, i gràcies a tu he sabut cap a on anar. Gràcies pels teus consells, ànims i per ser com ets.

Al futuro (no muy lejano) Dr. Carlos Ponce, por la alegría que me has aportado durante estos años, por esos piques en paddle (eso ha sido media), por los buenos momentos y el recorrido turístico por Sevilla y Granada (eh chino?!!), y porque igual que Àlvar, me has hecho ver el lado bueno de las cosas. Por todo ello gracias, gracias y gracias.

En aquests agraïments no poden faltar en Pau Barceló i en Xavier Lafuente, des de que ens vam conèixer a la carrera (2001), hem estat inseparables, som el "tripode", i encara que ara estem mes separats (geogràficament) que mai, no he deixat de sentir-me a prop vostre. Gràcies pel vostre suport en tot, heu estat i sou fonamentals en la meva vida. Gràcies per tot companys!!

A Lucia Struth y Natalia Guillén por haber colaborado en esta tesis, enseñándome a hacer "figuras molonas" y echándome una mano con la petrología de las inclusiones fluidas. También os quiero agradecer que me salvarais en esos momentos en los que no veía la luz al final del túnel, vosotras siempre encontrabais una salida.

A la nova i no tan nova fornada de “Precarios”: Àlvar Pastor, Carlos Ponce, Miquel Poyatos, Mireia Domènech, Lucia Struth, Marc Viaplana, Ana Isabel Martinez, Marta Roige, Salva Boya, Gemma de Vicente Bosch, Eudald, Victor, Edu Mascuñano... per compartir tots i cadascun dels dies dels últims quatre anys de la meva vida, pels “Friday beer”, per que sempre hi ha hagut algú de vosaltres per fer un descans i xerrar una estoneta. A tots vosaltres gràcies i molts ànims, mai us rendiu i tireu endavant!!

A Enrique Gómez y Eliseo Tesón, gracias por enseñarme todos los trucos necesarios, desde escribir un abstract o un poster, hasta la utilización de Canvas y Global Mapper, para poder sobrevivir durante la tesis.

Vull agrair l’esforç que han fet durant tots aquests anys de la meva tesis els professionals del Laboratori de Preparació de Làmines Primes de la UAB, en Jaume Ques, Lluis Gordón i en Marc Puigcerver. Sempre han complert amb la feina que els hi hem demanat!

També vull agrair la feina, que ens ha facilitat la vida a mi i a tots els becaris, de les tres Mosqueteres i en D’Artagnan del departament, les nostres “secres”, Silvia Ballbé, Sara Flotats, Glòria Gil i Teresa Puga.

A mi familia, a todos ellos, a los que están y a los que ya se fueron, mil millones de gracias por enseñarme, por educarme, por cuidarme, por apoyarme, por interesarse en mi y en el estado de la tesis todos los días, por celebrar todos los eventos importantes juntos, y por creer en mi. Especialmente quiero agradecer la paciencia y comprensión que han tenido mis padres y mi hermana durante estos años, sé que no ha sido fácil. And the last but not the least, a Neus Noguera, la persona que ha viscut de la manera més propera possible l’aventura de la meva tesis, des dels inicis fins al final, aguantant-ho tot, lo bo i lo dolent. Per això i moltíssimes coses més, gràcies Amoree.

Appendix

1. Location of hydrothermally altered samples analyzed for trace elements.

2. Location and results of the EMPA analyses performed on pyrites.

3. Location and results of the EMPA analyses performed on alunites and APS minerals.

4. Location of samples analyzed for stable isotopes (S, O and H).

1. Location of hydrothermally altered samples analyzed for trace elements.

Sample	Drill Core / Surface	Location	Elevation (masl)	Coordinates (°WGS84) Latitude	Longitude
0308-24.50	DC	Chontal edge	418 m	7.553503	-80.549597
0308-65.80	DC	Chontal edge	356 m	7.553503	-80.549597
0308-111.60	DC	Chontal edge	310 m	7.553503	-80.549597
9210-37.50	DC	La Pava	485 m	7.553891	-80.549785
9210-121	DC	La Pava	402 m	7.553891	-80.549785
9210-136	DC	La Pava	387 m	7.553891	-80.549785
9322-34	DC	La Pava	504 m	7.553800	-80.548254
9322-96	DC	La Pava	442 m	7.553800	-80.548254
9322-121	DC	La Pava	417 m	7.553800	-80.548254
9311-95	DC	La Pava	445 m	7.553721	-80.548643
9311-111	DC	La Pava	429 m	7.553721	-80.548643
9311-153	DC	La Pava	387 m	7.553721	-80.548643
9003-20	DC	La Pava	508 m	7.553838	-80.547904
9003-56	DC	La Pava	472 m	7.553838	-80.547904
LP220	S	La Pava	512 m	7.552939	-80.545198
LP225	S	La Pava	526 m	7.552832	-80.546476
LP235	S	La Pava	212 m	7.560740	-80.543110
CLP1	S	La Pava	477 m	7.553176	-80.550358
9315-87	DC	Cerro Quemita	661 m	7.561865	-80.519096
9315-120	DC	Cerro Quemita	628 m	7.561865	-80.519096
914-9.50	DC	Cerro Quemita	817 m	7.560368	-80.519259
914-22.85	DC	Cerro Quemita	803 m	7.560368	-80.519259
914-54.55	DC	Cerro Quemita	771 m	7.560368	-80.519259
914-82	DC	Cerro Quemita	744 m	7.560368	-80.519259
QT-01	S	Cerro Quemita	823 m	7.560532	-80.519223
QT-02	S	Cerro Quemita	826 m	7.560328	-80.519285
QA10	S	Cerro Quemita	837 m	7.560342	-80.519543
LP104	S	Cerro Quema	884 m	7.561511	-80.515021
LP107	S	Cerro Quema	930 m	7.561760	-80.513308
QA17B	S	Cerro Quema	899 m	7.561870	-80.514515
9343-21.50	DC	Cerro Idaida	705 m	7.555226	-80.507060
9343-50	DC	Cerro Idaida	676 m	7.555226	-80.507060
9343-77	DC	Cerro Idaida	649 m	7.555226	-80.507060
9343-80	DC	Cerro Idaida	646 m	7.555226	-80.507060

2. Location and results of the EMPA analyses performed on pyrites.

Sample	Alteration	Location	Elevation (masl)	Coordinates (ºWGS84) Latitude	Longitude	S	Fe	Co	Ni	Cu	Se	Ag	Cd	Sb	Total
9107-11.55	Vuggy Silica	La Pava	504 m	7.553503	-80.549597										
9107-11.55-4a						52.52	43.68	1.78	0.43	1.12	0.05	bdl	bdl	bdl	99.58
9107-11.55-4b						52.52	43.68	1.78	0.43	1.14	0.05	bdl	0.03	bdl	99.63
9107-11.55-1a						53.32	46.63	bdl	bdl	bdl	0.03	0.04	bdl	bdl	100.02
9107-11.55-1b						53.38	45.68	0.05	0.07	bdl	0.02	bdl	0.03	0.05	99.28
9316-173.2	Vuggy Silica	La Pava	374 m	7.554086	-80.549231										
9316-173.2-8a						53.25	45.53	0.08	0.07	0.13	0.02	bdl	bdl	bdl	99.08
9316-173.2-8b						53.34	46.72	bdl	bdl	0.09	bdl	bdl	bdl	bdl	100.15
9316-173.2-8c						53.93	45.90	bdl	bdl	0.17	0.02	bdl	bdl	bdl	100.02
9316-173.2-8.2a						53.72	45.76	bdl	bdl	0.24	bdl	bdl	bdl	bdl	99.72
9316-173.2-8.2b						53.28	45.77	bdl	bdl	0.29	bdl	bdl	bdl	0.07	99.41
9316-173.2-8.2c						53.69	44.98	bdl	bdl	1.56	bdl	0.03	bdl	0.05	100.31
9316-173.2-9						54.13	44.80	bdl	bdl	0.18	bdl	0.03	bdl	0.06	99.2
9316-173.2-10						53.50	46.39	bdl	bdl	0.07	bdl	bdl	bdl	bdl	99.96
9316-173.2-11int						53.37	45.95	bdl	bdl	0.10	bdl	0.03	bdl	0.07	99.52
9316-173.2-11e3						52.68	44.10	bdl	bdl	3.67	0.02	0.03	bdl	0.05	100.55
9316-173.2-11e4						54.14	44.86	bdl	bdl	0.59	bdl	bdl	bdl	bdl	99.59
9316-173.2-11e5						53.49	45.63	bdl	bdl	0.35	0.02	bdl	bdl	bdl	99.49
9316-173.2-11e6						53.48	45.48	bdl	bdl	0.64	bdl	bdl	bdl	0.05	99.65
9316-173.2-24						53.36	45.96	bdl	bdl	0.30	bdl	0.03	0.03	0.07	99.75
9316-173.2-19						53.77	46.34	0.02	0.02	0.06	0.02	bdl	bdl	bdl	100.23
9316-236	Vuggy Silica	La Pava	312 m	7.554086	-80.549231										
9316-236-28						53.38	45.44	bdl	bdl	0.57	0.02	bdl	bdl	0.05	99.46
9316-236-2						52.85	44.63	0.02	0.03	2.21	bdl	0.03	bdl	bdl	99.77
9316-236-1						53.35	46.58	bdl	bdl	bdl	0.02	bdl	bdl	bdl	99.95
9316-236-4						53.25	45.60	bdl	bdl	0.57	0.02	0.03	bdl	bdl	99.47
9316-236-6						53.52	45.20	0.04	0.06	1.44	bdl	0.04	bdl	0.05	100.35
9316-236-25						53.54	45.46	0.04	0.05	1.35	bdl	0.03	bdl	bdl	100.53
9316-236-22						53.15	44.65	0.04	0.02	1.20	0.02	0.04	bdl	bdl	99.29

Appendix 2. Location and quantitative analyses of pyrites from Cerro Quema. Element contet is expressed in wt %.

Sample	Alteration	Location	Elevation (masl)	Coordinates (°WGS84) Latitude	Longitude	S	Fe	Co	Ni	Cu	Se	Ag	Cd	Sb	Total
0308-51.8	Advanced Argillic	Chontal edge	370 m	7.553.503	-80.549.597										
0308-51.8-3						53.46	45.53	0.03	0.03	0.05	bdl	0.03	bdl	bdl	99.13
0308-51.8-8						53.31	45.97	bdl	bdl	0.18	bdl	bdl	0.03	bdl	99.49
0308-51.8-14						54.02	44.88	bdl	bdl	1.12	0.03	bdl	bdl	0.06	100.11
0308-51.8-1						53.61	46.06	bdl	bdl	0.24	0.02	bdl	bdl	bdl	99.93
0308-51.8-32a						53.35	44.61	0.02	bdl	1.72	bdl	0.03	0.03	0.06	99.82
0308-51.8-32b						53.51	46.51	bdl	bdl	0.19	0.02	0.04	bdl	bdl	100.27
0308-51.8-21						53.74	46.16	0.02	bdl	0.10	bdl	bdl	bdl	bdl	100.02
0308-51.8-22						53.51	46.25	bdl	bdl	0.24	bdl	bdl	bdl	0.05	100.05
0308-51.8-23						53.62	45.51	bdl	bdl	0.44	0.02	bdl	bdl	0.07	99.66
0308-73.6	Advanced Argillic	Chontal edge	349 m	7.553.503	-80.549.597										
0308-73.6-1						53.20	43.59	bdl	bdl	3.16	bdl	bdl	bdl	0.04	99.99
0308-73.6-2						53.55	46.12	bdl	bdl	0.14	bdl	bdl	bdl	bdl	99.81
0308-73.6-3b						53.27	46.27	bdl	bdl	0.44	0.02	bdl	bdl	0.06	100.06
0308-73.6-4						53.20	46.23	bdl	bdl	0.12	bdl	bdl	bdl	0.07	99.62
0308-73.6-5						53.36	46.23	bdl	bdl	0.19	0.03	bdl	0.03	bdl	99.84
0308-73.6-13						53.08	46.21	bdl	bdl	bdl	0.02	bdl	bdl	0.04	99.35
0308-73.6-16c						53.67	46.11	bdl	bdl	bdl	bdl	bdl	bdl	0.06	99.84
0308-73.6-18						53.70	46.53	bdl	bdl	bdl	bdl	bdl	bdl	0.05	100.28
0308-73.6-12						54.06	45.47	0.11	0.02	0.80	bdl	bdl	bdl	bdl	100.46
0308-73.6-8						53.56	45.95	bdl	bdl	0.12	bdl	bdl	bdl	0.06	99.69
9343-66	Vuggy Silica	Cerro Idaida	660 m	7.553.503	-80.549.597										
9343-66-01						53.49	45.43	bdl	bdl	0.37	bdl	0.03	bdl	bdl	99.32
9343-66-02						53.67	44.92	bdl	bdl	0.5	bdl	0.03	bdl	bdl	99.12
9343-66-03						53.1	46.09	bdl	bdl	0.24	bdl	bdl	0.03	bdl	99.46
9343-66-03b						53.55	46.16	bdl	bdl	0.08	bdl	0.03	bdl	0.05	99.87
9343-66-09						53.51	46.84	bdl	bdl	0.03	bdl	bdl	bdl	bdl	100.38
9343-66-04p						53.82	45.22	bdl	bdl	1.4	bdl	0.03	bdl	bdl	100.47
9343-66-04b						53.46	45.3	bdl	bdl	1.58	0.03	0.03	0.03	bdl	100.43
9343-66-04c						53.66	44.51	bdl	bdl	2.12	bdl	bdl	bdl	bdl	100.29
9343-66-13b						53.85	45.32	bdl	0.03	1.4	bdl	bdl	bdl	bdl	100.60
9343-66-23						53.44	46.34	bdl	bdl	0.44	bdl	bdl	bdl	bdl	100.22

Appendix 2 (continued)

3. Location and results of the EMPA analyses performed on alunite and APS minerals.

Sample	Alteration / Mineral	Location	Elevation (masl)	Coordinates (°WGS84) Latitude	Longitude	Al_2O_3	FeO Total	CaO	Na_2O	K_2O	P_2O_5	F	SO_3	CuO	As_2O_3	SrO	BaO	CeO	PbO	$(H_2O)^*$	Total
0308-51.8	Advanced Argillic	Chontal edge	370 m	7.553503	-80.549597																
0308-5180-2aa	Alunite					36.63	0.06	0.02	3.21	6.05	0.06	bdl	39.17	bdl	bdl	0.24	0.27	bdl	0.04	14.25	100
0308-5180-2bb	Alunite					36.14	0.07	0.02	3.17	6.11	0.16	bdl	39.26	bdl	bdl	0.37	0.31	bdl	bdl	14.39	100
0308-5180-2a	Alunite					35.86	0.05	0.02	4.22	4.31	0.25	0.33	38.43	0.10	0.04	0.51	0.42	bdl	0.10	15.36	100
0308-5180-2b	Alunite					35.54	0.12	0.20	2.33	6.86	0.43	0.03	37.55	0.17	0.01	0.17	1.07	0.43	bdl	15.09	100
0308-5180-2c	Alunite					35.57	bdl	0.22	2.26	5.36	0.55	0.17	37.85	0.07	bdl	0.56	0.84	0.20	0.33	16.02	100
0308-5180-2d	Alunite					35.68	bdl	0.15	3.23	5.80	0.41	0.47	38.61	0.05	0.01	0.48	0.69	0.10	0.12	14.20	100
0308-5180-2e	Alunite					35.62	0.13	0.19	2.93	5.94	0.56	bdl	37.93	0.02	0.03	0.52	bdl	0.09	bdl	16.04	100
0308-5180-3a	Alunite					33.43	0.14	0.17	3.77	3.56	2.42	0.06	35.85	0.08	bdl	3.39	0.38	0.27	0.16	16.32	100
0308-5180-3b	Alunite					33.87	0.07	0.09	3.61	5.81	0.33	0.3	38.35	bdl	bdl	0.22	0.16	bdl	0.10	17.09	100
0308-5180-5b	Alunite					36.16	0.04	0.36	3.54	5.78	0.46	0.23	38.39	bdl	0.09	0.19	0.12	0.14	bdl	14.50	100
0308-5180-5c	Alunite					35.27	0.08	0.24	3.16	5.52	1.23	0.35	36.80	0.23	0.06	0.39	1.49	0.86	0.06	14.46	100
0308-5180-5d	Alunite					35.78	0.05	0.10	3.90	5.34	0.19	0.03	38.14	bdl	0.03	0.52	0.16	0.08	0.10	15.58	100
0308-5180-9a	Alunite					35.62	0.04	0.02	3.36	5.60	0.25	0.36	37.70	bdl	0.03	0.57	bdl	0.15	0.20	16.10	100
0308-5180-9b	Alunite					35.97	bdl	0.01	4.79	4.06	0.19	0.12	40.22	bdl	0.07	0.42	0.12	bdl	bdl	14.03	100
0308-5180-9c	Alunite					35.49	0.26	0.01	4.53	2.87	1.70	bdl	36.69	0.10	bdl	3.29	0.3	0.09	0.26	14.41	100
0308-5180-11a	Alunite					36.51	bdl	0.08	4.36	4.56	0.25	0.36	39.68	bdl	0.06	0.41	0.23	0.11	bdl	13.39	100
0308-5180-11b	Alunite					33.60	2.16	0.23	4.62	1.98	3.20	0.55	34.34	bdl	0.02	3.28	1.73	0.59	0.26	13.44	100
0308-5180-24a	Alunite					35.88	0.01	0.28	4.51	4.04	0.59	0.17	40.05	0.10	0.04	0.31	0.16	0.15	0.09	13.62	100
0308-5180-29b	Alunite					36.28	0.11	0.03	3.95	5.11	0.19	bdl	39.29	0.06	0.12	0.43	bdl	0.04	0.10	14.29	100
0308-73.6	Advanced Argillic	Chontal edge	349 m	7.553503	-80.549597																
0308-7360-26a	APS					30.72	0.31	1.20	0.94	0.35	11.6	0.68	21.49	bdl	0.11	16.63	1.40	0.43	0.25	13.9	100
0308-7360-26b	APS					31.04	0.58	1.060	0.86	0.13	12.4	0.37	20.34	0.10	bdl	16.20	1.00	0.57	0.36	14.97	100
0308-7360-26c	APS					30.83	0.55	0.84	1.07	0.08	11.80	0.65	21.67	bdl	0.04	16.50	1.03	0.56	0.42	13.96	100
0308-7360-25a	APS					31.82	0.21	3.49	0.68	0.22	13.8	0.67	21.06	0.16	0.06	13.19	1.45	0.74	0.30	12.17	100
0308-7360-25b	APS					31.44	0.27	1.07	0.83	0.22	12.9	0.21	20.68	bdl	0.05	16.96	1.07	0.53	0.36	13.37	100
0308-7360-24a	APS					31.43	0.25	0.73	1.10	0.08	13.4	0.89	20.54	bdl	0.08	16.72	1.14	0.56	0.49	12.56	100
0308-7360-24b	APS					31.67	0.83	1.70	1.35	0.11	12.9	0.42	22.05	bdl	0.08	14.06	1.23	0.61	0.74	12.27	100
0308-7360-21a	APS					32.53	bdl	0.77	0.92	0.52	12.3	0.45	20.14	0.29	0.05	16.44	0.41	0.29	bdl	14.86	100
0308-7360-21b	APS					31.78	0.19	0.73	0.89	0.39	12.7	0.08	20.0	0.02	0.05	17.08	bdl	0.38	bdl	15.66	100
0308-7360-20a	APS					31.70	0.19	0.58	0.73	0.35	12.70	bdl	19.0	bdl	0.01	17.61	0.22	0.43	bdl	16.48	100
0308-7360-20c	APS					31.75	bdl	0.59	0.79	0.43	11.90	0.43	19.87	0.14	0.09	17.11	0.18	0.29	0.14	16.29	100
0308-7360-19a	APS					32.37	0.30	1.59	1.24	0.29	13	0.71	21.75	0.04	bdl	14.47	0.22	0.28	0.37	13.42	100
0308-7360-10a	APS					30.80	1.33	1.59	0.88	0.04	13.3	0.66	20.76	0.18	0.05	16.49	0.92	0.35	0.46	12.15	100
0308-7360-10b	APS					32.26	0.77	0.96	1.80	0.36	10.1	0.25	24.39	bdl	0.12	13.51	1.04	0.48	0.11	13.81	100
0308-7360-10c	APS					32.62	0.35	0.65	2.09	0.50	10.5	0.30	23.86	0.04	0.11	13.71	0.74	0.47	0.14	13.89	100
0308-7360-17a	APS					31.92	0.19	3.59	0.30	0.13	17.6	0.51	14.65	0.14	bdl	14.56	0.93	0.43	0.21	14.83	100
0308-7360-15a	APS					31.86	0.24	1.22	0.74	0.31	14.1	0.08	18.82	bdl	0.06	16.93	0.67	0.24	bdl	14.71	100
0308-7360-15b	APS					33.81	0.07	4.02	0.82	0.43	16.5	1.58	15.59	bdl	bdl	10.61	0.15	0.21	0.01	16.16	100
0308-7360-14a	APS					29.27	0.94	1.13	0.22	0.02	13.5	0.05	18.87	bdl	0.02	19.14	0.40	0.61	bdl	15.86	100
0308-7360-14c	APS					31.67	0.25	2.14	0.46	0.18	19	0.96	15.3	0.24	0.06	17.06	0.33	0.18	0.42	11.78	100
0308-7360-14d	APS					31.83	0.26	2.49	0.52	0.41	17.5	0.62	16.65	bdl	0.04	15.81	0.22	0.22	0.25	13.15	100

Appendix 3: Location and quantitative analyses of pyrites and APS minerals from Cerro Quema. Oxide content is expressed in wt %. * Calculated by difference.

4. Location of samples analyzed for stable isotopes (S, O and H).

Sample	Drill Core / Surface	Location	Elevation (masl)	Coordinates (ºWGS84)	
				Latitude	Longitude
0308-29	DC	Chontal edge	413 m	7.553503	-80.549597
0308-51	DC	Chontal edge	371 m	7.553503	-80.549597
0308-60	DC	Chontal edge	362 m	7.553503	-80.549597
0308-65	DC	Chontal edge	357 m	7.553503	-80.549597
0308-73	DC	Chontal edge	349 m	7.553503	-80.549597
0308-95	DC	Chontal edge	327 m	7.553503	-80.549597
0308-98	DC	Chontal edge	324 m	7.553503	-80.549597
0308-104	DC	Chontal edge	318 m	7.553503	-80.549597
0308-105	DC	Chontal edge	317 m	7.553503	-80.549597
0308-111	DC	Chontal edge	311 m	7.553503	-80.549597
0308-131	DC	Chontal edge	291 m	7.553503	-80.549597
0308-134	DC	Chontal edge	288 m	7.553503	-80.549597
QUE KAN	S	Chontal edge	380 m	7.554373	-80.534976
9210-16	DC	La Pava	507 m	7.553891	-80.549785
9322-78	DC	La Pava	460 m	7.553800	-80.548254
9311-106	DC	La Pava	434 m	7.553721	-80.548643
9311-153	DC	La Pava	387 m	7.553721	-80.548643
9316-182	DC	La Pava	365 m	7.554086	-80.549231
9316-190	DC	La Pava	357 m	7.554086	-80.549231
LP04	S	La Pava	212 m	7.560740	-80.543110
LP204	S	La Pava	287 m	7.544965	-80.542383
LP211	S	La Pava	444 m	7.552508	-80.542204
LP212A	S	La Pava	488 m	7.552739	-80.543656
LP213B	S	La Pava	491 m	7.552312	-80.543421
LP215	S	La Pava	506 m	7.552210	-80.544060
LP216	S	La Pava	528 m	7.552569	-80.545667
LP218	S	La Pava	510 m	7.552897	-80.544829
LP220	S	La Pava	512 m	7.552939	-80.545198
LP222	S	La Pava	513 m	7.553037	-80.545773
LP223	S	La Pava	520 m	7.552905	-80.546112
LP225	S	La Pava	526 m	7.552832	-80.546476
LP226	S	La Pava	524 m	7.552985	-80.546779
LP228	S	La Pava	533 m	7.553474	-80.547659
CLP4	S	La Pava	465 m	7.552721	-80.549952
QUE-51	S	La Pava	400 m	7.552455	-80.540572
914-59	DC	Cerro Quemita	767 m	7.560368	-80.519259
914-82	DC	Cerro Quemita	744 m	7.560368	-80.519259
9315-130	DC	Cerro Quemita	618 m	7.561865	-80.519096
QA05	S	Cerro Quemita	691 m	7.562193	-80.521998
QT-02	S	Cerro Quemita	826 m	7.560328	-80.519285
QA29	S	Cerro Quemita	820 m	7.562009	-80.516879
QA10	S	Cerro Quemita	837 m	7.560342	-80.519543
QA30	S	Cerro Quemita	786 m	7.561368	-80.518187
QA15A	S	Cerro Quema	923 m	7.562235	-80.513461
QA17B	S	Cerro Quema	899 m	7.561870	-80.514515
QA24	S	Cerro Quema	851 m	7.560411	-80.515163
QA32	S	Cerro Quema	911 m	7.561720	-80.514330
9343-36	DC	Cerro Idaida	690 m	7.555226	-80.507060
9343-56	DC	Cerro Idaida	670 m	7.555226	-80.507060
9343-66	DC	Cerro Idaida	660 m	7.555226	-80.507060
Pit-02	S	Pitaloza	365 m	7.643920	-80.646460